Characterization of the intracellular acidity regulation capacity of brain tumor cells in fluorescence imaging-Consequences for therapeutic optimization oftemozolomide

Alaa Tafech

THÈSE

Pour obtenir le grade de

DOCTEUR DE L'UNIVERSITÉ GRENOBLE ALPES

École doctorale : ISCE - Ingénierie pour la Santé la Cognition et l'Environnement
Spécialité : MBS - Modèles, méthodes et algorithmes en biologie, santé et environnement
Unité de recherche : Translational Innovation in Medicine and Complexity

Caractérisation de la capacité de régulation de l'acidité intracellulaire des cellules de tumeurs cérébrales en imagerie par fluorescence-Conséquences pour l'optimisation thérapeutique du témozolomide

Characterization of the intracellular acidity regulation capacity of brain tumor cells in fluorescence imaging-Consequences for therapeutic optimization of temozolomide

Présentée par :

Alaa TAFECH

Direction de thèse :

Angélique STEPHANOU CHARGEE DE RECHERCHE, Université Grenoble Alpes	Directrice de thèse

Rapporteurs :

OLIVIER SEKSEK
Chargé de recherche HDR, CNRS DELEGATION ILE-DE-FRANCE SUD
ANNABELLE BALLESTA
Chargé de recherche HDR, INSERM PARIS ILE- DE-FRANCE CENTRE EST

Thèse soutenue publiquement le **13 décembre 2022**, devant le jury composé de :

OLIVIER SEKSEK Chargé de recherche HDR, CNRS DELEGATION ILE-DE-FRANCE SUD	Rapporteur
ANNABELLE BALLESTA Chargé de recherche HDR, INSERM PARIS ILE- DE-FRANCE CENTRE EST	Rapporteure
WALID RACHIDI Professeur des Universités, UNIVERSITE GRENOBLE ALPES	Président
ANTOINE DELON Professeur des Universités, UNIVERSITE GRENOBLE ALPES	Examinateur

Invités :

MAÏTÉ VERREAULT

Abstract

A well-known feature of tumor cells is high glycolytic activity leading to acidification of the tumor microenvironment through extensive lactate production. This acidosis promotes processes such as metastasis, aggressiveness and invasiveness that has been associated to a worse clinical prognosis. Moreover, the function and/or expression of transporters involved in regulation of intracelluar pH (pH_i) might be altered.

In this context, the aim of this thesis was first to characterize the capacity of a tumor to regulate intracellular acidity by measuring the pH_i of two glioma cell lines: the F98 cell line (rat glioma) and the U87-MG cell line (human glioblastoma). Therefore, we have developed a new ratiometric method that allows the combination of pH-sensitive fluorescent probes and confocal microscopy to characterize the pH_i regulatory capacity and pH resistance of F98 and U87 cell lines in 2D monolayer cultures and in 3D spheroids. This method makes it possible to best exploit the capacities of the confocal microscope.

Our result show that the tumor regulation of acidity is not the same for the two cell lines and as a consequence, our results do not support the common idea that tumor cells behave in a similar way. On the other hand, pH_i regulation appears highly cell-dependent. In 2D monolayer cultures, we have found that F98 rat glioma cells do not regulate intracellular acidity and may preserve protons inside the cells by activating the V-ATpase pump at acidic pH to bring H^+ ions into lysosomes. However, we have found that human glioblastoma U87 cells are able to regulate intracellular acidity and may use the Na^+/H^+ exchanger to export H^+ ions outside the cells. Comparison of the measurements performed on 2D monolayer cultures and 3D spheroids exhibits some differences. Our results show that extracellular acidity may inhibit energy metabolism or protein synthesis and prevent the regulation of exchanges such as Na^+/H^+ in 3D spheroids.

Another aim of the thesis was to assess the efficacy of Temozolomide (TMZ). TMZ is the cornerstone drug used against brain tumors. It has the particularity to be highly pH-dependent. Therefore, the effect of TMZ was studied on our two cell lines by manipulating the extracellular pH (pH_e). The results has allowed us to show that drug efficiency depend on the cell type and on the pH_e, which gives an argument for considering pH as a personalized therapeutic target for future research based on the combination of TMZ with pH-regulating agents.

Based on our original results, we found that the use of our developed fluorescent method can be a valuable tool to assess metabolic status in glioma models and can therefore be used to characterize cells from patient biopsies to better adapt the therapy.

Contents

Introduction **1**

1 State of art **5**
1.1 Origin of tumor acidity . . . 5
1.2 Regulation of intracellular acidity . . . 9
1.2.1 The family of Na^+/H^+ exchangers (NHEs) . . . 10
1.2.2 The enzyme V-ATPase . . . 12
1.2.3 Proton-lactate transporters (MCTs) . . . 12
1.2.4 Carbonic anhydrases and HCO_3^- transporters . . . 13
1.3 Warburg effect and acidity . . . 14
1.4 Consequences of acidity . . . 16
1.4.1 Acidity and tumor invasion . . . 16
1.4.2 Acidity and cellular plasticity . . . 17
1.4.3 Acidity and immunosuppression . . . 17
1.4.4 Acidity and resistance to treatments . . . 17
1.5 Techniques and aim of pH measurement . . . 18
1.5.1 pH microelectrodes . . . 19
1.5.2 ^{31}P NMR spectroscopy . . . 20
1.5.3 Weak acids and bases . . . 21
1.5.4 Fluorescence microscopy . . . 22
1.6 Glioma and glioblastoma . . . 24
1.6.1 Classification of gliomas . . . 24
1.6.2 Glioblastoma treatments . . . 25
1.6.3 TMZ, a methylating agent . . . 25
1.6.4 Development of temozolomide resistance . . . 28
MGMT Can Repair TMZ-Induced DNA Alkylation . . . 28
DNA mismatch repair (MMR) system and temozolomide resistance . . . 29
The role of glioma stem cells in temozolomide resistance . . . 29
1.7 Manipulating tumor acidification as a cancer treatment strategy . . . 30
1.8 Extracellular acidity and chemoresistance . . . 31

2 Materials and methods **41**
2.1 The cell models . . . 41
2.1.1 Experimental tumor model . . . 41
The U87-MG model . . . 41

The F98 model . . . 42
The development of tumor spheroid experiments . . . 43
2.2 Cell culture conditions . . . 47
2.3 Cell handling . . . 47
2.3.1 Trypsinization and subculture . . . 47
2.3.2 Cell freezing . . . 48
2.3.3 Cell counting . . . 48
2.3.4 Counting methods for mortality/viability . . . 48
2.3.5 Loading cells with pH probes . . . 49
2.4 Fluorescence microscopy . . . 50
2.4.1 Confocal microscopy . . . 50
2.4.2 Principle of fluorescence . . . 52
2.4.3 Characteristic parameters of fluorescence . . . 56
Fluorescence lifetime . . . 56
Quantum yield of fluorescence . . . 59
2.4.4 Emission and excitation spectra in fluorescence . . . 59
2.4.5 Fluorophores . . . 60
Organic fluorophores . . . 60
Quantum dots . . . 61
2.4.6 Fluorescent proteins . . . 61

3 Fluorescent indicators for intracellular pH: a comparative study between SNARF-4F and BCECF 65
3.1 SNARF-4F . . . 66
3.1.1 In vitro fluorescence spectra of SNARF-4F . . . 68
Non-permeable version . . . 68
Permeable version . . . 70
3.1.2 Measurement of intracellular potassium ions concentration . . . 72
3.1.3 Intracellular pH calibration . . . 74
3.2 BCECF . . . 76
3.2.1 In vitro fluorescence spectra of BCECF, non-permeable version . . . 78
3.2.2 Intracellular pH calibration . . . 82
3.3 Screening of the pH probes . . . 85

4 Evaluation of the pH drift in the culture medium used for cell incubation during *in vitro* studies 91
4.1 Introduction . . . 91
4.2 The buffer system . . . 91
4.3 DMEM pH Drift . . . 93
4.4 Predicted pH at equilibrium . . . 96
4.5 Conclusion . . . 99

5 Intracellular pH adaptation to changing extracellular pH **101**
5.1 Introduction . . . 101
5.2 Intracellular pH adaptation . . . 103
5.2.1 Methodology . . . 103
5.2.2 Overall pH_i adaptation dynamics . . . 104
5.2.3 Adaptation of F98 cells . . . 106
5.2.4 Adaptation of U87 cells . . . 108
5.2.5 Conclusion . . . 110
5.3 Resistance to extracellular pH changes . . . 110
5.3.1 Long-term mortality . . . 112
5.3.2 Short-term mortality . . . 112
5.4 Intracellular pH heterogeneity . . . 115
5.4.1 Methodology . . . 115
5.4.2 pH_i heterogeneity at the cell population level . . . 117
5.4.3 pH_i heterogeneity at the intercellular level . . . 118
5.5 Conclusion . . . 124

6 Intracellular pH evaluation in 3D spheroids **127**
6.1 Introduction . . . 127
6.2 The spheroids . . . 128
6.3 Formation of spheroids . . . 129
6.4 Fluorescence microscopy . . . 129
6.5 Image processing . . . 132
6.6 Intracellular pH in tumor spheroids . . . 138
6.6.1 Intracellular pH and spatial heterogeneity . . . 138
6.6.2 pH_i gradients in the spheroid . . . 140
pH_i in F98 Spheroids . . . 140
pH_i in U87 Spheroids . . . 140
6.7 Interpretation . . . 141
6.8 2D *vs.* 3D cultures . . . 143
6.9 Conclusion . . . 144

7 Extracellular pH as a therapeutic target to optimize the efficacy of temozolomide **149**
7.1 Introduction . . . 149
7.2 Drug dose-response . . . 149
7.2.1 Cell viability and IC_{50} values . . . 150
7.3 Toxicities of TMZ in F98 and U87 monolayer cultures (2D) . . . 150
7.3.1 Methodology . . . 150
7.3.2 Results . . . 153
7.4 Toxicities of TMZ in F98 and U87 spheroids (3D) . . . 156
7.4.1 Methodology . . . 156
7.4.2 Results . . . 158
7.5 Conclusion . . . 160

Conclusion and Perspective **165**

A Intracellular pH evaluation in 3D spheroids **167**

A.1 pH_i in tumor spheroids 167

Bibliography **171**

Introduction

This thesis subject is part of the virtual tumor development project on which the BCM team (Biologie Computationnelle et Modélisation) has been working for several years. The purpose of this project is to make personalized medicine operational and effective for the treatment of solid tumor cancers in general and brain tumors in particular. Therefore, the setting of the virtual tumor, that is to say the equations of the mathematical model, requires making it possible to measure many quantities specific to the tumor and its environment, in order to better understand how the environment influences tumor evolution, and conversely how the tumor modifies its environment.

Initially, it was planned to measure several bio-physiological parameters such as the oxygen gradient, glucose uptake and extra/intracellular pH (pH_e/pH_i) to the core of the tumor mass using fluorescent probes. As we found that pH_i is a super complex parameter to measure, we chose, instead of measuring multiple physiological variables, to refocus on the pH measurements since cell acidity regulation capacity is a major characteristic of tumor cells that is often related to the cell aggressiveness in terms of survival/resistance and invasiveness. More precisely, a well-known feature of tumor cells is high glycolytic activity which is exploited by PET imaging to locate tumor masses and diagnose cancer (Zhu, Lee, and Shim, 2011). The by-product of glycolysis, lactate, is associated to an increased acidity which helps eliminate normal cells unable to adapt, while tumor cells survive due to their better ability to regulate their pH_i. It was found that tumor cells could maintain a higher pH_i under acidic external conditions (Sharma et al., 2015).

In this context, the aim of this thesis was first to characterize the capacity of a tumor to regulate intracellular acidity by measuring the pH_i of two glioma cell lines: The F98 cell line (rat glioma) and the U87-MG cell line (human glioblastoma). Thereby, fluorescence microscopy methods were widely developed other the past thirty years as a reliable device to measure the pH_i. By the protonation of a chemical function, it is possible to modify the spectroscopic properties of the molecule and to obtain a fluorescent probe sensitive to the variation in proton concentration, and therefore to the pH. Benefiting from a strong expertise in cellular and tissue imaging within our team, pH-sensitive probes have been coupled with confocal microscopy to characterize the pH_i regulatory capacity of F98 and U87 cell lines.

The pH-sensitive fluorescent probe SNARF-4F was first used to measure pH_i. However, during the course of our experiments, we encountered a problem with the fluorescence spectrum of this probe which was found seriously altered. It appeared that the probe stability

had expired which explained the loss of its properties. It was not possible to get a new batch rapidly so we were constrained to replace it by the BCECF probe. Whereas the SNARF-4F probe requires a unique excitation wavelength, the BCECF probe must be excited by two excitation wavelengths: 440 nm and 488 nm, which doubles the acquisition time. Another drawback was that the 440 nm was missing on our confocal microscope. Because of our material limitations, we have developed a method to measure the intracellular/extracellular pH with the BCECF probe, based on the available excitation wavelengths, which makes it an original work. Although the BCECF probe was not intended to be used, we have found, according to the spectral method that we have developed, that it is the most suitable probe for characterizing the regulatory capacity of pH_i of glioma cells.

On the therapeutic aspect, the cornerstone drug used against brain tumors - temozolomide (TMZ) - is known to have an activity that is highly dependent on the acidity of the microenvironment. It has been shown that slightly more basic pH_i values in cancer cells favor the damage induced by TMZ in tumor cells (Zhang, Stevens, and Bradshaw, 2012). However, since tumor cells can acidify their microenvironment, this may influence the efficacy of TMZ. Therefore we focused in the thesis on optimizing the effects of the molecule temozolomide on our two cell lines by manipulating extracellular acidity. The results will set the stage for a realizable clinical application in the short term. Stéphanou and Ballesta, 2019 developed a mathematical model using U87-MG cells to improve TMZ antitumor efficacy. In this model, the cellular, spatial and pH heterogeneity of the tumor microenvironment were examined. Therefore, our experimental results characterizing the cell ability to regulate its pH_i as a function of pH_e, allows the model to highlight potential ways for improving the efficacy of TMZ on tumor cells.

This manuscript has been organized into 7 chapters describing the successive stages of this research. **Chapter 1** concerns a bibliographic study on the origin of acidity in cancer cells and the various mechanisms existing in tumors to prevent acidification of the intracellular environment. Moreover, it presents the consequences of acidity on the tumor environment as well as the role of acidity in the evolution of the therapeutic response of tumors. **Chapter 2** is devoted to the materials and methods used for the realization of this work. **Chapter 3** is devoted to the methodology developed to measure intracellular acidity using an original (extended) ratiometric method using fluorescence spectra that circumvents our materials limitations. During the experiments, we noticed a drift in the pH of the DMEM culture medium used for cell incubation during *in vitro* studies. Normally this drift can be controlled either by adding bicarbonate (HCO_3^-) or by increasing the percentage of carbon dioxide (CO_2) in the incubator. Since we planned to measure in parallel the evolution of the pH_i and pH_e, we chose not to control this drift. Moreover, the drift evolution of the culture medium can easily be quantified which is the purpose of the **Chapter 4**. This chapter presents a simple model to predict the pH at equilibrium. **Chapter 5** is dedicated to the study of the regulation of intracellular acidity of our two tumor cell lines of interest in 2D monolayer cultures. The spectral method developed in Chapter 3 was therefore applied to evaluate the pH_i to changing pH_e. In addition, resistance to pH_e changes was assessed by evaluating cell death. 3D tumor spheroid

model is accepted as a primary model of solid tumors because it reproduces the evolution of the states of oxygenation and acidity of the tumors as a function of their growth and their size. Consequently, **Chapter 6** is devoted to the evaluation of the pH_i in 3D spheroids. A comparison between the results obtain in 2D monolayer cultures and 3D spheroids is made. Finally, **Chapter 7** is dedicated to the study of the effect of pH_e on the efficacy of the drug TMZ, and to the search for the optimal pH_e to maximize the effect of this molecule on the two cell lines, U87 and F98.

Chapter 1

State of art

1.1 Origin of tumor acidity

Acidity is a well-known feature of the tumor microenvironment. It is observed in a variety of solid tumors (Vaupel, Kallinowski, and Okunieff, 1989; Kallinowski and Vaupel, 1988; Chiche, Brahimi-Horn, and Pouysségur, 2010). The pH can be very heterogeneous within the same tumour, with localized acid zones. pH measurements using electrodes have shown that the pH can reach 5.9 in brain tumors, with an average value at around 6.8 while the pH in normal brain tissue is around 7.1 (Vaupel, Kallinowski, and Okunieff, 1989). The question is: where does this acidity come from ?
Let's first define what metabolism is.
Metabolism is the set of chemical reactions that take place within a living organism to enable it to stay alive, reproduce, develop and respond to its environment. It is composed of two opposing mechanisms: catabolism, which extracts energy from nutrients, by degradation of energy molecules (carbohydrates, lipids, etc.); and anabolism, which makes it possible to synthesize the constituents necessary for the structure and proper functioning of cells. We can therefore define *Energy Metabolism* as all the chemical reactions, within a cell, producing ATP (adenosine triphosphate), the cellular energy stock. There are mainly two metabolic pathways in the cell to produce ATP: mitochondrial respiration and fermentation. The common starting point for both pathways is glycolysis and the use of one or the other depends on the availability of oxygen and the level of proliferation of the cell.
In the presence of oxygen (O_2), most differentiated cells metabolize glucose to pyruvate by glycolysis, then completely oxidize most of this pyruvate to carbon dioxide (CO_2) during the Krebs cycle in the mitochondrial compartment. This reaction allows maximum production of adenosine triphosphate (ATP) and limited production of lactate (ionized form of lactic acid). It is the mitochondrial respiration or the oxidative phosphorylation (OXPHOS), which produce a lot of ATP by metabolizing glucose. Conversely, anaerobic glycolysis, or fermentation, is used by several cell types to supply lactate to another cell type nearby, as in the example of the metabolic coupling between astrocytes and neurons (Turner and Adamson, 2011). This reaction converts glucose to lactic acid in the absence of oxygen, producing large amounts of lactate and little ATP (Figure 1.1). Note that glycolysis produces less ATP per mole of glucose than OXPHOS, but allows rapid generation of ATP than OXPHOS (Koppenol, Bounds, and Dang, 2011).

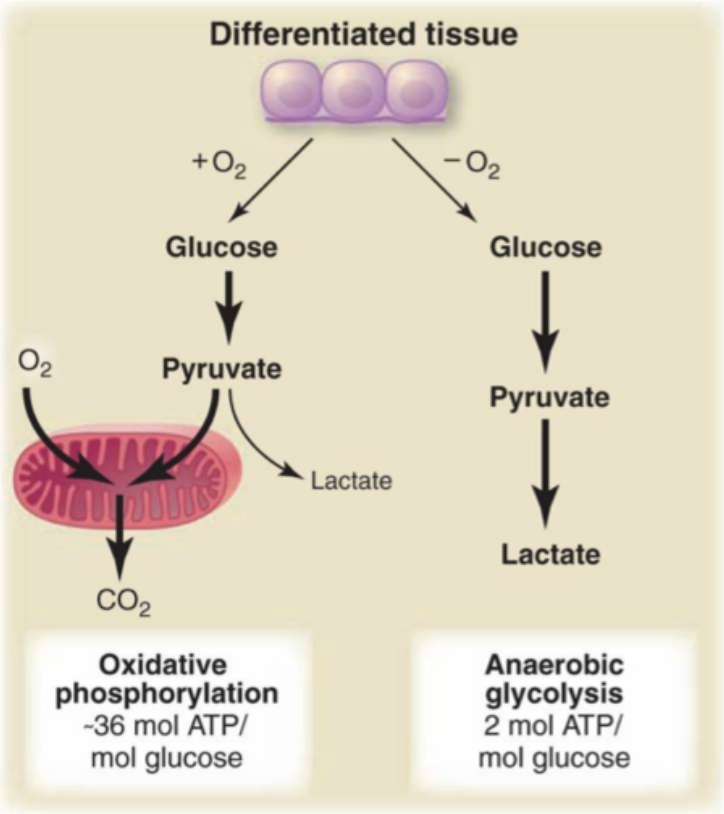

FIGURE 1.1: Schematic representation of oxidative phosphorylations (or mitochondrial respiration) and anaerobic glycolysis (or fermentation). In the case of differentiated tissues, glucose is metabolized to pyruvate via glycolysis and in the presence of O_2, pyruvate is completely oxidized to CO_2 in the mitochondria to produce ATP. On the other hand, in the absence of O_2, pyruvate is transformed into lactate, which allows glycolysis to continue, but producing little ATP. (Extract from Heiden, Cantley, and Thompson, 2009)

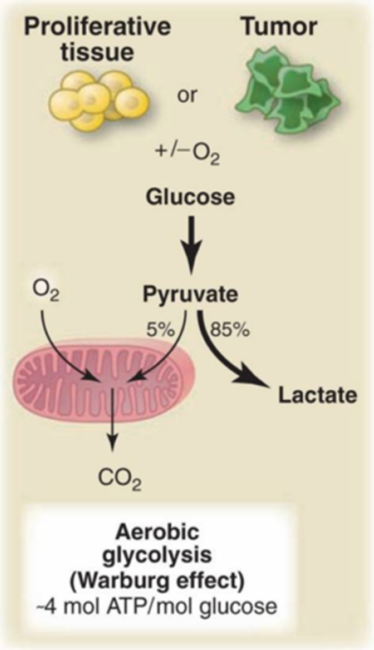

FIGURE 1.2: Schematic representation of aerobic glycolysis known as the "Warburg effect". Warburg noted that cancer cells ferment glucose to lactate even when there is enough oxygen to support oxidative phosphorylation. (Extract from Heiden, Cantley, and Thompson, 2009)

Cells in the proliferative state need energy and organic resources in order to reproduce the components of the cell (DNA, membranes, proteins). Glucose is essential because, apart from ATP, it also provides the metabolic intermediates that take part in anabolic reactions. In the case of tumor cells, the majority develop a more glycolytic than oxidative metabolism, often accompanying a greater aggressiveness of these tumors. This had led Warburg to suspect a deficit in mitochondrial function responsible for this metabolic orientation (Warburg, 1926; Warburg, 1956). It now appears that mitochondria function normally in tumor cells and that the blocking of OXPHOS constitutes an adaptive event (see the section "Warburg effect and acidity") (Figure 1.2).

In addition to the role of glucose, oxygen (O_2) is an essential molecule for cell survival since it is used as a final electron acceptor during the production of energy by mitochondrial respiration. Oxygen can diffuse up to a distance of about 100 μm from a blood vessel and this is why the presence of many vessels is necessary to supply all the cells of a tissue (Kerbel and Folkman, 2002) (Figure 1.3). As it develops, the tumor destroys the microvascular network which ensures the physiological and homogeneous oxygenation of the tissue. Tumor cells that divide very quickly are therefore large consumers of oxygen and nutrients and will then quickly run out of resources by dividing. They then enter a quiescent state, where they drastically reduce their metabolism and no longer divide. Activation of the Hypoxia-Inducible Factor (HIF) family of transcription factors is one of the main oxygen-responsive signalling pathways that allows the adaptation of hypoxic tumor cells to this hostile environment (Figure 1.3).

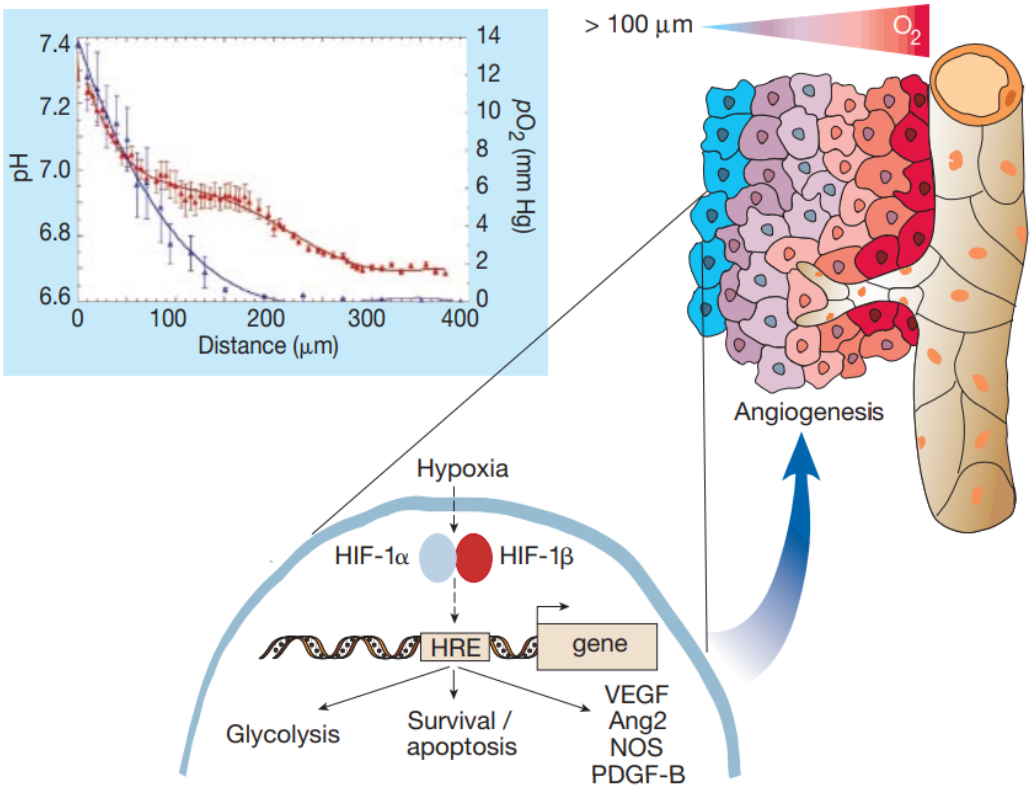

FIGURE 1.3: Role of hypoxia in tumor angiogenesis. Tumor cells that proliferate abnormally quickly run out of resources and become hypoxic. This state of hypoxia triggers the production of HIF proteins, which themselves will stimulate the production of growth factors which will stimulate angiogenesis. The main angiogenic factors expressed in hypoxia are VEGF, NOSs and PDGF. Inset: relationship between the distance of tumor cells from nearby vessels and their degree of hypoxia (blue symbols) and acidosis (red symbols). (Extract from Carmeliet and Jain, 2000)

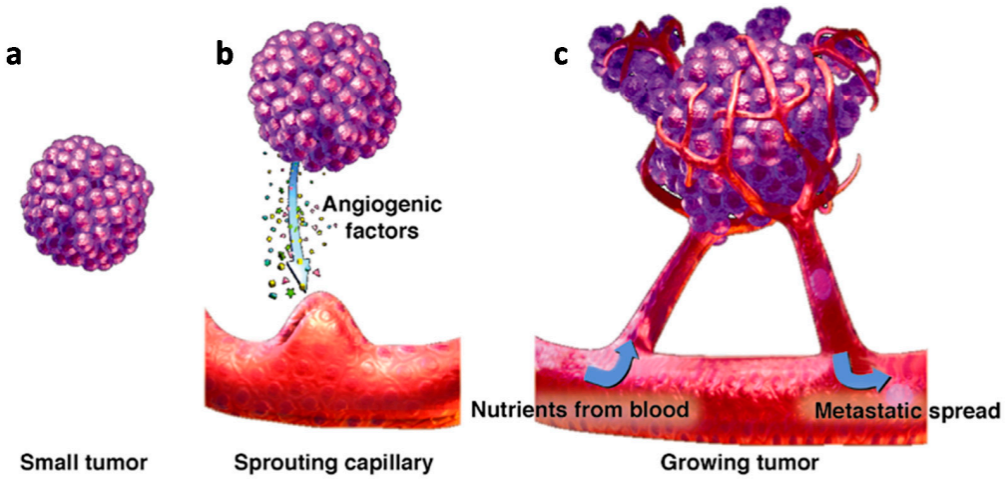

FIGURE 1.4: Angiogenesis and tumor growth. From left to right: the avascular and hypoxic tumor secretes growth factors (VEGF). These will bind to endothelial cells constituting the wall of blood vessels and promote their proliferation and migration to the tumor. This results in the formation of an intra-tumor blood network. This is called a vascular or vascularized tumour. (Extract from Loizzi et al., 2017)

Therefore, hypoxic tumor cells activate the HIF pathway that leads to the production of VEGF (vascular endothelial growth factor), which stimulates the growth of new vessels. The tumor is then vascularized. This process is called angiogenesis or neovascularization (Figure 1.4). Some cells return to the proliferative state where they can divide, and the tumor can thus continue to grow. Even if hypoxia is harmful for both healthy cells and tumor cells, the latter have the ability to adapt to it in several ways and even seem to take advantage of the tumor microenvironment, via various interactions, to promote their growth and dissemination (Serres, O'Brien, and Sibson, 2014).

Furthermore, in the case of hypoxia, the majority of tumor cells are not able to produce ATP via OXPHOS due to low O_2 levels. In order to adapt to this harmful environment, HIF signalling shifts energy production from OXPHOS in the mitochondria towards glycolysis, allowing hypoxic tumor cells to continue to produce ATP despite the low O_2 levels. Due to their significant glycolytic activity, hypoxic tumor cells secrete a large amount of lactate and H^+ ions, which can lead to changes in the pH_i of cancer cells. To help deal with the excess production of lactate and H^+ ions, tumor cells activate a number of pH regulating proteins (such as CAIX, NHE1, MCT4 and V-ATPase) to export lactate and H^+ ions and keep the intracellular pH (pH_i) within the physiological level. Once excreted, lactate and H^+ ions induce a decrease in extracellular pH (pH_e) leading to acidification of the tumor microenvironment (Figure 1.5).

1.2 Regulation of intracellular acidity

Tumor cells are generally associated with alkaline pH_i values of 7.1 to 7.6 and acidic pH_e values of 6.2 to 6.9 (Druzhkova et al., 2015), whereas, normal cell are found with a lower pH_i

(7.0–7.2) than that in the environment in physiological conditions (7.3–7.4) (Shirmanova et al., 2015; Gillies et al., 2002). We then tall about an inverse pH gradient for tumor cells. The fact that pH_i is significantly higher than pH_e in tumors demonstrates the existence of powerful mechanisms to prevent acidification of the intracellular environment (Roos and Boron, 1981; Madshus, 1988; Zhuang et al., 1984). The tools used by tumor cells to regulate their pH_i are varied and depend on the cell type. Several pH regulatory proteins show increased expression (often modulated by the transcription factor HIF-1) or activity in tumor cells. These redundant proteins of tumor pH regulation include: Na^+/H^+ exchangers (NHEs) such as NHE1 (Barathova et al., 2007), V-ATPase (Vacuolar-type Adenosine TriPhosphatase) (Hinton et al., 2009), the monocarboxylate transporters (MCTs) such as MCT1, MCT2, MCT3, and MCT4 (Enerson and Drewes, 2003), Carbonic Anhydrases such as CAII, CAIX, and CAXII (Barathova et al., 2007; Supuran et al., 2010), and the HCO_3^- transporters (Pouysségur, Dayan, and Mazure, 2006) (Figure 1.6). The role of each regulator will be detailed in the following paragraphs. Distinct mechanisms can also be set up in cells with different invasive or metastatic potentials (Sennoune et al., 2004; Montcourrier et al., 1997). A different subcellular localization of pH regulators has been demonstrated in a model of brain tumors (Grillon et al., 2011).

1.2.1 The family of Na^+/H^+ exchangers (NHEs)

Sodium-proton exchangers play a major role in the regulation of pH_i. These Na^+/H^+ exchangers (NHEs) allow the electroneutral exchange of a Na^+ for an H^+. A 2:2 stoichiometry has also been proposed (Fuster, Moe, and Hilgemann, 2004). This family includes nine isoforms (NHE-1 to NHE-9) with varied subcellular and tissue distributions. Only three have been identified in the regulation of pH_i: NHE-1, NHE-2 and NHE-3. NHE-2 and NHE-3 have been localized only in the intestine and kidney while NHE-1 is abundantly expressed throughout the body. NHE-1 is localized at the level of the plasma membrane of the cell and its role is to expel an H^+ ion in exchange for the entry of a sodium Na^+ ion, thereby increasing the pH_i. NHE-1 have a great potential to maintain normal pH_i (Figure 1.6). Johanna Chiche and his collaborators reported the following experiment: the injection of a large quantity of H^+ ions into a hamster expressing NHE-1, NHE-2 and NHE-3 gives rapid recovery from a normal pH_i, suitable for its survival. Contrariwise, mutated cells in which a lack of NHE-1 is observed did not recover their pH_i after the injection of H^+ and died in less than an hour due to the persistent acidification (Chiche, Brahimi-Horn, and Pouysségur, 2010).
The ubiquitous NHE-1 isoform is the only one whose activity has been associated with several properties of cancer cells (Cardone, Casavola, and Reshkin, 2005; Harguindey et al., 2005; Stock and Schwab, 2009). The activity of NHE-1 also seems to be involved in the phenomena of resistance to anti-cancer drugs. Cells resistant to chemotherapy agents generally have a more alkaline cytoplasmic pH and more acidic intracellular vesicles than cells sensitive to these agents (Larsen, Escargueil, and Skladanowski, 2000). It has been shown that the expression and activity of NHE-1 were increased in cells resistant to doxorubicin (DOX) and that inhibition of NHE-1 by a pharmacological inhibitor restores sensitivity to this anti-cancer agent (Miraglia et al., 2005). Inhibition of NHE-1 is also involved in the action of certain

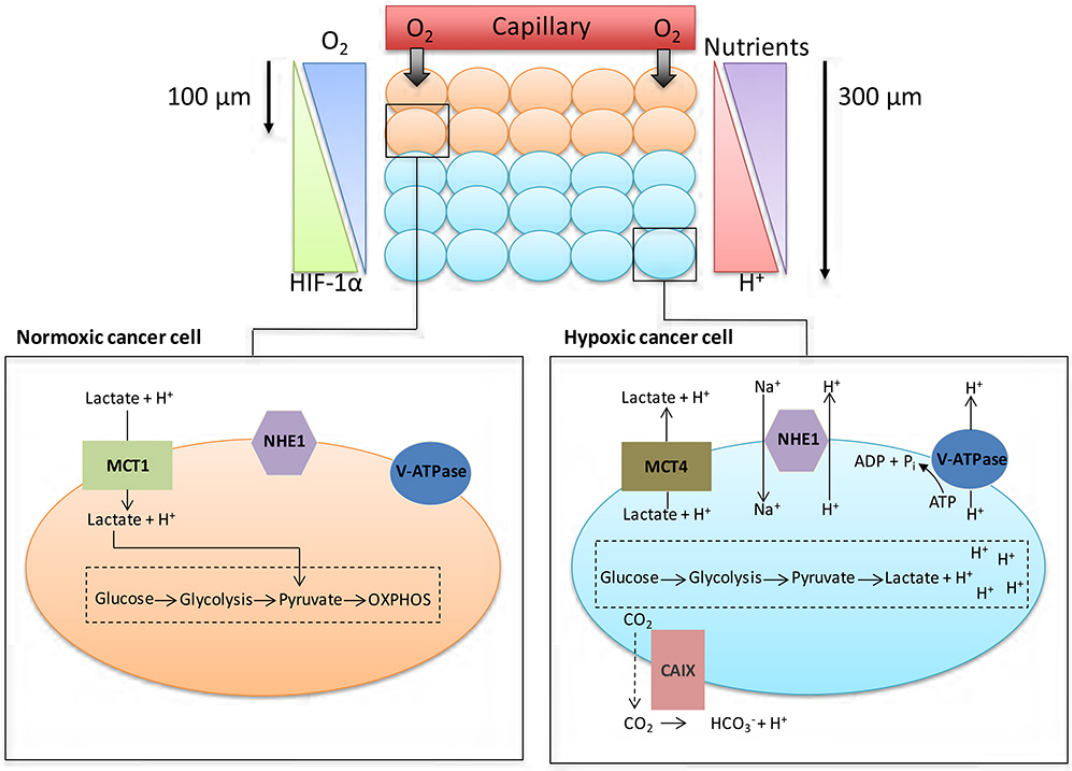

FIGURE 1.5: Cancer cell metabolism, HIF and pH. Oxygen and other nutrients in the blood are carried by the capillaries to the tissues. Due to the oxygen diffusion limit, tumor cells have to deal with different oxygen (O_2) tensions. Normoxic cancer cells surrounding the blood capillary produce energy by oxidative phosphorylation (OXPHOS). However, hypoxic cancer cells are poorly oxygenated and express high levels of HIF. They are not able to acquire energy via OXPHOS and the HIF signalling shifts energy production from OXPHOS in the mitochondria towards glycolysis, allowing hypoxic cancer cells to continue to produce energy despite the low O_2 levels. To maintain intracellular energy levels, cells under hypoxic conditions promote glycolysis, leading to increased glucose uptake and thus increased H^+ production. To help cope with the excessive production of H^+ ions, hypoxic cells put in place numerous regulatory proteins; these proteins include CAIX, NHE1, MCT4 and V-ATPase. Excessive production and export of H^+ ions by cancer cells induces extracellular acidification in the tumor. (Extract from Ward et al., 2020)

anti-cancer agents that induce cancer cell apoptosis such as paclitaxel (Reshkin et al., 2003) and cisplatin (CIS) (Rebillard et al., 2007).

1.2.2 The enzyme V-ATPase

The vacuolar-type proton pumping ATPase (V-ATPase) is a multiprotein complex using the energy of ATP hydrolysis to electrogenically transport protons (Brown, Gluck, and Hartwig, 1987; Forgac, 1989). It is an enzyme catalyzing the following reaction:
ATP + H_2O + $H^+_{intracellular}$ $\rightarrow$ ADP(Adenosine diphosphate) + phosphate + $H^+_{extracellular}$
V-ATPase is expressed at the plasma membrane of cancer cells where it has a role in regulating pH_i (Martinez-Zaguilan, 1992; Martinez-Zaguilan et al., 1993) and consequently contributes in the modification of pH_e. Its expression at the plasma membrane level and its activity are found in highly invasive cancer cells and it is proposed that its activity is correlated with the aggressiveness of cancer cells (Martínez-Zaguilán et al., 1998; Sennoune et al., 2004).
Targeting V-ATPase activity has been proposed as a new cancer treatment strategy (Spugnini, Citro, and Fais, 2010). A V-ATPase inhibitor molecule, esomeprazole used as an acid pH activated prodrug, decreases tumor growth and tumor pH gradient *in vivo* (Milito et al., 2009). V-ATPase inhibitors could also be used in the context of resistance to chemotherapy. Indeed, the expression of several V-ATPase subunits is increased by a chemotherapy agent, cisplatin (Murakami et al., 2001; Torigoe et al., 2002). This increase in expression is involved in chemoresistance phenomena, it has therefore been proposed that inhibition of V-ATPase would increase the cytotoxicity of cisplatin and could be a new strategy to avoid resistance to this compound.

1.2.3 Proton-lactate transporters (MCTs)

Monocarboxylate transporters (MCTs) allow the transport of lactate, ketone bodies or pyruvate. This family includes 14 isoforms of which only the first four play a role in pH_i regulation. The MCT1, MCT2, MCT3 and MCT4 isoforms are electroneutral membrane cotransporters of protons and lactate with a stoichiometry of 1:1.
In cancer cells, significant expression of MCT1 and MCT4 has been demonstrated. MCT4 allows the export of lactate produced by glycolytic (hypoxic) cancer cells, which will then be captured by MCT1 expressed in oxidative cancer cells located at the periphery of the tumor (Sonveaux et al., 2008). MCT1 allows the export of lactate outside the cell, but also the import inside it. Whereas, MCT4 allows the export of lactate outside the cell but is unsuitable for importing it.
MCT1 and MCT4 have an *in vitro* role in the invasiveness of lung cancer cells (Izumi et al., 2011) and MCT4 is involved in the migration of breast cancer cells (Gallagher et al., 2007). MCT1 expression has been shown to be correlated with glioma progression (Froberg et al., 2001).
The use of an MCT1 inhibitor, α-cyano-4-hydroxycinnamate (α-CHC) has been proposed in order to inhibit the entry of lactate into oxidative cells which will then have to use glucose as an energy substrate, and which will not be therefore more available to the glycolytic cells in

the center of the tumor (Sonveaux et al., 2008). The use of α-CHC shows a decrease in tumor growth and radiosensitization in mouse tumor models (Sonveaux et al., 2008). Similar effects are found when the expression of MCT1 is inhibited by an siRNA (Végran et al., 2011). Other inhibitors have been identified (Bueno et al., 2007; Ekberg et al., 2007). No specific MCT4 molecule is available and a targeting problem may arise since MCT4 is located in glycolytic cells far from blood vessels.

1.2.4 Carbonic anhydrases and HCO_3^- transporters

The regulation of cell pH involves, in addition to protons, bicarbonate ions. The carbon dioxide/bicarbonate buffer system helps regulate pH and is the most important physiological buffer system. Carbonic anhydrases are able to catalyze the reaction of CO_2 with H_2O to produce bicarbonates (HCO_3^-) and protons (H^+): $CO_2 + H_2O \rightleftharpoons H^+ + HCO_3^-$. These bicarbonates can be transported into cells to neutralize protons and increase intracellular pH. The transport of bicarbonate ions can be carried out by various co-transporters or exchangers using different associated ions.

- **Carbonic anhydrases**

Carbonic anhydrases (CA) form a superfamily comprising 16 isoforms which catalyze the reversible hydration of CO_2 into HCO_3^- and H^+, and are mainly involved in gas exchange. They can be anchored in the plasma, cytoplasmic, mitochondrial membranes or even secreted (Gilmour, 2010; Pastorekova et al., 2004). Among the active enzymes, five carbonic anhydrases are cytosolic (CAI, CAII, CAIII, CAVII and CAXIII), five are membrane-associated and oriented towards the extracellular environment (CAIV, CAIX, CAXII, CAXIV and CAXV), two are mitochondrial (CAVA and CAVB) and CAVI is secreted. Three are devoid of catalytic activity CAVIII, CAX and CAXI. CAs are involved in many physiological phenomena including respiration and transport of CO_2 and HCO_3^- to the tissues and the lungs, pH and CO_2 homeostasis, certain biosynthetic reactions and bone formation or resorption.
High expression of CAIX and CAXII has been found in breast cancer cells (Bartošová et al., 2002; Ivanov et al., 2001) and in many other types of cancers (Chiche, Brahimi-Horn, and Pouysségur, 2010). CAIX and CAXII are membrane-bound and their catalytic site is oriented towards the outside of the cell. Thus, CO_2, produced by cellular respiration and which diffuses freely outside the cell, is hydrated into protons and bicarbonate ions (HCO_3^-). This action participates in the acidification of the extracellular environment (Švastová et al., 2004), but has also been shown to regulate pH_i (Chiche et al., 2008; Parks, Chiche, and Pouyssegur, 2010; Parks et al., 2013; Swietach et al., 2009). The expression of CAIX and CAXII is induced by hypoxia via the HIF-1 transcription factor (Chiche et al., 2008). Their expression can also be increased even in normoxia in the case of mutations making HIF-1α constitutively active (Grabmaier et al., 2004; Ivanov et al., 1998). In addition, the activity of CAIX is increased by an acid medium such as that found in tumors (Alterio et al., 2009). In hypoxia, induction of CAIX expression contributes to acidifying the extracellular environment of cancer cells and therefore participates in pH regulation (Chiche et al., 2008; Li et al., 2009).
An intracellular carbonic anhydrase, CAII, also seems to be found in certain cancers such as

brain cancers (Parkkila et al., 1995) and to be associated with a poor prognosis in medulloblastomas (Nordfors et al., 2010) while its expression is associated to better survival in gastrointestinal stromal tumors (Parkkila et al., 2010). There are also compensation relationships since the reduction in CAIX expression induces an increase in CAII expression and vice versa (Pan et al., 2006).
Particular attention should be given to CAIX since this isoform is found very infrequently in healthy tissues (in certain parts of the gastrointestinal tract), but is expressed in many tumor tissues, probably due to its hypoxic induction but also to the selective advantage it confers on tumor cells that express it (Parks, Chiche, and Pouysségur, 2013). CAIX represents a particularly interesting therapeutic target and is the subject of intense research around the development of specific inhibitors (Neri and Supuran, 2011).

- **HCO_3^- transporters**

These proteins are mainly grouped into three classes: electroneutral Cl^-/HCO_3^- exchangers of the SLC4 (solute carrier 4) family; the NBC (Sodium-Bicarbonate Cotransporter) family of Na^+/ HCO_3^- co-transporters; and anion transporters of the SLC26 family. These transporters allow the importation of HCO_3^- bicarbonates which are the main buffer species for H^+ hydrogen ions, thus contributing to alkalizing the cytoplasm of the cell.
Little is known about the involvement of bicarbonate transporters in cancer cells. These transporters have been proposed to be involved in pH regulation of cancer cells in recent reviews (Harguindey et al., 2009; Pouysségur, Dayan, and Mazure, 2006; Swietach, Vaughan-Jones, and Harris, 2007). Their involvement was initially studied by the use of a pharmacological inhibitor, DIDS, which is not very specific for a single transporter and also inhibits channels permeable to Cl^- ions. This inhibitor decreases the pH_i of cancer cells *in vitro* (Rotin et al., 1987) and decreases tumor growth *in vivo* but has a toxicity limiting its potential therapeutic use (Yamagata and Tannock, 1996).

1.3 Warburg effect and acidity

In the 1920s, the biochemist Otto Warburg (1883-1970)[1] was the first to show that in the presence of oxygen, cancer cells do not oxidize the pyruvate resulting from glycolysis via the mitochondrial OXPHOS, but convert it mainly into lactate (Warburg, 1926). His subsequent research convinced him that this dysregulation of energy metabolism was due to an irreversible dysfunction of the mitochondrial functions of tumor cells. Otto Warburg hypothesized that an irreversible alteration of mitochondrial respiration is at the origin of the development of cancer (Warburg, 1956); a hypothesis ignored for more than fifty years by a large part of the scientific community, so much so that metabolism was not part of the "Hallmarks of cancer" listed in the famous review by Douglas Hanahan and Robert Weinberg published in 2000 (Hanahan and Weinberg, 2000). It was not until they were updated in 2011 that abnormal metabolism made its appearance with the mention of "deregulating cellular

[1]German physician, physiologist and biochemist. He was awarded the Nobel Prize in Physiology or Medicine in 1931.

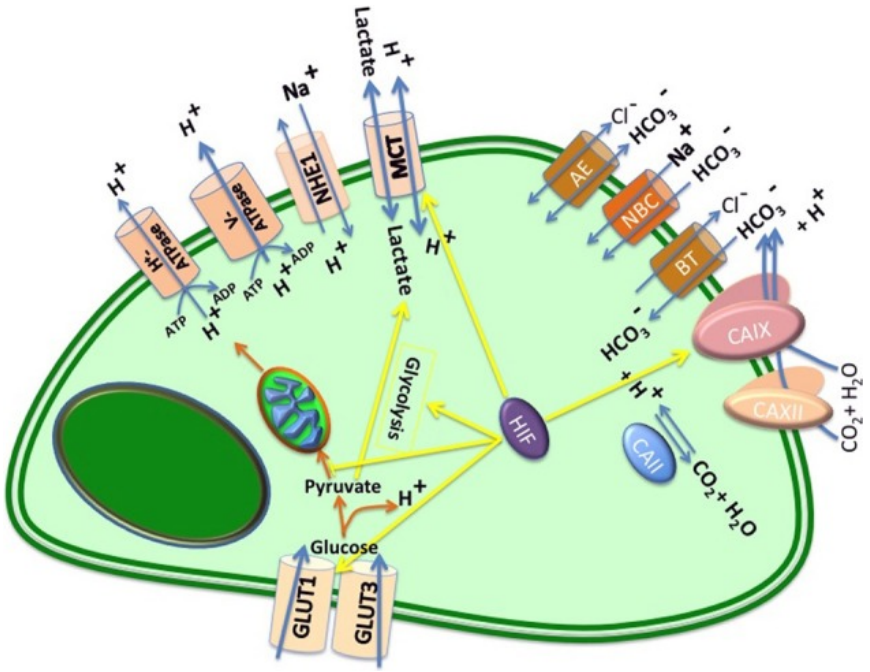

FIGURE 1.6: Regulation of intracellular pH (pH_i) in cancer cells. Cancer cells survive in an acidic environment by coordinating the function of pH-regulating proteins, such as NHE1, CAs, MCTs, V-ATPase, HCO_3^- transporters. Tumor hypoxia promotes the expression of certain proteins involved in the regulation of metabolism and pHi via the HIF transcription factor. (Extract from Damaghi, Wojtkowiak, and Gillies, 2013)

energetics" (Hanahan and Weinberg, 2011).

In honor of its discoverer, the activation of glycolysis under aerobic conditions has been dubbed the "Warburg effect", and at the same time that this process was admitted, it became a paradox to be resolved: why malignant cells having, a priori, an increased need for ATP to proliferate, do they not use the OXPHOS pathway, whose energy yield is significantly higher ?

Today, with the progress of knowledge on the origin and mechanisms of malignant transformation, Warburg's hypothesis on the origin of uncontrolled cell proliferation is no longer accepted for two reasons. The first is that aerobic glycolysis is not directly related to malignancy. Many mammalian cell lines (lymphocytes and fibroblasts) develop aerobic glycolysis under proliferating conditions (Lunt and Heiden, 2011). In cultured lymphocytes, after stimulation of proliferation, it has been shown that these cells convert a significant amount of consumed glucose into lactate (Roos and Loos, 1973; Wang, Marquardt, and Foker, 1976; Hedeskov, 1968). The second reason is that the development of aerobic glycolysis may be independent of whether the mitochondria are functional or not. Indeed, several works have proven that mitochondria function normally in cancer cells and that the blocking of oxidative phosphorylation constitutes an adaptive event (Razungles et al., 2013; Ward and Thompson, 2012; Gentric, Mieulet, and Mechta-Grigoriou, 2017).

In addition, recent study has investigated the impact of environmental acidity on tumor mitochondrial function, (Wu, Ying, and Hu, 2016). The authors of this review reported that cancer cells reverted to OXPHOS, when they were exposed to lactic acidosis, a common

factor in tumor microenvironment. To draw this conclusion, they quantitatively determined the percentage of ATP production from glycolysis and OXPHOS with and without lactic acidosis. They found that in the absence of lactic acidosis, cancer cells exhibited excessive glycolysis and produced a large amount of lactate; while, in the presence of lactic acidosis, cancer cells showed a low level of glycolysis and produced a negligible amount of lactate. These quantitative data supported therefore their notion that cancer cells reverted from Warburg effect to OXPHOS phenotype under acidic conditions.
My teammate Pierre Jacquet has described in his thesis manuscript a simplified model of cellular energy metabolism, to test the role of pyruvate in the distribution of fluxes towards respiration or fermentation, to specify the importance of lactate and to include glycolytic inhibition by acidity. This model was based on recent publications and experimental data highlighting the role of acidity in the regulation of metabolism. The results obtained from this model showed, with a view to the production of ATP, that in order to keep a constant level of pyruvate it was necessary to direct the glycolytic fluxes towards fermentation when this exceeded the activity maximum of the pyruvate dehydrogenase (PDH) complex. Conversely, when the glycolytic flow is reduced by acidity, it is necessary to consume lactate. Thus, the oxidative activity is maintained as much as the oxygen level allows and gradually transitions to fermentation as long as the acidity is not too high, a transition dictated by the maintenance of the pyruvate concentration. This model tends to show that the Warburg effect is not necessarily an inherent characteristic of the tumor cell, but a spontaneous and transient adaptation mechanism to a disturbed environment (Jacquet and Stéphanou, 2021).

In addition to its influence on the Warburg effect , acidity in the tumor microenvironment may have many effects on the evolution of cancer and its progression to malignancy. It has been proposed that exposure to chronic acidosis may induce genome instability through chromosome breakages and translocations driving somatic evolution (Morita et al., 1992; Xiao et al., 2003). Moreover, acidity may contribute to metastatic progression by increasing the degradation of the extracellular matrix surrounding cancer cells (Ibrahim-Hashim and Estrella, 2019; Brisson et al., 2012). On the other hand, acidity can be cytotoxic, inhibit cancer cell proliferation, and promote stress response and cell apoptosis (Ohtsubo et al., 1997; Williams, Collard, and Paraskeva, 1999; Putney and Barber, 2003; Smallbone, Maini, and Gatenby, 2010). Taken together, acidosis has been described as a defining hallmark of the tumor microenvironment. However, the mechanisms by which cancer cells, immune cells, and blood vessels sense acidosis and respond to it are yet to be completely established but may be advantageous for a more comprehensive understanding of tumor biology.

1.4 Consequences of acidity

1.4.1 Acidity and tumor invasion

It has been established that extracellular acidity plays an important role in the process of tumor invasion. Acidity promotes tumor invasion by two main mechanisms: on the one hand,

acidity induces toxicity on normal cells, whereas tumor cells are resistant to acid stress; as normal cells die, tumor cells continue to proliferate and invade therefore this open space. On the other hand, the acidity induces the degradation of the extracellular matrix, via the release and activation of proteases such as cathepsin B (Bourguignon et al., 2004; Rozhin et al., 1994) and of matrix metalloproteases (MMPs) such as MMP-1, 2 and 9 (Yang et al., 2010; Kato et al., 2005, which are generally believed to be involved in local invasion and tissue remodeling. In a xenograft model with breast and colon cancer cells, Estrella et al., 2013 observed a correlation between acidity and tumor invasion. In tumors, areas with the highest invasion corresponded to areas of lowest pH. Interestingly, systematic treatment with sodium bicarbonate decreased the proton gradient in the tumor and prevented tumor invasion (Robey and Nesbit, 2013).

1.4.2 Acidity and cellular plasticity

Although the role of extracellular acidity in regulating the stem state of cancer cells has been less characterized, there are few studies on the regulation of cellular plasticity by acidity.
In a study published in 2010, the acidic condition was shown to stimulate the development of a cancer stem cell phenotype (Hjelmeland et al., 2010). Exposure of glioma cells to an acidic culture medium (pH 6.5) promotes the expression of stem cell markers such as Olig2, Oct4 and Nanog and increases the secretion of angiogenic factors such as VEGF. This happens in particular through increasing the expression of HIF-2α involved in the phenotype of stem cells and the growth of tumor cells. Additionally, lactate has been shown to attract human mesenchymal stem cells to tumour cells and heighten stem cell migration (Rattigan et al., 2012).

1.4.3 Acidity and immunosuppression

During their development, malignant tumors are able to evade the response of the immune system (Hanahan and Weinberg, 2011). Recent studies have shown that the anti-tumor immune response is modulated by the tumor microenvironment, including acidity.
Lactic acid produced by tumor cells inhibits the production of cytokines from cytotoxic T lymphocytes *in vitro* (Fischer et al., 2007). Activated T cells themselves use glycolysis and rely on the efficient secretion of lactic acid. Lactic acid blocks the efflux of lactate produced in the tumor environment and thus disrupts T cell metabolism. In another study, treatment with the proton pump inhibitor esomeprazole, by reducing tumor acidity, restored the functioning of T lymphocytes (Calcinotto et al., 2012).

1.4.4 Acidity and resistance to treatments

Despite advances in the development of new therapeutic strategies, a major underlying factor in cancer-related death remains treatment resistance.
The cytoplasmic membrane functions as a semi-permeable physical barrier that separates the intracellular and extracellular environment. Small and uncharged molecules can easily diffuse through the membrane, while the passage of charged molecules is relatively more difficult. On

the other hand, the diffusion of uncharged chemotherapeutic agents can be altered by changes in the pH of the tumor environment. Thus for slightly basic molecules such as doxorubicin, the extracellular acidity that can be found in the tumor microenvironment can limit their passage through the membrane of cancer cells, compromising their anti-tumor efficacy. This has been shown in *in vivo* and *in vitro* studies.
Extracellular acidity may also play a role in drug resistance by increasing the activity of P-glycoprotein (P-gp), which is involved in drug efflux. Activation of the p38 MAP Kinase signaling pathway by acidity is involved in the activation of P-glycoprotein. Therefore, inhibition of the p38 pathway restores the sensitivity of tumor cells to chemotherapeutic agents.

Until very recently, research and development of anti-cancer drugs focused only on tumor cells, with the development of conventional chemotherapy agents generally targeting the proliferation of cancerous cells, then more targeted agents acting on proteins characteristic of the tumor or on neovascularization. However, due to a very limited improvement in prognosis and an accumulation of our knowledge on the role of acidity in the evolution and therapeutic response of tumors, much attention has currently been focused on strategies targeting the tumor acidity. The different strategies that directly target tumor acidity or exploit characteristics of acidity are now being developed and have begun to show promising results.
A first strategy targeting tumor acidity consists in studying drugs that can be activated under acidic conditions to have a better specificity of the treatment. We cite for example the molecule of our interest TMZ, the fundamental molecule used against glioblastoma (Stéphanou and Ballesta, 2019). Another strategy consists of inhibiting the various proteins involved in maintaining pH_i, which is crucial for the survival of tumors in an acidic environment, using small molecule inhibitors or antibodies. Among the targeted proteins, one can find in particular the NHEs, MCTs, CAs, NBCs (Na^+/HCO^- co-transporters) and V-ATPase (Andersen, Moreira, and Pedersen, 2014; Parks, Chiche, and Pouysségur, 2013; Neri and Supuran, 2011). Tumor acidity is also exploited in the development of nanoparticles which release cytotoxic agents under acidic conditions in order to obtain a better distribution of molecules in the tumor tissue (Lee, Gao, and Bae, 2008; Song et al., 2014).

1.5 Techniques and aim of pH measurement

Although changes in pH_i had been observed much earlier, the oldest method of what might loosely be described as pH_i measurement was employed in 1912 by Michaelis and Davidoff with red blood cells (For a review see Caldwell, 1956). Using platinum/hydrogen electrodes, they noted that red cell lysis caused a change in bulk pH. Although cell lysis was the most appropriate method for estimating pH_i, the potentially serious problems with this technique were recognized early on. For example, the metabolism continues after cell lysis and leads to a drop in pH due the production of lactic acid and carbon dioxide (CO_2). Therefore, various studies in the field of intracellular pH has been characterized by better developments in measurement techniques, by increasing knowledge of the mechanism of control of pH_i,

and by progress in establishing relationships between pH_i and cellular metabolism (Table 1.1 and Table 1.2).

1.5.1 pH microelectrodes

One of the methods developed to measure pH_i is the pH-sensitive microelectrodes method (Thomas, 1974). Although this method is technically very exacting, it has provided very important information. It is particularly suitable for providing a direct, continuous monitoring of local pH and has been used extensively to measure cytosolic pH.
Due to the existence of electrical potential difference across the cell membrane, two electrodes must enter the cell to measure the pH_i. A reference microelectrode filled with potassium chloride (KCl) to measure the membrane potential, and a pH sensitive microelectrode to measure a combination of pH and membrane potential. By subtracting the potential recorded by the two electrodes, one obtains an electric potential proportional to the local pH.
Using this method, intracellular pH measurement was performed in papillary muscle cells of streptozotocin-induced diabetic rats (Lagadic-Gossmann, Chesnais, and Feuvray, 1988). The aim of this study was to investigate the *in vivo* regulation of pH_i following an intracellular acid or alkaline loading in diabetic rats. Accordingly, diabetes was induced in male Wistar rats by the injection of streptozotocin into the femoral vein. The results show differences between diabetic and normal muscles in the regulation of pH_i in response to induced acidity, suggesting that diabetes is associated with a change in the activity of the Na^+/H^+ exchange (Moore, 1983), a major way for the export of H^+ ions from cells during acidity (Fuster, Moe, and Hilgemann, 2004).
pH-sensitive microelectrode has been further used to measure the pH_i of mammalian cardiac cells. The first measurement *in vivo* was performed by Ellis and Thomas, 1976 who studied the effect of CO_2 on the pH_i of Purkinje fiber cells cut from sheep ventricles. The results showed that the pH_i was strongly influenced by CO_2 in the equilibration gas. The mean pH_i in the presence of CO_2 is close to 7.02 and is significantly lower than when CO_2 is absent.
In fact, when the dimensions of the cells are too small, such as epithelial cells, it is difficult and often impossible to accommodate two separate electrodes in the same cell. In this case, two different cells can be penetrated and a different membrane electrical potential can be noted by the reference microelectrode and the pH-sensitive microelectrode. The measurement of pH_i is therefore carried out by calculating the average values of the electrical potentials of several penetrations (Zeuthen, 1980). In order to circumvent most of these problems, a double-barrelled pH microelectrode was introduced (Hemptinne, 1980). It allow the penetration of both electrodes into the same cell, measuring thus the same membrane potential.
A repetitive pH_i measurement of Purkinje fiber cells was obtained using the double-barreled pH microelectrode (Hemptinne, 1980). The results show that the pH_i varies between 7.1 and 7.2 which is, however, significantly greater than that reported by Ellis and Thomas, 1976. It has been reported that this difference is probably due to the different HCO_3^- concentration in the control solution, compared to that used in the Ellis and Thomas publication.
Hagberg, Larsson, and Haljamae, 1983 measured *in vivo* the pH_i of rabbit skeletal muscle fibers using the double-barreled pH microelectrode. The pH_i of 7.00 ± 0.09 found in this study

was lower than that found in mouse soleus fibers *in vitro* using pH-sensitive microelectrodes (7.07) (Claire and Thomas, 1977) or in rat soleus using double-barrelled electrodes (7.1-7.2) (Hemptinne, 1980). Hagberg, Larsson, and Haljamae, 1983 assumed that the higher bath pH and the lower level of CO_2 in the studies of Claire and Thomas, 1977 and Hemptinne, 1980 could explain this small discrepancy. In addition, the pH_i could be different in the soleus (composed mainly of red fibers) than in the predominantly white gastrocnemius muscle.
pH-sensitive microelectrodes have been widely used for pH_i measurements, but since they can cause cell membrane damage and cytosolic leakage that will alter pH_i measurements, their use has been rather limited. In addition, the use of pH-sensitive microelectrodes is impossible on mobile cells such as amoebae (Heiple and Taylor, 1980).

1.5.2 ^{31}P NMR spectroscopy

Following the pioneering work of Moon and Richards (Moon and Richards, 1973), who, in 1973, used the principle of the variation of the chemical shift of mainly cytosolic inorganic phosphate (P_i) with pH, phosphorus nuclear magnetic resonance (^{31}P NMR) spectroscopy was used as a non-invasive pH_i measurement technique. In this case the cells are incubated in the presence of probes such as phosphate or methylphosphonate comprising ^{31}P which penetrate into the cells.
Several cardiac pH measurements were performed using ^{31}P NMR spectroscopy (Salhany, 1979; Brindle et al., 1988; Clarke et al., 1993; Schroeder et al., 2009). Since cardiac cellular acidosis has been introduced as one of the central mechanisms to explain irreversible cell damage during ischemia (Williamson et al., 1976), cardiac cellular pH is therefore an important parameter to measure in various types of ischemic states. For example, a ^{31}P NMR measurement of cardiac pH was performed in isolated rat heart during ischemia and reperfusion (Clarke et al., 1993). The results show that in the pre-ischemic rat heart, the pH_i was approximately 7.15. After 4 min of ischemia, the pH_i decreased to approximately 6.16. On reperfusion, pH_i returned to pre-ischemic levels within 2.5 min.
^{31}P NMR spectroscopy has also been used to monitor renal intracellular pH (Ackerman et al., 1981; Adam, Koretsky, and Weiner, 1985; Adam, Koretsky, and Weiner, 1986). It has been suggested that intracellular acidification could be a primary signal that stimulates renal ammoniagenesis (Tannen, 1978). Therefore, knowing renal intracellular pH may be a key issue in understanding the regulation of ammoniagenesis. In this context, intrarenal pH was measured *in vivo* in perfused rat kidneys where an acidification, from pH 7.4 to pH 6.9, was induced by addition of hydrochloric acid (HCl) to the perfusion medium (Adam, Koretsky, and Weiner, 1985). The results showed that kidney pH fell from 7.20 to 6.75, and reached a plateau of pH 6.85, 30 min after addition of HCl. In parallel, it was found that the rate of ammonia (NH_3) production at 7.4 was doubled when the perfusate was acidified to pH 6.9. This is therefore consistent with the hypothesis that intracellular acidification may participate in the stimulation of ammoniogenesis.
Besides measuring intracellular pH, ^{31}P NMR spectroscopy has also been used to visualize and quantify the phosphorylated metabolites which are directly involved in energy metabolism. We will cite as an example, ATP (adenosine triphosphate) which constitutes the main source

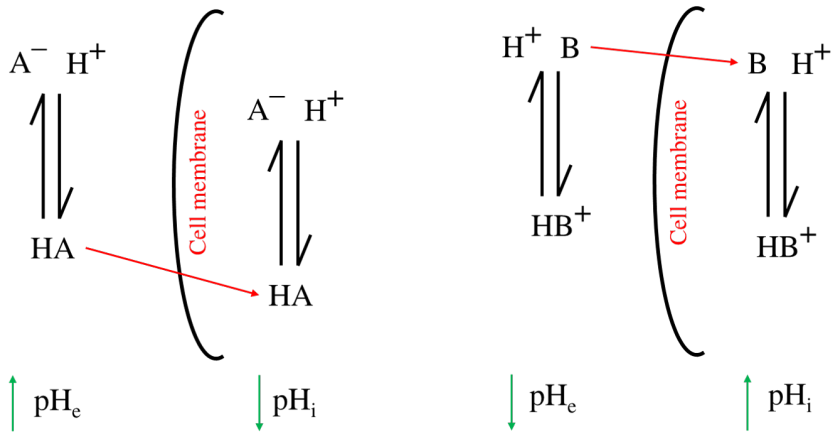

FIGURE 1.7: Diagram illustrating the effects on local pH when weak acids (HA) or weak bases (B) are present.

of energy of the organism, phosphocreatine which is an energy buffer (it makes it possible to maintain the concentration of available ATP constant) and the inorganic phosphate P_i which is the substrate for the ATP synthesis reaction. In addition to quantification, ^{31}P spectra provide unique access to dynamic parameters such as the speed of ATP synthesis (Lei, Ugurbil, and Chen, 2003; Lei et al., 2003). Although this method can provide very important information, it remains little used. This is due to relatively high equipment costs and the need to work with suspensions of high cell concentrations. In addition, it has the disadvantage of giving relatively long analysis times (spectrum acquisition) which do not make it possible to see rapid variations in pH_i (Leyval et al., 1997; Imai and Ohno, 1995; Molenaar, Abee, and Konings, 1991).

1.5.3 Weak acids and bases

Weak acids and bases distribution method has also been introduced to measure intracellular pH (Brown and Garthwaite, 1979). The basis of this method is the use of weak acids HA when $pH_i > pH_e$ or of weak bases B when $pH_i < pH_e$. The neutral species of these probes diffuses freely through the membrane while the ion is impermeable. The weak protonated acid, HA, transports its proton across the membrane and can then dissociate inside the cell, lowering intracellular pH and increasing extracellular pH (pH_e). The weak deprotonated base B will penetrate, leaving a proton behind, and will tend to pick up a proton inside the cell, raising the pH_i and lowering the pH_e (Figure 1.7). In the case of a weak acid, $[HA]_i$=$[HA]_e$ at equilibrium. And since the acid dissociates on both sides, it is therefore assumed that the dissociation constant is the same in the extracellular and intracellular media. From this equilibrium the following equation results:

$$K_a = \frac{[H^+]_i[A^-]_i}{[HA]_i} = \frac{[H^+]_e[A^-]_e}{[HA]_e} \tag{1.1}$$

Under this condition and if $pH_e > pK_a + 1$, most of the acid is ionized on both sides of the membrane, and measurement of the acid distribution ratio allows calculation of intracellular

pH at equilibrium. Since the extracellular pH can be easily measured, the calculation of the pH_i then becomes possible. The quantities of ionized acid are assayed by titrimetry, or by radiometry in the case of labeled probes such as acetate and methylamine (Padan, Zilberstein, and Schuldiner, 1981).

Waddell and Butler, 1959 measured the pH_i of skeletal muscle of the dog using the weak acid DMO (5,5-Dimethyl-2,4-oxazolidinedione). The effects of various treatments altering the pH or the pCO_2 (plasma CO_2) of plasma were studied. In 11 dogs, the calculated pH_i values of normal, resting muscle were all in the range of 6.96 to 7.10 with an average of 7.04. The greatest changes in muscle pH_i are those produced by increasing blood carbon dioxide tension. The pH_i of muscle is lowered by a high tension of carbon dioxide whether or not the blood pH is lowered. Lowering blood pH, by intravenous infusion of hydrochloric acid (HCl), has less effect in lowering muscle pH_i than does high tension of carbon dioxide. While raising blood pH, after sodium bicarbonate ($NaHCO_3$) injection, raise muscle pH_i only to a small extent.

Although this technique is easy, accurate and applicable to small cells, its use is limited by the fact that it requires the destruction of the tissue and therefore cannot easily be used to measure pH_i changes over time. In addition, the presence of acidic or basic molecules can disrupt the establishment of the electrochemical gradient (Molenaar, Abee, and Konings, 1991).

1.5.4 Fluorescence microscopy

Another method developed over the past thirty years to deal with these drawbacks is fluorescence microscopy. By the protonation of a chemical function, it is possible to modify the spectroscopic properties of the molecule and to obtain a probe sensitive to the variation of the proton concentration.

Currently, pH sensitive probes are often in the esterified form of the probe (AM). The presence of these ester groups facilitate the diffusion of fluorophores through the cytoplasmic membrane. Inside the cells and under the action of intracellular esterases, the ester groups are cleaved and the more or less negatively charged probes are retained intracellularly and are then potentially fluorescent.

Gores et al., 1989 used the BCECF-AM probe to measure the pH_i in cultured rat hepatocytes after ATP depletion by metabolic inhibition with KCN (potassium cyanide) and iodoacetate acid (IAA)(chemical hypoxia). KCN and IAA block cellular ATP formation through inhibition of oxidative phosphorylation and glycolysis, respectively. During chemical hypoxia at extracellular pH (pH_e) of 7.4, pH_i dropped from 7.36 to 6.33 within 10 min and remained at 6.1-6.5 for 30-40 min (plateau phase). Subsequently, pH_i began to increase, and cell ensued within minutes as evidenced by nuclear staining with propidium iodide. Exposure of hepatocytes to acidic pH_e simultaneously with KCN and IAA produced a slightly greater drop in pH_i, prolonged the plateau phase of intracellular acidosis and delayed the onset of cell death. In addition, inhibition of Na^+/H^+ exchange with amiloride also produced an increase of cell survival and prolongation of the plateau phase of intracellular acidosis. The results suggest that intracellular acidosis after ATP depletion protects against hepatocellular death from ATP depletion, a phenomenon that may represent a protective adaptation against hypoxia-induced

stress (Gores et al., 1989).
It has been suggested that such an alteration in the pH_i of brain cells could contribute to neurological dysfunctions in patients with AIDS. Therefore, Makutonina et al., 1996 used the BCECF-AM probe to quantitate pH_i in HIV-1-infected T cells (human immunodeficiency virus type 1). The results obtained show that infection of RH9 cells, an established line of CD_4^+ T-lymphoblastoid cells, with HIV-1 resulted in a significant decrease in pH_i from 7.2 in mock-infected cells to approximately 6.6 by days 4 after infection, when cells were undergoing acute cytopathic effects. Fluorescence concentration analysis using BCECF indicated that the pH_i in persistently infected cells that survived the acute cytopathic effects of HIV-1 was approximately 6.8 to 7.0, values which are modestly lower than those inmock-infected cells. The mechanism by which HIV reduces pH_i in CD_4^+ T-lymphoblastoid cells is not established in this study. However, prior studies indicated that HIV infection induces intracellular acidification in lymphocytes due to dysfunction of the plasma membrane ion transport system Na^+/H^+ (Garry et al., 1988; Voss et al., 1996). Exposure to gp120, the HIV-1 surface glycoprotein (SU), activates the Na^+/H^+ exchange system, resulting in an increase in active transport of protons out of the cell and intracellular alkalinization. The results of these studies sugest that alterations in pH_i may mediate certain cytopathic effects of HIV-1, thereby contributing to depletion of CD_4^+ T lymphocytes in patients with AIDS.
Salvi, Quillan, and Sadée, 2002 evaluated The performance of 3 pH-sensitive probes, SNARF-1-AM, BCECF-AM, and Cell-Tracker Green CMFDA in chinese hamster ovary (CHO), human embryonic kidney (HEK293), and 2 Human colon carcinoma (Caco-2) cells for measuring pH_i changes in a multi-well plate format. The stability of pH_i measurements was strongly affected bye the rate of the probe efflux, which was found to depend on the pH-sensitive probe, temperature, pH_e, cell type, and the use of transport inhibitors to prevent probe export. The results show that the performance of the CellTracker Green CMFDA was significantly better with respect to cellular probe efflux. Therefore, this probe was selected for use in further studies with CHO, HEK293, and Caco-2 cells. To investigate whether the effect of hypertonic stress on pH_i can be detected, the medium was made hypertonic by addition of sucrose. The exposure of HEK293 and CHO cells to hypertonic medium induced a pH_i increase of 0.08 pH unit and 0.16 pH unit respectively, whereas no significant pH_i rise was observed in Caco-2 cells. To examine whether the activation of G-protein coupled receptors was connected to a pH_i change, acetylcholine was injected into HEK293-M1 and CHO-M1 cells. In both cell lines expressing a high level of muscarinic receptors, activation by acetylcholine did not cause any significant pH_i response compared with wild type cells. Similarly, stimulation of endogenously expressed β-adrenergic receptors by isoproterenol had no effect. The effects of human dipeptide transport activity on pH_i were also investigate in this study. A pH_i decrease of 0.15 pH unit was observed in CHO cells expressing the human H^+/peptide transporter PEPT1 upon addition of dipeptide substrates. The authors of this study succeeded in developing a rapid fluorimetric assay using the multi-well plate format to measure pH_i change in living cells and examine pH_i changes induced by various effectors.

A large number of fluorescent probes, or fluorophores, have been developed for pH_i sensing;

these probes have the advantage of low toxicity to cells and are not metabolized (Molenaar, Abee, and Konings, 1991). In addition the specificity of localization which can allow the exclusive study of certain cellular compartments such as lysosomes of macrophages (Ohkuma and Poole, 1978). Since its introduction by Tsien in the early 1980s, 2',7' bis(carboxyethyl)-5(and 6)-carboxyfluorescein (BCECF) has been by far the most widely used pH-sensitive fluorescent probe (Tsien, 1981).
As part of the thesis, two pH-sensitive fluorescent probes were selected for their characteristics and they were controlled in order to define the most suitable for characterizing the regulation of the intracellular acidity of brain tumor cells. The study of these two probes will be detailed in Chapter 3.

1.6 Glioma and glioblastoma

In this thesis we chose to focus on the study of brain tumor cells. Therefore we have selected two cell lines frequently used in the literature and well documented: The F98 cell line (rat glioma) and the U87-MG cell line (human glioblastoma). These two cell lines will be presented in detail in the next chapter.

1.6.1 Classification of gliomas

Gliomas are tumors of glial origin. They present 28% of primary tumors and 80% of malignant tumors of the brain and central nervous system (Ostrom et al., 2014). Their incidence is 18.7 cases (including 7.2 malignant cases) per 100,000 persons per year in the USA (Ostrom et al., 2014) and 3.2 cases per 100,000 persons per year in France (Clavreul et al., 2019); It is the 4th cause of tumor mortality in adults and the 2nd cause in children after leukemia. According to their cellular composition (oligodendrogliomas, oligoastrocytomas, astrocytomas), their histological characteristics and their degree of malignancy, gliomas are classified into 4 grades by the WHO (World Health Organization) (Louis et al., 2007). Grade I gliomas correspond to benign tumors with a low potential for proliferation, well demarcated and which can be completely removed by surgery. Grade II gliomas are infiltrative in nature and, despite low proliferative potential, may reappear after surgery. These tumors can progress to higher grade tumors such as diffuse low-grade astrocytomas, anaplastic astrocytomas and glioblastomas. Grade III describes lesions with much greater malignancy; this type of tumor is treated with chemotherapy and radiotherapy. Grade IV astrocytomas, also called glioblastomas, form very invasive tumours, highly proliferative, with the appearance of areas of necrosis and hypoxia and the phenomena of angiogenesis (Figure 1.8); there is also an inflammatory area around the tumor. Due to the highly infiltrating nature of glioblastomas, surgical resection of the macroscopically affected area is not sufficient to eliminate all tumor cells, leading to recurrences and a median of 14.6 months, despite radio- and chemotherapeutic treatments, which makes this pathology one of the cancers with the darkest prognosis.

Glioblastomas represent 54.7% of gliomas and 45.6% (the most frequent form) of all primary malignant brain tumors (Figure 1.9). One of the obvious difficulties in the treatment

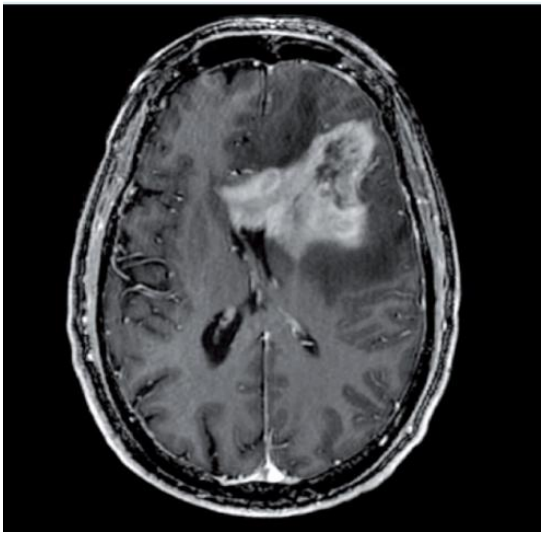

FIGURE 1.8: Magnetic resonance imaging (MRI) of high-grade glioblastoma.
(Extract from Ly, 2014)

of gliomas is their particular location. The brain is a sensitive organ, with an organization as complex as it is fragile, and even a benign brain tumor, due to its volume and the non-deformable nature of the cranial box, can compress certain regions of the brain and induce significant damage depending on the area concerned. On the other hand, the presence of the blood-brain barrier constitutes a major problem since most drugs cannot pass through.

1.6.2 Glioblastoma treatments

Since the 1970s, radiotherapy has been used as part of the treatment of glioblastoma, after surgical excision if it has taken place. It consists of using radiation, or irradiation, to destroy cancer cells by blocking their ability to multiply, while preserving the best possible healthy tissues and surrounding organs. The impact of chemotherapy in the first line treatment of glioblastomas has been introduced more recently.
Chemotherapy is the use of a drug-based approach to treating cancer. It can be delivered locally or systemically. The systemic administration of a molecule is however limited for the treatment of brain tumors due to the presence of the blood-brain barrier, protecting the brain parenchyma from substances present in the blood. On the contrary, during local chemotherapy, the therapeutic agent is directly administered, thus making it possible to deliver high concentrations of molecules, while overcoming the blood-brain barrier.
Since 2005, the treatment of glioblastomas has been relatively standardized. After the most optimal surgical resection, radiotherapy of the surgical bed is carried out and associated with a systemic adjuvant chemotherapy by Temozolomide (TMZ) (Stupp et al., 2005; Stupp et al., 2009).

1.6.3 TMZ, a methylating agent

Temozolomide is a DNA alkylating agent discovered in the early 1980s, and which is now a reference in the treatment of glioblastomas. Temozolomide has the ability to cross the

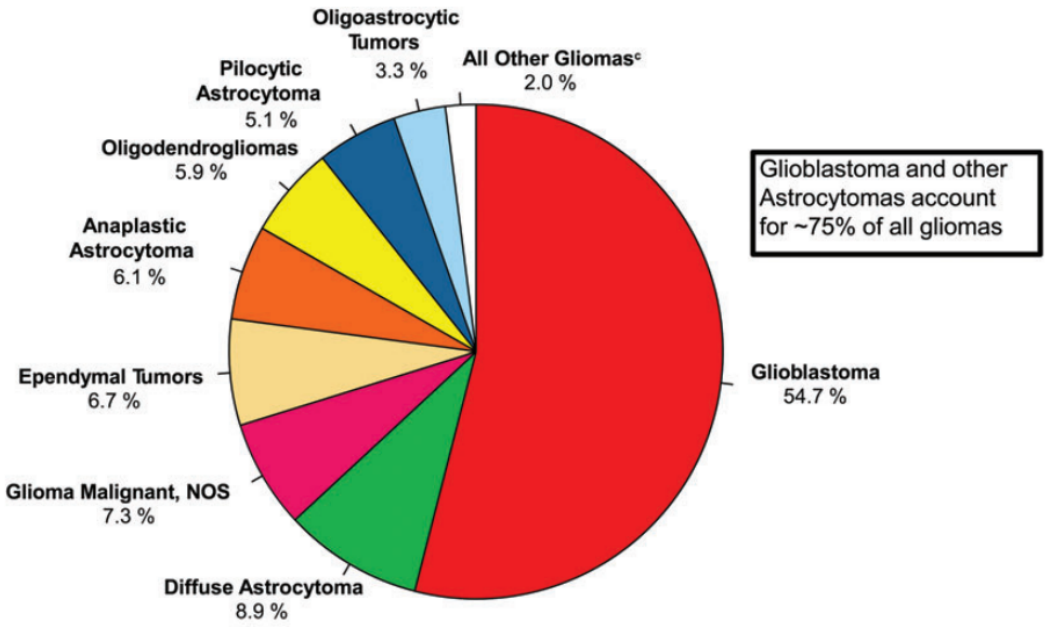

FIGURE 1.9: Distribution of cerebral and CNS gliomas by histological subtype according to the CBTRUS report (Ostrom et al., 2014).

blood-brain barrier and has excellent biodistribution in the central nervous system as well as high stability at acidic pH, allowing its oral administration. The activation of this molecule takes place via the spontaneous conversion of temozolomide into 3-methyl-(triazen-1-yl) imidazole-4-carboxamide (MTIC), which is subsequently degraded into a methyldiazonium cation, the DNA-methylating species. The methyldiazonium cation activates the DNA repair system MMR (mismatch repair) which will lead to DNA breaks and trigger cell death via the p53 protein (Denny et al., 1994; Ballesta et al., 2014; Thomas et al., 2017).

Once activated, TMZ preferentially methylates the purine bases of DNA at the N7 position of guanines in the guanine-rich regions (N7-meG; 60-80%), but it also methylates at the N3 position of adenines (N3-meA ; 10-20%) and in position O6 of guanines (O6-meG ; 5-10%) (Tentori and Graziani, 2002) (Figure 1.10). N7-meG and N3-meA methylations are the most abundant and induce replication fork arrest. They are quickly repaired via base excision repair (BER). N7-meG are not cytotoxic, on the other hand, N3-meA lesions are lethal for the cell if they are not repaired. The cytotoxicity of lesions caused by TMZ therefore depends on the cellular repair system but it is generally due to methylations at the O6 position of guanines (Strobel et al., 2019).

O6-meG can be directly repaired if the cell expresses the enzyme MGMT (methylguanine methyltransferase). Otherwise, O6-meG cause a mismatch with thymine (not cytosine) during DNA replication which triggers the mismatch repair system (MMR). MMR exclusively recognizes only thymine and excises it, with O6-meG remaining in place on the opposite strand. Thus several futile cycles of excision then reinsertion of thymine are linked together causing single-strand breaks in the DNA. These breaks lead to the collapse of the replication fork and the formation of DNA double-strand breaks (Mojas, Lopes, and Jiricny, 2007). The absence of MGMT and a functional MMR are therefore the two essential conditions for the

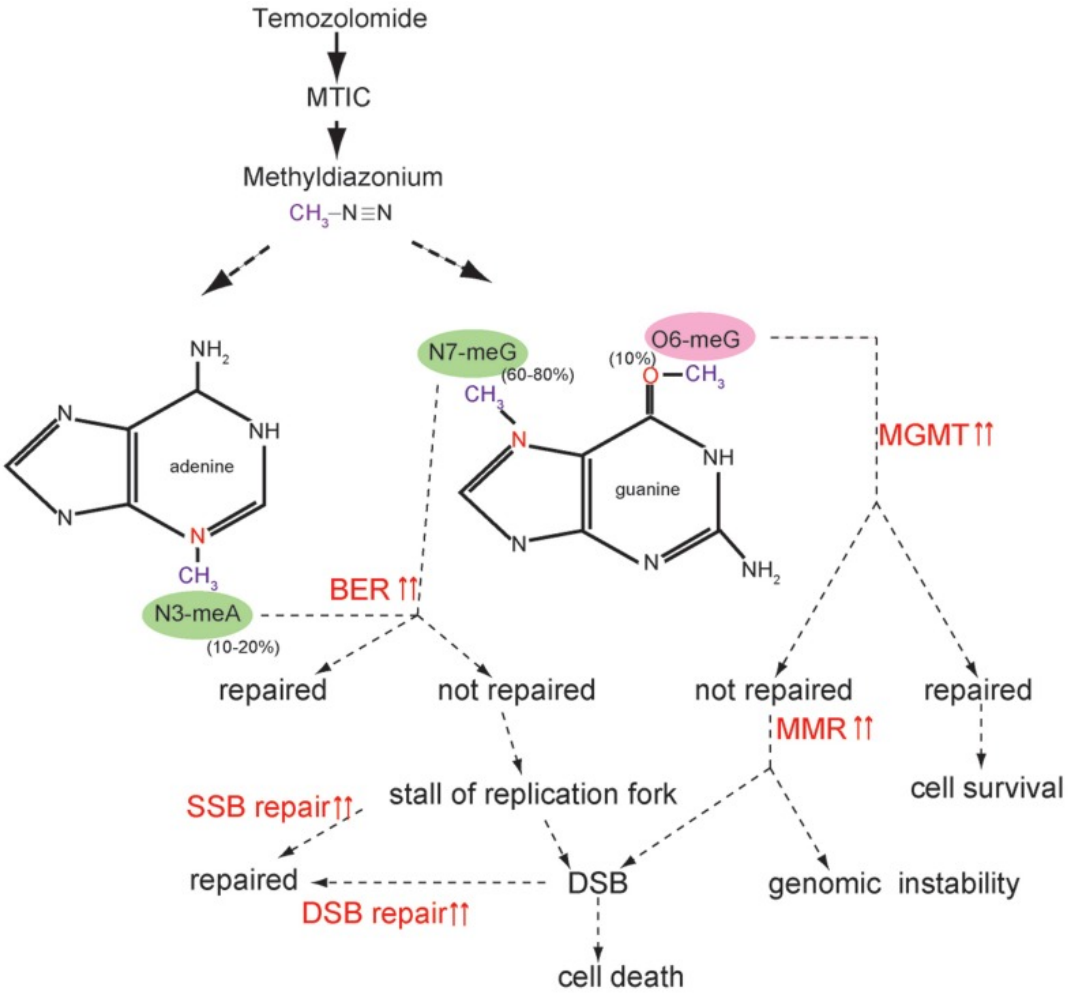

FIGURE 1.10: Mechanisms of TMZ cytotoxicity and activated DNA repair pathways. Extract from Yoshimoto et al., 2012.

cytotoxicity of TMZ by O6-meG.

Despite the treatment's promise, the use of TMZ as an oral chemotherapy agent has certain limitations. Unfortunately, more than 50% of GBM patients treated with TMZ do not respond to therapy (Lee, 2016; Singh et al., 2020). In addition, some patients subsequently suffer from recurrences or their tumor continues to grow. This represents treatment failure that is commonly associated with the phenomenon known as drug resistance, which is a major problem with TMZ treatment. This phenomenon has been linked to the expression of O6-methylguanine-DNA methyltransferase, but the mismatch repair system (MMR) and the presence of cancer stem-like cells in tumors have also been related to TMZ resistance. Each mechanism will be presented in more detail in the next section.

1.6.4 Development of temozolomide resistance

MGMT Can Repair TMZ-Induced DNA Alkylation

MGMT (O^6-methylguanine-DNA methyltransferase) is often considered as a prominent contributor to TMZ resistance due to its direct role in counteracting DNA alkylation damage (Chen et al., 2018; Singh et al., 2020). The MGMT gene encodes a DNA damage repair protein that helps maintain genomic stability through mismatch repair. Under TMZ treatment, MGMT can remove the methyl group in O^6-methylguanine thereby neutralizing the TMZ-induced DNA damage and reducing the overall efficacy of the drug (Singh et al., 2020). MGMT is normally found in large quantities in the liver and is expressed in small quantities in the brain (Verbeek et al., 2008). In tumors, MGMT exists in high concentrations in breast, ovarian and lung cancers, whereas it is not very active in pancreatic cancers or malignant melanomas. In the case of gliomas, there is a wide variability, however there is a very strong correlation between its expression and resistance to alkylating agents. With regard to GBM, the link between protein expression and resistance has not been clearly established. The only commonly accepted correlation is that of the methylation of the MGMT promoter with the response to TMZ, which makes it the first predictive marker of response to chemotherapy with alkylating agents (Karayan-Tapon et al., 2009).
MGMT gene inactivation is a common epigenetic event in tumorigenesis. Epigenetic methylation is carried out on cytosines located in CpG islands thanks to DNMTs (DNA methyltransferases). The hypermethylation of the CpG islands of the MGMT promoter inhibits the binding of transcription factors and allows the silencing of the gene. Between 45 and 70% of patients newly diagnosed with GBM show MGMT methylation (Salvati et al., 2020). This methylation is associated with a significant survival benefit after TMZ treatment and radiotherapy compared to radiotherapy alone. However, the analysis of MGMT expression in gliomas by immunocytochemistry or by enzyme activity test gives contradictory results. The heterogeneity of glioma biopsies is yet another complicating factor. It is possible that MGMT promoter methylation is only a marker of a more general epigenetic dysregulation suggesting that other genes may be more relevant to clinical outcome.

DNA mismatch repair (MMR) system and temozolomide resistance

Mismatch repair (MMR) is a DNA repair mechanism that works by correcting mismatched nucleotide base pairings; this process takes place during DNA synthesis and is fundamental in the cytotoxicity induced by O^6-MeG.
The MMR system is composed of several subunits that join to form heterodimers. In the absence of MGMT, O6-MeG pairs with thymine. Recognition of O6-MeG-T mismatches by the MutSα subunit (which is composed of MSH2 and MSH6 subunits) of the MMR pathway is a crucial step for the initiation of programmed death in response to alkylation damage. Indeed, the activation of the MSH2/MSH6 dimer leads to a deletion/insertion loop which ultimately produces double-strand breaks and triggers apoptosis. MMR status therefore influences the response to genotoxins and TMZ-induced cytotoxicity depends on a functional MMR. Mutations of MSH6 are frequently found in recurrent GBMs having been treated with TMZ in the first line (Yip et al., 2009). In cells mutated for MSH6 the O6-MeG are not recognized. Where the absence of MGMT sensitizes the cells, the loss of a functional MMR allows the cell to tolerate damage and continue in its cycle. Therefore, if the MMR system is mutated or inactivated, TMZ tolerance increases in GBMs because the erroneous O6-MeG:T pairs may not be recognized, leading to continued DNA replication and resistance to TMZ treatment (Johannessen, Bjerkvig, and Tysnes, 2008; Messaoudi, Clavreul, and Lagarce, 2015; Thomas et al., 2017).

The role of glioma stem cells in temozolomide resistance

Tumors are known to contain a relatively small subpopulation of cancer cells with stem-like properties, called cancer stem cell or CSCs (Shackleton et al., 2009). Indeed, these cells divide slowly and are capable *in vivo* of remaining within tumors in a quiescent state, a state which protects them from molecules used in chemotherapy such as TMZ. Thanks to this property, they can spread again, leading to tumor relapse. In addition, these cells preferentially express efflux pumps on their surface, in particular ATP binding cassette (ABC) transporters, which will continuously expel antitumor drugs out into the extracellular environment. These cells then become impermeable to the molecules used in chemotherapy (Frank et al., 2005). On the other hand, they are able to protect themselves from the pro-apoptotic effects caused by chemotherapy by secreting specific proteins, in particular the proinflammatory cytokine IL-4 as in the case of colon cancer (Todaro et al., 2007).
CSCs have been isolated in various solid tumors including breast, prostate, colon, brain, pancreas, lung, liver, bladder, ovary and others (Visvader and Lindeman, 2012; Kreso and Dick, 2014). While the criteria for defining GSCs are still evolving, the most widely accepted and used GSC markers include CD133, CD44, CD15, CD70, S100A4, ALDH1A3, Nanog, SOX-2, and Nestin (Mesrati et al., 2020). Several *in vitro* studies have suggested that cells containing CSC markers are more resistant to TMZ exposure (Llaguno et al., 2009; Chen et al., 2012)

Despite the fact that TMZ was discovered more than three decades ago, it is a drug that

will be present not only for the treatment of GBM but also for the treatment of a large number of tumor pathologies. However, there are serious drawbacks, mostly related to inherent and acquired resistance, which may contribute to the poor prognosis. Therefore, there is an urgent need for novel therapeutic strategies that enhance the benefits of TMZ.

1.7 Manipulating tumor acidification as a cancer treatment strategy

According to drug responsiveness, drug resistance can be categorized as intrinsic or acquired resistance. Intrinsic drug resistance may be defined as the pre-existence of resistance mechanisms before therapy is initiated, whereas acquired resistance develops after initial therapy (Holohan et al., 2013; Ji et al., 2019). However, metabolic alterations in the tumor microenvironment develop in both intrinsic and acquired resistances, thus playing a key role in regulating the biological mechanisms that lead to the decreased drug sensitivity of cancer cells (Mahoney et al., 2003; Mccarty and Whitaker, 2010).

Advanced stages of cancer are associated with increased levels of glucose uptake and extracellular acidification of tumor microenvironment. As a reminder, it is recognized that extracellular acidity is a consequence of poor blood perfusion, low oxygen availability and cellular energy metabolism. The tumor cells predominantly rely on increased glycolysis and lactic fermentation, resulting in a higher production of hydrogen ions and lactate. To prevent intracellular acidification, cells secrete H^+ ions and lactate into the extracellular space, and due to decreased blood perfusion, the extracellular medium will be acidified (Smallbone et al., 2005; Chiche, Brahimi-Horn, and Pouysségur, 2010; Justus, Dong, and Yang, 2013; Parks, Cormerais, and Pouysségur, 2017). Today, acidic extracellular pH is considered a new hallmark of cancer (Andreucci et al., 2020; Piasentin, Milotti, and Chignola, 2020; Pérez-Herrero and Fernández-Medarde, 2021; Audero, Prevarskaya, and Pla, 2022) and, is a major feature of the malignant solid tumor microenvironment (Smallbone et al., 2005; Zhou, Liotta, and Petricoin, 2015).

Acidosis of the tumor microenvironment leads to a selection of cancer cells with a stem cell phenotype, with a greater invasive and metastatic potentials, and failure with treatment strategies involving chemotherapy (Smallbone et al., 2005; Moellering et al., 2008; Fang, Gillies, and Gatenby, 2008; Estrella et al., 2013; Pillai et al., 2019). The association between extracellular acidity and increased chemotherapeutic resistance has been reported in previous *in vitro* and *in vivo* studies on human melanoma (Fernández, 1983), osteosarcoma (Avnet et al., 2016), prostate carcinoma (Thews et al., 2006), colon (Cheng and To, 2012, breast (Fan et al., 2012) and human oral squamous cell carcinoma (Visioli et al., 2014). Therefore, the following paragraph is devoted to a literature review in order to elucidate the biological mechanisms underlying acidosis-induced chemotherapy resistance (Table 1.3 and Table 1.4). It should be noted that no study combining extracellular acidity and chemotherapeutic resistance has been reported on glioma.

1.8 Extracellular acidity and chemoresistance

ABC transporters, also known as primary active transporters, are a wide family of proteins involved in the transport of hydrophobic compounds against their concentration gradients, from a wide variety of substrates, including peptides, lipids, and chemotherapeutic agents (Tarling, Aguiar Vallim, and Edwards, 2013; Gillet and Remacle, n.d.). ABC transporters use the energy provided by the hydrolysis of ATP at the level of NBD domains (nucleotide binding domain) to function. Genes encoding ABC transporters are grouped into subfamilies according to their domain organization and amino acid homology. In humans, seven subfamilies have been identified (ABCA to ABCG).
Cheng and To, 2012 assessed *in vitro* the regulation of ABCG2 transporter in human colon carcinoma, HCT-116, and S1 and its resistant S1M1-80 cell lines overexpressing ABCG2, in response to acidic pH. The data revealed increased regulation of ABCG2 gene transcription, with the exception of the S1 cell line, under extracellular acidity, and increased resistance to the drugs cisplatin (CIS) and mitoxantrone (Cheng and To, 2012).

Federici et al., 2014 et al have investigated the role of both extracellular acidosis and exosome release in resistance of different malignant cell lines (human breast cancer, human metastatic melanoma and human colon carcinoma) to cisplatin. They demonstrated that tumor cell lines exhibited different sensitivity to the cisplatin and that the acid culture condition reduced sensitivity to cisplatin in all tumor cell lines tested compared to the same cells cultured at neutral pH. In addition, the results showed that acidic pH increased exosome release by tumor cells with a higher accumulation of cisplatin, which may be one of the mechanisms by which cells protect themselves by expelling the drug. Melanoma cells pre-treatment with lansoprazole, a proton pump inhibitor (PPI), induced a 50% reduction of the amount of cisplatin present in the exosomes purified from the cell culture supernatant, as compared to the exosome purified from supernatant of cell cultures that were not treated with lansoprazole. This supported the hypothesis that pretreatment with a proton pump inhibitor may lead to both exosome release inhibition and an increased drug retention by tumor cells (Federici et al., 2014).
The most important human ABC transporter involved in drug disposition is ABCB1 also known as multidrug resistance protein 1 (MDR1) or P-glycoprotein (Pgp) (Genovese et al., 2017). P-glycoprotein prevents cellular uptake of a large number of structurally and functionally diverse compounds by acting as an efflux pump and transporting the chemotherapeutics out of the cell and, in this way causes multidrug resistance (MDR) (Lam et al., 2001; Ponte-Sucre, 2007).
A group of researchers have been working on the impact of extracellular acidity on the activity of Pgp and the cytotoxicity of chemotherapeutic drugs (Thews et al., 2006). They found that exposing prostate carcinoma cells (AT1) to an acidic extracellular environment (pH 6.6) for a period of 3 to 6 hours doubled the activity of Pgp and reduced the cytotoxic efficacy of two chemotherapeutic drugs, daunorubicin (DNR) and cisplatin. In order to assess the cytotoxic activity of the chemotherapeutic drugs, the relative caspase 3 (a proapoptotic protein) activity

normalized with respect to untreated control cells was measured. With cisplatin, caspase 3 activity was significantly reduced by the acidic environment compared to normal pH. However, even though cisplatin-induced caspase 3 activation was markedly reduced in the acidic microenvironment, overall cell death was not significantly different in cells incubated with cisplatin at different pH levels. These results indicate that the cytotoxicity of cisplatin was only marginally affected by the acidic microenvironment. In contrast, DNR induced cell death was markedly reduced by the acidic microenvironment. In order to investigate the underlying mechanisms by which extracellular pH may influence pGP activity, changes in intracellular levels of calcium ions (Ca^{2+}) and protein kinase C (PKC) were measured. It was found that the increased Pgp activity under acidic conditions was related to the decreased intracellular calcium levels and inhibition of PKC. Based on the results of these experiments, the authors concluded that the chemoresistance to chemotherapeutic agents generated by extracellular acidosis may be the result of an increase in Pgp activity which, in turn, is potentially caused by a decrease intracellular calcium concentration and PKC activity (Thews et al., 2006).

Thews et al., 2014 studied the cytotoxicity of three chemotherapeutic drugs, DNR, CIS and docetaxel (DOC) and, their dependence on Pgp activity during acidosis were analyzed. *In vitro* and *in vivo* experiments were performed using the same treatments and the same cell lines as in their previous study. Under acidic (pH 6.6) conditions, they observed a decrease in cytotoxicity of DNR or DOC whereas cisplatin-induced cell death was almost pH-independent. The Pgp inhibitor (verapamil) reversed the acidosis-induced chemoresistance against DNR and DOC. The cytotoxicity *in vivo* was assessed by forcing glycolytic metabolism "acidosis treatment") in the tumor tissue. *In vivo* results confirmed that induction of acidity in animals reduced the cytotoxicity of DNR and DOC, whereas the cytotoxicity of CIS remained almost independent from the tumor pH. Thus, it was suggested that when there are clinical indications for DAU and DOC treatment, the Pgp-mediated chemoresistance can be counteracted by inhibition of the drug transporter (Thews et al., 2014).

In an acidic microenvironment, combined chemotherapy and proton pump inhibitors have been shown to increase the sensitivity of cancer cells to treatment. Avnet et al., 2016 injected osteosarcoma cells into immunodeficient mice (NOD/SCID animals) and treated them with the chemotherapeutic drug DOX and omeprazole, a proton pump inhibitor targeting lysosomal acidity. Exposing to an acidic pH_e significantly increased the number and acidity of lysosomes, and the combination of DOX with omeprazole significantly enhanced DOX cytotoxicity. In addition, the results of this study demonstrated that mice treated with the combination of DOX and omeprazole showed a higher necrotic index, smaller tumor volumes and less body weight loss compared to the groups treated with DOX alone. Therefore, it can be inferred that proton pump inhibitor drugs may offer novel solutions to overcome drug resistance.

The role of V-ATPase in the efficacy of chemotherapy treatment has been evaluated in breast cancer. Fan et al., 2012 observed that LASS2 (Homo sapiens longevity assurance homolog 2 of yeast LAG1) is able to enhance breast cancer chemosensitivity by counteracting the acidic

tumor microenvironment by inhibiting proton pump V-ATPase activity. Low expression of LASS2 was associated with poor prognosis in breast tumors. The results showed that the overexpression of LASS2 in MCF-7/ADR breast cancer cells increased the effect of several chemotherapeutic agents (DOX, CIS, and 5-fluorouracil (5-FU)). In these cells, they detected that LASS2 inhibited the function of V-ATPase by binding to its C-subunit. This effect was mediated by a significant increase in pH_e and lysosomal pH, and DOX that was previously sequestered in the cytosol was released in the nuclei of cells, inducing increased rates of apoptosis. These results suggest that LASS2 is involved in chemotherapeutic outcomes and that low expression of LASS2 may predict drug resistance.

Visioli et al., 2014 investigated the effect of acidic pH stress on tumor-associated endothelial cells (TECs) and found that the mechanisms underlying cell adaptation and resistance to antiangiogenic chemotherapeutic agents may depend on the activation of the unfolded protein response (UPR). Primary human dermal microvascular endothelial cells (HDMECs) cultured in acidic conditioned medium showed increased expression of the UPR marker (Grp78, glucose-regulated protein 78) and concomitantly greater resistance to cytotoxicity induced by the drug Sunitinib. Inhibition of GRP78 resensitizes HDMECs to drug treatment. Therefore, this work suggested that UPR induction in endothelial cells under acidic pH conditions may results in therapeutic failures in response to chemotherapy. Targeting Grp78, the key component of the UPR pathway, may provide a promising alternative in cancer treatment.

3D tumor spheroids have also found application in assessing tumor resistance, since they reproduce the tumor microenvironment conditions in a more accurate way and provide more physiologically relevant information and more predictive data for *in vivo* tests. Mellor and Callaghan, 2011 used such a model to evaluate chemoresistance in colorectal adenocarcinoma cells (DLD-1), colon adenocarcinoma cells (HT29) and ovarian adenocarcinoma cells (NCI^{ADR}). The accumulation and distribution of doxorubicin (DOX), a chemotherapeutic drug, were measured in tumor spheroids. DOX is fluorescent, and thus allows detection by confocal microscopy. Tumor spheroids demonstrated a high level of DOX in cells on the tissue surface. An inner ring, only in the DLD-1 and HT29 cell lines, consistent with the hypoxic zone, was almost completely devoid of DOX staining, reflecting poor intracellular accumulation in this zone. In addition, the authors of this study observed that the pH was acidic (6.9–7.0) in all the cell lines exposed to hypoxia. The influence of Pgp on doxorubicin accumulation was examined under hypoxic conditions in TS comprising all three cell types. The inibition of Pgp by the modulator Tariquidar (XR9576) increased the accumulation of DOX in all the three cell lines evaluated. The study concluded that exposure of 3D tumor spheroids to hypoxia generates an acidic microenvironment; this leads to increased expression of drug transporters and, therefore, a decrease in DOX-induced cytotoxicity (Mellor and Callaghan, 2011).

For a better understanding of the biological mechanisms governing acidity-induced resistance to chemotherapeutics, more comprehensive studies exploring these mechanisms are needed.

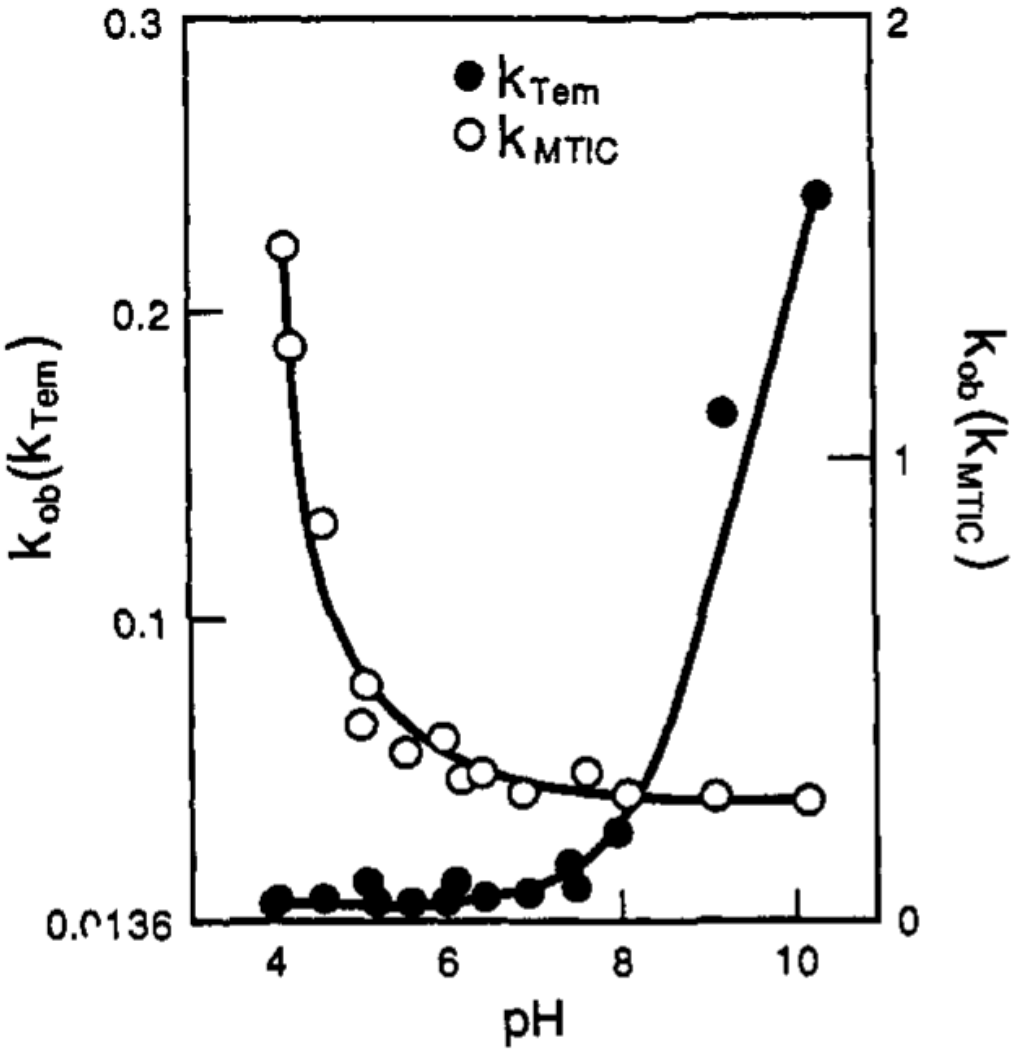

FIGURE 1.11: Graph representing the stability constant (k_{ob}) as a function of the pH of Temozolomide (TMZ) and of MTIC. Extract from Denny et al., 1994.

These studies are required to provide guidance to future cancer treatment and achieve better outcomes. However, given the above, it is clear that for the success of cancer treatment, the pH of the tumor microenvironment is a critical criterion.

In fact, both TMZ and MTIC degradation rates are highly pH-dependent as they exponentially increase and decrease with pH values, respectively (Figure 1.11). There is therefore only a small range of pH allowing the hydrolysis of TMZ into MTIC and then into the alkylating group of DNA (Denny et al., 1994). As tumor cells exhibit different regulation of intracellular and extracellular pH, this can influence the efficiency of TMZ, although this has not been studied experimentally up to our knowledge. Indeed, it's necessary to investigate the optimal pH values, that affect the successive stages of TMZ transformation into its active compound. The realization of which allows to increase TMZ exposure benefit both in terms of efficacy and tolerability.

Stéphanou and Ballesta, 2019 have designed a complete theoretical framework to study the antitumor efficacy of TMZ, integrating the effect of pH_e, the spatial configuration of the tumor and the microenvironment. Based on the relationship between pH_e and pH_i for a given cell type, it provides quantitative predictions regarding the differential impact of TMZ on cancer cells and optimal pH values leading to greater amount of DNA damage. Therefore, by experimentally characterizing the cell ability to regulate its pH_i as a function of pH_e, the model highlights potential ways for improving the efficacy of TMZ on tumor cells.
In this context and as part of the thesis, I experimentally characterized the regulation of pH_i, as a function of pH_e, of two glioma cell lines and determined the optimal pH for the efficacy of TMZ on both cell lines. The results has allowed us to show that drug efficiency depend on the cell type and the pH_e, which gives an argument for considering pH as a personalized therapeutic target for future research based on the combination of TMZ with pH-regulating agents.

Author and year	Type of cell studied	Cell model	pH_i measurement	aim of the study	Main results
Michaelis and Davidoff (1912)(For a review see Caldwell, 1956)	Blood/Red blood cells	*in vitro*	Platinum/hydrogen electrode	Blood pH measurement	The red cell lysis caused a change in bulk pH
Lagadic-Gossmann, Chesnais, and Feuvray, 1988	Papillary muscle cells of streptozotocin-induced diabetic rats	*in vivo*	pH-sensitive microelectrode	Investigate the regulation of pH_i following an intracellular acid or alkaline loading in diabetic rats	The results show differences between diabetic and normal muscles in the regulation of pH_i in response to induced acidity, suggesting that diabetes is associated with a change in the activity of the Na^+/H^+ exchange (Moore, 1983), a major way for the export of H^+ ions from cells during acidity
Ellis and Thomas, 1976	mammalian cardiac cells	*in vivo*	pH-sensitive microelectrode	Study the effect of CO_2 on the pH$-i$ of Purkinje fiber cells cut from sheep ventricles	The pH_i was strongly influenced by CO_2 in the equilibration gas. The mean pH_i in the presence of CO_2 is close to 7.02 and is significantly lower than when CO_2 is absent
Hemptinne, 1980	mammalian cardiac cells	*in vivo*	Double-barreled pH microelectrode	pH_i measurement of Purkinje fiber cells	The results show that the pH_i varies between 7.1 and 7.2 which is, however, significantly greater than that reported by Ellis and Thomas, 1976. It has been reported that this difference is probably due to the different HCO_3^- concentration in the control solution, compared to that used in the Ellis and Thomas publication
Hagberg, Larsson, and Haljamae, 1983	Rabbit skeletal muscle fibers	*in vivo*	Double-barreled pH microelectrode	pH_i measurement in rabbit skeletal muscle fibers	A mean pH_i of 7.00 (in 8 animals) was obtained

TABLE 1.1: Intracellular pH, techniques and aim of its measurement.

Author and year	Type of cell studied	Cell model	pH_i measurement	aim of the study	Main results
Clarke1993	Isolated rat heart	*in vitro*	^{31}P NMR spectroscopy	Measurement of cardiac pH during ischemia and reperfusion	In the pre-ischemic rat heart, the pH_i was approximately 7.15. After 4 min of ischemia, the pH_i decreased to approximately 6.16. On reperfusion, pH_i returned to pre-ischemic levels within 2.5 min
Adam, Koretsky, and Weiner, 1985	Rat kidneys	*in vitro*	^{31}P NMR spectroscopy	Measurement of intrarenal pH in perfused rat kidneys an acidification, from pH 7.4 to pH 6.9, was induced by addition of hydrochloric acid (HCl) to the perfusion medium	Kidney pH fell from 7.20 to 6.75, and reached a plateau of pH 6.85, 30 min after addition of HCl. In parallel, it was found that the rate of ammonia (NH3) production at 7.4 was doubled when the perfusate was acidified to pH 6.9
Waddell and Butler, 1959	Skeletal muscle	*in vitro*	Weak acid (DMO)	Measurement of dog skeletal muscle pH_i using DMO weak acid. The effects of various treatments altering the pH or the pCO_2 of plasma were studied	The calculated pH_i values of normal, resting muscle were all in the range of 6.96 to 7.10 with an average of 7.04. The greatest changes in muscle pH_i are those produced by increasing blood carbon dioxide tension
Gores et al., 1989	Rat hepatocytes	*in vitro*	BCECF-AM	pH_i measurement in cultured rat hepatocytes after ATP depletion by metabolic inhibition with KCN (potassium cyanide) and iodoacetate acid (IAA)(chemical hypoxia)	Exposure of hepatocytes to acidic pH_e simultaneously with KCN and IAA produced a slightly greater drop in pH_i, prolonged the plateau phase of intracellular acidosis and delayed the onset of cell death. Inhibition of Na^+/H^+ exchange with amiloride also produced an increase of cell survival and prolongation of the plateau phase of intracellular acidosis

TABLE 1.2: Intracellular pH, techniques and aim of its measurement.

Author and year	Type of cancer studied	Cell model	pH assessed	Drug tested	Mechanisms evaluated	Main results
Mellor and Callaghan, 2011	colorectal adenocarcinoma (DLD-1), colon adenocarcinoma (HT29) and ovarian adenocarcinoma (NCI^{ADR})	*in vitro*	6.9–7.0 and 7.2–7.3	Doxorubicin (DOX)	Growth of tumor spheroids in normoxia and hypoxia, intracellular accumulation of DOX, and inhibition of Pgp by tariquidar (XR9576)	The distribution and accumulation of DOX were heterogeneous in all cell lines evaluated. The acidity generated by hypoxia decreased the accumulation of DOX in tumor spheroid. The inibition of Pgp by tariquidar (XR9576) increased the accumulation of DOX in tumor spheroids
Avnet et al., 2016	Osteosarcoma	*in vivo*	6.5 and 7.4	DOX	Combined treatment of DOX and omeprazole (a proton pump inhibitor targeting lysosomal acidity)	The combined treatment of DOX with omeprazole showed a higher necrotic areas, smaller tumor volumes and less body weight loss
Fan et al., 2012	Breast cancer (MCF-7/ADR)	*in vitro* and *in vivo*	DOX, CIS, and 5-fluorouracil (5-FU)	Acid pH (unknown value)	Induction of LASS2 expression	The overexpression of LASS2 in MCF-7/ADR breast cancer cells increased the effect of several chemotherapeutic agents. LASS2 inhibited the function of V-ATPase. More Dox entered the cells and stayed in the nuclei of cells, inducing increased rates of apoptosis
Visioli et al., 2014	Endothelial cells from human oral squamous cell carcinomas (OSCC)	*in vitro*	Sunitinib	pH 6.0–6.4	Activation of UPR: quantification of Grp78 in endothelial cells and cytotoxicity using SRB	Extracellular acidity increased expression of the UPR marker (Grp78) and its inhibition reversed the drug sensitivity to Sunitinib

TABLE 1.3: Literature review to elucidate the biological mechanisms underlying acidosis-induced chemotherapy resistance.

Author and year	Type of cancer studied	Cell model	Drug tested	pH assessed	Mechanisms evaluated	Main results
Cheng and To, 2012	Human colon carcinoma HCT-116, and S1 and its ABCG2-overexpressing resistant S1M1-80 cell lines	*in vitro*	Cisplatin (CIS) and mitoxantrone	5.00	Regulation of ABCG2 under adverse conditions within the tumor microenvironmen (Hypoxia, glucose deprivation and acidosis)	Glucose depletion, decreased extracellular pH and hypoxia can all upregulate ABCG2 transcript level and apparently leading to multidrug resistance. Acidic pH did not significantly alter the level of ABCG2 in S1 cells
Federici et al., 2014	MCF7 (human breast cancer), Me30966 and Me501 (human metastatic melanoma), and SW480 (human colon carcinoma) cell lines	both *in vitro* and *in vivo* experiments	CIS	Experiments were performed in acidic (pH 6.0–5.0), buffered (pH 7.4) and unbuffered media	Cisplatin cellular resistance and effects of proton pump inhibitor (lansoprazole) on cisplatin tumor uptake	Treatment with lansoprazole increased the intracellular absorption of cisplatin and reduced the amount of cisplatin present in the exosomes
Thews et al., 2006	Rat prostate cancer (AT1)	*in vitro*	Daunorubicin (DNR) and CIS	6.6 and 7.4	Caspase 3 Activity and Cell Toxicity Assay	Exposure to acidic extracellular environment doubled Pgp activity and reduced cytotoxic efficacy of CIS and DNR
Thews et al., 2014	Rat prostate cancer (AT1)	*in vitro* and *in vivo*	DNR, CIS, and docetaxel (DOC)	6.6 and 7.4	Measurement of apoptosis induction (caspase 3) and cell survival	Acidity reduced the cytotoxicity of DAU, CIS, and DOC. The Pgp inhibitor (verapamil) reversed the acidosis-induced chemoresistance against DNR and DOC

TABLE 1.4: Literature review to elucidate the biological mechanisms underlying acidosis-induced chemotherapy resistance.

Chapter 2

Materials and methods

2.1 The cell models

2.1.1 Experimental tumor model

Although less close to medicine and the human patient, *in vitro* studies are particularly important. They are often the first step in testing for new treatment protocols. *In vitro* experiments are also excellent sources of data and information on the microscopic behavior of the phenomena studied. Not having the technical and practical limitations of *in vivo* approaches, they also make it possible to compare a theoretical model of a microscopic phenomenon with a particularly large amount of data, which makes it possible to validate a more robust model and, also to potentially easily test a prediction that a model could produce with a new experiment. *In vitro* experiments can also be a step in *in vivo* experiments. For example, the implantation of a micro-tumor formed *in vitro* in a small animal (*in vivo*) makes it possible to evaluate, in a more reproducible way, the development of a tumor and the effect on it of new treatments. *In vitro* studies can also produce larger statistics compared to *in vivo* studies. Despite these advantages, *in vitro* studies cannot reproduce all the conditions encountered *in vivo*, for example blood circulation or the presence of the immune system. These limitations imply that *in vitro* results should not be transposed too quickly to *in vivo* cases (Lenting et al., 2017).

Tissue, organ or cell culture techniques in nutrient media outside the body are part of *in vitro* models. These cultures may have special environmental conditions close to those *in vivo*. One can distinguish classic cell cultures such as 2D models or more sophisticated three-dimensional 3D cultures with the characteristics of organs or tissues *in vivo*. Several types of in vitro cell cultures can be distinguished: primary cells and cell lines. The use of primary cell cultures is limited by their availability, repeatability, and use in long-term studies due to their limited lifespan, but transformed cell lines are widely used. The different glioma cell lines that I used in this thesis are presented below.

The U87-MG model

The first cell line used during the experiments is U-87 MG from the American Type Culture Collection (ATCC). This is one of the first cell lines established from a human glioblastoma in the 1960s (Pontén and Macintyre, 1968). This line was established from an astroctoma

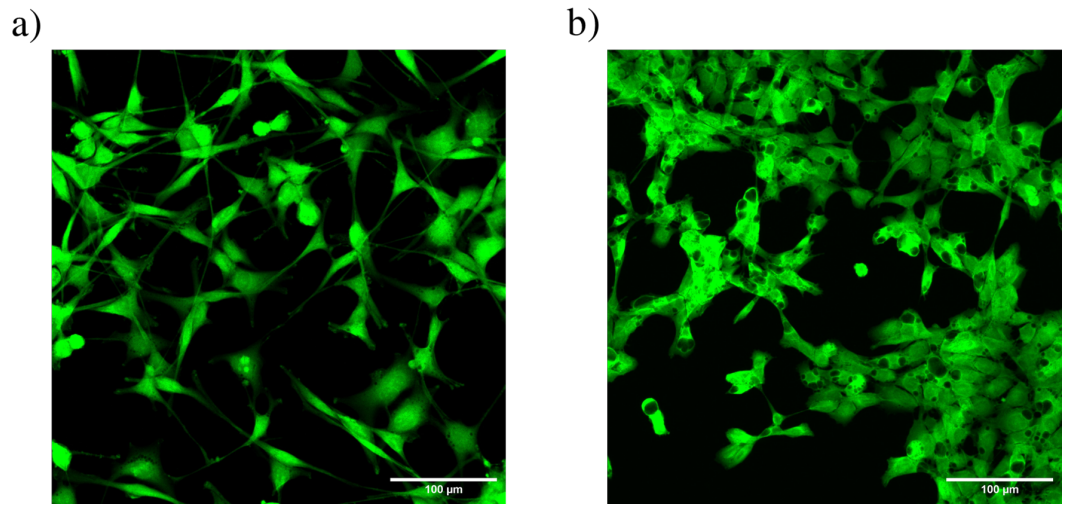

FIGURE 2.1: Confocal fluorescence images recorded after loading cells with the BCECF pH-probe using an excitation wavelength of 488 nm. a) U87-MG cells b) F98 cells. scale bar: 100μm. 2048×2048 pixels

line showing areas of necrosis. These cells have been described as having an atypical morphology: often polynuclear with very fine membrane extensions, hence the name MG for "malignant glial" (Figure 2.1, a)). U87-MG cells have a mean doubling time of 30.8 ± 2.5 h (Oraiopoulou et al., 2017), which is the slowest division between the cell types we use. Additional lines were subsequently developed based on the MGs. The U87-MG belong to the U- series established at Uppsala University. This line has a rapid proliferation and the sequencing of its genome revealed good stability despite wide use for more than 40 years (Clarke, Butowski, and Chang, 2010).

Since the 1960s, animal models of human brain tumors have been a real challenge in experimental neuro-oncology. Although there is no model that perfectly simulates the behavior of high-grade human gliomas, rodent models still allow the development of innovative therapeutic strategies. Ideally, valid brain tumor models should be derived from glial cells, grow predictably and reproducibly *in vitro* and *in vivo*, be weakly or ideally not at all immunogenic, have growth and response to therapies that resemble those human glioma cells (Barth, 1998). Hence the F98 cell model presented in the next section.

The F98 model

Initially, the F98 tumor model was created by Wechsler (in Dr. Koestner's laboratory; Ohio State University) by intravenously injecting a single dose of nitrosurea (N-ethylN nitrosourea) into a pregnant Fischer rat. This induced on the litter, spontaneous tumors which were isolated and classified into various cell lines, including the F98 glioma. Its in vivo histopathological analysis allowed it to be classified as an anaplastic or undifferentiated glioma (Ko, Koestner, and Wechsler, 1980; Barth, 1998). This very aggressive F98 model grows invasively from

the start of its development. It is also weakly immunogenic[1], which brings it closer to human gliomas.
It is reported in the literature that other types of tumors, notably C6 and 9L gliosarcomas which are immunogenic, are not good models for studies on immunocompetent rats if the objective is to prolong and measure animal survival. In fact, during certain studies it was observed that the C6 and 9L models could trigger a specific immune response and regress spontaneously (Barth, 1998; Barth, Yang, and Coderre, 2003). With the F98 glioma model, the injection of a hundred tumor cells is enough to cause the death of 100% of untreated rats (Barth et al., 2000). Thus, an increase in the median or mean survival of the animals can only be attributed to the treatment tested.
The cell line used in the laboratory comes from ATCC. The cells are predominantly spindle-shaped (Figure 2.1, b)) and have an in vitro doubling time of approximately 18 hours (Mathews et al., 2012).

The development of tumor spheroid experiments

Due to their spatial structure, spheroid cultures constitute an intermediate biological model between 2D cell cultures, in culture flasks, and animal models. Spheroid experiments make it possible to realistically reproduce the growth of a tumor at the avascular stage and in particular the heterogeneity observed within a tumor (Hirschhaeuser et al., 2010). Indeed, some mechanisms present in tissues are not expressed in 2D cell cultures (Pampaloni, Reynaud, and Stelzer, 2007). For example, in the case of experiments with permanent supply of nutrients and oxygen, the growth of 2D cell cultures is exponential and unlimited while for spheroids, the limitation of the supply of nutrients and oxygen, due to the diffusion inside the spheroids, makes it possible to observe a natural saturation of their growth (Folkman and Hochberg, 1973). This limitation of growth is only possible by the appearance of a crown of proliferating cells on the surface as well as cells in a quiescent phase, or even a necrotic core, in the center of the spheroid. Spheroid experiments thus make it possible to simulate changes in the microenvironment of a tumor during the early stages of its growth, as well as the appearance of new phenotypes, such as the appearance of quiescent cells or necrosis following the limited diffusion of nutrients and oxygen in the center of the spheroid (Freyer and Sutherland, 1985; Sutherland, 1988).
Based on these advantages, I developed during the thesis an *in vitro* platform optimizing the 3D glioma model (spheroid) and the required analysis tools. This allows us, using this platform, to assess the capacity of glioma cells to regulate their intracellular acidity and therefore to optimize the efficacy of glioblastoma treatment by TMZ.
Therefore, GFP (green fluorescent protein) spheroid cultures were plated at density of 1000 cells/well (Day0) and allowed to grow for a total of 27 days (Figure 2.2). This growth was monitored by confocal imaging by taking each day of experience a Z-stack image for each spheroid. Starting from one pole of each spheroid, the excitation is carried out by optical sections along the Z axis (confocal z-stack) through the spheroid with a Z-slice spacing of 5

[1] An element is said to be immunogenic when it is recognized as foreign by the body, i.e. it causes the formation of a specific antibody capable of neutralizing it.

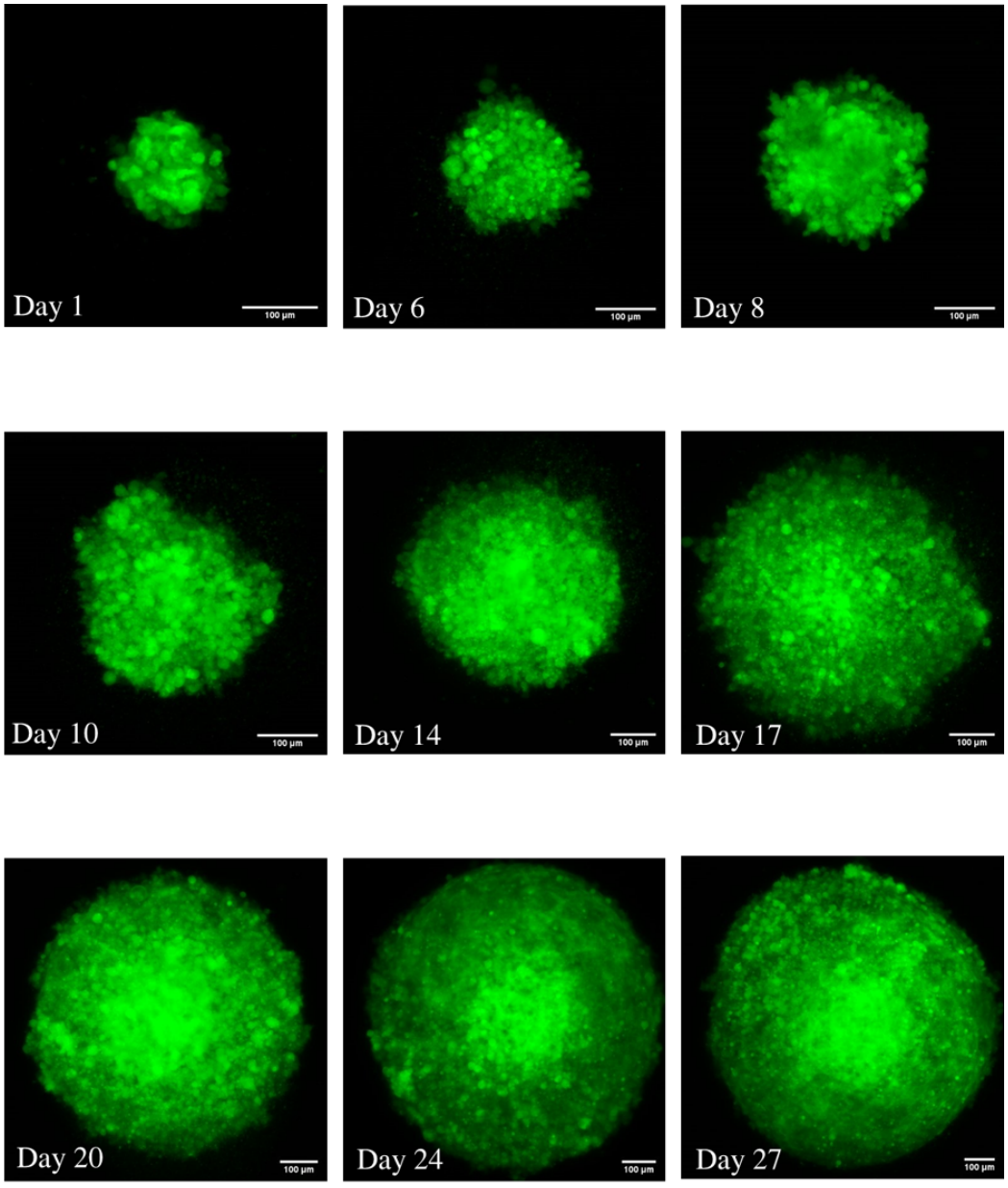

FIGURE 2.2: Suspension 3D cultures. Growth of U87 spheroids over a period of 27 days. Growth was monitored by confocal imaging by taking each day of experience a Z-stack image for each spheroid. Excitation = 488 nm. Scale bar = 100 μm

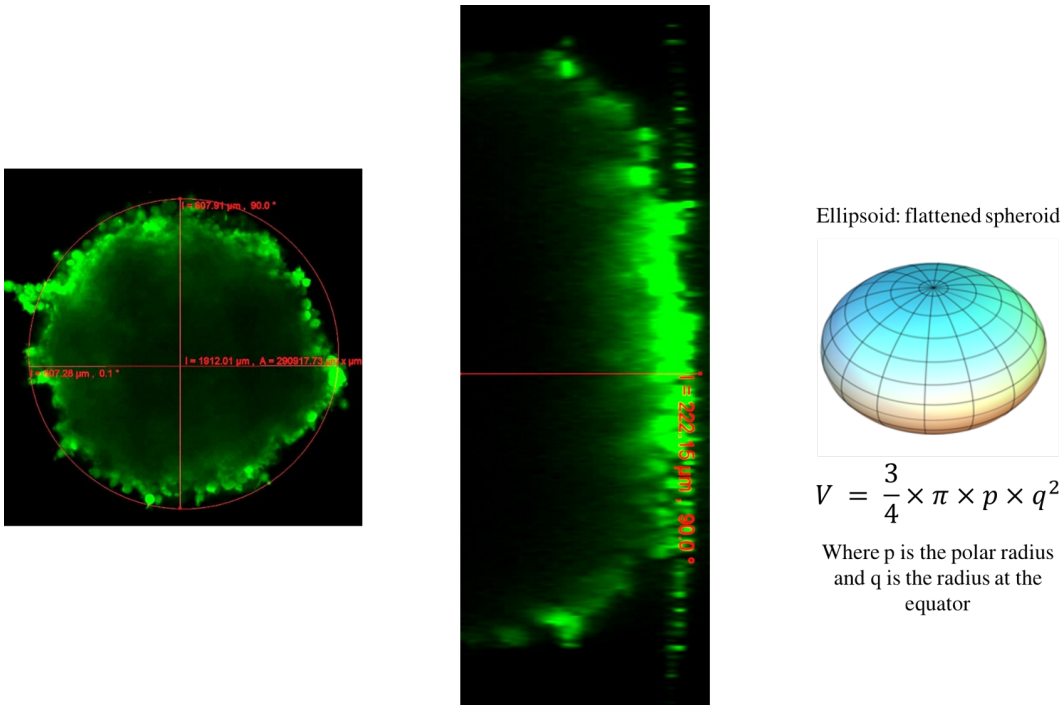

FIGURE 2.3: The method used to predict the volume of spheroids. With imageJ, the maximum depth of penetration (predicted polar radius) as well as the radius at the equator were measured.

μm between adjacent optical planes. The penetration depth of imaging was very restricted, which limits the ability to image the entire spheroid. Therefore, the volume of the spheroids was predicted by measuring by imageJ the maximum depth of penetration (predicted polar radius) as well as the radius at the equator. The predicted volume of the spheroids is therefore given by the following equation:

$$V = \frac{3}{4} \times p \times q^2 \tag{2.1}$$

Where p is the polar radius and q is the radius at the equator (Figure 2.3).

All spheroid cultures demonstrated a significant increase in relative size over the period of imaging (Figure 2.4). U87 spheroids proliferate more slowly than F98 spheroids. Beyond D21, the F98 spheroid has reached the plateau phase, where the spheroid has occupied the entire surface of the well and does not have enough space to proliferate. Until day 27, the U87 spheroids have enough space to grow.

In addition, another plateau phase was observed on the growth curve of F98 spheroids. This phase begins from day 10 to day 17. We hypothesized that this phase could be a form of resting state, or quiescence, in which cells reside until they receive the appropriate signals - for example, growth factors - stimulating them to re-enter and progress through the cell cycle. Previous studies reported that beyond a diameter of 500 μm, most spheroids develop hypoxia leading to a necrotic core surrounded by a viable rim of cells (Kunz-Shughart, Kreutz, and Knuechel, 1998; Hirschhaeuser et al., 2010). Where these conditions prevail, they contribute to a type of cell death, necrosis. Our results are in good agreement with this hypothesis. F98 and U87 spheroids began to develop hypoxia from D9 and D14, respectively. The images on

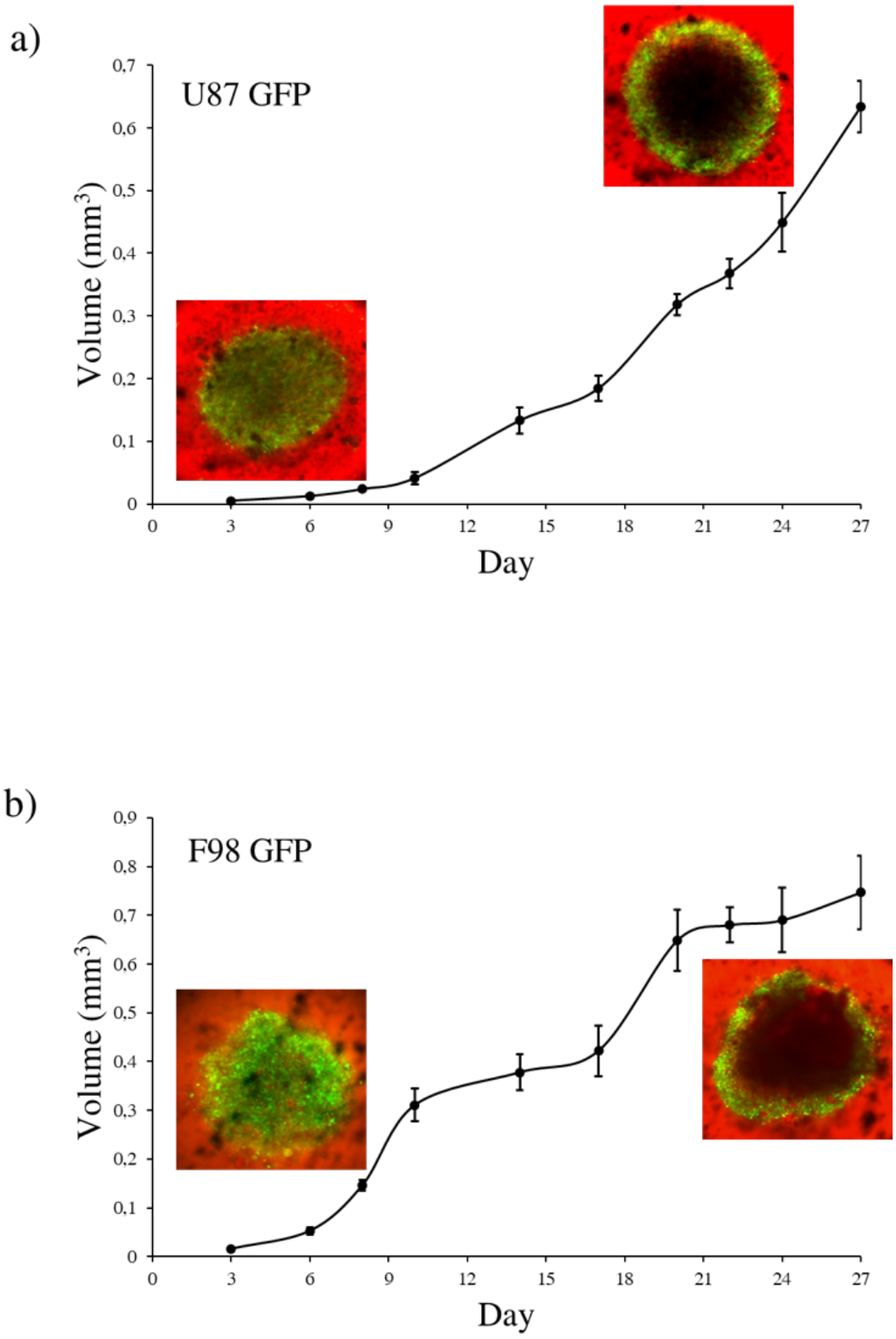

FIGURE 2.4: Tumor spheroid growth. 96-well CELLSTAR® round bottom ultra-low attachment plates were used to generate a) U-87 MG and b) F98 spheroids (a single spheroid per well). Analysis was carried out using ImageJ. Values are means ± SD (n = 5 spheroids/timepoint

the growth charts show the center of the spheroid composed of hypoxic and dead cells, which are not fluorescent (Figure 2.4).
A final remark noted on the images of the spheroids is related to the morphology of the spheroids. The U87 spheroids showed a more compact structure than the F98 spheroid. It has been reported that the compact spheroid formation is associated with contractile behavior and an invasive phenotype (Sodek, Ringuette, and Brown, 2009).

As already stated, spheroids are 3D models closer to the tumor than 2D models of cell cultures, reproducing *in vitro* its organization as well as its microenvironment. It is more suitable for modeling tumors at advanced stages of their growth. These spheroid models were used, within the framework of this thesis, to better understand the response to the treatments used, also making it possible to study the regulation of intracellular pH and the particular modalities of response to drugs in 3D structures.

2.2 Cell culture conditions

Cell culture conditions need to be controlled as well as possible in order to avoid any risk of cell contamination by bacterial or fungal organisms and any risk of cell population drift. For this, the cell culture is carried out in a dedicated room that is as clean as possible. The manipulations are carried out in a sterile manner under a microbiological safety station (PSM), with previously autoclaved equipment and sterile purchased solutions to allow the retention of a large number of bacteria. The absence of antibiotics in the culture medium makes it possible to detect bacterial contamination more quickly and to eliminate cell cultures if necessary. The morphology of the cells as well as some properties such as proliferation are checked regularly in order to ensure the proper maintenance of the cells. Apart from the manipulations, the flasks containing the cells are placed in a controlled atmosphere incubator saturated with humidity at a temperature of 37°C and containing 95% air and 5% carbon dioxide CO_2.

2.3 Cell handling

2.3.1 Trypsinization and subculture

F98 and U87 MG cells are cultured in adhesion in plastic flasks in the presence of a nutrient medium (5 or 10 mL for 25 or 75 cm^2 flasks respectively). The culture medium is composed of DMEM with 4.5% glucose (Dublbecco's Modified Eagle's Minimum medium; Dominique DUTSCHER, Bernolsheim, France), supplemented with 10% fetal bovine serum (FBS, Dominique DUTSCHER) and 2mM glutamine. It will be characterized as "complete medium" in the following. This medium is preheated to 37°C before being brought into contact with the cells. The cells are always incubated in an incubator at 37°C in a humid atmosphere, composed of 95% air and 5% CO_2 and divide in a single layer until confluence. They are subcultured about twice a week: After removing the medium and rinsing the cells with 1x PBS

(Phosphate Buffer Saline, Dominique DUTSCHER), 1 or 3 mL of trypsin are applied to the flasks of 25 or 75 cm^2 respectively (Trypsine -EDTA 0.05%, Sigma-Aldrich, Saint-Quentin Fallavier, France). The trypsin acts for 5 minutes in the incubator then its action is stopped by adding complete medium (same volume as that of the trypsin). The cells are centrifuged (5 minutes, 1500 rpm) and the cell pellet is taken up in complete medium in order to reseed the cells at a lower concentration.
During experiments, cells were seeded at a concentration of 1000 cells/well in 96-well flat ClearLine® plates or in 96-well CELLSTAR® round bottom ultra-low attachment plates for 2D monolayar cultures or 3D spheroid cultures, respectively. The outer wells were not used due to the evaporation edge effect during long term culturing.

2.3.2 Cell freezing

The cells are detached using tripsin (as described above), then the cell pellet is taken up in 1 or 3 mL, for 25 or 75 cm^2 flasks respectively, of medium containing 10% DMSO which is transferred into a cryotube. The cryotubes are then placed in a freezing box, containing isopropanol which allows a slow decrease in cell temperature (1 °C/min), this box is placed in a freezer at –80 °C. The next day, the cryotubes are placed in a Dewar of liquid nitrogen (–196 °C) this process allows long-term storage of the cells.

2.3.3 Cell counting

The different cell culture protocols usually require knowing the number of cells in the suspensions used. There are different ways to perform cell counting, for example directly by counting with a microscope, using a special counting slide (counting chamber or hemacytometers), or by automatic cell counter. In the laboratory we use a handheld automated cell counter (Scepter) as well as two types of hemocytometers which differ by their grid: Malassez chamber (1 rectangle = 0.01 mm^3, 1 band = 0.1 mm^3, the chamber = 1 mm^3) and Thoma chamber (1 rectangle = 0.004 mm^3, the chamber = 0.1 mm^3).

2.3.4 Counting methods for mortality/viability

Countess Automated Cell Counter
The countess automated cell counter is a benchtop automated cell counter that performs cell count and viability measurements using the standard trypan blue stain. It is supplied with disposable countess cell counting chamber slides that contain two enclosed chambers to measure two different samples or perform replicates of the same sample. A drop of trypan blue/cell mixture (10 μL) is applied to the chamber, therefore, the cell counting occurs in the central location of the counting chamber and the volume counted is 0.4 μL, the same as counting four (1 mm × 1 mm) squares in a standard hemocytometer. A single sample measurement within a minute provides the following data:

- Live and dead cell concentration/mL
- Total cell concentration/mL

- Viability (% live cells to total cells)
- Average live and dead cell size
- Cell images
- Graphical data representation

MTT test

Cell viability was studied by a colorimetric technique that evaluates the effects of an external treatment: the tetrazolium salt reduction method or MTT test.

The MTT test is based on the transformation of yellow colored tetrazolium salts (3-(4,5-dimethylthiazol-2-yl)-2,5-diphenyltetrazolium bromide or MTT) into violet crystals of formazan by predominantly mitochondrial succinate dehydrogenase, which is only active in living cells. The crystals insoluble in aqueous solvents are solubilized in DMSO before carrying out a reading by spectrophotometer.The intensity of the color reaction measured at 570 nm or optical density is directly proportional to the number of living cells. In our experiments the MTT test was used to study the effect of TMZ as a function of extracellular pH in order to find the optimal pH for TMZ efficacy. The cells are seeded on D0 in a 96-well plate at the rate of $1*10^4$ cells per well in 200 μL of culture medium. On D3, the cells were incubated 48 hours with TMZ in different extracellular pH for a final volume of 100 μL per well. At the end of the incubation period, 10 μL of an MTT solution is added to achieve a final concentration of 0.5 mg/mL. The cells were then incubated for 3 h at 37°C, 5% CO_2 and protected from light. The Formazan crystals formed after incubation were dissolved by adding 100 μL of dimethylsulfoxide to each well. Finally, the number of live cells was quantified by an absorbance reading at 570 nm. The viability is expressed as a percentage of living cells relative to the control.

2.3.5 Loading cells with pH probes

The fluorescent probes were loaded into cells with their cell-permeable ester derivatives that are hydrolysed by cytosolic esterases to yield fluorescent intracellularly trapped probes.

Suspended cells were cultured in 96 well flat bottom ultra low attachment plates (Dominique Dutscher, France). They are seeded on day 1 at a density of 1×10^3 cells per well in a volume of 200 μL of complete medium and allowed to adhere for 48 hours before experiment. After that, cells were incubated in serum-free DMEM medium with 5 μM of probe prepared from a 1 mM stock-solution in DMSO, for 30 minutes at 37°C and 5% CO_2. FBS serum may contain endogenous esterase activity. Therefore, loading medium should be serum-free to keep extracellular hydrolysis of the AM ester to a minimum. Once loaded with the probe, cells were washed three times at 37°C, to remove the probe not taken up by the cells, with 200 µL of serum-free DMEM of the pH that was desired for the observation. The preparation is then placed on the stage of the confocal microscope (Zeiss LSM 710) and the acquisition begins after the selection in the observed fields of a population of cells, by reducing the opening of the pinhole (see details below).

Unlike the introduction of probes by microelectrodes, the method by incubation of the probe

in esterified form is ideal for preserving as much as possible the cell integrity (Nett and Deitmer, 1996).

2.4 Fluorescence microscopy

The last fifty years have seen the appearance of a large number of new techniques such as scanning tunneling microscopy or atomic force microscopy, making it possible to observe the surface of objects at the scale of the atom. Fluorescence microscopy has also established itself as a method of choice for biological applications. It is indeed possible using immunochemical methods to specifically label certain molecules using antibodies coupled with fluorophores. By exciting these fluorophores at the right wavelength, we obtain images with better contrast. However, fluorescence microscopy does not allow three-dimensional reconstructions and the images obtained are often surrounded by a blurred halo due to the fact that the fluorescence observed consists of not only that collected from the focal plane, but also from all parts of the specimen irradiated with excitation light. In order to solve this problem, Marvin Minsky patented in 1957 a new system allowing to overcome these parasitic fluorescences: confocal microscopy was born (for a review see Merchant et al., 2005). The development of lasers as an excitation source allowed the expansion of this method during the 1980s.

2.4.1 Confocal microscopy

Confocal microscopy is a method that also uses the fluorescence properties of certain molecules (Conchello and Lichtman, 2005). However, unlike conventional fluorescence microscopy, it makes it possible to obtain better images by eliminating the out-of-focus light or glare in specimens whose thickness exceeds the immediate plane of focus. The images obtained, called optical sections, are therefore of greater sharpness. Similarly, the motorization of the objective along the z axis makes it possible to produce optical sections at different levels of the sample in order to be able to obtain three-dimensional reconstructions afterwards. Confocal microscopy is a scanning microscopy, that is to say that the sample is considered as a grid and that the excitation and the acquisition of the signal will take place successively for all the points. Each grid point then corresponds to a pixel in the final image.
The light source in confocal microscopy must be particularly intense and focused, which is why lasers are used as sources in the majority of cases (table 2.1).
If we follow the optical path, the laser beam will first be reflected by a dichroic mirror before being sent to an XY scanner which will allow scanning of the entire area of interest in the specimen. The beam will then cross the objective and excite the fluorophores. The fluorescence emitted will be collected by the objective, reflected again by the XY scanner then it will cross the dichroic mirror, a converging lens and the confocal diaphragm before arriving on the detector. In general, the detector used is a photomultiplier tube (PMT) whose signal will be amplified before being processed by a computer to reconstruct the image. There are also filters between the dichroic mirror and the PMT to select the fluorescence wavelengths collected (Figure 2.5).
The central element of the system is the confocal diaphragm (called pinhole) located in front

Laser	Excitation lines	Power (in mW)
Argon (Ar)	458	5
	476	5
	488	20
	514	20
Argon-Krypton (Ar-Kr)	488	3-15
	568	3-15
	647	3-15
Helium-Neon (He-Ne)	543	1,2
	633	10

TABLE 2.1: Characteristics of the main lasers used in confocal microscopy.

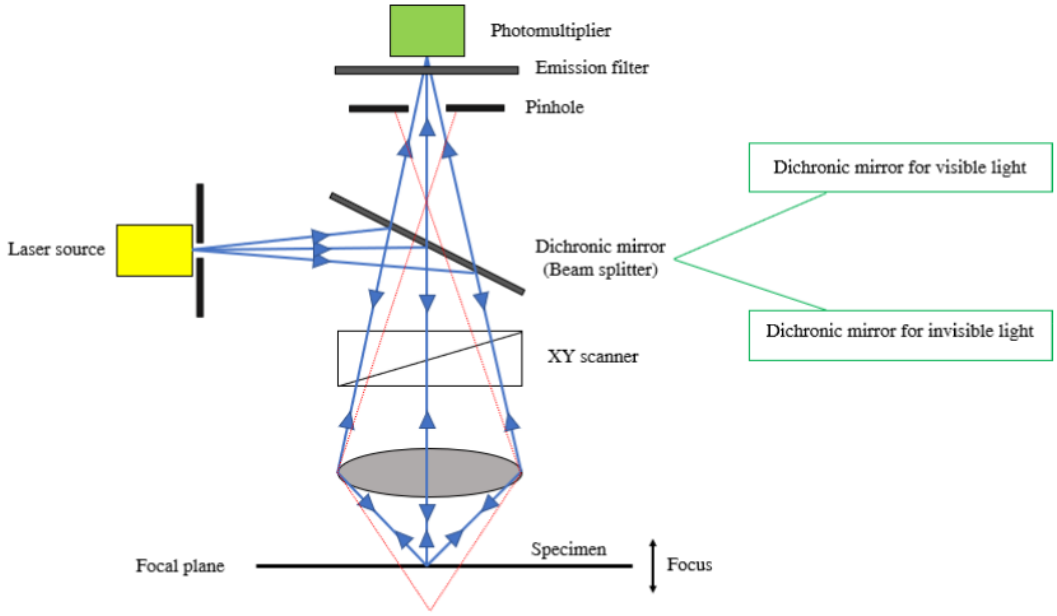

FIGURE 2.5: Scheme of a confocal microscope. The pinhole placed in front of the photomultiplier stops all signals not coming from the focal plane (red line).

of the PMT at the level of the focal plane conjugate with that of the objective (hence the name "confocal"). The pinhole will stop the fluorescence beams that have not been emitted at the level of the focal plane of the objective, the parasitic fluorescence therefore does not reach the detector. The thickness of the optical section varies according to the aperture of the confocal diaphragm. The smaller the aperture, the thinner and sharper the slice will be. However, from a certain value (limit of resolution), closing the diaphragm no longer leads to an increase in quality but a reduction in light intensity.

Advantages and disadvantages

Since the early 1990s, confocal microscopy has established itself in many research laboratories. By using staining techniques similar to those used in fluorescence microscopy (fluorescent dyes, immunochemistry, transgenesis), it is possible to obtain images with better lateral resolution as well as three-dimensional information.

Its main disadvantages remain the photobleaching of the fluorophores, the cellular photodamage induced by the focusing of a laser with a high power and the cost of an excitation laser source lower than 450 nm. However, it remains the reference method for all studies carried out on cells.
In *in vivo* imaging, the depth of observation has also been improved to allow studies up to 200 μm deep in the brainTomita et al., 2005. Despite this, this depth remains insufficient to conduct experiments covering the entire thickness of the cerebral cortex, for example. The use of confocal microscopy for intravital studies is therefore limited by the fact that excitation photons as well as fluorescence photons are scattered during their passage through significant thicknesses of tissue.

In this project, a laser scanning confocal microscope Zeiss LSM 710 was used. It rests on an anti-vibration table to stabilize the assembly. It is an inverted microscope especially suitable for live cell imaging and photobleaching experiments, equipped with a cage incubator for temperature control and CO_2 supply (Figure 2.6). Below is the microscope specifications:

Light source
Halogen lamp for bright-field microscopy (white light illumination)
■ a contrast image of the specimen can be directly observed through the eyepiece.

Laser Lines
■ Diode 405 nm
■ Argon 458 nm, 488 nm, 514 nm
■ Helium-Neon 543 nm, 633 nm

Objectives
Magnification / Numerical aperture
■ 10×/0.3 EC plan-Neofluar (Zeiss)
■ 20×/0.5 EC plan-Neofluar (Zeiss)
■ 63×/1.4 Oil Plan-Apochromat (Zeiss)
■ 63×/1.2 W C-Apochromat (Zeiss)

Detectors
2 PMTs for fluorescence, 1 PMT for differential interference contrast (DIC)

Acquisition software
Zen 2010 (Zeiss)

2.4.2 Principle of fluorescence

The term fluorescence was introduced by Georges Stokes who published his work describing this phenomenon in 1852 (Stokes, 1853). The term comes from fluorite (CaF_2), which is the mineral used in his experiments. He showed that when this mineral was exposed to ultraviolet

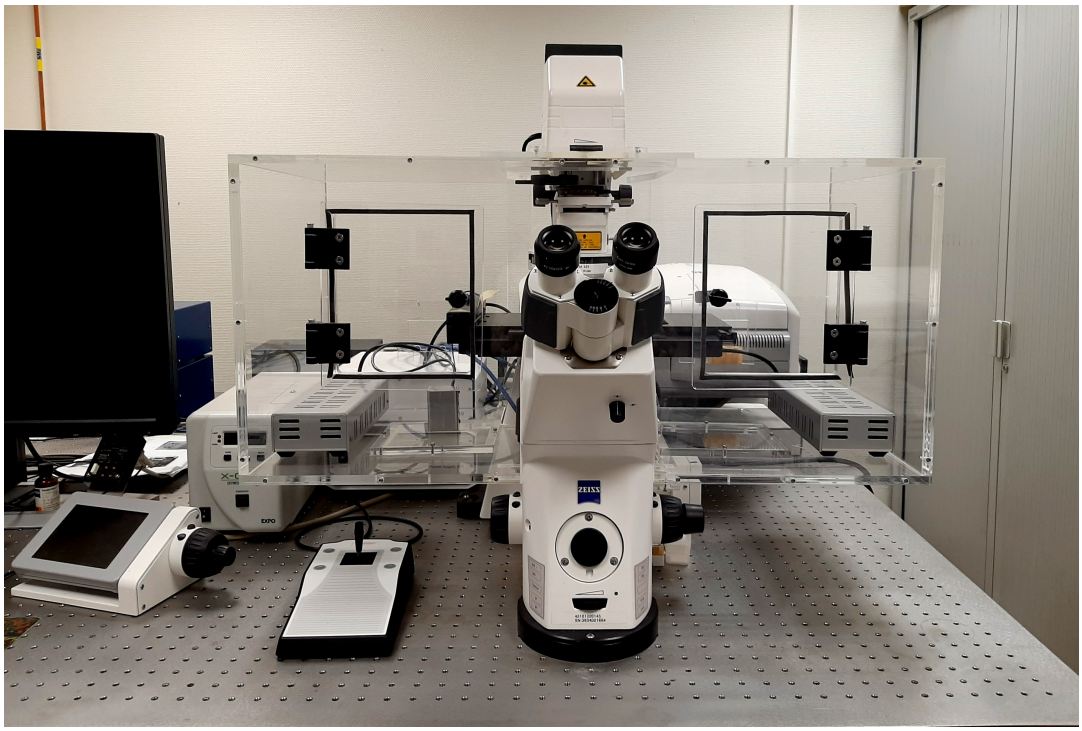

FIGURE 2.6: The ZEISS LSM 710 confocal laser scanning microscope used. Our incubation chamber allows control over temperature, CO_2 and humidity to permit live-cell imaging experiments.

light, it emitted blue light.

Fluorescence is a radiative physical phenomenon, i.e. involving the emission of photons. We are talking about a fluorophore or fluorescent probe, a molecule that has the ability to emit fluorescence. When such a molecule in its ground state absorbs light energy, for example a photon of energy $h\nu$, alterations in the electronic, vibrational and rotational states of the molecule can occur. This energy can allow an electron to pass from a fundamental level S_0 to an excited state S_2 with change of orbital of the electron. This transition to the excited state occurs very quickly (a few femtoseconds). This excited state S_2 has a very short lifetime (on the order of a nanosecond). Conformational changes and interactions with the surrounding molecules cause the molecule to pass from the excited state S_2 to a more stable excited state S_1: this is the internal conversion which lasts about 10^{-12}s.

From there, different processes can occur:

- or else the electron will pass from state S_1 to state S_0 by re-emitting the energy in the form of a spontaneous photon of energy $h\nu'$ (because of the internal conversion, $h\nu' < h\nu$, therefore the emission wavelength is greater than that of absorption). This process is called fluorescence and lasts from 10^{-12}s to 10^{-8}s. During this process, the spin of the electron considered does not change orientation.

- or else the electron will pass from S_1 to S_0 by undergoing a non-radiative de-excitation.

- finally, the electron can pass, thanks to an intersystem conversion, from the singlet state S_1 to an excited triplet state T_1 (this transition $S_1 \rightarrow T_1$ has a probability of occurring much lower than that of the transition $S_1 \rightarrow S_0$). There is then a change of the spin of the electron. This

inversion makes de-excitation more difficult, and the emission of a photon to return to the S_0 state will then be much slower: from 10^{-5}s to 10^{0}s. This is called phosphorescence.
In the following, we will only focus on fluorescence. Such a process is more easily identifiable since the spontaneous emission occurs within nanoseconds of the extinction of the excitatory radiation. It is a rapid conversion of absorbed radiation into re-emitted energy, without energy storage.

Thanks to the work of Alexander Jablonski (1898-1980), a Polish physicist who worked on the different transition moments for the absorption and emission of a fluorophore (Jablonski, 1933), we have a very practical tool for understanding the phenomena of luminescence: the Jablonski energy diagram (Figure 2.7). This diagram represents the different energy levels involved in the absorption and emission of light by a fluorophore as well as the notions of absorption spectrum and emission spectrum of a fluorophore, which are characteristic of the energy structure of the fluorophore (Figure 2.8). Indeed, to allow the transition from the fundamental state S_0 to the excited state S_1, it will take an energy at least equal to the energy difference between the highest sub-level of the fundamental level and the lowest sub-level of level S_1. This explains that there is an energy below which we will not be able to excite the fluorophore, i.e. a maximum wavelength. On the other hand, with shorter wavelengths, there will always be a non-zero probability of exciting the fluorophore. And it is the opposite for the emission spectrum. We also notice that the different sub-levels, as well as the instability of the excited level, will widen the emission spectrum around the resonance frequency of the considered transition. This makes it possible to explain the spread shape of the absorption and emission spectra and in particular the asymmetry of each of the two, but also the symmetry, the "mirror" effect between the two spectra for the simplest species.
The difference between the wavelength where absorption is maximum and that where emission is maximum is called the Stokes shift (Figure 2.9). This quantity is very important for fluorescence imaging: it is indeed necessary to work with fluorophores which have a sufficiently large shift so that we can reject the excitation light and only collect the fluorescence signal.
When working with fluorophores, certain artefacts are unavoidable and can alter the measurements (Lichtman and Conchello, 2005). In principle, a fluorophore can perform an unlimited number of cycles between the ground state and the excited state. But after irradiation, the molecule in the excited state is more reactive and the conditions under which these fluorophores are used limit the number of cycles. Generally, it is estimated that good fluorophores can perform between 10,000 and 40,000 cycles before permanently losing their fluorescent character. Photobleaching is the term for all processes that cause an irreversible decline in the fluorescence signal. At the molecular level, there are several means of bleaching and the photochemistry is not completely understood for most fluorophores. In a fairly basic way, it appears that this bleaching is the consequence of an energy transfer between the triplet state of the fluorophore and an oxygen molecule. The oxygen molecule thus excited in a singlet state is reactive and will participate in irreversible chemical reactions with organic molecules (polymerization, oxidation, dissociation, isomerization, etc.). These reactions can

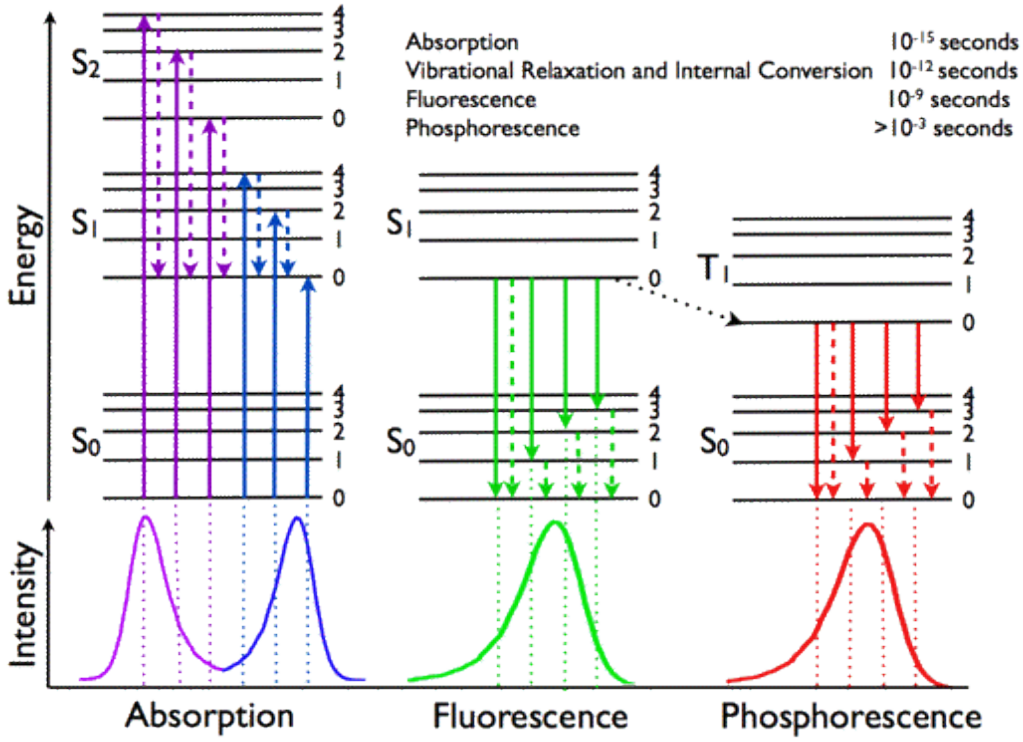

FIGURE 2.7: Jablonski diagram. On this diagram, the main radiative de-excitations of a molecule are represented. The singlet electronic states are denoted S_0 (fundamental), S_1, S_2 for the first and second excited electronic state. The first and second triplet electronic states are denoted T_1 and T_2. Different vibrational levels are associated with each electronic state. Absorption and emission processes are represented by solid arrows while vibrational relaxations and intersystem conversions are represented by dotted arrows [http://www.photobiology.info/Visser-Rolinski.html].

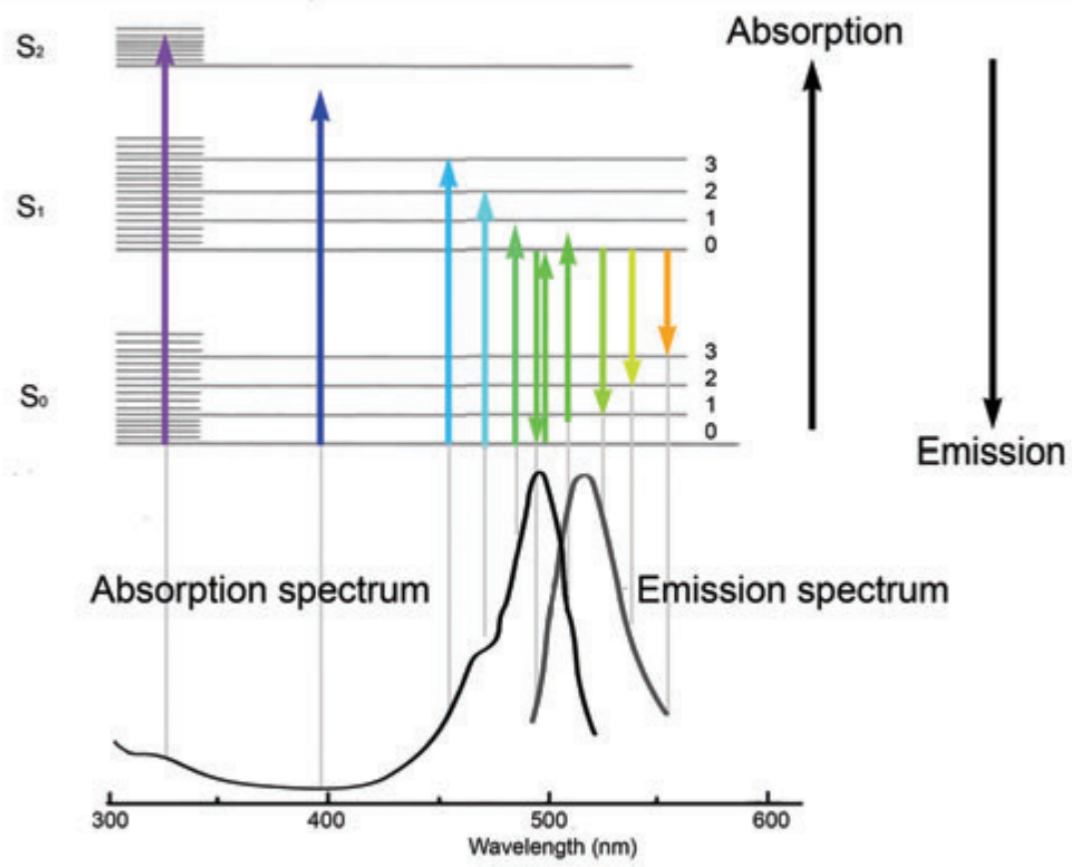

FIGURE 2.8: Jablonski diagram and FITC (Fluorescein-5-isothiocyanate) absorption and emission spectra. The gray lines connect the wavelength of the spectrum to the corresponding energy transition (Lichtman and Conchello, 2005)

alter the fluorophore and inactivate its ability to fluoresce. This singlet oxygen can also cause phototoxicity to the sample. But skilfully used, this photobleaching can also prove to be a tool. Let us cite as an example the case of FRAP (Fluorescence Recovery After Photobleaching), where a small volume of the sample is photobleached and by observing the way in which the fluorescence reappears in this volume, certain properties, in particular diffusion, of the sample studied are deduced.

It is also possible that the fluorophore, by interacting in a non-covalent manner with its molecular medium, loses, but reversibly this time, its fluorescence. This "damping" of fluorescence is called "quenching". This property can also be used to provide additional information about the sample. FRET (Förster Resonance Energy Transfe) is an example of collisional or dynamic quenching of the fluorophore in the excited state (Jares-Erijman and Jovin, 2003).

2.4.3 Characteristic parameters of fluorescence

Fluorescence lifetime

During the fluorescence emission, all the molecules present on the first excited state S_1 will be able to return to the ground state S_0 by two processes corresponding to a non-radiative de-excitation (whose probability is noted K_{nr}) and to the emission of fluorescence (whose

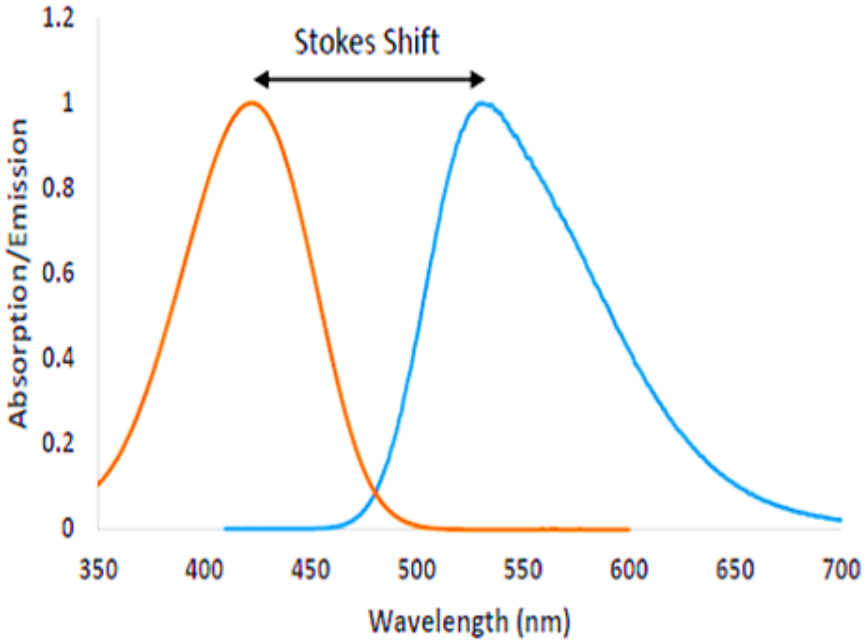

FIGURE 2.9: Absorption (orange) and emission (blue) spectra of Coumarin 153 dye illustrating the Stokes shift (Bakhoda et al., 2018).

probability is noted K_r).

Let N(t) be the population of fluorophores in the excited state, the depopulation of the excited state will depend on the two probabilities of radiative and non-radiative de-excitation and is given by the differential equation below:

$$-\frac{dN(t)}{dt} = (K_r + K_{nr})N(t) \tag{2.2}$$

Which allows us to obtain the evolution of this population over time:

$$N(t) = N_0 \exp(-\frac{t}{\tau}) \tag{2.3}$$

With

$$\tau = \frac{1}{K_{nr} + K_r} \tag{2.4}$$

Fluorescence emission being a random process, this quantity τ characterizes the average lifetime of molecules in the excited state, and is called the fluorescence lifetime. It can be seen that the fluorescence lifetime depends on the characteristics of the chosen fluorophore but also of its environment. It will thus provide additional information to the intensity measurement, by providing information on molecular interactions and on the physico-chemical environment of molecules. Its value in biological media is typically between 1 and 10 ns. Moreover, the fluorescence lifetime has the advantage of being independent of the concentration of the fluorophore (therefore of the level of expression of the latter in biological cells), of the characteristics of the excitation and therefore constitutes a measure relative, specific for the observed fluorophore.

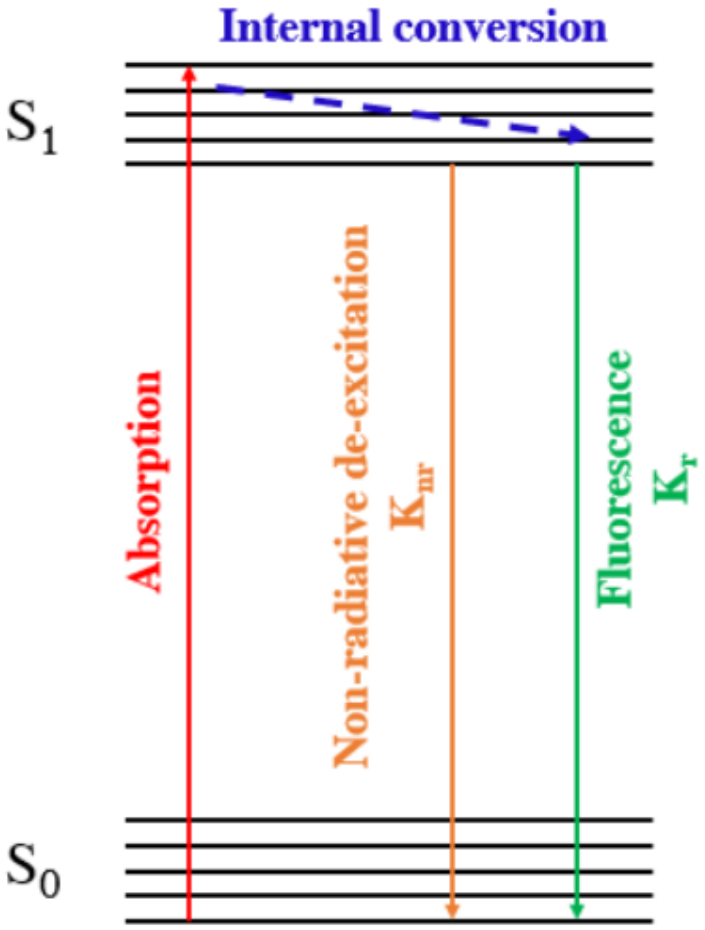

FIGURE 2.10: Simplified Jablonski diagram

Quantum yield of fluorescence

An important parameter relating to fluorescence intensity is the fluorescence quantum yield η. The latter is the quotient of the number of photons emitted over the number of photons absorbed. Assuming that all the absorbed photons allow the transition to the excited state S1, the latter will depopulate in two ways: each absorbed photon will either allow the emission of a fluorescence photon, or allow a non-radiative de-excitation. Therefore, the quantum yield is given by:

$$\eta = \frac{K_r}{K_{nr} + K_r} \tag{2.5}$$

This yield is between 0 and 1 and will therefore approach to 1 when the radiative de-excitation will become predominant with respect to the non-radiative de-excitation ($K_{nr} \langle\langle K_r$)

2.4.4 Emission and excitation spectra in fluorescence

Fluorescence data are generally presented in the form of spectra (excitation or emission) made up of several hundred measurement points. The emission spectrum is a curve representing the intensities of fluorescence released by the fluorophore during the radiative transition towards the different resonance levels of the ground state. In other words, it shows that the amount of light emitted is wavelength dependent. In this case, the excitation wavelength is fixed, and only the emission wavelength varies. Unlike IR spectra, fluorescence emission spectra often show a single band with a single maximum sometimes accompanied by one or more shoulders. The shape of the emission spectrum of a fluorophore varies according to the chemical structure of the excited molecule but also according to the physico-chemical characteristics of its close environment (Lakowicz, 1999).

The excitation spectrum is obtained by observing at one wavelength the intensity emitted as a function of the excitation wavelength. As the fluorescence intensity is proportional to the number of photons absorbed, the excitation spectra are very close, but not identical, to the absorption spectra. The excitation spectrum represents the effectiveness of different excitation wavelengths in causing fluorescence, and indicates which wavelengths give intense fluorescences (Lakowicz, 1999; Albani, 2008).

The traditional methods of processing fluorescence spectral data are based on the only determination of the fluorescence intensity at the wavelength corresponding to the maximum of emissions (Lakowicz, 1999). Today in fluorescence spectroscopy, the ratiometric method is generally used in order to reduce artefacts during measurements. Indeed, error signals are caused by inaccuracies in the concentration of fluorophore, the length of the optical path, the possibility of leakage of the fluorophore or even due to the phenomenon of photobleaching. To do this, the ratio of fluorescence intensities measured at the isosbestic[2] wavelength and at the maximum wavelength is calculated so that the measurements are independent of the fluorophore concentration (Haugland, 2005).

[2]The isosbestic point is a specific wavelength where the intensity is independent of pH.

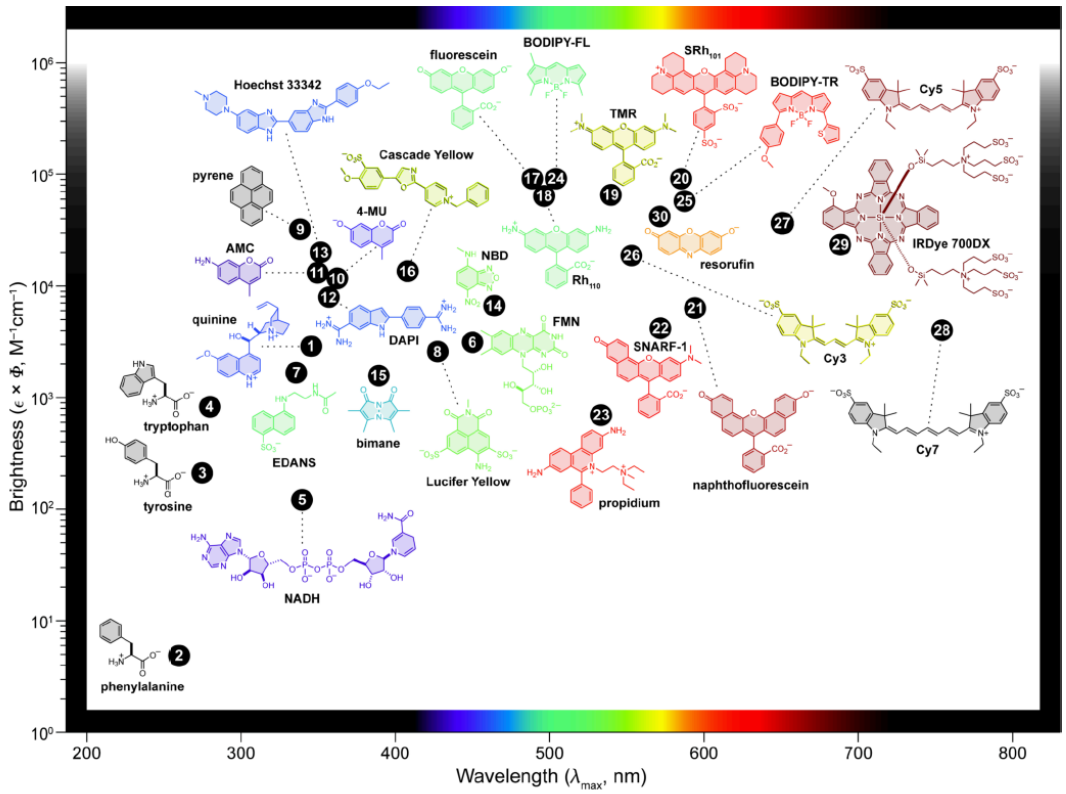

FIGURE 2.11: Representation of the main families of organic fluorophores classified according to their brightness and their maximum emission (Lavis and Raines, 2008).

2.4.5 Fluorophores

One of the main goals of technical improvements in microscopy over the years has been to increase the ability to distinguish what is interesting (the signal) from what is not (the background). Due to its shift in wavelength between excitation and emission, fluorescence has asserted itself as an essential tool, particularly in the observation of living organisms. Indeed, by using appropriate spectral selection tools, we will be able to collect only the fluorescence signal, and therefore have a contrast of very good quality. There are different types of fluorophores which are used in fluorescence microcopy depending on the samples observed and the processes and phenomena studied:

Organic fluorophores

Over the past 40 years, many organic fluorophores have been developed for bioimaging as illustrated in Figure 2.11. Today, organic fluorophores are reagents of choice for studying many biological phenomena and this in very different contexts: from *in vitro* to *in vivo*. The particular physico-chemical properties of certain molecules make it possible to use them directly in the fluorescent labeling of cells or of certain organelles ("staining" Haugland, 2005; Zhu et al., 2016; Xu et al., 2016). However, the most used approach is based on the association of the fluorophore with another molecule (most often a biomolecule or a biopolymer) with the aim of monitoring the latter and its possible interaction with a biological target ("biomolecule

labelling" Gonçalves, 2008; Dean and Palmer, 2014; Chen, Tsao, and Keillor, 2015). Finally, they are increasingly used in the design of "smart" probes for the measurement of certain cellular parameters (pH for example), for the detection of a large number of chemical species playing a key biological role (ROS , RNS, biological thiols, metal anions and cations for example) or enzymatic activities (Shieh and Bertozzi, 2014; Lang et al., 2020).
Generally, the organic fluorophores have high quantum yields and sufficient Stokes shifts to easily separate the fluorescence signal from the excitation light and allow multiple labeling without spectral overlap.
In this project, we are interested in measuring the pH inside glioma cells since cell acidity regulation capacity is a major characteristic of tumor cells. In this regard, Molecular probes offers a variety of organic fluorophores, their conjugates and other agents, for pH measurements mainly used for biological systems. Therefore, within the framework of this study, two organic fluorophores were pre-selected for their characteristics and subsequently, they were checked in order to define the most suitable one for our pH measurements. These two fluorores are the BCECF and SNARF-4F. They will be presented in detail in Chapter 3.

Quantum dots

In order to overcome the shortcomings of organic fluorophores, fluorescent probes made from nanomaterials, quantum dots, have been developed and are used for applications in biology and medicine (Bailey, Smith, and Nie, 2005). Indeed, these probes have a high brightness (linked to their high quantum efficiency) and a higher photostability, which makes these particles less sensitive to photobleaching. In addition, these probes offer fluorescence emission wavelength tunability which is a direct function of their size. They also have a wide absorption spectrum allowing the use of a single excitation source and having different possible emission wavelengths. Thanks to their longer fluorescence lifetime (10-50 ns), inorganic fluorescent particles make it possible to follow processes in larger time windows or offer larger signal variation quantification dynamics compared to organic fluorescent molecules . However, these inorganic particles have certain disadvantages such as their size which remains much greater than that of organic fluorophores and can disturb a biological system. On the other hand, most QDs are toxic (core formed of heavy metals such as CdSe), which is troublesome for applications in the living environment.

2.4.6 Fluorescent proteins

The major turning point in the use of microscopy in cell biology took place with the Green Fluorescent Protein (GFP) which resulted in a Nobel Prize in 2008 for Martin Chalfie, Osamu Shimomura and Roger Tsien (Chalfie et al., 1994; Shimomura, Johnson, and Saiga, 1962; Ormö et al., 1996).They first discovered and purified aequorin, which emits in the blue, then identified GFP, which emitted in the green after excitation in the ultraviolet (Shimomura, Johnson, and Saiga, 1962). Indeed, by genetic encoding, this fluorescent protein can be produced directly by the cell and it makes it possible to specifically mark the proteins that one wishes to study. The first use of this GFP took place in 1994 by the team of Martin

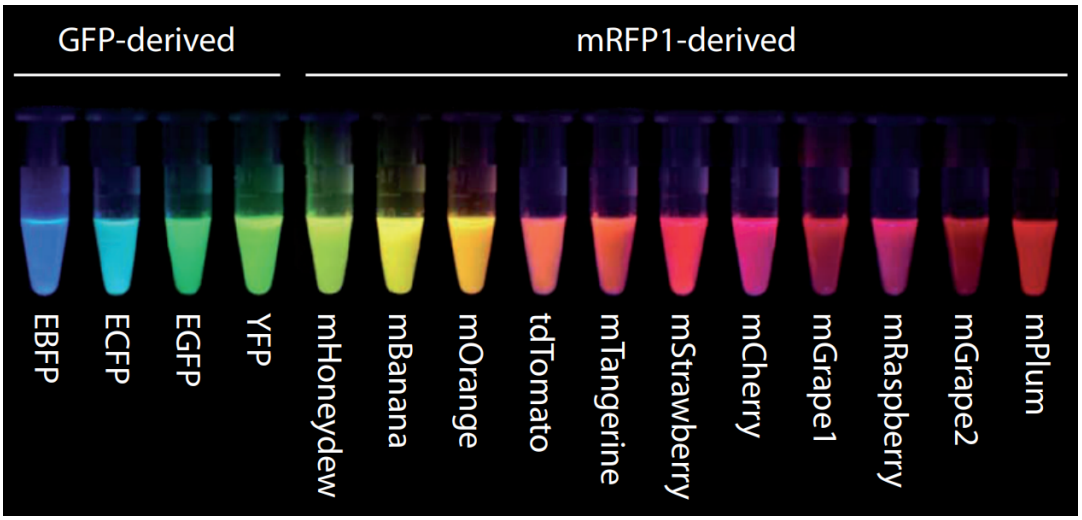

FIGURE 2.12: Image of emission spectra of different fluorescent proteinsRino et al., 2009

Chalfie (Chalfie et al., 1994). The researchers expressed GFP in C.elegans under the control of a promoter of a gene coding for a beta-tubulin. They were thus able to link the different intensities of fluorescence according to the cells with the level of expression of the gene. They also showed that mutations within this fluorophore could lead to a red or blue shift in the emission spectrum of GFP. This paved the way for the development of many GFP derivatives to cover the spectrum of light.Improved versions of GFP called Enhanced GFP (eGFP) have been developed that can be up to 35 times brighter than wild-type GFP (Heim and Tsien, 1996; Zhang, Gurtu, and Kain, 1996). Other derivatives of GFP have been generated such as CFP (Cyan Protein Fluorescent) (Heim and Tsien, 1996) or CyPet (Nguyen and Daugherty, 2005), which emit more towards blue or as mCitrine (Griesbeck et al., 2001), Venus (Nagai et al., 2002) and Ypet (Nguyen and Daugherty, 2005) which are YFPs (Yellow Fluorescent Protein) which emit more in the yellow.

In the same way that GFP was discovered to exist in living organisms, DsRed is a fluorescent protein that was discovered in the sea anemone Discosoma and whose emission spectrum is in the red. Its spectrum, which is significantly separated from GFP, thus makes it possible to develop two-color approaches in the same system. However, DsRed is a tetrameric protein (Ranganathan, Wall, and Socolich, 2000) and its maturation rate is slow. Maturation is a post-translational step during which the rearrangement of the protein makes it possible to acquire its fluorescence property. This time is highly variable among different fluorescent proteins (Balleza, Kim, and Cluzel, 2017). Thus DsRed has also undergone series of development by mutagenesis in order to improve its properties. First, its mRFP1 monomer could be isolated. This one has a better maturation but a lower quantum yield and a less good photostability (Campbell, 2001). From this monomer, other proteins have been obtained such as mCherryShaner et al., 2004. This turns out to have a correct maturation time (although less than GFP) and better photostability. Figure 2.12 illustrates the coverage of the visible spectrum by a set of fluorophores derived from GFP or from the DsRed monomer (Rino et al., 2009).

These proteins are the basis of very powerful tools called biosensors. In theory, it is possible to express these proteins in fusion with one or more proteins of interest in living models and thus to have access to localization, diffusion, concentration or even distribution in living organisms.Their use often has an advantage of specificity compared to other labeling techniques such as immunofluorescence and is more suitable for living organisms (Toseland, 2013).

The development of new fluorescent proteins is still relevant. The challenges are to develop proteins whose maturation time will be as short as possible, whose brightness will be as high as possible, whose stability against photobleaching or pH, for example, will be as high as possible (Campbell, 2001) and with the best possible quantum yield.

Chapter 3

Fluorescent indicators for intracellular pH: a comparative study between SNARF-4F and BCECF

At the end of the 19th century, fluorescent probes such as rhodamine, acridine orange and fluorescein, the most widely used in biology, appeared (Steyern, Josefsson, and Tågerud, 1996; Mirrett, 1982; Minta, Kao, and Tsien, 1989). There are two categories, intrinsic and extrinsic probes. First of all, the intrinsics are those already present in the biological sample. These include, for example, aromatic amino acids, purines, pyrimidines, certain enzymatic cofactors (NADH) and vitamins (Georgakoudi et al., 2008). While extrinsic probes are added for the analysis of a non-fluorescent compound, and serve to label a specific constituent (Liu et al., 2020; Hawe, Sutter, and Jiskoot, 2008). Fluorescent molecules that intercalate with various molecules can be used to study enzymatic activity, intracellular pH or even cell viability (Tourkya, 2009). In short, there is a wide variety of substances that can be used in fluorescence and useful for biological studies. However, the use of these molecules is increasingly extending to other applications due to the development of fluorescent molecules with specific characteristics.

In this regard, Molecular Probes^{TM} offers a variety of fluorescent pH probes, with their conjugates and other agents, for pH measurements and which are mainly used for biological systems. In general, they can be classified into two groups. The first group includes fluorescent pH probes which exhibit a single fluorescence emission peak (fluorescein for example (Slyusareva et al., 2011)). For these probes, the fluorescence excitation profile is pH-dependent and the shape of the emission spectra remains almost constant. Hence, the ratiometric pH measurement is implemented when the excitation is performed at two excitation wavelengths and the fluorescence emission is measured at one wavelength. In other words, ratiometric pH measurement allow the observation of variations in the emission intensity ratio, hence the name *ratiometric*, by measuring the fluorescence at two separate excitation wavelengths. The second group exhibits a dual fluorescence emission peak (Carboxy SNARF-1 for example (Magg and Albert, 2007)). Here, each protonated or deprotonated forms exhibits characteristics emission and/or absorption spectra. Shifts between spectra obtained for protonated and deprotonated species can be exploited in order to perform a ratiometric measurement. Two

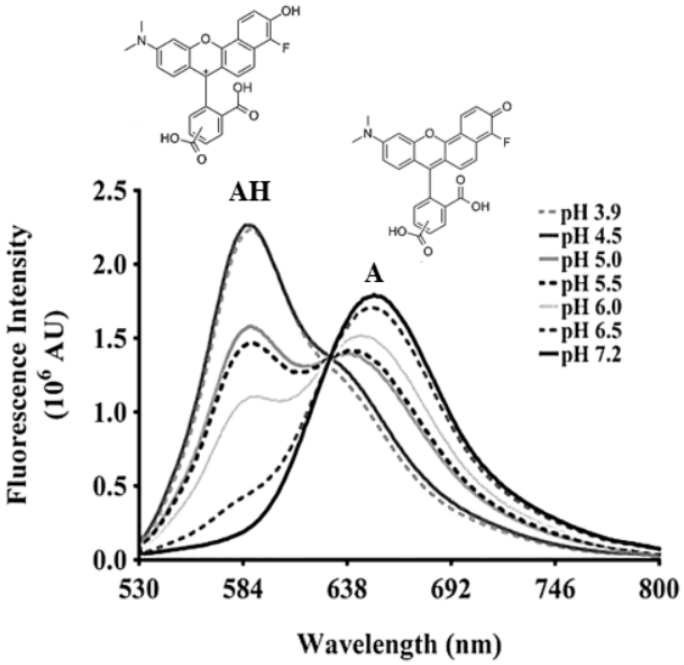

FIGURE 3.1: Fluorescence emission spectra of SNARF-4F in aqueous samples ranging in pH from ~ 4 to 7 (Hight et al., 2011). When in solution, SNARF-4F exists under two forms: the acidic or protonated form (AH) and the basic or deprotonated form (A). The equilibrium of the acid-base reaction is driven by the law of mass action. Samples were excited at 523 nm.

situations occur, either the excitation is performed at two excitation wavelengths and the fluorescence emission is measured at one wavelength, or the excitation is performed at only one excitation wavelength and fluorescence emission is measured at two emission wavelengths. Under certain conditions, ratiometric measurement makes pH determination independent of the probe concentration or optical path length because pH is related to the ratio (in excitation or emission) at two characteristic wavelengths.

As part of this study, two fluorescent probes were pre-selected for their characteristics and subsequently they were checked in order to define the most suitable for our study. As a reminder, it is a question of characterizing the regulatory capacity of intracellular pH of two glioma cell lines using fluorescence microscopy. This has consequences for treatment planning since the main drug used against glioblastoma is highly pH dependent.

3.1 SNARF-4F

The measurement of pH in fluorescence microscopy is based on the protonation and deprotonation of functional groups[1] as a function of pH, modifying the spectroscopic properties of the probes. Among these, the seminaphtarhodafluor (SNARF) family has shown interesting analytical properties for their applications in biological conditions (deMello, 2006; Li et al., 2013; Bastús et al., 2014). Carboxy SNARF-1 was widely used from this family to monitor

[1]In organic chemistry, a functional group is a specific group of atoms or bonds within molecules that have their own characteristic properties, regardless of the other atoms present in a molecule.

pH_i. It can be excited by the 488 or 514 nm spectral lines of the argon-ion laser. This advantage had made carboxy SNARF-1 exceptionally suitable for both confocal laser scanning microscopy and flow cytometry. However, the relatively high pK_a (~ 7.5) of carboxy SNARF-1 has limited its cellular applications. This motivated to modify the existing SNARF-1 probe by fluorinating its benzo[c]xanthene ring system (Liu, Diwu, and Leung, 2001). Therefore, new fluorescent probe was synthesized and characterized as new dual-emission pH probe with pK_a values of ~ 6.4. The low pK_a value of 6.4 for SNARF-4F make this probe exceptionally suitable for pH_i measurement in the range from about 6.0 to 7.5 with confocal laser scanning microscopy and flow cytometry.

When in solution, SNARF-4F exists under two forms: the acidic or protonated form (AH) and the basic or deprotonated form (A). Therefore, the fluorescence signal is due to the contribution of these two forms with relative contributions depending on the pH of the medium under test (Figure 3.1). Thus, at pH values well below its pK_a, the probe exists predominately in a protonated state and exhibits maximum fluorescence emission at 580 nm when excited at 523 nm. Whereas, SNARF-4F exists in a predominately deprotonated state at pH values well above the pK_a and exhibits maximum fluorescence emission at 640 nm when excited at 523 nm (Figure 3.1). Shift obtained between the spectra of the protonated and deprotonated species can be used to perform a ratiometric measurement for more accurate pH determinations. In this case, pH is directly related to the ratio of the fluorescence intensities measured at two emission wavelengths, typically about 580 nm and 640 nm. These two emission wavelength can be minimally affected depending on the medium under test or even the excitation light used. Besides being a single excitation-dual emission fluorescent probe, SNARF-4F can be used as a dual excitation-single emission fluorescent probe. In such case, the excitation of SNARF-4F is performed at two excitation wavelengths and the fluorescence emission is measured at one emission wavelength, 580 nm or 640 nm. pH measurements are therefore made by determining the ratio of fluorescence intensities measured at both excitation wavelengths and fixed emission at 580 nm or 640 nm.

There are two types of SNARF-4F probes: the SNARF-4F-AM and SNARF-4F (Figure 3.2). The first has an acetoxymethyl ester (AM) group which makes the probe neutral, allowing it to cross cell membranes. Once inside the cell, intracellular esterases will cleave the ester group of the molecule, releasing the charged groups and trapping the probe in the cytoplasmic compartment (Tsien, 1981; Graber et al., 1986). The second is devoid of this AM group. The molecule therefore cannot enter the cells and remains in the extracellular compartment. The esterified version is therefore used to measure the intracellular pH (pH_i) while the non-permeable version is used to measure the extracellular pH (pH_e).

In our project, SNARF-4F (SNARF-4F 5-(and-6)-carboxylic acid *cell impermeant) and SNARF-4F-AM (SNARF-4F 5-(and-6)-carboxylic acid, acetoxymethyl ester, acetate *cell permeant) have been purchased from Molecular Probes^{TM} (Oregon USA). Upon receipt, they have been stored away from light at a temperature of -20°C. SNARF-4F was provided as a lyophilized solid in units of 1 mg while SNARF-4F-AM was supplied in sets of 10 × 50 μg vials of lyophilized solid. For each probe, a stock solution is prepared at 0.1 mM in DMSO and then is divided into 10 μL aliquots in microtubes (Eppendorf) which are stored at -20°C.

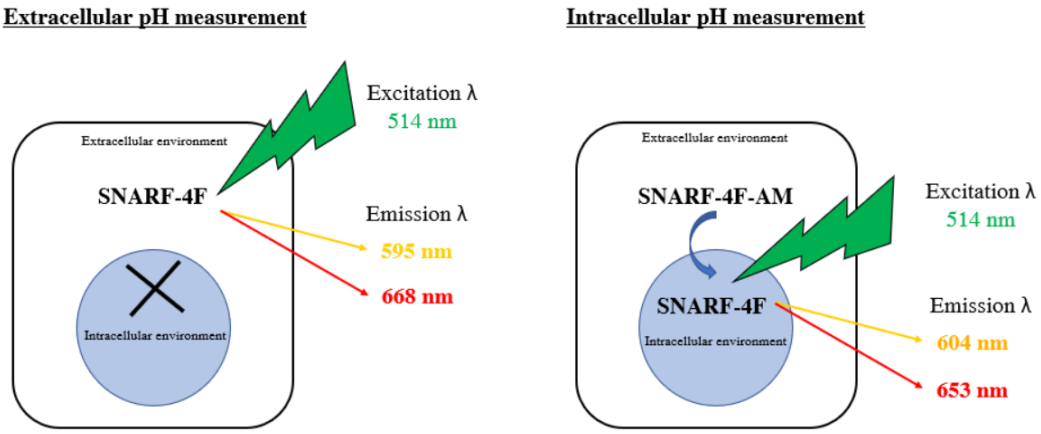

FIGURE 3.2: Schematic representation of the use of the two fluorescent probes SNARF-4F and SNARF-4F-AM for extracellular and intracellular pH measurements respectively.

3.1.1 In vitro fluorescence spectra of SNARF-4F

Non-permeable version

In order to measure the emission spectra of SNARF-4F, an initial experiment was performed using the non-permeable version of SNARF-4F (5µM) in a serie of pH-adjusted DMEM free-serum medium, from 4.0 to 8.4 with 0.2 pH increments. The pH of the DMEM medium was measured with a pH meter and adjusted to obtain a range of pH from 4.0 to 8.4 using 0.1 M HCl or 0.1 M NaOH solutions. The fluorescence of the probe was examined using an excitation light at 514 nm provided by an argon ion-laser and the fluorescence emission was recorded in the 420-720 nm range.

As shown in Figure 3.3, when excited at 514 nm, SNARF-4F exhibits a pH-dependent wavelength shift with emission maxima at 599 and 668 nm, and an isosbestic point[2] at 638 nm. In parallel, looking at Figure 3.4, the probe displayed a strong deep red fluorescence in neutral/basic medium ($\lambda_{em,max}$ = 668 nm). In contrast, when the pH of the medium was down-regulated to more acidic values, the fluorescence gradually changed from deep red to yellow-orange ($\lambda_{em,max}$ = 559 nm). Thus, increasing acidity was accompanied by yellow-shifts for emission spectra when the pH changed from neutral to acidic. Therefore, as a dual emission probe, SNARF-4F can be used to deduce pH from the ratio of the fluorescence intensities emitted at the two wavelengths corresponding to the emission maxima. One says that SNARF-4F is a dual-emission ratiometric fluorescence probe. The two emission wavelengths used for this ratiometric measurement are 599 nm and 668 nm for this probe. We found that the ratio between the fluorescence intensities at 599 nm and 668 nm (I_{599nm}/I_{668nm}) displayed a ~ 15-fold enhancement (from 0,119 at pH 8.4 to 1,787 at pH 4.0) (Figure 3.5). A good linearity (R = 0.99) between the fluorescence ratio ($R=I_{559nm}/I_{668nm}$) and pH in the range of 6.2 to 7.2 was obtained, suggesting that this probe had the potential to detect pH_i

[2]The isosbestic point is the wavelength where the intensity is independent of pH.

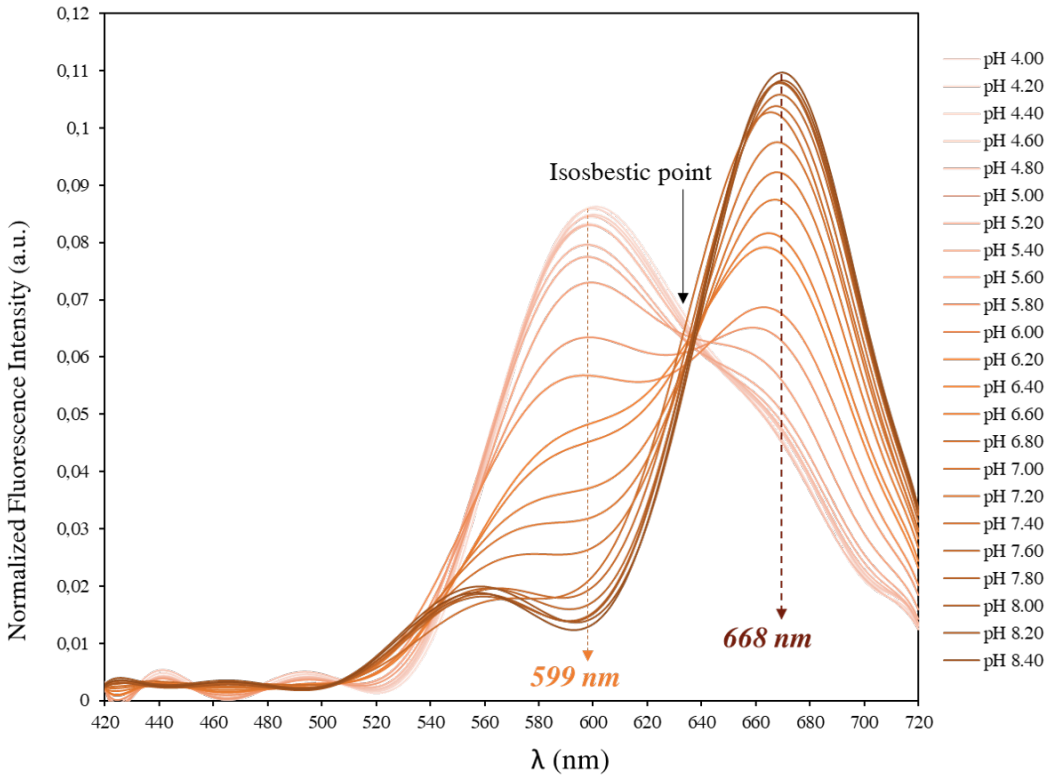

FIGURE 3.3: Emission spectra of SNARF-4F (5.0 μM) in DMEM medium at various pH values. SNARF-4F exhibits a double emission peak with an isosbestic point at 638 nm. Excitation wavelength was 514 nm. N=1.

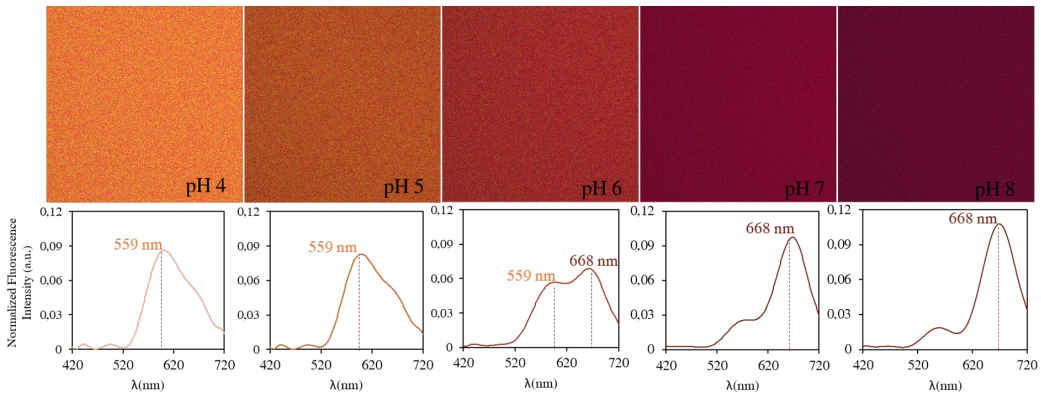

FIGURE 3.4: Fluorescence images of SNARF-4F in DMEM medium from pH 4.0 (left) to pH 8.00 (right) under 514 nm excitation. For each pH, we present the average emission spectrum over the entire image (2048×2048 pixels).

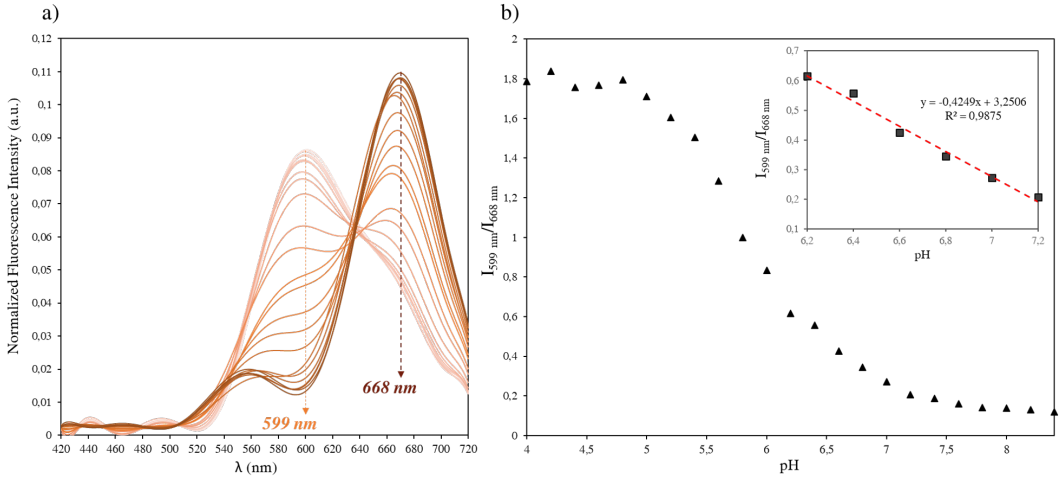

FIGURE 3.5: a) The two emission wavelengths used for the ratiometric pH measurement for SNARF-4F: 599 nm and 668 nm. b) Ratio of fluorescence intensity (I_{599nm}/I_{668nm}) of SNARF-4F (5.0 µM) in DMEM medium at different pH values. Inset: the linear relationship between I_{599nm}/I_{668nm} and pH value (6.2 to 7.2).

(6.2-7.2) in a ratiometric manner. This linearity allows us to use the following equation to therefore estimate the extracellular pH (pH_e) from the values of the fluorescence ratio:

$$R = \frac{I_{559nm}}{I_{668nm}} = -0,4249 \times pH_e + 3,2506 \tag{3.1}$$

valid in the range pH_e 6.2-7.2.

Therefore,

$$pH_e = -2,353 \times R + 7,65 \tag{3.2}$$

Permeable version

To measure the intracelluar pH with the fluorescent pH probe, SNARF-4F has been loaded into cells by incubation with the acetoxymethyl ester (AM) form: SNARF-4F-AM (Figure 3.2). As a reminder, once inside the cell, the ester is supposed to be hydrolyzed by intracellular esterases, releasing the proton-sensitive probe which is fluorescent and unable to permeate the membrane, thereby being trapped inside of the cell (Graber et al., 1986).
Therefore, in this context, U87 and F98 cells were grown in a complete cell culture medium for 2 days. Culture medium was then changed to DMEM free-serum medium (pH ~ 7.4) to avoid extracellular hydrolysis of AM ester caused by the presence of serum which may contain endogenous esterase activity. After 40 min incubation with 5 μM of SNARF-4F, cells were washed 3 times with fresh medium (pH ~ 7.4) to remove the probes not taken by the cells and thus were incubated for 1 hour with the pH desired for observation (Figure 3.6).
The emission spectra of SNARF-4F-AM have been recorded using an excitation wavelength at 514 nm in the 420-720 nm range. In ordre to reduce, as low as possible, the photobleaching of samples, the laser beam was scanned across them only once for each image. One scan for

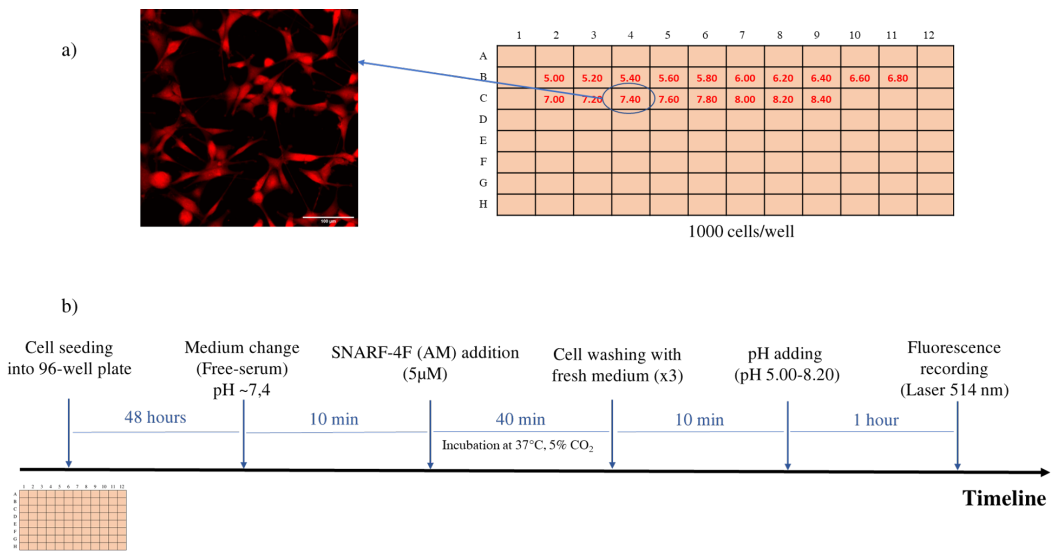

FIGURE 3.6: a) Confocal fluorescence image of U87 cells after one hour of incubation with SNARF-4F in a DMEM culture medium at pH 7.4. Cells were seeded in a flat 96-well ClearLine® plate. b) The experimental timeline for recording the emission spectra of SNARF-4F-AM in glioma cells at various pH values.

a 2048×2048 pixels per image lasted approximately 7 s. Figure 3.7 (b) shows the emission spectra of SNARF-4F-AM in F98 cells. As can be seen, in comparison with its non-permeable version (Figure 3.3 or Figure 3.7 (a)), SNARF-4F-AM emission spectra were altered by the intracellular milieu. The shape of the emission spectra of SNARF-4F-AM was markedly different particularly at higher values of pH. As the pH was dropped, the emission spectra showed much less visible conversion than expected to the high pH spectral form. It was reported that this difference was not an artifact of incomplete hydrolysis of the acetoxymethyl ester (AM) that was used to load the probe into the cells (Owen, 1992). Nevertheless, SNARF-4F-AM incorporated into the cell responded to pH_e changes similarly to SNARF-4F.

Cell Type	Intracellular potassium (mM)
Human lymphocytes	137 ± 11
Mouse lymphocytes	139 ± 11
Rat lymphocytes	15 ± 10
U266	74 ± 13
JY	96 ± 9
HUT-78	106 ± 8
Common carp sperm	60 ± 7

TABLE 3.1: Intracellular free potassium ion concentration of different cells. Displayed data are means ± S.D. values calculated from three independent samples (Balkay et al., 1997).

Therefore, because the pH-dependent spectra of SNARF-4F are significantly different when the probe is loaded in cells, in situ calibration is generally required for each cell line (Owen, 1992). The most widely used calibration method is the nigericin method (Thomas et al., 1979; Seksek et al., 1991; Seksek and Bolard, 1996; Bond and Varley, 2005). The presence

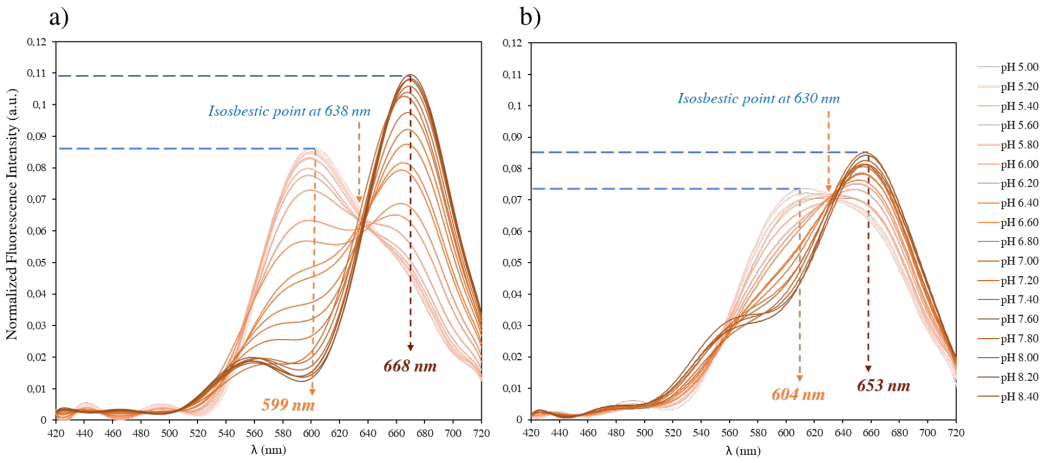

FIGURE 3.7: Comparaison between the emission spectra of **a)** SNARF-4F in DMEM medium and **b)** SNARF-4F-AM in F98 cells at various pH values. Excitation wavelength was 514 nm.

of nigericin in the solution whose concentration of potassium ions (K^+) is similar to that of the cells will create an exchange potassium/proton at the level of cell membranes in order to equilibrate the pH of the solution with the pH inside the cell. It is thus a method which depends on the knowledge of the intracellular [K^+].

Reviewing the research literature, no study is found allowing us to know the intracellular concentration of K^+ ions in our glioma cells. However, from the study of Balkay et al., the table 3.1 shows the intracellular potassium ion concentration of different cells (Balkay et al., 1997). The measured data show that intracellular potassium concentration is a well cell-dependent parameter and fall into the range between 50 mM and 150 mM. This parameter was measured using the "null point" concept (Babcock, 1983). It will be further detailed in the following paragraph. Therefore, based on this concept, the potassium ion concentration was well measured for our U87 and F98 glioma cells.

3.1.2 Measurement of intracellular potassium ions concentration

In order to use the SNARF-4F to measure the intracellular pH of glioma cells in confocal microscopy, it is first necessary to calibrate the fluorescent probe in each cell line. As mentioned above, the best established technique for the intracellular calibration of probes which sense pH is the method of Thomas et al (Thomas et al., 1979). This method uses nigericin K^+/H^+ exchange to bring pH_i to defined levels.

As a representative of carboxylic ionophores, nigericin allows exchange of potassium ions K^+ with hydrogen ions H^+ across their concentration gradients. So, when cells are suspended in medium whose potassium ion concentration is approximately equal to that inside the cells, hydrogen ions move freely and pH_i tends to equal pH_e. One says pH_i is “clamped” at pH_e (Pressman and deGuzman, 1977). This method depends on knowing the intracellular potassium concentration. It is therefore required to evaluate the intracellular K^+ concentration. This concentration was measured by the nigericin null-point technique, modified from the

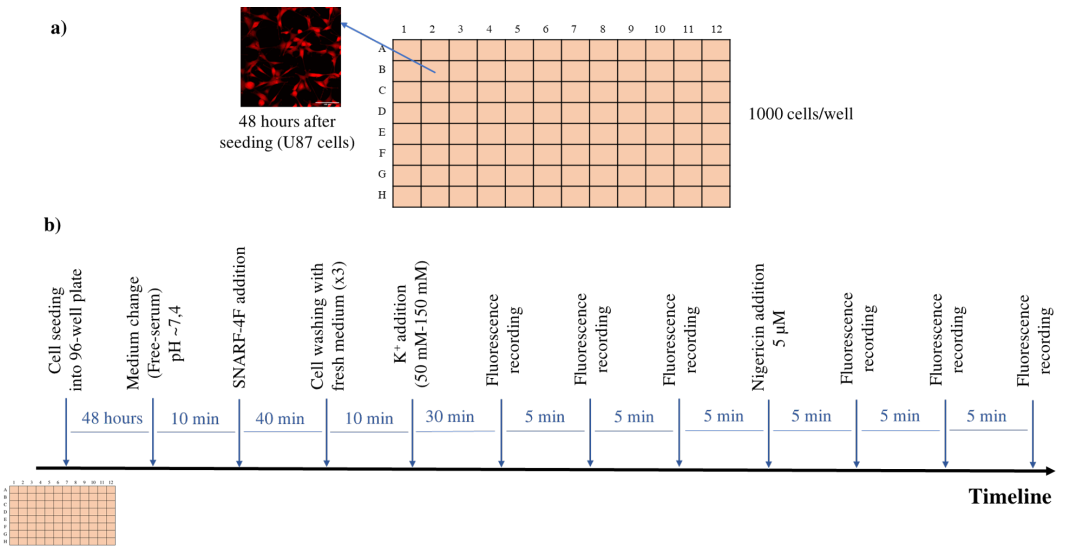

FIGURE 3.8: a) Cells were seeded at a concentration of 1000 cells/well in a flat ClearLine® plate (96 wells). Confocal fluorescence images were recorded after loading cells with the SNARF-4F probe using an excitation wavelength of 514 nm. b) Experimental timeline to measure the intracellular potassium ions concentration.

method of Babcock (Babcock, 1983).

The ability of the carboxylic ionophore nigericin to promote the exchange of H^+ for K^+ can be used to lower or raise the intracellular pH by placing in the medium, respectively, K^+ lower or higher than the intracellular concentration. This exchange of H^+ and K^+ ions by nigericin implies that:

$$\frac{[H^+]_i}{[H^+]_e} = \frac{[K^+]_i}{[K^+]_e} \tag{3.3}$$

If extracellular and intracellular K^+ concentrations are approximately equal, $[K^+]_i = [K^+]_e$, there is no net movement of potassium ions, and hydrogen ions can move freely down their concentration gradient. The pH_i is therefore set at the pH of the medium (pH_i=pH_e). This provides then the basis for a null point determination of intracellular K^+ concentration (Babcock, 1983).

Therefore, to measure the intracellular K^+ concentrations, U87 and F98 cells were grown in a complete cell culture medium for 2 days in a 96-well flat plate. Culture medium were then changed to DMEM free-serum medium (pH ~ 7.4) to avoid extracellular hydrolysis of AM ester caused by the presence of serum. After 40 min incubation with 5 μM of SNARF-4F, cells were washed 3 times with fresh medium (pH ~ 7.4) to remove the probes not taken by the cells. The cells were then exposed to different DMEM media with different concentrations of K^+ ions (50 mM to 150 mM with 20 mM increments). 30 minutes after incubation, fluorescence spectra were recorded from the samples every 5 minutes over a period of 15 minutes. 5 µM of nigericin were then added to the wells and spectra were recorded every 5 minutes over a period of 15 minutes (Figure 3.8).

As we have not yet calibrated the experimental system, i.e. we do not have the calibration equations which allows us to measure the pH_i from the fluorescence ratio. Therefore, we

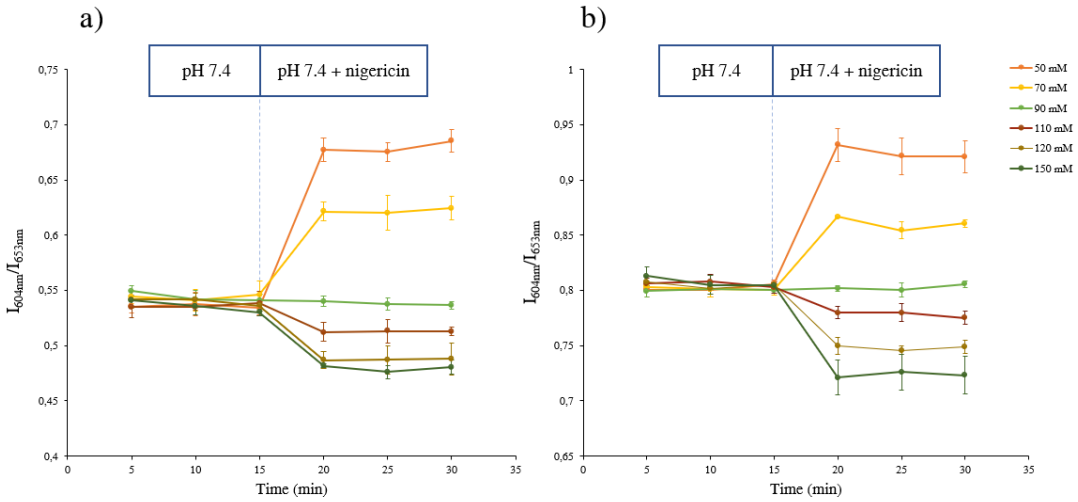

FIGURE 3.9: Effects of nigericin with varying extracellular K^+ concentrations on I_{604nm}/I_{653nm} in a) F98 cells b) U87 cells. In the presence of nigericin, a 50-70 mM [K^+] increases I_{604nm}/I_{653nm}, whereas high [K^+] (110-150 mM) decreases I_{604nm}/I_{653nm}. The estimated [K^+] of 90 mM has little effect on I_{604nm}/I_{653nm} ("null point").

will monitor the pH_i as a function of the fluorescence ratio. It has been noted that the pH is inversely proportional to the fluorescence ratio as shown in Equation 3.1.

In this context, at each fluorescence recording, the fluorescence ratio, I_{604nm}/I_{653nm}, is measured and plotted against the set $[K^+]_e$ as shown in Figure 3.9. In the presence of a 50-70 mM K^+ concentration, I_{604nm}/I_{653nm} promptly rise, i.e. pH_i promptly fell, consistent with a rapid proton influx that balanced the K^+ efflux. Exposure to a 90 mM K^+ concentration minimally affected pH_i, whereas a high K^+ concentration (110-150 mM) fell I_{604nm}/I_{653nm}, i.e. raised pH_i, consistent with adequate functioning of the probe-ionophore system and the "null point" concept.

Thus, using the ionophore nigericin in the presence of 90 mM K^+ lead to calibrate the pH_i with the controlled pH_e and the pH-dependent spectral shifts exhibited by carboxy SNARF-4F allow calibration of the pH response in terms of the ratio of fluorescence intensities I_{604nm}/I_{653nm} measured at two different wavelengths (604 nm and 653 nm).

3.1.3 Intracellular pH calibration

As mentioned above, the calibration of the intracellular pH is based, after loading the cells with the pH probe, on an equilibrium of the intracellular pH with the extracellular pH of the culture medium which value is known. In other words, it consists in imposing the pH_i at known values and determining for each of these values the fluorescence ratio. To impose the pH_i, the addition of nigericin in the culture medium, whose ionic composition in K^+ is similar to that of the treated cells, allows to equilibrate the intracellular pH with the pH of the medium by creating a membrane antiport K^+/H^+.

Therefore, as a first step, the calibration solutions are prepared so that they contain a concentration of 90 mM of K^+ ions and 5 μM of nigericin. The pH is adjusted by adding HCl or

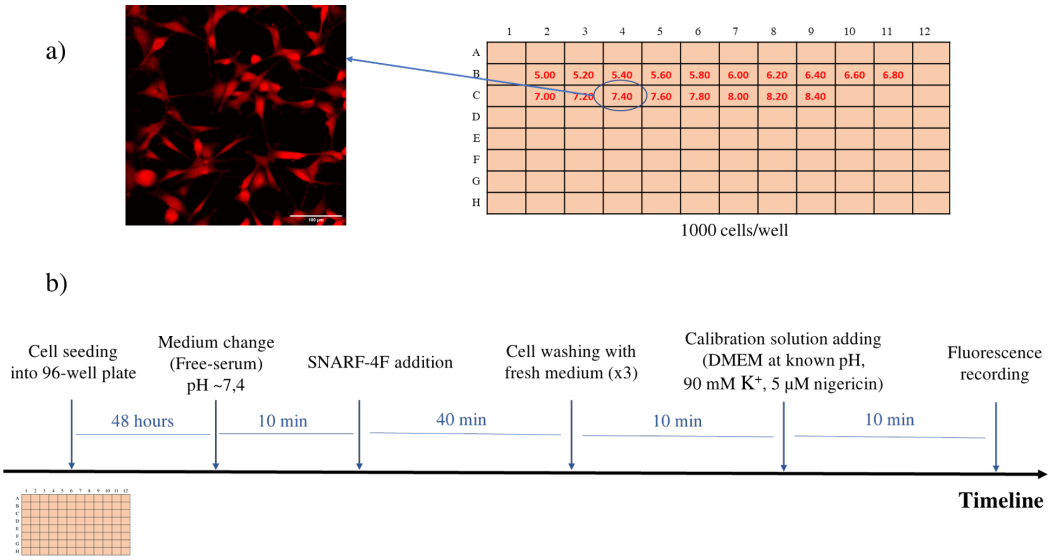

FIGURE 3.10: a) Cells were seeded at a concentration of 1000 cells/well in a flat ClearLine® plate (96 wells). Confocal fluorescence images were recorded after loading cells with the SNARF-4F probe using an excitation wavelength of 514 nm. b) Experimental timeline to calibrated the intracellular pH of glioma cells.

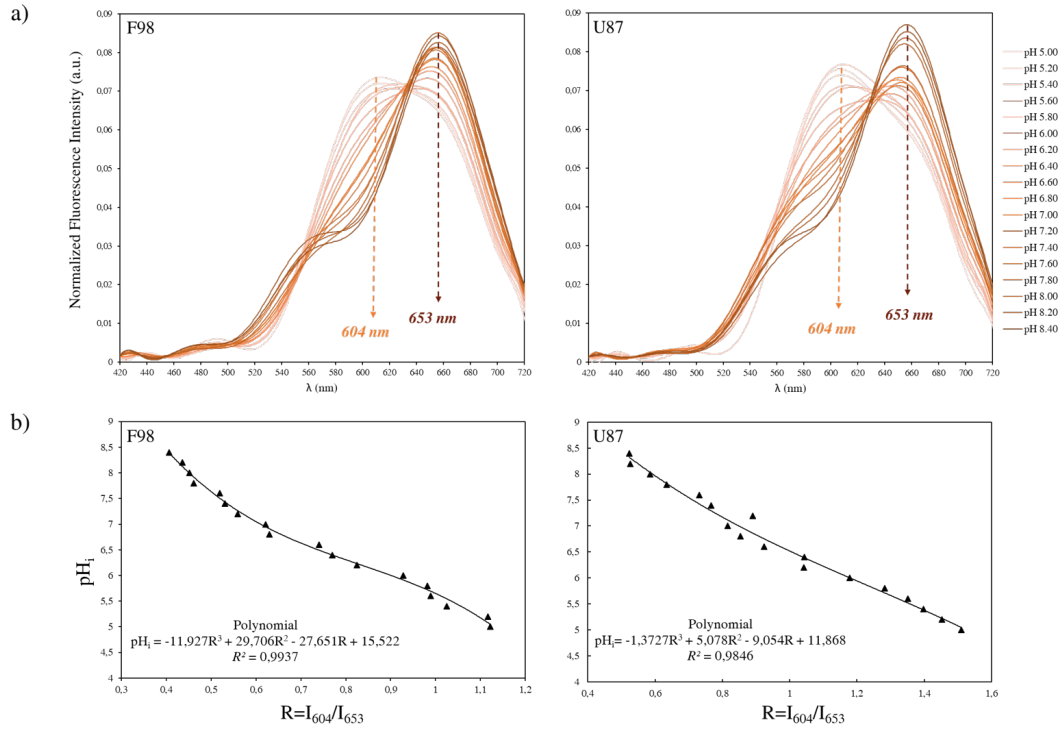

FIGURE 3.11: Calibration of SNARF-4F in F98 and U87 cells. a) Calibration emission spectra of SNARF-4F within F98 and U87 cells. The pH-controlled DMEM medium contained 90 mM of K^+ ions and the intracellular pH was equilibrated with the extracellular by the addition of nigericin. Excitation wavelength was 514 nm. b) The calibration curves of the intracellular pH produced with the SNARF-4F probe in the F98 and U87 cells. These curves are obtained from the fluorescence emission ratios (I_{604nm}/I_{653nm}) recorded for each pH value.

NaOH in order to obtain solutions in a pH range of 5 to 8.4. Once loaded with the pH probe, the cells were exposed to different calibration solutions with different pH values. 10 minutes later, the fluorescence of the probe was examined using an excitation light at 514 nm and the fluorescence emission was recorded in the 420-720 nm range (Figure 3.10). Figure 3.11 shows the pH-dependent emission spectra of SNARF-4F in U87 and F98 cells at various pH values of the calibration DMEM solution. In such conditions, the intracellular pH value is equal to the pH value of the calibration solution (pH_i=pH_e). The transition from one pH_i value to another is accompanied by a corresponding variation in the fluorescence intensity ratio R= I_{604nm}/I_{653nm}. Each pH_i value corresponds to a fluorescence intensity ratio allowing to plot the calibration curve: R = f(pH_i). The calibration curves obtained are presented in Figure 3.11 (b).

3.2 BCECF

Introduced by Tsien et al. in 1982 (Tsien, 1981), the 2',7'-bis(carboxymethyl)-5(6)-carboxyfluorescein probe (BCECF, Figure 3.12 (a)) is the most widely used fluorescent probe for intracellular pH measurement. Based on a fluorescein core, it has the advantages of a high fluorescence quantum yield in basic medium (84%) and a pK_a equal to 7.0 adapted to physiological pH. Thanks to its 4 carboxylate groups deprotonated at neutral pH and therefore carrying a negative charge, the fluorophore is well retained in the cell, which prevents a dilution of the signal throughout the organism. These same negative charges, on the other hand, prevent entry into the cell. It is therefore necessary to protect the carboxylate groups in the form of acetoxymethyl esters. These are then cleaved by esterases present in the cytoplasm.
The emission spectrum characteristics of BCECF after in vitro excitation with several wavelengths are reported in Figure 3.12 (b). The fluorescence intensity of the probe depends on the pH value, and it reaches a maximum amplitude when the probe is excited at about 488 nm. At the same time, the analysis of the emission spectrum of the probe shows that the fluorescence intensity is also sensitive to pH and that this intensity is maximum when the emission wavelength is equal to 537 nm. The shape of the emission spectra remains constant and the use of a single excitation wavelength (488 nm) does not make it possible to obtain an emission signal indicating only the variations in fluorescence linked to a change in pH_i. The decrease in fluorescence intensity can be the result of a bleaching of the probe following repeated excitations, or a direct consequence of the decrease in the concentration of BCECF due to leakage phenomena. In order to record only fluorescence variations due to pH variations, a second excitation wavelength is used, at 440 nm. The fluorescence intensity, at this wavelength, is independent of pH and reflects the intracellular probe concentration. Therefore, the use of the fluorescence ratio (R = F488/F440) makes it possible to avoid any variations in fluorescence independent of pH.
In the case of a confocal microscope, 440 nm Helium–Cadmium laser line is used for excitation in combination with the 488 nm Argon laser line. Thus, this combination allows pH measurement in the terms of the ratio of fluorescence intensities (R=F488/F440) measured at these two excitation wavelengths and fixed emission at 537 nm.

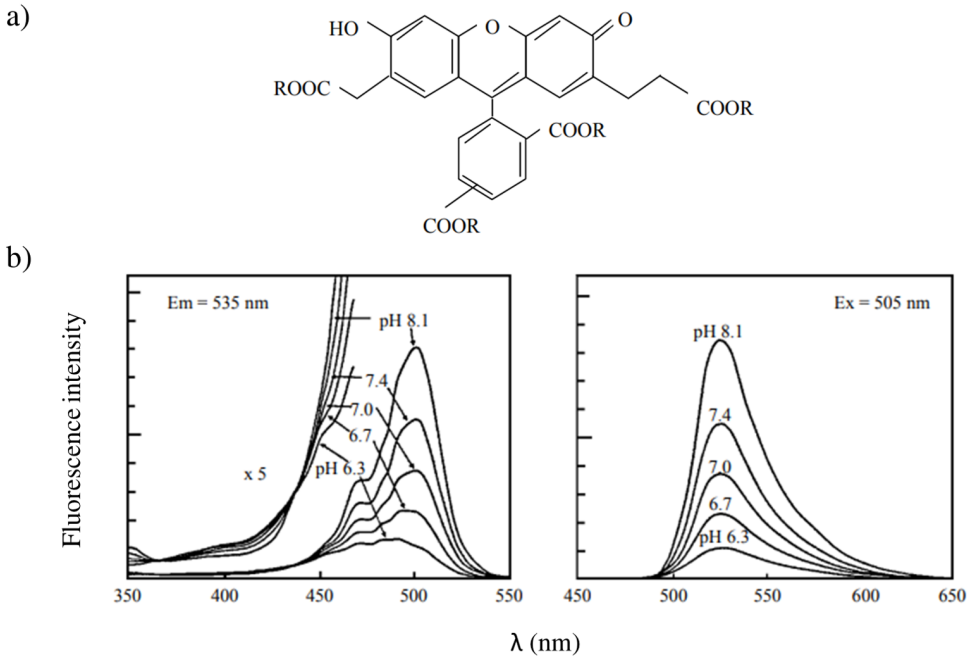

FIGURE 3.12: Specific characteristics of the BCECF. a) Structure of the BCECF molecule. The presence of carboxylic radicals gives the molecule a pK close to 7.00. In its permeant form, the R radicals are acetoxymethyl ester groups (Rink, Tsien, and Pozzan, 1982). b) The excitation spectrum represents the variation in fluorescence intensity as a function of pH. We note that the maximum amplitude of the response is obtained for an excitation at ~ 488 nm. The 5× enlargements of the region below 470 nm clearly illustrate the excitation isosbestic point at ~ 440 nm. The emission spectrum shows that the intensity of the emitted light also increases with pH. This variation is greatest around 537 nm (Loiselle and Casey, 2010).

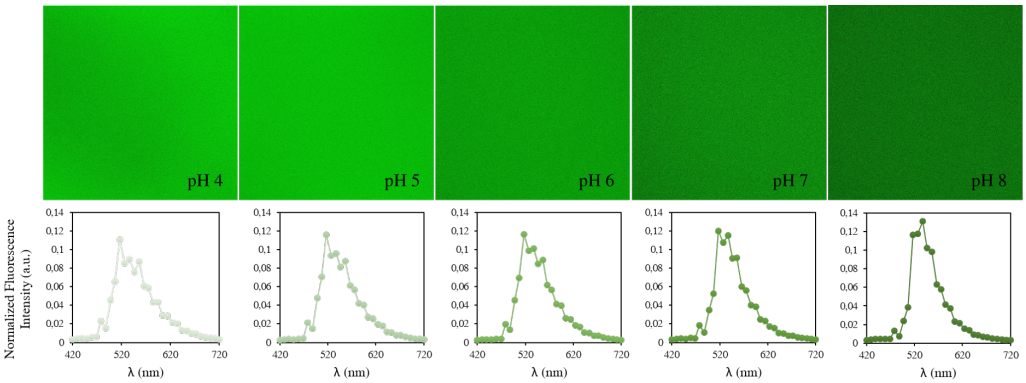

FIGURE 3.13: Fluorescence images of BCECF in DMEM medium from pH 4.0 (left) to pH 8.00 (right) under 405 nm excitation. For each pH, we present the average emission spectrum over the entire image (2048×2048 pixels).

On our Zeiss LSM 710 confocal microscope, 6 laser lines are present: Diode 405 nm, Argon 458 nm, 488 nm, 514 nm and Helium-Neon 543 nm, 633 nm. Therefore, one of the appropriate excitation wavelengths, i.e. 440 nm, used to ratiometrically measure the intracellular pH with the BCECF probe is missing. As a dual-excitation probe, BCECF must be excited by two excitation wavelengths. therefore, the first question that we asked was about the possibility of using of an another excitation wavelength, than the 440 nm laser, in combination with the 488 nm laser or even the possibility of using two other lasers, which do not even include the 488 nm, among the lasers we have. Hence the call for a study to find a method of intracellular pH measurement that overcome the material limitations of our confocal microscope. This study will be detailed in the following paragraphs.

3.2.1 In vitro fluorescence spectra of BCECF, non-permeable version

As mentioned above, to ratiometrically measure the intracellular pH, BCECF is typically excited by two wavelengths: 440 nm and 488 nm. As we do not have the laser 440 nm, the goal was first to know if there is another excitation that can be used in combination with the 488 nm laser or whatever two other lasers among the lasers we have. Therefore, the first step of our study consists in finding among the lasers that we have those which can be used to excite the BCECF. To answer that, an initial experiment was performed using the non-permeable version of BCECF (5μM) in a serie of pH-adjusted DMEM free-serum medium, from 4.0 to 8.4 with 0.2 pH increments. The fluorescence of the probe was examined at each of the six lasers installed on our confocal microscope and the fluorescence emission was recorded in the 420-720 nm range. We have found that among the six lasers, BCECF can be excited by four: 405 nm, 458 nm, 488 nm and 514 nm. Whether it is the excitation wavelength or the pH of the tested solution, the BCECF shows strong green fluorescence with a maximum emission intensity at around 537 nm (Figure 3.13). The emission spectra, of the non-permeable version of the BCECF, recorded at each excitation wavelength are shown in Figure 3.14. The analysis of the emission spectra shows that the longer excitation wavelength gives the higher fluorescence intensities in all emission wavelengths we explored (420–720 nm). Namely, 514 nm produced the highest fluorescence values. Whatever the excitation wavelength, the

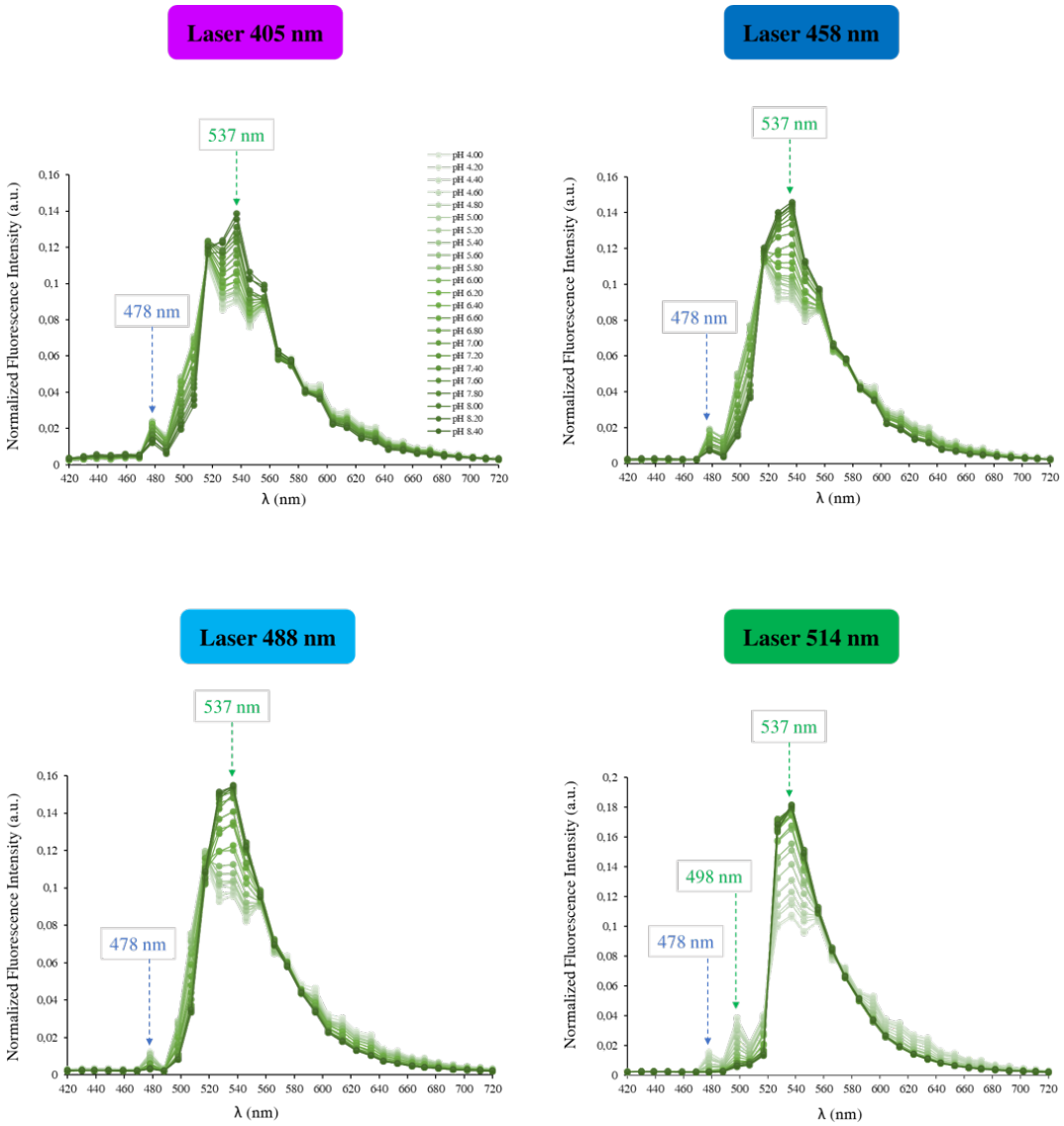

FIGURE 3.14: BCECF (5μM) emission spectra at 405 nm, 488 nm, 458 nm and 514 nm excitation wavelengths, in DMEM free-serum medium at various pH values. The pH of the medium was measured with a pH meter and adjusted to obtain a range of pH from 4.0 to 8.4 with 0.2 pH increments using 0.1 M HCl or 0.1 M NaOH solutions. The remarkable emission wavelengths taken for the ratiometric measurements are represented by arrows

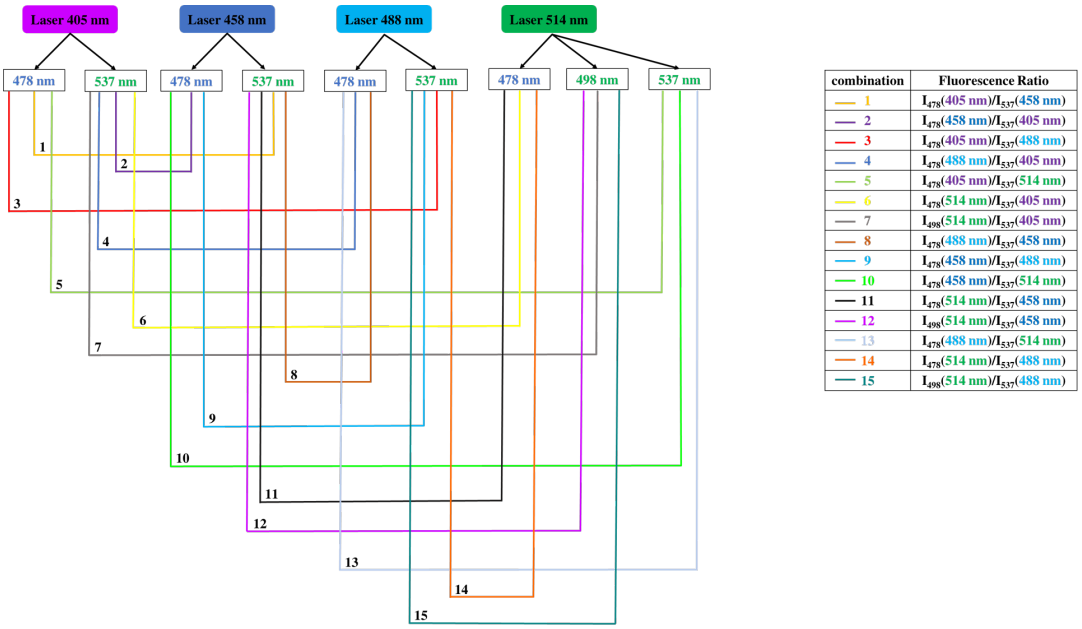

FIGURE 3.15: The 15 combinations made between two remarkable emission wavelengths noted on the emission spectra of the non-permeable version of the BCECF. For each combination, the ratio of fluorescence intensities measured at the two remarkable emission wavelengths is monitored as a function of pH.

fluorescence intensity of the probe is maximum when the emission wavelength is around 537 nm (red arrow). Another remarkable emission wavelength, common among all spectra, is noticed. It is located at 478 nm (blue arrow). In spite of this remarkable feature, its fluorescence intensity is small. The fluorescence intensities around 478 nm decrease when the pH increases, while those of around 537 nm increase at the same conditions. Only for the 514 nm laser, a third remarkable emission wavelength is noticed. It is located at 498 nm and responds to the pH changes similarly to 478 nm (green arrow).

As its name suggests, the ratiometric method is based on the use of a ratio between two fluorescence intensities measured at two emission wavelengths. A relationship between the pH and this ratio is therefore established. Starting from this principle, we suggested to measure the ratio between all the remarkable emission wavelengths noticed on the emission spectra of BCECF (Figure 3.14). The goal was to find a combination of two emission wavelengths allowing to detect the pH as a function of the fluorescence ratio. As the BCECF is used as a dual excitation probe, the two emission wavelengths are chosen separately from two different laser lines. In total, 15 combinations were made between the remarkable emission wavelengths. These combinations are shown in Figure 3.15. Every combination shows first the two laser lines used and therefore the emission wavelength chosen for each. For example the combination 1 (in yellow) shows that the two lasers used are 405 nm and 458 nm. For the 405 nm laser the emission wavelength is fixed at 478 nm while for the 458 nm laser the emission wavelength is fixed at 537 nm. Once the two emission wavelengths are fixed, the ratio (R) of the fluorescence intensities measured at these two emission wavelengths is monitored as a function of the pH. This allows us to construct for each combination the curve

Combination		Regression			
		Linear		Polynomial, degree 3	
		R^2	% error (δ)	R^2	% error (δ)
1	I_{478}(405 nm)/I_{537}(458 nm)	0,97	3,46	0,98	2,98
2	I_{478}(458 nm)/I_{537}(405 nm)	0,95	4,29	0,96	3,72
3	I_{478}(405 nm)/I_{537}(488 nm)	0,98	2,79	0,98	2,62
4	I_{478}(488 nm)/I_{537}(405 nm)	0,92	5,77	0,94	4,83
5	I_{478}(405 nm)/I_{537}(514 nm)	0,94	4,89	0,98	2,67
6	I_{478}(514 nm)/I_{537}(405 nm)	0,79	7,83	0,92	5,32
7	I_{498}(514 nm)/I_{537}(405 nm)	0,86	6,36	0,95	3,71
8	I_{478}(488 nm)/I_{537}(458 nm)	0,92	5,71	0,94	4,81
9	I_{478}(458 nm)/I_{537}(488 nm)	0,95	4,26	0,97	3,34
10	I_{478}(458 nm)/I_{537}(514 nm)	0,93	4,24	0,98	2,53
11	I_{478}(514 nm)/I_{537}(458 nm)	0,79	7,80	0,91	5,34
12	I_{498}(514 nm)/I_{537}(458 nm)	0,86	6,48	0,94	3,82
13	I_{478}(488 nm)/I_{537}(514 nm)	0,88	6,52	0,94	4,55
14	I_{478}(514 nm)/I_{537}(488 nm)	0,79	7,95	0,89	5,79
15	I_{498}(514 nm)/I_{537}(488 nm)	0,85	6,56	0,92	4,45

FIGURE 3.16: The coefficient of determination R^2 and the percent error δ for each regression applied on the data points of each laser combination. In green, the 4 best combinations with a coefficient of determination R^2 of 0.98 and a percent error smaller than 3%.

R = f(pH). The 15 curves are presented in the Annex 1. Above each curve is noted the corresponding combination. Statistically, two types of regression were used to estimate the relationship between the pH and the fluorescence ratio. The goal was to find a best-fit line that best expresses the relationship between the data points. To get a idea of how many data points fall within the results of the line formed by the regression equation, the coefficient of determination "R^2" or "R squared" was determined. The higher the coefficient, the higher the percentage of points crossed by the fit line. Among the 15 combinations, we found 4 combinations (1, 3, 5 and 10) with a coefficient of determination of 0.98 by applying a polynomial fit of degree 3. This means that 98% of the data points fall within the regression line. This higher coefficient is an indicator of a better goodness of fit for the observations.
Since we take a measurement on the pH of the DMEM medium which has a reference value according to the pH meter, the percent error δ makes it possible to evaluate the importance of the difference between the pH value effectively measured and the reference value. It is recommended to have a percent error in the range of 0-3%. The table 3.16 shows the coefficient of determination R^2 and the percent error δ obtained for each regression which made on the data points of each laser combination. The combinations 1, 3, 5 and 10 shows, for a given regression (marked in green in the table 3.16), a percent error lowest than 3%. This confirms the choice of the best lasers combination with the highest coefficient of determination anf the lowest percent error.
The four best combinations are presented in the Figure 4.21. It shows for each combination which two lasers must be used to excite the BCECF probe as well as the emission wavelength which must be fixed for each laser line in order to measure the fluorescence ratio. We have

found that the 405 m laser can be used, instead of the 440 nm laser, in combination with the 488 nm laser for ratiometric measurements of pH. The originality of this study is based on the different possibilities of exciting the BCECF probe in the case of pH measurements. In the literature, only one method has been proposed to measure the pH with the BCECF probe. It consists of using the 440 nm laser in combination with the 488 nm laser and fixing the emission intensity at 537 nm. It is said that "some problems are opportunities and solutions to other problems". Due to our material limitations, we have found several ways to excite the BCECF probe in order to ratiometrically measure the pH. The first way is to use the 405 nm laser in combination with the 458 nm laser and setting the emission wavelength at 478 nm for the 405 nm laser and at 537 nm for the 458 nm laser. In this case, a polynomial regression of degree 3 is applied on the data points (R^2=0,98, δ=2,98%). The second way consists of using the 405 nm laser in combination with the 488 nm laser and setting the emission wavelength at 478 nm for the 405 nm laser and at 537 nm for the 488 nm laser. In this case, a well-fitting linear regression results was obtained for the observed data (R^2=0,98, δ=2,79%). It's interesting to apply this excitation method since it is generally known that the fluorescence ratio is linearly related to the pH variation. The 3rd way to measure the pH is to use of the 405 nm laser in combination with the 514 nm laser by setting the emission wavelength at 478 nm for the 405 nm laser and at 537 nm for the 514 nm laser. In that event, a polynomial regression of degree 2 is applied on the data points (R^2=0,98, δ=2,66%). The last method allows us to use the 458 nm laser in combination with the 514 nm laser and setting the emission wavelength at 478 nm for the 458 nm laser and at 537 nm for the 513 nm laser. Here, a polynomial regression of degree 3 is applied on the data points (R^2=0,98, δ=2,53%).

BCECF	Laser 1	Laser 2	Emission wavelenght 1	Emission wevelenght 2	Fluorescence Ratio
Combination 1	405 nm	458 nm	478 nm	537 nm	$I_{478(405nm)}/I_{537(458nm)}$
Combination 3	405 nm	488 nm	478 nm	537 nm	$I_{478(405nm)}/I_{537(488nm)}$
Combination 5	405 nm	514 nm	478 nm	537 nm	$I_{478(405nm)}/I_{537(514nm)}$
Combination 10	458 nm	514 nm	478 nm	537 nm	$I_{478(458nm)}/I_{537(514nm)}$

TABLE 3.2: The spectral configurations of the 4 best laser combinations allowing ratiometric pH measurements with BECEF. Each combination shows the two excitation wavelengths to be used to excite the BCECF as well as the corresponding emissin wavelengths for the measurement of fluorescence ratios.

For our extracellular pH measurements, we chose the second method of excitation of the BCECF probe, which allowed us to apply a regression of smallest degree (linear) thus giving the lowest percent error. This method allows the implementation of the ratiometric pH measurement by exciting the pH probe with the 405 nm and 488 nm laser. The emission wavelength is fixed at 478 nm for the 405 nm laser and at 537 nm for the 488 nm laser. The calibration curves used to measure the extracellular pH is shown in Figure 3.17.

3.2.2 Intracellular pH calibration

Like SNARF-4F, the pH-dependent spectra of BCECF are significantly different when the probe is loaded into cells (Figure 3.18). Therefore, a calibration is carried out, for each cell

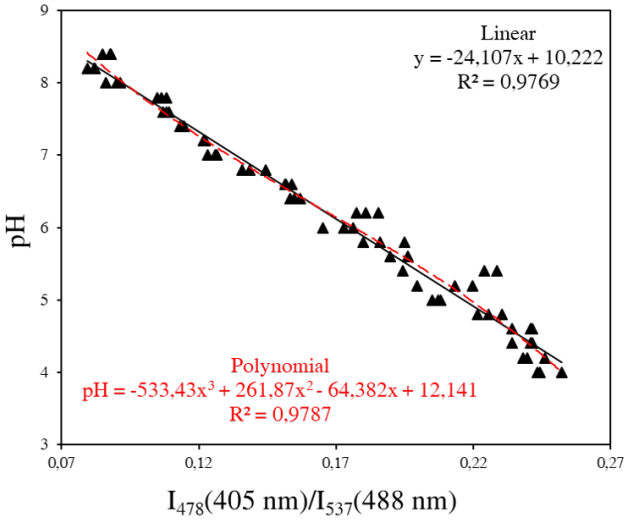

FIGURE 3.17: The calibration curve of the extracellular pH produced with the BCECF probe in the DMEM free-serum medium. The fluorescence of the probe was examined with two lasers: 405 nm and 488 nm. The emission wavelength was fixed at 478 nm for the 405 nm laser and at 537 nm for the 488 nm laser (N=3).

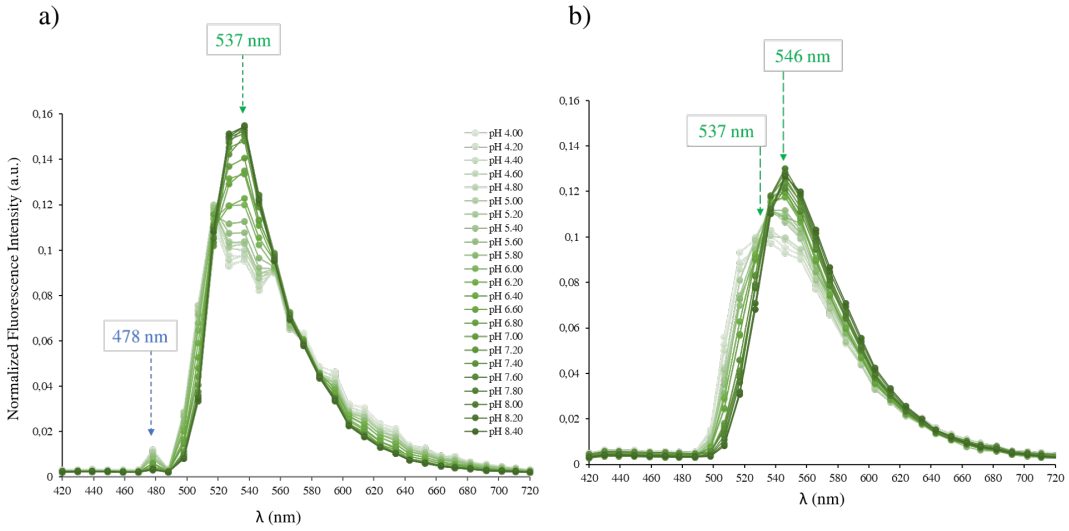

FIGURE 3.18: Difference between the emission spectra of BCECF in a) DMEM free-serum medium and b) in F98 cells at various pH values. Excitation wavelength was 488 nm.

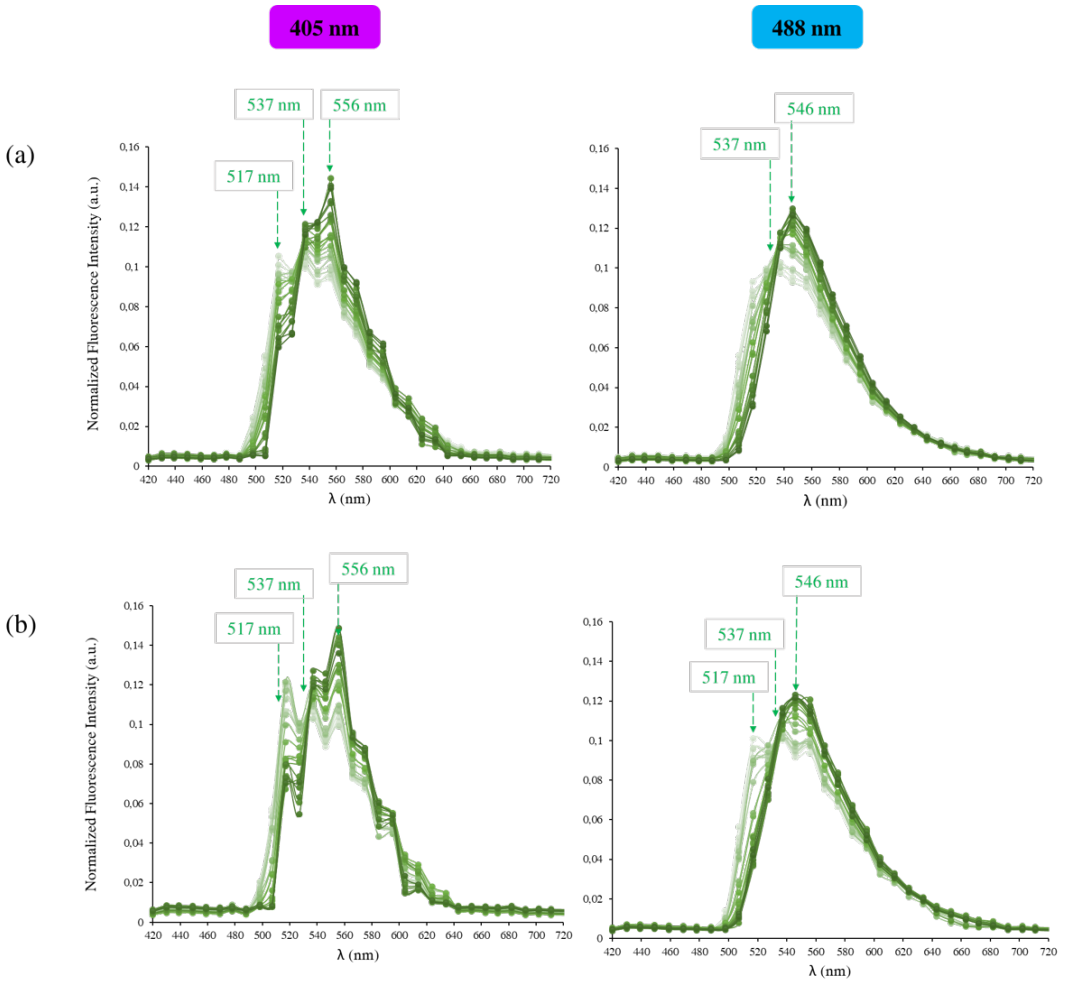

FIGURE 3.19: BCECF (5μM) emission spectra at 405 nm (left), 488 nm (right) excitation wavelengths, in (a) F98 and (b) U87 at various pH values. The remarkable emission wavelengths taken for the ratiometric measurements are represented by arrows.

line, using the DMEM free-serum medium containing 5 μM of nigericin, 90 mM of KCL, and adjusted to a pH range from 4.0 to 8.4 using 0.1 M HCl or 0.1 M NaOH solutions. Once loaded with the pH probe, cells were consecutively exposed to 405 nm and 488 nm laser lines. The fluorescence emission was recorded in the 420-720 nm range. Figure 3.19 shows the emission spectra of BCECF in U87 and F98 cells at various pH values of the calibration DMEM solution. When inside cells, the remarkable emission wavelengths noted on the emission spectra of the permeable version of BCECF have differed from those noted in the emission spectra of the non-permeable version of BCECF. Therefore, it is required to find among the first the two emission wavelengths adapted to the measurement of intracellular pH. Always based on the principle of the ratiometric method, a combination of two remarkable emission wavelengths may allow us to evaluate the intracellular pH as a function of the ratio of fluorescence intensities. In this context, we have analyzed all the combinations that can be made between two given remarkable emission wavelengths. For each cell line, the analyzed combinations are presented in the Figure 3.20. For each combination, the ratio of fluorescence

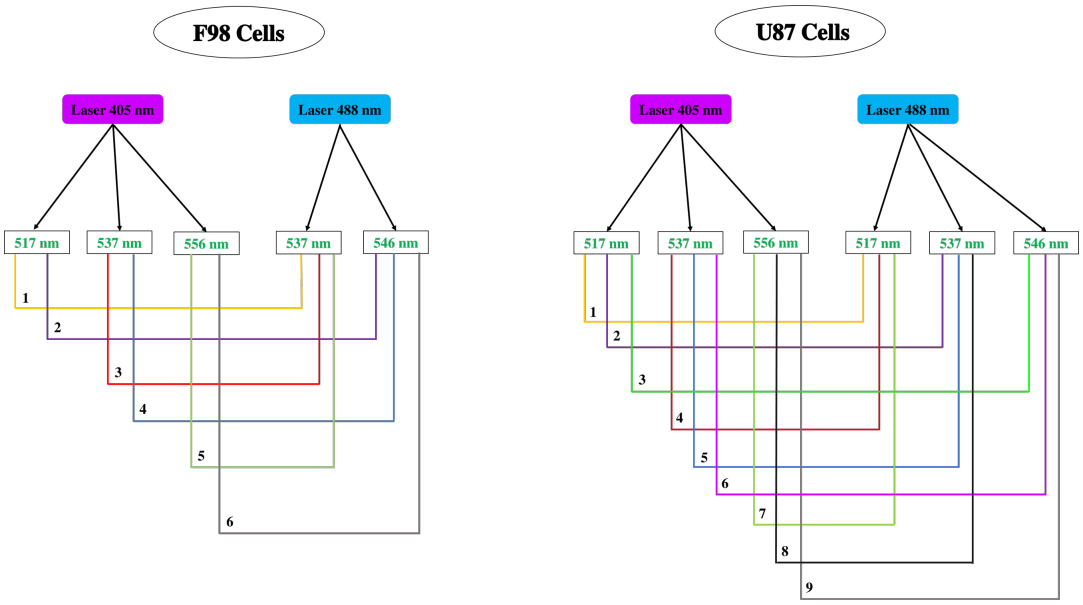

FIGURE 3.20: The combinations made, for each cell line, between two remarkable emission wavelengths noted on the emission spectra of the permeable version of the BCECF (BCECF-AM). For each combination, the ratio of fluorescence intensities measured at the two remarkable emission wavelengths is monitored as a function of pH.

intensities measured at the two remarkable emission wavelengths is monitored as a function of pH and the curve $R = f(pH_i)$ is thus constructed (Annex 2). As the analysis of the extracellular case, two types of regression (linear and polynomial) were used to estimate the relationship between the pH and the fluorescence ratio and to find the best-fit line that best expresses the relationship between the data points. The percent error δ was also calculated to evaluate the importance of the difference between the pH_i value effectively measured and the reference value. We have found that the best method to measure the intracellular pH of F98 cells is to set the emission wavelength at 517 nm for the 405 nm laser and 546 nm for the 488 nm laser. In this case the pH is monitored as a function of the fluorescnece ratio $R=I_{517nm}/I_{546nm}$. Whereas for U87 cells, the intracellular pH is measured by fixing the emission wavelength at 556 nm for the 405 nm laser and at 517 nm for the 488 nm laser. In this case the pH is monitored as a function of to the fluorescnece ratio $R= I_{517nm}/I_{556nm}$ (Figure 3.21).

3.3 Screening of the pH probes

As part of this study, two fluorescent probes were tested to measure the intracellular pH of glioma cells. In evaluating these probes, whole emission spectra, either in the extracellular or in cells, were analyzed.

SNARF-4F is a fluorescent pH probe that exhibits changes in spectral shape associated with its protonated and deprotonated forms in solution. When excited at 514 nm, solutions predominantly containing the deprotonated form (A) display a deep red long-wavelength band with a maximum situated at 668 nm, which drops and shifts to the yellow-orange upon acidification of the solution. The changes are accompanied by the appearance of a new band peaking

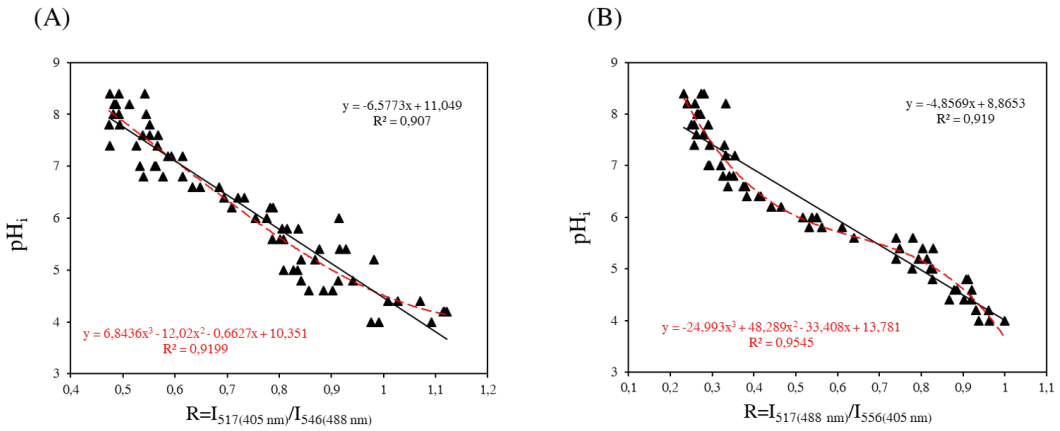

FIGURE 3.21: The calibration curve of the intracellular pH produced with the BCECF probe in (A) F98 and (B) U87 cells (N=3).

at 599 nm, which can be assigned to the fluorescence of the protonated species (HA). This shift between protonated and deprotonated species allows us to use the ratio of fluorescence intensities (R= I_{599nm}/I_{668nm}) from the probe at two emission wavelengths (599 nm and 668 nm) for more accurate pH determinations. Note that in the case of cells, these two emission wavelengths have minimally shifted to 604 nm and 653 nm. SNARF-4F is therefore used as a single excitation-dual emission probe where the excitation is performed at only one excitation wavelength and fluorescence emission is measured at two emission wavelengths. This approach is called emission ratiometric measurement. However, BCECF probe does not exhibit significant changes in the spectral shape between the protonated and deprotonated species and the analysis of the probe's emission spectra shows that the intensity of the emitted light is dependent on the pH as well as the environment of the probe such as the concentration, the photobleaching and the surrounding ions of the probe. Therefore, the use of one excitation wavelength does not make it possible to obtain the fluorescence variations only linked to a change in pH. A second excitation wavelength is then used. This approach is called excitation ratiometric measurement. With two excitations, the manipulation time with the BCECF will be 2 times longer than that of the SNARF-4F.

Due to material limitations on our confocal microscope, we have developed a method to measure the intracellular/extracellular pH with the BCECF probe, based on the available excitation wavelengths. We have found that the two excitation wavelengths 405 nm and 488 nm are the two appropriate wavelengths, among those available on our confocal, for pH measurements with the fluorescent probe BCECF. Therefore, Table 3.3 summarizes the spectral configurations for pH_e and pH_i measurements with the BCECF probe.

The pH probe, whether SNARF-4F or BCECF, was introduced into cells due to the acetoxymethyl ester group (AM). Once inside the cell, the ester is supposed to be hydrolyzed by ubiquitous intracellular esterases, releasing the proton-sensitive probe which is fluorescent and unable to permeate the membrane, thereby being trapped inside of the cell. In view of the results obtained in figure 3.22, we have found that the entry of BCECF-AM inside the cells and the action of esterases are more rapid than those of SNARF-4F-AM. 20 minutes of incubation is sufficient for BCECF while SNARF-4F requires at least 40 minutes. In

BCECF	Extracellular pH	Intracellular pH (F98 cells)	Intracellular pH (U87 cells)
Excitation 1	405 nm	405 nm	488 nm
Excitation 2	488 nm	488 nm	405 nm
Emission 1	478 nm	517 nm	517 nm
Emission 2	537 nm	546 nm	556 nm
Fluorescence ratio	$I_{478nm(405nm)}/I_{537nm(488nm)}$	$I_{517nm(405nm)}/I_{546nm(488nm)}$	$I_{517nm(488nm)}/I_{556nm(405nm)}$

TABLE 3.3: The spectral configurations for pH_e and pH_i measurements with the BCECF probe.

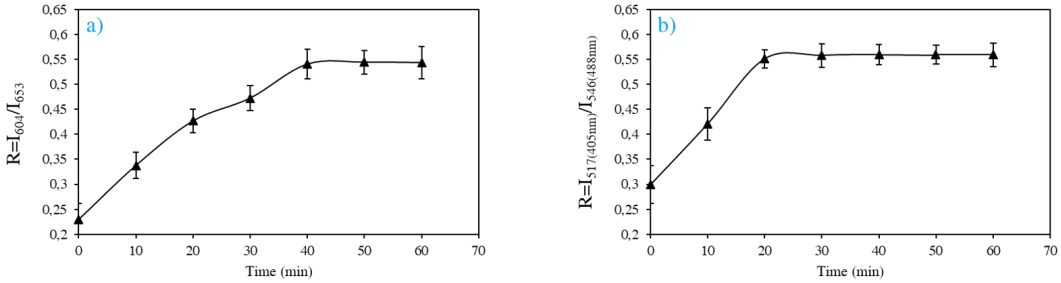

FIGURE 3.22: Determination of the incubation time of SNARF-4F-AM (a) and BCECF-AM (b) in F98 cells.

these cases, neither the fluorescence intensities nor the fluorescence ratio increase. It can be assumed that at these stages all of the probes have been deesterified.

Images of the cells incubated with the pH probes were taken by confocal microscopy before washing the culture medium (Figure 3.23). A significant background noise is noticed with the SNARF-4F-AM probe (Figure 3.23, a)) which requires a washing of the culture medium after the incubation period. On the other hand, the images obtained with the BCECF-AM show a strong fluorescence in the cells while the extracellular medium presents an almost negligible background noise (Figure 3.23, b)), without the need for washing the culture medium. This is a sign that the molecules are entering the cell extremely quickly. This very rapid internalization of the probe can be explained by, on the one hand, the small size of the probe which allows it to easily cross the cell membrane and on the other hand, by the low hydrophilicity of the molecule which makes it possible to retain this one in the cell.

SNARF-4F has been synthesized to be a promising fluorescent sensitive pH probe in the 6-7.5 pH range. This is in great agreement with the results that we have obtained after the spectral study of this probe in confocal microscopy. The emission ratiometric measurements with the SNARF-4F probe allowed us to conclude on the sensitivity of this probe in the range of pH 6.2-7.2 (Figure 3.24).

However, it was reported that BCECF probe allows measurements in the physiological pH range of 6.8–7.4. In such a case, the typical ratiometric method is to use the two excitation wavelengths 440 nm and 488 nm and fix the emission at 537 nm. Herein lies the distinguishing point of our study. Despite the material limitations on our confocal microscope, the method that we have developed using the available excitation wavelenghts has allowed us to increase drastically the range of validity of the BCECF probe. We have found that the use of the two excitations wavelengths 405 nm et 488 nm allows us to detect the intracellular pH in 4-8.4 pH range (Figure 3.24).

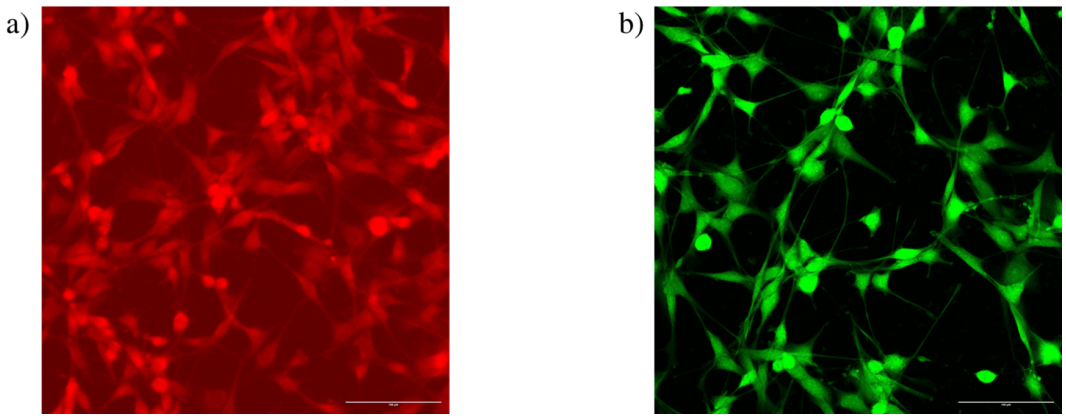

FIGURE 3.23: Fluorescence images of U87 cells incubated with a) SNARF-4F and b) BCECF. They were taken by confocal microscopy before washing the culture medium. Scale bar : 100 μm. 2048×2048 pixels.

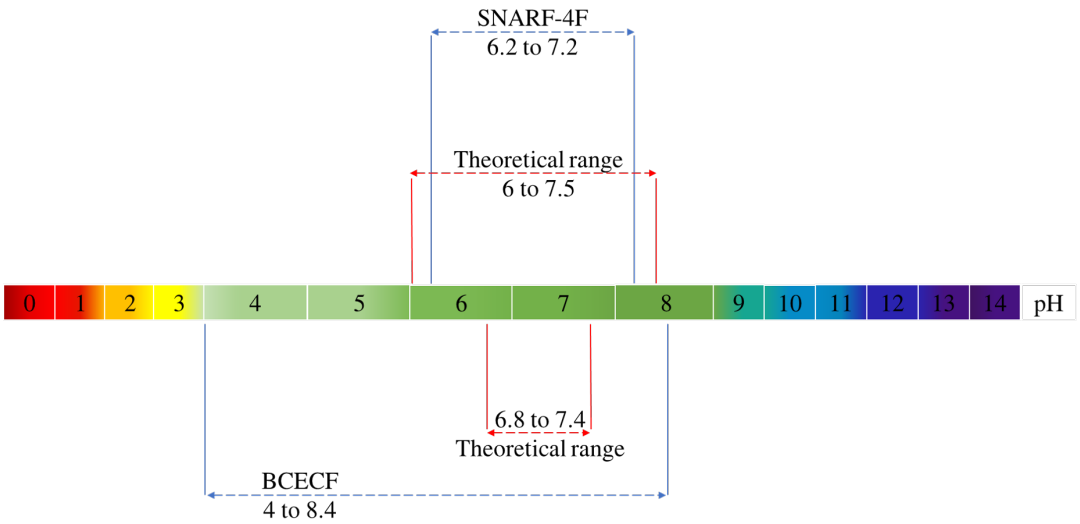

FIGURE 3.24: The ranges of validity of the BCECF and SNARF-4F probes.

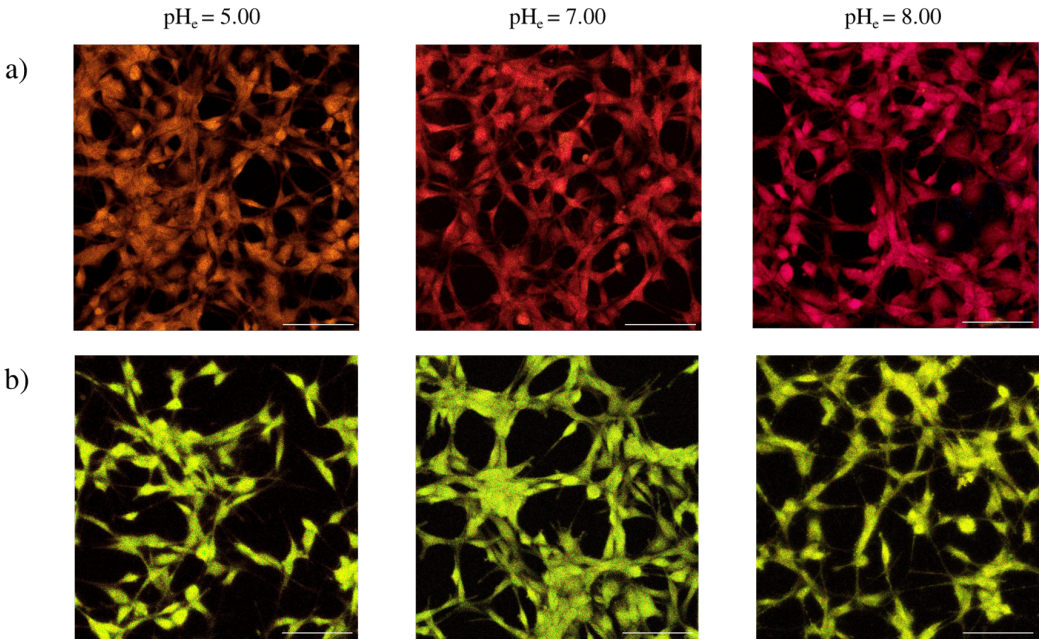

FIGURE 3.25: The change in the fluorescence signal of SNARF-4F after the loss of its physical characteristics. a) SNARF-4F signal before the loss of its physical characteristics. b) SNARF-4F signal after the loss of its physical characteristics.

In fact, it was not planned at the beginning of this study to use the BCECF probe. We have chosen from the start the SNARF-4F probe due to its ability to detect pH in the physiological range. However, during the experiments, a noticeable change in the SNARF-4F fluorescence signal was observed, rendering the probe unusable.

In a characteristic way, SNARF-4F exhibits a significant pH-dependent emission shift from yellow-orange to deep red fluorescence under acidic and basic conditions, respectively. In spite of that, the fluorescence shift of SNARF-4F has completely disappeared and a yellowish-green fluorescence was observed whatever the pH tested (Figure 3.25). First, we have assumed that SNARF-4F lost its physical and mechanical properties through degradation caused by more or less aggressive environmental factors such as storage temperature, humidity, light, chemical agents etc. Therefore, we have contacted Thermo fisher Scientific^{TM} to explain the problem encountered with the SNARF-4F, and they have sent us two boxes of this probe to test them. Unfortunately, we have found the same spectral problem encountered with the first box. As the 3 boxes come from the same lot, we have then assumed that this lot was expired. Another contact took place with thermo fisher Scientific^{TM} to know the production date of the new lot of SNARF-4F, they told us that it will be in 4-5 months. For this reason, we have asked to send us another fluorescent probe for the measurement of intracellular pH. Here, we have chosen the BCECF probe, the most widely used probe to measure the intracellular pH in the physiological range.

Although the BCECF probe was not intended to be used, we have found, according to the spectral method that we have developed, that it is the most suitable probe for characterizing

the regulatory capacity of intracellular pH of glioma cells. In summary, the data of each fluoescent probe as well as their characteristics have been grouped together to affirm our selection of the most suitable fluorescent probe for our project (Table 3.4).

	SNARF-4F	**BCECF**
Advantages	Short acquisition time (1 laser)	Reasonable price The most widely used High aqueous solubility Rapid internalization Wide range of pH (4- 8.4)
Disadvantages	High price long incubation time Problem of dissolving (significant background noise) Restricted pH range (6.2-7.2)	Long acquisition time (2 lasers)
Conclusion	Discarded	Selected

TABLE 3.4: Characteristics of pH-sensitive fluorescent probes

Chapter 4

Evaluation of the pH drift in the culture medium used for cell incubation during *in vitro* studies

4.1 Introduction

A cell culture medium is essentially composed of mineral salts, amino acids, vitamins and energy elements, each of which performs a specific function (Table 4.1). These elements act on the growth and adhesion of cells, the osmotic balance and the pH of the medium. However, other elements are added to the cell culture medium so that the cells can proliferate. In this section we are interested in the buffering capacity of the culture medium which thus characterizes the capacity to buffer the pH, to limit its modifications and variations. DMEM (Dulbecco's Modified Eagle Medium) is the culture medium used for our cell experiments.

Basic elements	Function	Added elements	Function
Amino acids	Growth, viability	Antibiotics	Antibacterial
Vitamins	Proliferation	Serum	Growth, adhesion
Mineral salts	osmotic balance membrane potential	Buffer	pH stabilization
Carbon source	Growth, oxidative stress		

TABLE 4.1: Function of basic and added elements defining a cell culture medium

4.2 The buffer system

Let's first consider the blood buffer system (Figure 4.1).
The body consumes sugars and fats, uses oxygen and produces water and carbon dioxide. When these reaction are not complete, weak metabolic acids are formed, leading to a decrease in blood pH. The bicarbonate buffer system is an acid-base homeostatic mechanism involving the balance of bicarbonate ion (HCO_3^-) and carbon dioxide (CO_2) in order to maintain a constant pH in the blood and duodenum, among other tissues, in order to support proper metabolic functions. Carbon dioxide (CO_2) reacts with water (H_2O) to form carbonic acid

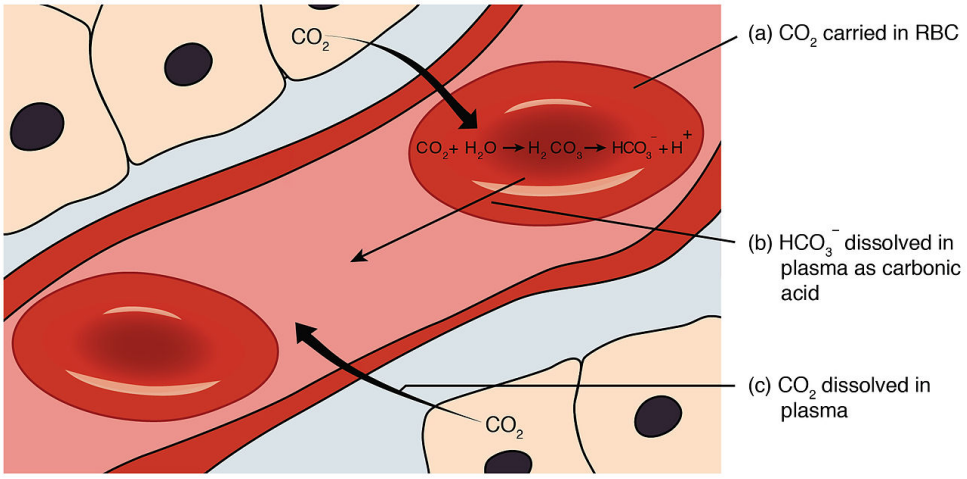

FIGURE 4.1: Carbon dioxide, a byproduct of cellular respiration, is dissolved in the blood, where it is taken up by red blood cells (RBC) and converted to carbonic acid (H_2CO_3) by carbonic anhydrase. Most of the carbonic acid then dissociates into bicarbonate (HCO_3^-) and hydrogen ions (H^+) (https://courses.lumenlearning.com/suny-dutchess-ap1/chapter/transport-of-gasesno-content/).

(H_2CO_3), which in turn rapidly dissociates to form bicarbonate ion (HCO_3^-) and a hydrogen ion (H^+) as shown in the following reaction (Meldrum and Roughton, 1933; Widmaier, Raff, and Strang, 2014; Oxtoby, Gillis, and Butler, 2015):

$$CO_2 + H_2O \rightleftharpoons H_2CO_3 \rightleftharpoons H^+ + HCO_3^- \tag{4.1}$$

As with any buffer system, the pH is balanced by the presence of both a weak acid (e.g. H_2CO_3) and its conjugate base (e.g. HCO_3^-) so that any excess acid or base introduced into the system is neutralized: In tissues, cellular respiration produces carbon dioxide as a waste product. As one of the primary roles of the cardiovascular system, most of this CO_2 is rapidly removed from the tissues by its hydration to bicarbonate ion (Sadava et al., 2014). The bicarbonate ion present in the blood plasma is transported to the lungs, where it is dehydrated into CO_2 and released during expiration. These hydration and dehydration conversions of CO_2 and H_2CO_3, which are normally very slow, are facilitated by carbonic anhydrase (CA) in the blood and duodenum. While in the blood, the bicarbonate ion serves to neutralize acid introduced into the blood by other metabolic processes (e.g. lactic acid, ketone bodies). Similarly, all bases (e.g. urea resulting from protein catabolism) are neutralized by carbonic acid H_2CO_3.

The most active blood buffering system is the CO_2/bicarbonate buffer which accounts for 75% of the buffering capacity. CO_2 stabilizes the pH at values compatible with cell activity, i.e. between 7.35 and 7.45 (Hamm, Nakhoul, and Hering-Smith, 2015). Failure of the buffer system leads to acid-base imbalance, such as acidemia (pH < 7.35) and alkalemia (pH > 7.45) in the blood (Rhoades, 2013).

In cell culture (Figure 4.2), an incubator is used to maintain 5% CO_2 into the atmosphere,

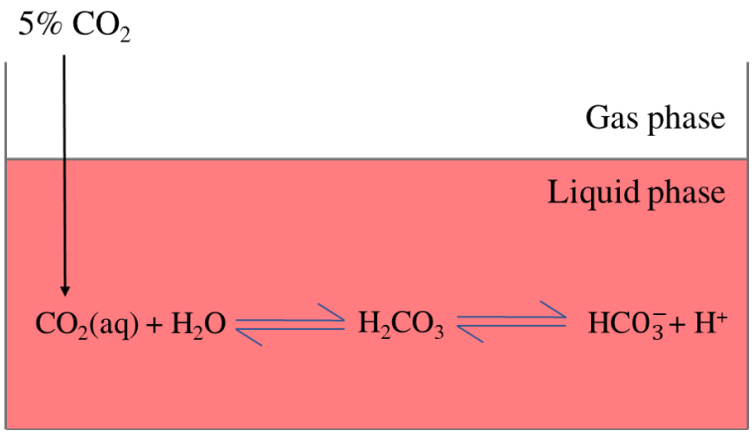

FIGURE 4.2: Mechanism of CO_2 buffering system in cell culture.

which means that the partial pressure of CO_2 corresponds to:

$$P_{CO_2} = \frac{\%\,CO_2}{100} \times Atm = 0.05\,Atm = 5.06\,kPa \tag{4.2}$$

Therefore, the concentration of aqueous CO_2, [CO_2(aq)], is determined using Henry's law:

$$[CO_2(aq)] = K_{CO_2} \times P_{CO_2} = 3.0 \times 10^{-2}\,\frac{mole}{L.Atm} \times P_{CO_2}(Atm) = 1.5 \times 10^{-3} M \tag{4.3}$$

Where K_{CO_2} is the Henry's constant of CO_2 (3.0x 10^{-2} $\frac{mole}{L.Atm}$ at 37°C in blood/culture medium).
Thus, the pH of the culture medium depends on the concentration of carbonate ions present in solution. In the case of DMEM (0.044M of HCO_3^-), the pH is, using the equation of Henderson–Hasselbalch:

$$pH = 6,1 + \log\frac{[HCO_3^-]}{[CO_2(aq)]} = 7.56 \text{ at } 37°C \tag{4.4}$$

which is slightly above the physiological range around 7.4. However, in most cases, the lactic acid and CO_2 evolved by growing cultures and will offset and correct this high pH. This is especially the case when working with high density cultures in DMEM or with particularly fast growing cultures. Otherwise, it is recommended to use a higher percentage of CO_2. In theory, DMEM requires 10% of CO_2, but most cell culture protocols set the value to 5% CO_2 with this medium and there is little information available to advise on the impact of using higher CO_2 concentrations with DMEM.

4.3 DMEM pH Drift

During confocal experiments, cells were seeded at low concentration in a 96-well plate (1000 cell/well, 200 µL/well) and incubated in a humidified atmosphere of 5% CO_2 at 37°C. When handling with a pH of 7.4, an excessive increase in the pH of the DMEM was noticed. This

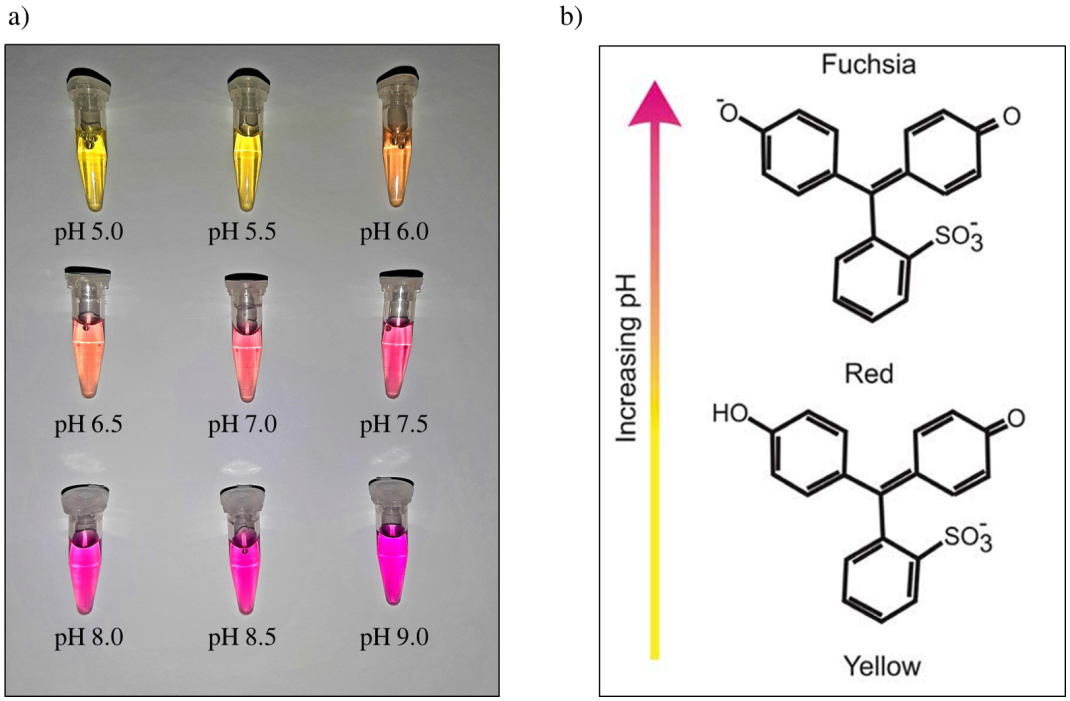

FIGURE 4.3: Phenol red is commonly used as a visible pH indicator of cell culture media. a) Phenol red turns from yellow to bright fuchsia from acid pH to alkaline pH, at physiological pH it gives an orange-red color to culture media. Image b (taken from Held, 2018) shows the structure of phenol red.

increase in pH was first noticeable from the color of the phenol red present in the solution. In fact, phenol red, also known as phenolsulfonphthalein, is a visible pH indicator that exhibits a gradual transition from yellow to fuchsia from acidic to alkaline pH (Figure 4.3). Therefore, with an initial pH of 7.4, a fuchsia color of the culture medium was observed after 8 hours, suggesting a pH above 8.0. With the pH meter, we found a value of 8.28. In order to know if the presence of cells is responsible for this increase in medium pH, comparisons were made between plates with cells (U87 and F98) and a plate without cells. Cells were seeded at a density of 1000 cells/well and allowed 48 hours for attachment and used the following day for testing. After incubation with 5 µM of BCECF, cells were washed 3 times with fresh medium and thus were incubated with the pH desired for observation. For the plate without cells, we simply put the pH to be tested in the wells. The 3 plates (plate of U87 cells, plates of F98 cells and plate without cells) are all maintained at 5% CO_2 and 37°C. Media with a pH of 5.00, 6.00 and 7.40 were tested. Thus, pH measurements of the medium were performed every 2 hours for 8 hours using the pH meter in the cases of the plates without cells and the BCECF probe in the cases of the plates with cells. Another measurement was also made on a plate without cells, outside the incubator and at room temperature. The results of the measurements are shown in Figure A.2. Firstly, the initial pH of the DMEM medium increases over time for all the conditions performed and, the pH measured outside the incubator is significantly higher (~ 0.04% CO_2 and ~ 20°C). At 5% CO_2, and at 37°C, the 3 curves (F98 cells, U87 cells and without cells) are almost identical, thus suggesting that the pH drift is independent of the cells. The increase in pH is significant when the initial pH of the medium is 7.40 (+0.88 pH

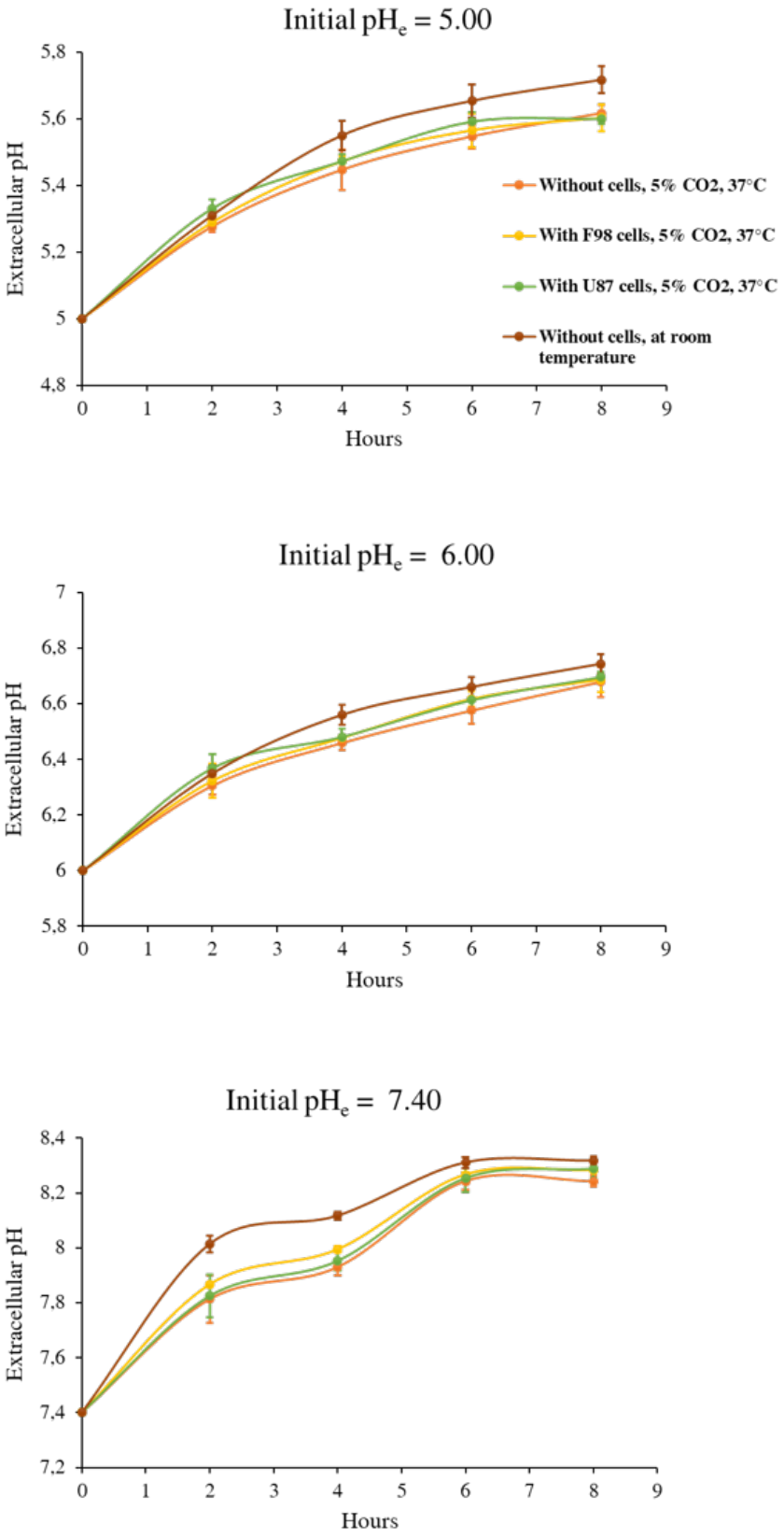

FIGURE 4.4: pH drift of DMEM medium incubated under different conditions. Media with a pH$_e$ of 5.00, 6.00 and 7.40 were tested (N=3).

units over 8 hours). An increase of about 0.63 pH units was noticed for an initial medium pH of 5.00, and about 0.70 pH units for an initial medium pH of 6.00. This is explained by the fact that DMEM medium is buffered for high CO_2 (10%). Reducing the CO_2 level (5% in our case) decreases the amount of H^+ ions generated by the hydration of CO_2, pushing the equilibrium (equation 5.1) towards a higher $[HCO_3^-]$ and lower $[H^+]$, that is, a more basic medium.
In order to know if the medium pH reaches a steady state (or equilibrium) after 8 hours, or if it continues to change beyond 8 hours, we used a simple method (described in the following paragraph) allowing to predict the medium pH at equilibrium. This method is based on the initial concentrations of both reactants and products in reaction (5.1) and makes it possible to describe the progress of this reaction in terms of the evolution of the quantities of the species over time.

4.4 Predicted pH at equilibrium

As already seen, pH is defined by the following equation:

$$pH = -\log_{10}[H^+] \tag{4.5}$$

where $[H^+]$ denotes the molar hydrogen ion concentration. The latter is therefore given by:

$$[H^+] = 10^{-pH} \tag{4.6}$$

At equilibrium,

$$pH_{eq} = -\log_{10}[H^+]_{eq} \tag{4.7}$$

and

$$[H^+]_{eq} = 10^{-pH_{eq}} \tag{4.8}$$

where pH_{eq} denotes the pH of the aqueous solution at equilibrium and $[H^+]_{eq}$ denotes the molar hydrogen ion concentration at equilibrium.
Moreover, when the concentration values of all the substances at equilibrium are known, then it is possible to calculate the equilibrium constant (K_{eq}) given by the following equation:

$$K_{eq} = \frac{[HCO_3^-]_{eq} \times [H^+]_{eq}}{[CO_2(aq)]_{eq}} \tag{4.9}$$

Where, $[HCO_3^-]_{eq}$ and $[CO_2(aq)]_{eq}$ represent the concentrations of HCO_3^- and $CO_2(aq)$ at equilibrium, respectively.

For culture medium at 37°C,

$$K_{eq} = 8.0 \times 10^{-7} \tag{4.10}$$

Therefore, using the expressions of K_{eq}, it is necessary to know the $[HCO_3^-]_{eq}$ and $[CO_2(aq)]_{eq}$ to find then $[H^+]$, or in other words the pH, with equation (4.9). However, it is sometimes impossible to experimentally know all the concentrations of the substances present at equilibrium. If one knows the initial concentration of reactants and products, it is possible to predict all equilibrium concentrations algebraically. This is done using an Initial-Change-Equilibrium (ICE) table. An ICE table is a simple matrix formalism used to calculate the changing concentrations of reactants and products in reversible equilibrium reactions (Table 4.2). This method first lists the concentrations of both products and reactants, before any changes occur. This is the initial stage. Then, the change is listed, in the form of addition or subtraction of a specific concentration required for the reaction to reach equilibrium. Alternately, the addition or subtraction of an unknown amount is listed in the form of + or - x M, and the value of x is solved for. Note that the change of each quantity must be in accordance with the stoichiometry of the reaction. Finally, the equilibrium concentration is listed, which is the initial concentration after it has undergone the change described. Once this row is completed, its contents can be plugged into the equilibrium constant equation to solve x. This is algebraically written:

$$K_{eq} = \frac{([HCO_3^-]_i + x) \times ([H^+]_i + x)}{[CO_2(aq)]_i - x} = 8.0 \times 10^{-7} \tag{4.11}$$

Starting from a given pH, and knowing the initial concentrations of the chemical species in question, we can therefore solve the quadratic equation obtained whose unknown is x, and therefore find the concentration of H^+ ions at equilibrium ($[H^+]_{eq}$= $[H^+]_i$ + x) and consequently the equilibrium pH (Equation 4.7). Table 4.3 summarizes the predicted pH at equilibrium for each initial pH tested, from 5.0 to 8.4 with 0.2 pH increments. Using the fit equations of the experimental data (Figure 4.5), one can predict the time required to reach the equilibrium state (Table 4.3).

Chemical species	CO_2	H^+	HCO_3^-
Initial	$[CO_2]_i$	$[H^+]_i$	$[HCO_3^-]_i$
Change	-x	+x	+x
Equilibrium	$[CO_2]_{eq}$=$[CO_2]_i$ - x	$[H^+]_{eq}$= $[H^+]_i$ + x	$[HCO_3^-]_{eq}$ =$[HCO_3^-]_i$ + x

TABLE 4.2: An useful tool in solving equilibrium problems is an ICE Table (Initial-Change-Equilibrium Table). By using the balanced equation and the various initial concentrations, one can deduce all the missing concentrations or express them in terms of unknowns (variable x).

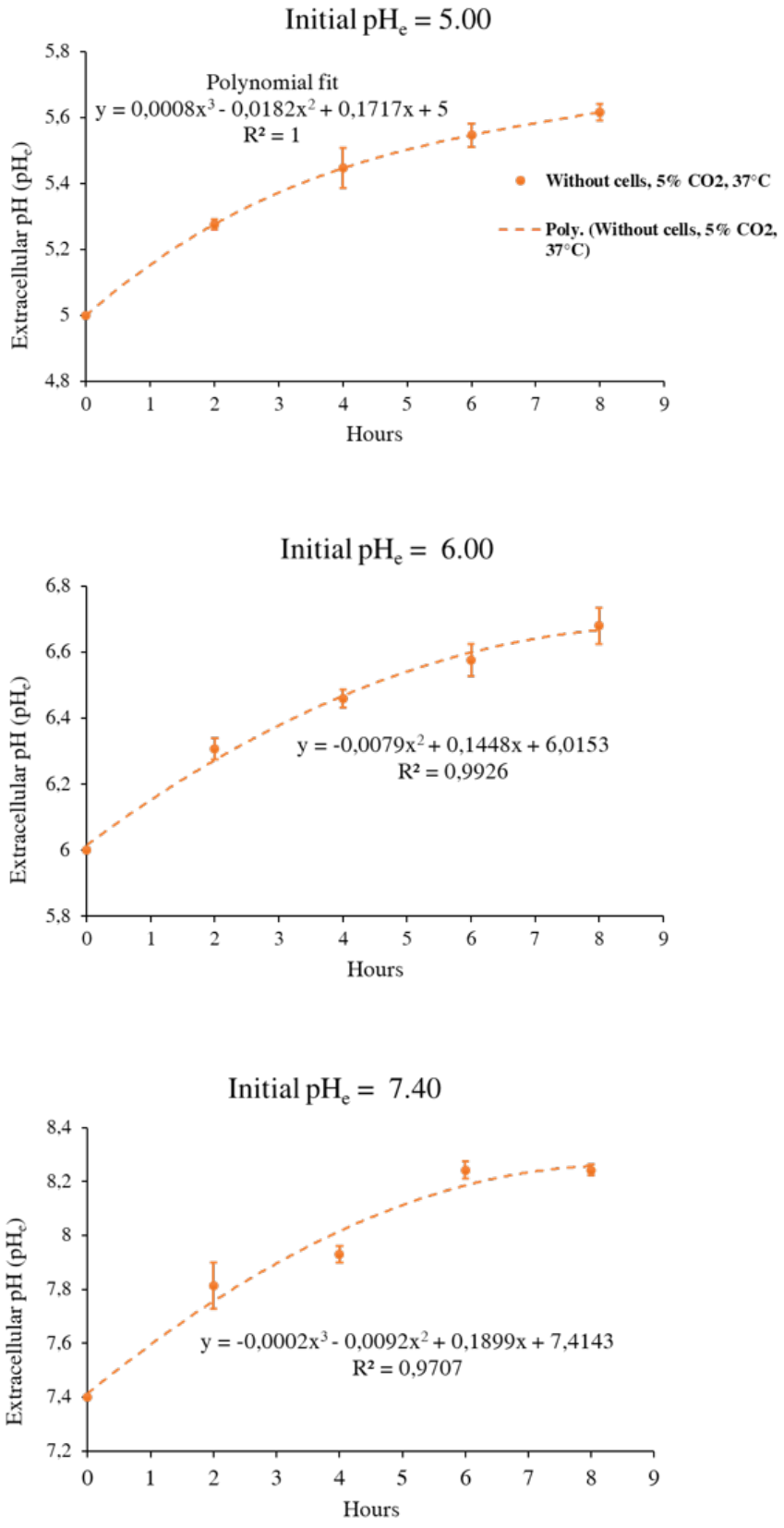

FIGURE 4.5: pH drift of DMEM medium (at 5% CO_2 and 37°C) and the fit equations of the experimental data used to predict the time taken to reach equilibrium.

Initial pH	pH at 8 hours	Predicted pH at equilibrium	Predicting time taken to reach equilibrium (hours)
5.00	5.61	6.07	14.2
5.20	5.74	6.16	12.9
5.40	5.84	6.32	12.2
5.60	5.95	6.65	12.4
5.80	6.30	6.78	11.8
6.00	6.68	6.91	9.9
6.20	6.87	7.08	9.7
6.40	7.12	7.33	9.3
6.60	7.46	7.53	8.4
6.80	7.53	7.67	8.9
7.00	7.56	8.07	11.0
7.20	7.88	8.15	10.7
7.40	8.24	8.52	8.9
7.60	8.45	8.63	9.2
7.80	8.47	8.71	9.5
8.00	8.47	8.76	9.2
8.20	8.55	8.81	9.1
8.40	8.57	9.01	10.9

TABLE 4.3: Predicted pH at equilibrium using the method of ICE table

4.5 Conclusion

With the classically used protocols, a relatively rapid and notable rise in the pH of the DMEM culture medium (Dublbecco's Modified Eagle's Minimum medium, PAN-Biotech) has been observed, and values greater than 8.5 could be reached after 8 hours of incubation.
After quantifying the pH drift of the DMEM culture medium, we conclude that increasing the CO_2 level of the incubator can be a worthwhile exercise to avoid significant pH fluctuations. Theoretically, returning to the equation of Henderson–Hasselbalch (Equation 4.4) increasing the CO_2 level decreases the ratio $\frac{[HCO_3^-]}{[CO_2(aq)]}$ and therefore the pH. However, a higher CO_2 percentage will displace oxygen in the incubator, reducing therefore the oxygen available to the cells. CO_2 percentages higher than 10% are not recommended. Additionally, bicarbonate supplementation may be effective in improving buffering performance. Increasing the concentration of HCO_3^- ions, decreases the ratio $\frac{[HCO_3^-]}{[CO_2(aq)]}$ and therefore the pH of the culture medium.
In our experiments, we always take into account the pH drift of culture medium to comment and interpret our results.

Chapter 5

Intracellular pH adaptation to changing extracellular pH

5.1 Introduction

It has become evident that the intracellular pH (pH_i) is an important regulator of metabolism and many cell functions such as cell proliferation (Kapus et al., 1994; Pouysségur et al., 1982; Denker et al., 2000), cell cycle progression (Turchi et al., 2000; Putney and Barber, 2003) and differentiation (Uzman et al., 1998; Boussouf and Gaillard, 2000). In general, the pH_i of normal cells is lower than the extracellular pH (pH_e), with pH_i and pH_e values typically in the ranges of 7.0–7.2 and 7.3–7.4, respectively. Tumor cells are generally associated with alkaline pH_i values of 7.1 to 7.6 and acidic pH_e values of 6.2 to 6.9 (Shirmanova et al., 2015; Gillies et al., 2002). This reversed pH gradient is considered to be a hallmark of cancer (Sharma et al., 2015), promoting tumor growth, invasion, and metastasis of cancer cells via various mechanisms. Therefore it appears that the measurement of pH_i in tumors presents an interest for monitoring the progression of cancers and the responses of cancer cells to various treatments.

In 1889, Stephen Paget introduced the "Seed and Soil" theory that metastasis did not occur randomly but rather responded to a cooperation between tumor cells (Seed) and their specific microenvironment (Soil) (Paget, 1889). For many years, Paget's concept was ignored and even more with the emergence of genetics (Heston, 1948; Strong, 1950). It was not until the mid seventies and onwards that a relatively small group of oncologists revisited Paget's hypothesis and paid attention to the interactions between cancer cells and the tumor microenvironment (Onuigbo, 1975; Fidler, 2003). Auerbach (Auerbach, 1988), for example, cites Paget: "*The best work in the pathology of cancer is done by those studying the nature of the seed. They are like scientific botanists; and he who turns over the records of cases of cancer is only a ploughman, but his observations of the properties of the soil may also be useful*". Auerbach then express his own opinions about cancer researchers who study the tumor microenvironment: "*Those individuals who study the properties of the host environment should not be ignored. Not only are the observations of the 'soil' useful, they provide essential information without which we will not be able to understand the nature of the metastatic process*". A huge increase in the number of publications dealing with the

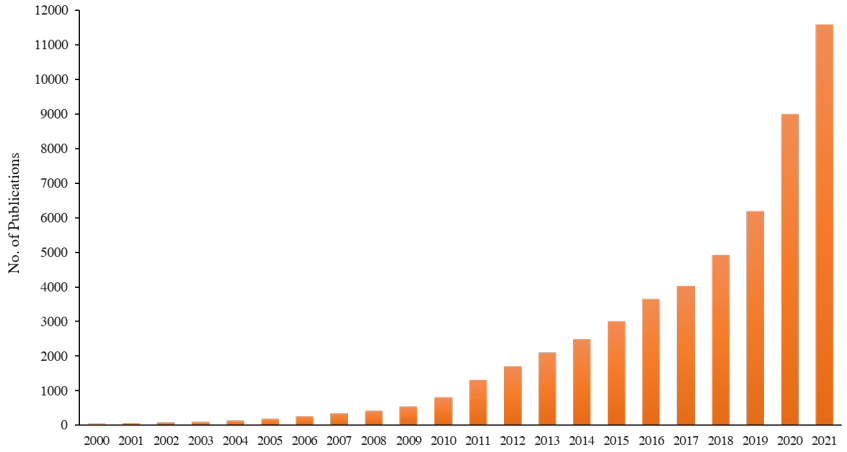

FIGURE 5.1: Evolution of the number of publications related to the tumor microenvironment during the period: 2000-2021. Results obtained from the Pubmed database by searching by keywords "Tumor microenvironment" or "Tumour microenvironment".

tumor microenvironment occurred from 2000 to 2021 (Figure 5.1). Moreover, a recent study shows that the majority of cancer-related deaths are the result of resistance of metastases to conventional treatments or therapies used successfully in the treatment of primary cancers (Wang, Zhang, and Chen, 2019). The changes that the tumor cell undergoes, induced by the microenvironment, are greatly responsible for the the phenomenon of chemoresistance. As a consequence, the tumor microenvironment has become a privileged target to study new approaches for the treatment of cancers.

A change in microenvironmental pH is one of the important stress-inducing events in cancer. Moreover, accumulating evidence shows that acidic pH_e enhances the invasive behavior of cancer cells and promotes the development of cancer by allowing the inhibition of apoptosis, consequently hindering tumor treatment (Martínez-Zaguilán et al., 1996). In addition, acidic pH_e affect markedly the response of tumors to various treatments such as chemotherapy and radiotherapy. For instance, the acidic pH_e increases the cellular uptake of weakly acidic drugs such as chlorambucil (Brophy and Sladek, 1983) and melphalan (Skarsgard et al., 1995) and thus increases the effect of the drugs. In contrast, the acidic pH_e retards the uptake of weakly basic drug such as doxorubicin (Born and Eichholtz-Wirth, 1981; Hindenburg et al., 1989) and mitoxantrone (Jähde, Glüsenkamp, and Rajewsky, 1990; Vukovic and Tannock, 1997), thereby reducing the cytotoxic effects of the drugs. A better understanding of pH_e control mechanisms in tumors can therefefore lead to an effective tumor treatment strategy. In this context, the pH sensing method developed in Chapter 2 has been applied: ratiometric imaging of the BCECF probe was performed in monolayer cell cultures and the evaluation of the pH_i to changing pH_e was made by using the calibration curves already obtained for each cell line (U87 and F98).

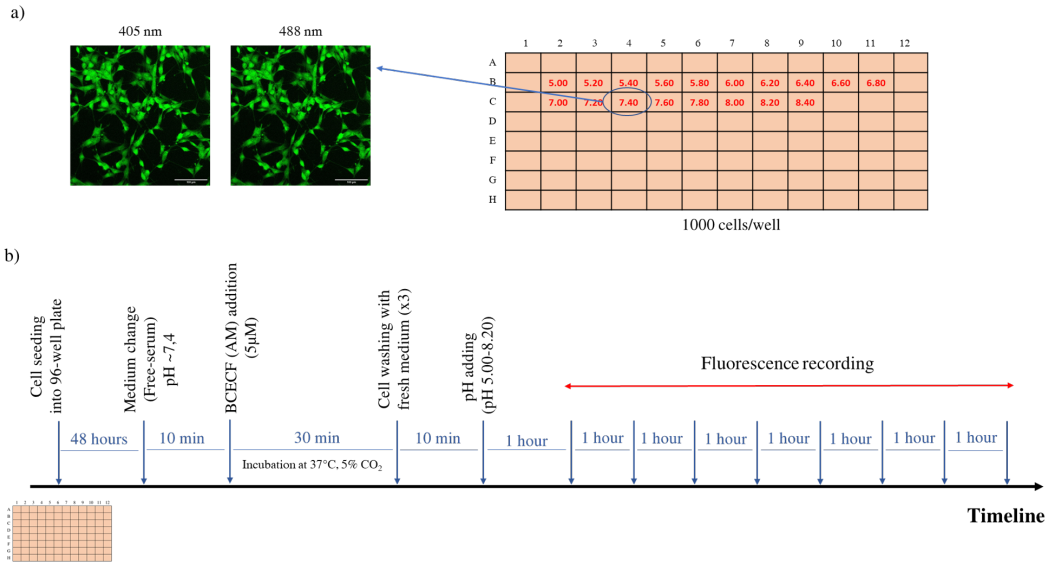

FIGURE 5.2: a) Cells were seeded at a concentration of 1000 cells/well in a flat ClearLine® plate (96 wells). Confocal fluorescence images were recorded after loading cells with the BCECF probe using excitation wavelengths of 405 nm and 488nm. b) Experimental timeline to measure the intracellular pH of glioma cells over a period of 8 hours.

5.2 Intracellular pH adaptation

5.2.1 Methodology

In order to assess the effects of pH_e on glioma cells, U87 anf F98, we established simple *in vitro* culture systems to maintain a pH_e ranging from 5 to 8.4 at 37°C under 5% CO_2, using HCl or NaOH in the culture medium. Therefore, identical culture conditions were applied for each cell line and two flat ClearLine® plates presenting inserts of U87 and F98 cells were seeded at a concentration of 1000 cells/well with 200 µL of culture medium. 48 hours after seeding, the culture medium was replaced with serum-free DMEM medium of pH ~ 7.4. As a reminder, culture medium should be serum-free to avoid extracellular hydrolysis of AM ester caused by the presence of serum which may contain endogenous esterase activity. Cells were incubated for 30 min with 5 μM of BCECF-AM and then rinsed 3 times with fresh medium (pH ~ 7.4) to remove the probes not taken by the cells. Once loaded with the pH probe, the cells were incubated under varying pH conditions and the effect of pH_e on pH_i was monitored over a period of 8 hours (Figure 5.2). Every hour, and at each pH_e tested, confocal fluorescence images were recorded by exciting the cells at 405 nm and 488 nm. The intensity ratio of the two emission wavelengths was calculated pixel-to-pixel, and the pH_i is thus determined using the calibration curves previously established in Chapter 3. The dynamic changes of pH_i as a function of pH_e are presented in Figure 5.3.

In order to properly study the pH_i regulation of glioma cells, it is important to take into account the drift of the culture medium pH discussed in Chapter 3. In this context, parallel measurements of pH_e were carried out every hour, for 8 hours, using the non-permeable version of the BCECF probe. The results obtained are shown in Figure 5.4. Therefore, looking

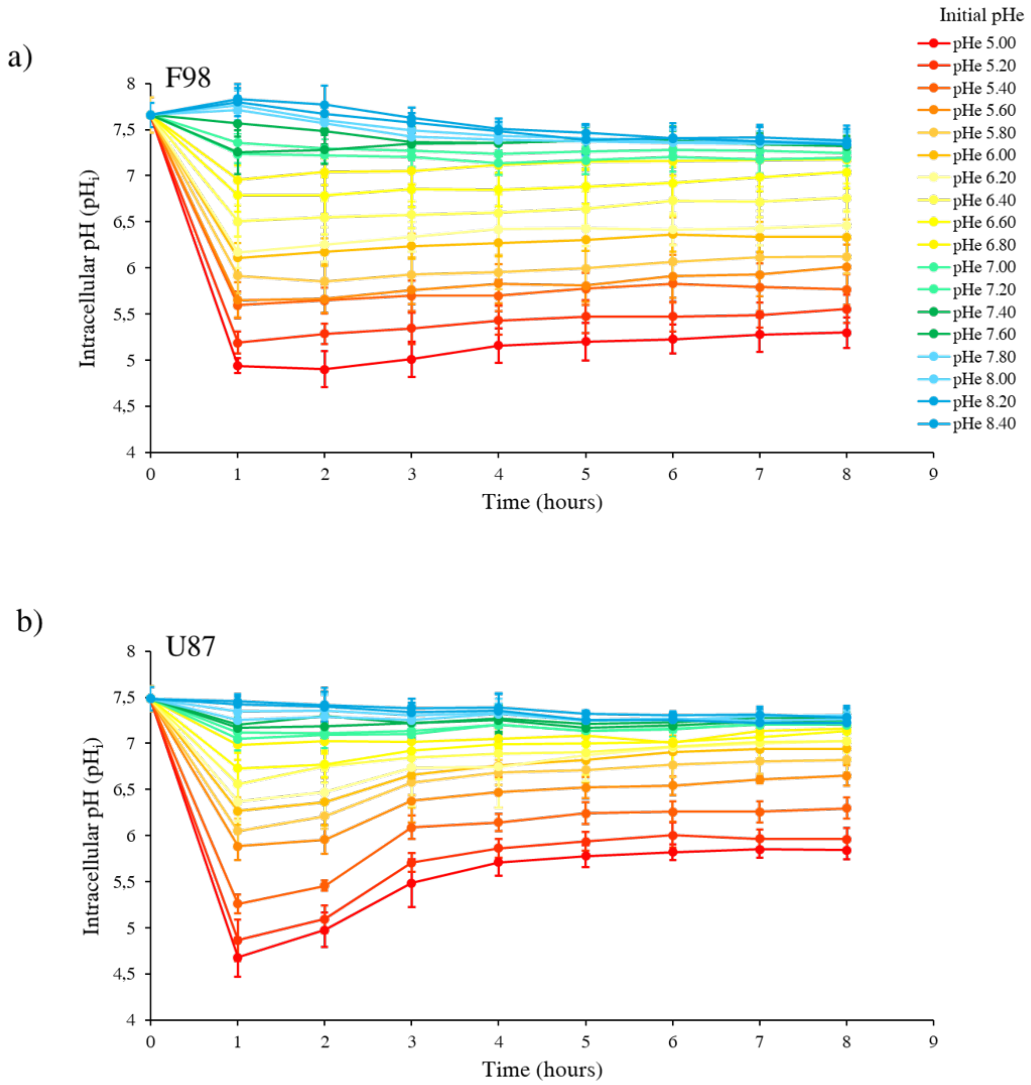

FIGURE 5.3: The effect of pH_e on pH_i of F98 (a) and U87 (b) cells as a function of time. Cells labeled intracellularly with pH sensitive fluorescent probe BCECF, were incubated under varying pH_e levels and monitored over time. Points are mean (± SD) of three experiments.

in parallel at Figure 5.3 and Figure 5.4, a pH_e value can be associated to a corresponding pH_i value measured at the same instant. Thus, as another way to display the effect of pH_e on pH_i, the relationship between pH_e and pH_i for the two cell lines is shown in Figure 5.5.

5.2.2 Overall pH_i adaptation dynamics

Figure 5.3 shows the effect of pH_e on the pH_i of U87 and F98 cells as a function of time. On the short term (~ 1 hour), the sudden change of pH_e creates a shock on the cells since the pH_i of both cell lines almost instantly take the value of the pH_e. Beyond that, the pH_i regulation process takes 2 hours to produce some effect and one more to reach a stationnary state. On the longer term, after 4 hours and up to 8 hours, the pH_i remains stable and is specific to the cell line.

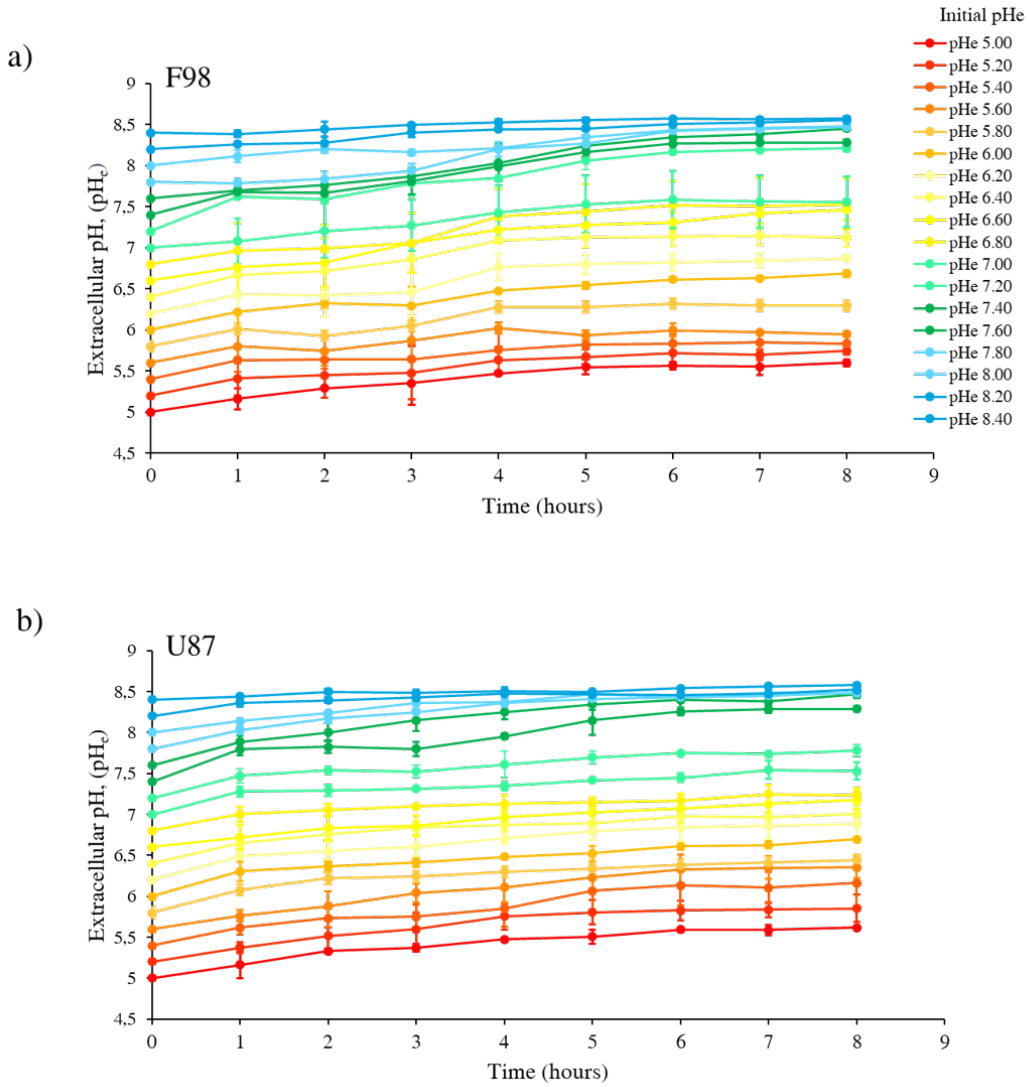

FIGURE 5.4: The evolution of the pH$_e$ of F98 (a) and U87 (b) cell cultures over time. Cells were seeded in 96-well plates and incubated under varying pH$_e$ levels in the presence of 5μM of BCECF (non-permeable version). Points are mean (± SD) of three experiments.

In order to be able to understand pH_i changes in the cell it is necessary to measure the basal pH_i, i.e. the pH_i associated to the pH_e of the culture medium before external pH_e changes. In other words, pH_i was first measured at time zero in complete medium at the growth phase of the cells. In this initial condition, pH_i was 7.65 ± 0.13 For F98 cells and 7.48 ± 0.12 for U87 cells.

5.2.3 Adaptation of F98 cells

For F98 cells, we note first of all that the curves giving the pH_i as a function of the pH_e are almost always under the axis pH_i=pH_e, which means that the pH_i is always lower than the pH_e (Figure 5.5, a). For this F98 cell line, we not that there is no inversion of the pH gradient as usually documented in tumors cells. In addition, a quasi-linear increase in pH_i with pH_e in the range of pH_e 5.0-7.2 is observed, and the measures are very close to the pH_i=pH_e axis. Moreover, the dependence of pH_i as a function of time is low in the acidic pH_e range, as the curves are almost superimposed. However, the range with the higher pH_e values, shows a marked dependence of pH_i as a function of time. The pH_i of F98 cells decreases over approximately 4 hours before being less influenced after 5 hours. At that time, the relationship between pH_i and pH_e exhibits a plateau for pH_e above 7.2. F98 cells have therefore the ability to progressively adjust with time their pH_i under basic conditions (above 7.2).

As already mentioned, the F98 cells have a pH_i of 7.65 ± 0.13 in the basal state (Figure 5.3, a). Lowering the pH_e, for example, to 5.00 rapidly decreases pH_i to 4.94 ± 0.08 (after 1 hour). This decrease of the pH_i corresponds to the rise of hydrogen ions (H^+) inside the F98 cells.
It has been reported that the main mechanism responsible for pH_i changes is related to the movement of H^+ ions across the plasma membrane (Izutsu, 1972; Baltz, Biggers, and Lechene, 1993; Doyen et al., 2022). Extracellular acidification stimulates the passive influx of H^+ ions into the cell by increasing the permeability of the plasma membrane, resulting in a decrease in pH_i (Carmelo, Santos, and Sá-Correia, 1997).
As acidic pH_e limits the availability of bicarbonate ions (HCO_3^-) and thereby reduces both passive and dynamic HCO_3^--dependent buffering, tumor cells are thought to use the sodium-hydrogen exchanger (NHE exchanger) to recover from intracellular acidification. However, their poor recovery during this assay suggests that NHE activity is low in F98 glioma cells. This is in great agreement with the study by Glunde et al., 2002, which showed that extracellular acidification inhibits the activity of NHE-1 exchanger (sodium-hydrogen exchanger isoform-1) in glioma cell lines (C6 and F98).

For basic pH_e, F98 cells maintain a physiological level of pH_i around 7.4, more precisely 7,33 ± 0.13. Going from an initial state of pH_i 7.65 ± 0.13 to 7.33 ± 0.13, a passive influx of H^+ ions into the cell is imposed. Although basic pH_e limits the availability of H^+ ions in the

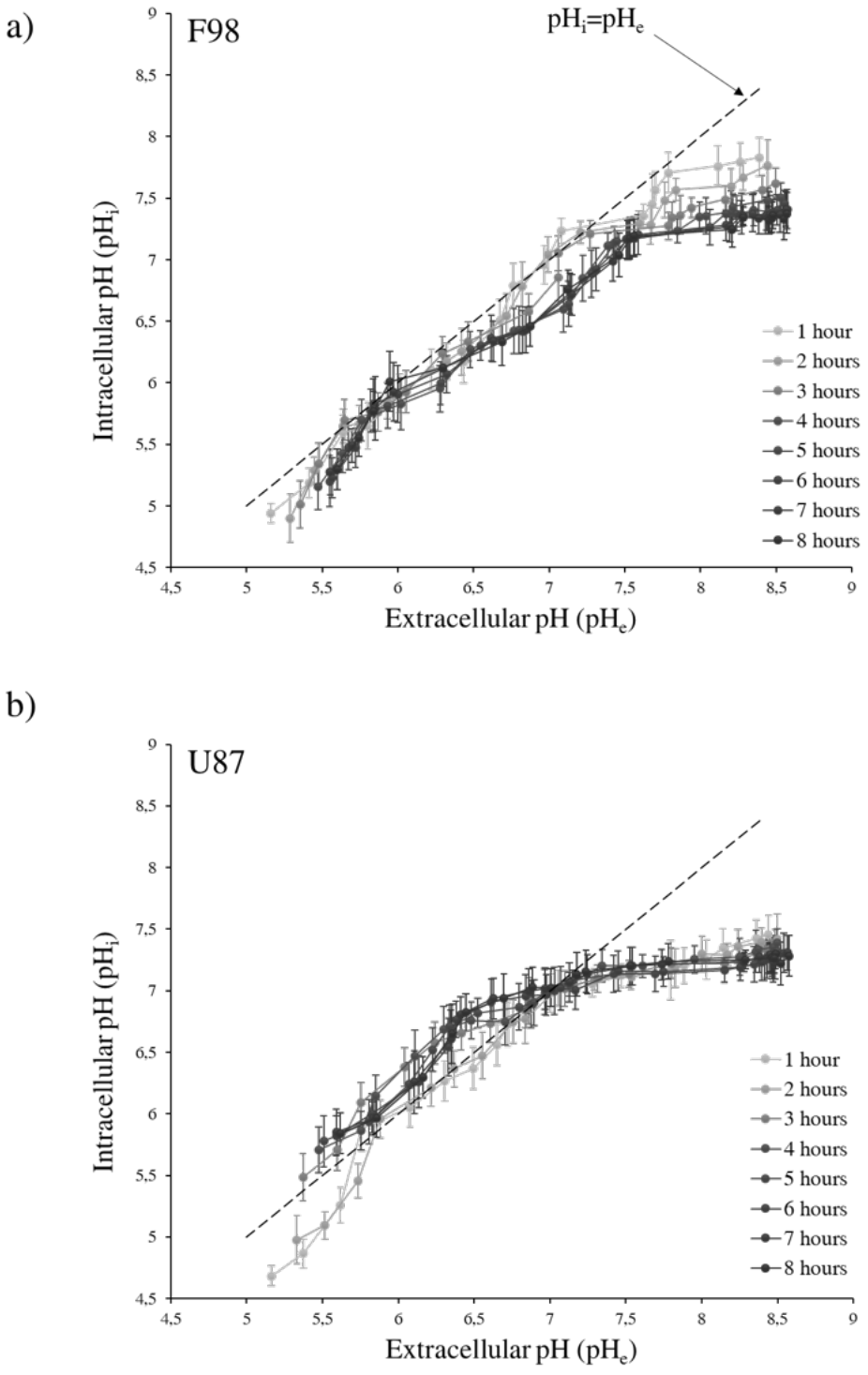

FIGURE 5.5: Relationship between pH_e and pH_i of F98 (a) and U87 (b) cells *in vitro*. The cells were maintained at pH_e 7.4 before exposure to a new pH_e. pH_i and pH_e were measured over time using the pH sensitive fluorescent probe BCECF. Basal pH_i was 7.65 ± 0.13 for F98 cells and 7.48 ± 0.12 for U87 cells. Points are mean (± SD) of three experiments.

culture medium, H^+ ions are generated by the hydration of CO_2 according to the reaction:

$$CO_2 + H_2O \rightleftharpoons H_2CO_3 \rightleftharpoons H^+ + HCO_3^- \tag{5.1}$$

Inside the cells, the incoming H^+ ions will be sequestered by the bicarbonate ions (HCO_3^-), thus increasing the pH_i. This is, however, not the case with F98 cells. As the F98 cells have lowered their pH_i, it can be assumed that the F98 cells used the Cl^-/HCO_3^- exchanger to export the HCO_3^- ions outside the cells. Once the HCO_3^- ions are exported, H^+ ions are no longer sequestered leading therefore to a decrease in pH_i. The Cl^-/HCO_3^- exchanger has been identified as an essential regulator particularly activated following an alkaline incubation (Lacoste, Harvey, and Ehrenfeld, 1991; Vilariño et al., 1998; Rivarola et al., 2005): activation of Cl^-/HCO_3^- exchanger decreases the rate of acidification during recovery of pH_i from extracellular alkaline incubation.

5.2.4 Adaptation of U87 cells

For U87 cells, we notice first of all that the curves of pH_i according to pH_e are almost systematically above the axis pH_i=pH_e, in the range of pH_e 5.0-6.8, meaning that the pH_i is higher than the pH_e which is in agreement with the reverse pH gradient described in tumor cells (Figure 5.5, b). U87 cells are able therefore to increase their pH_i under acidic condition. In addition, a time dependence of pH_i is also noted in this pH_e range: the pH_i increases over 3 hours before being less influenced after 4 hours. However, in the zone of $pH_e > 6.8$, the curves of pH_i are always under the axis pH_i=pH_e and the pH_i is completely independent of time (superimposed curves). U87 cells have therefore the ability to rapidly maintain a pH level close to the physiological one for pH_e above 6.8.

In their basal state, U87 cells have a pH_i of 7.48 ± 0.12 (Figure 5.4, b). Lowering the pH_e, for example, to 5.00, decreases pH_i to 4.75 ± 0.14 (after 1 hour). First, the rapid drop in pH_i is due to the passive influx of H^+ ions into the cell. However, unlike F98 cells, U87 cells have reduced their intracellular acidity to 5.81 ± 0.12 after 8 hours. Therefore, considering the low HCO_3^--dependent buffering at acidic pH, it can be suggested that U87 cells used the dynamic NHE exchanger to recover from intracellular acidification. The plasma membrane isoforms of this protein extrude 1 intracellular H^+ ion in exchange for 1 extracellular Na^+ ion, leading thus to an increase in pH_i.

For basic pH_e, U87 cells maintain a pH_i level close to physiological pH, more precisely 7.25 ± 0.03. Going from an initial state of pH_i 7.48 ± 0.12 to 7.25 ± 0.03, U87 cells use, like the F98 cells, the Cl^-/HCO_3^- exchanger to export the HCO_3^- ions outside the cells and to recover from alkaline incubation by decreasing pH_i. The temporal dependence of pH_i observed with F98 cells can be explained by the fact that the pH_i of F98 cells at time zero is higher than that of U87 cells (by about 0.2 pH units).

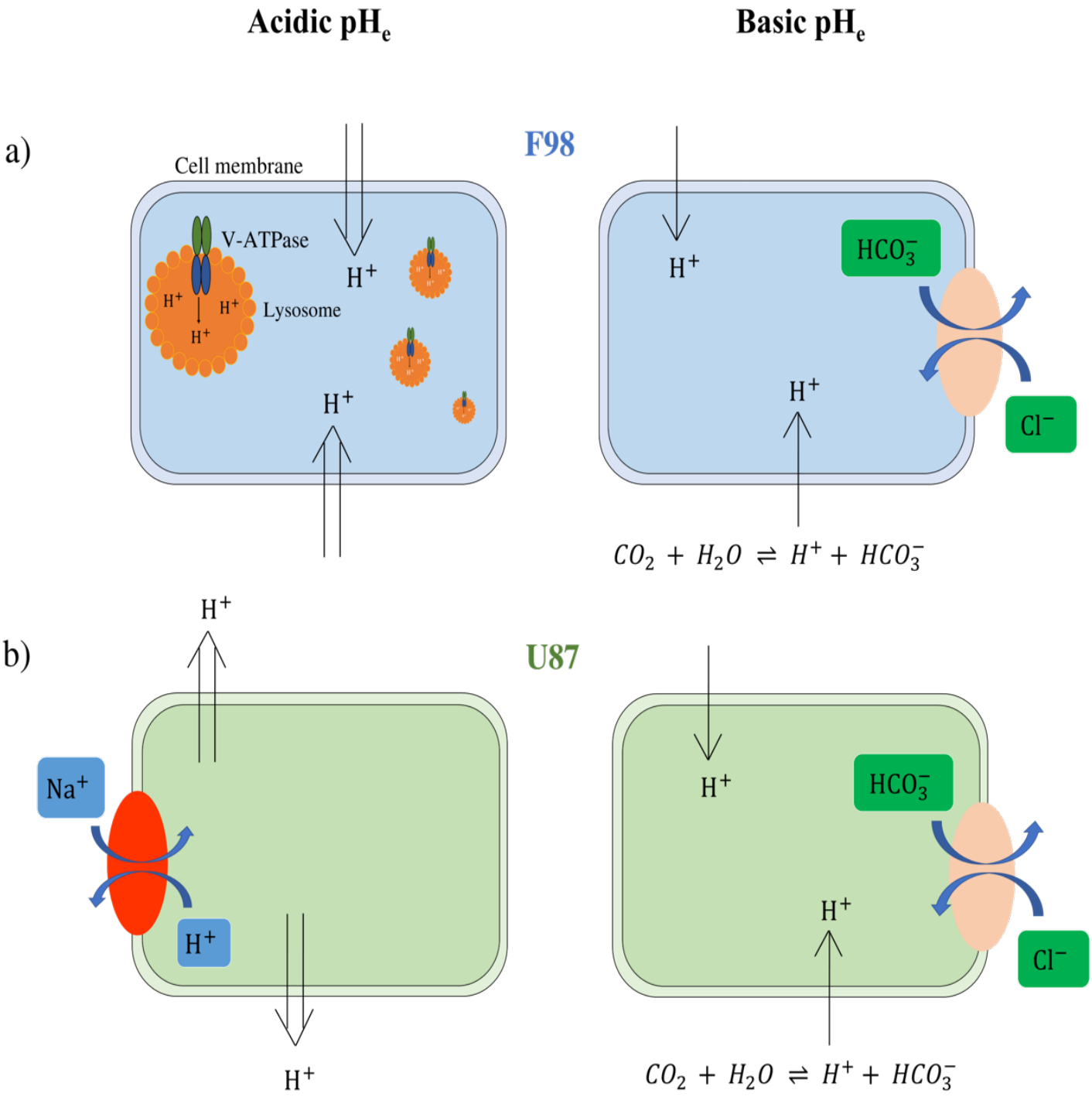

FIGURE 5.6: Intracellular pH$_i$ regulatory mechanisms of F98 (a) and U87 cells (b). We found that F98 cells are not able to regulate acidic pH and H$^+$ ions remains inside the cells. Therefore, another mechanism is probably involved. We assumed that the F98 cells activated the V-ATpase pump to encapsulate the protons in the lysosomes. On the other hand, U87 cells are able to regulate intracellular acidity by exporting protons outside the cells. We assumed that U87 cells used the NHE-1 exchanger to export protons in exchange with Na$^+$ ions. Both cell lines are able to regulate basic pH. We hypothesized that the cells used the Cl$^-$/HCO$_3^-$ exchanger to export the HCO$_3^-$ ions outside the cells and thus maintain a pH$_i$ level close to the physiological one.

5.2.5 Conclusion

In order to survive the dynamic nature of pH in tumors, cancer cells require the ability to sense minute pH changes and respond appropriately to maintain pH_i homeostasis. In other words, it is the ability to regulate pH_i. Regulation of pH_i starts with changes in the expression or activity of several plasma membrane molecules such as pumps and transporters that facilitate protons efflux. Thus, a strength in understanding the pH_i regulation of tumors is the understanding of proton transport across the plasma membrane. Therefore, we have experimentally characterized in monolayer cultures the pH_i-regulating capacity of two glioma cell lines using fluorescence microscopy. We observed that the pH_i regulation is not the same for the two cell lines. Firstly, under acidic conditions, U87 human glioblastoma cells are able to reduce intracellular acidity by exporting protons outside the cells. In other words, U87 cells are able to regulate acidic pH. We assumed that U87 cells used the NHE-1 exchanger to export protons in exchange with Na^+ ions. However, we found that F98 cells are not able to regulate acidic pH and H^+ ions have been maintained inside cells. Therefore, another mechanism might be involved since high pH_i degrades intracellular proteins and prevents normal functioning of the cell machinery. We assumed, as we will see in the next section, that the F98 cells activate the pump V-ATpase to encapsulate the protons in the lysosomes. On the other side, we found that both cell lines are able to regulate basic pH. We hypothesized that the cells used the Cl^-/HCO_3^- exchanger to export the HCO_3^- ions outside the cells and thus maintain a pH_i level close to the physiological one. All of these mechanisms are summarized in Figure 5.6.

Many recent studies have shown that the cancer cells exhibit a higher resistance to acidity due to a better ability to regulate their pH_i (Swietach et al., 2014; Estrella et al., 2013; Corbet and Feron, 2017). As we end up with two tumor cell lines that do not regulate their acidity in the same way, we were interested in evaluating the effects of acidification of the tumor microenvironment on the mortality of those glioma cells. To do this, cells were grown in culture media with different pH_e values for 72 hours. The cells were then subjected to trypan blue exclusion assays to evaluate mortality. The results are therefore presented in the following paragraph.

5.3 Resistance to extracellular pH changes

In order to assess *in vitro* the resistance to pH_e changes of glioma cells, U87 and F98 cells were seeded at a concentration of 5×10^4 cells/mL into a 24-well plate and incubated for 48 hours at 37°C in a humid atmosphere containing 5% CO_2. After 48 hours of growth, the culture medium was removed and replaced with the test medium with a pH_e ranging from 4.0 to 9.0. To assess cell mortality, the trypan blue stain was used. Trypan blue stains dead and dying cells whose membrane integrity is damaged. The culture medium was removed from each well and 200 μL of trypsin was added per well to remove the cells. The removed cells were then re-suspended in 800 μL of culture medium. The cell suspensions were diluted 1:1 (v:v) with 0.4% trypan blue and then a 10 μL mixture was transferred to a cell count slide.

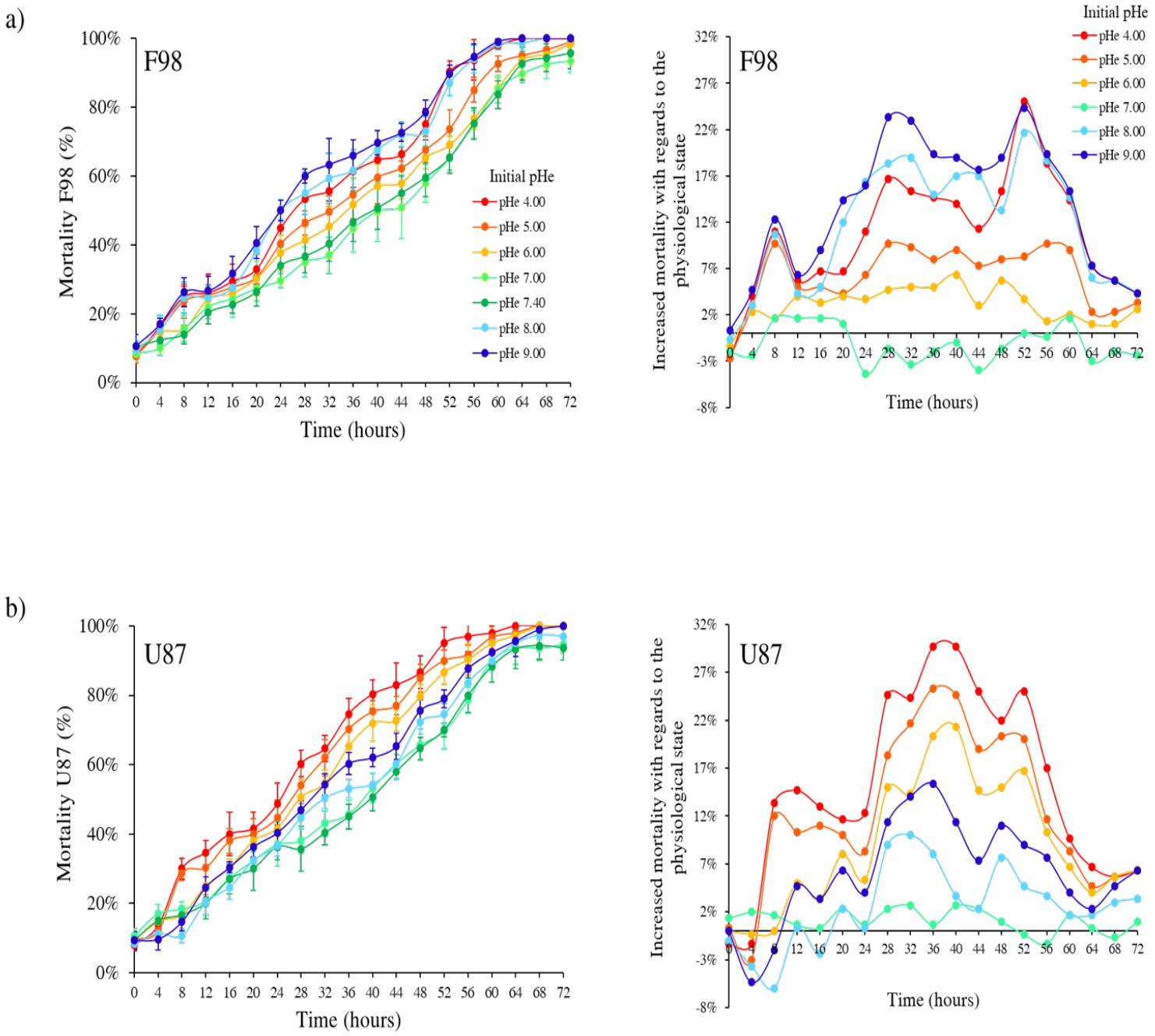

FIGURE 5.7: Effects of pH_e on cell mortality of F98 (a) and U87 (b) cells. The right graphs show the evolution of the percentage of dead cells (over the entire number of cells of the population) with time. The left graphs show the excess mortality compared to the control (which is the standard culture medium with a physiological pH of 7.4). Data are expressed as mean ± SE.

Cell mortality was monitored using an automated cell counter over a period of 72 hours and the number of dead cells was measured every four hours for each pH_e tested. The results are shown in Figure 5.7. To assess cell mortality, two graphics are used. The first one simply shows the evolution of the percentage of dead cells (over the entire number of cells of the population) with time. The second represents the excess mortality compared to the control (which is the standard culture medium with a physiological pH of 7.4). We note that it can be negative if the mortality is reduced compared to the control condition.

5.3.1 Long-term mortality

In the long term, we have found that both cell lines resist to high acidic conditions over 48 hours and, at least 15% of cells are alive. After 72 hours, the cells are almost all dead. Beyond 28 hours, cell mortality becomes significant and the excess mortality, compared to the control state, reaches nearly 25% for certain pH_e (Figure 5.7, right). At 28 hours, F98 mortality is higher for extreme acidic (4.00) and basic (9.00) pH_e with a mortality of approximately 53% and 60% respectively. However, U87 mortality is higher for acidic pH_e with cell mortalities of approximately 60%, 54% and 51% at pH_e 4.00, 5.00 and 6.00, respectively. It appears that F98 cells seem to have a higher resistance to acidity than U87 cells, whereas, U87 cells have a higher resistance to basicity than F98 cells.
In order to determine how glioma cells resist changes in pH_e, it is important to make the relationship between cell mortality and pH_i adaptation. However, since we have not studied long-term pH_i adaptation of glioma cells, nothing can be said about long-term interpretation. Therefore, the following paragraph is dedicated to the short-term analysis.

5.3.2 Short-term mortality

In this part, cell mortality was analyzed over the period when we studied pH_i adaptation, i.e. 8 hours (Figure 5.8). Therefore, within 4 hours, F98 cells show a mortality of 16% and 15% when incubated with a pH_e of 4.00 and 5.00 respectively. Four hours later, the percentage of mortality increases to approximately 24% and 23% for the same pH_es respectively. At the same time, within 4 hours, U87 cells show a mortality of 14% and 12% when incubated with a pH_e of 4.00 and 5.00 respectively. Four hours later, the percentage of mortality increases to approximately 31% and 30% for the same pH_es respectively. The increased mortality after 4 hours is slightly bigger for U87 cells than for F98 cells which might suggests a delayed reaction to acidity for U87 cells.
A significant difference between U87 and F98 mortality was observed under basic conditions. At 8 hours, the F98 mortalities were approximately 25% and 26% for pH_e 8.00 and pH_e 9.00, respectively. While, U87 mortalities were approximately 11% and 15% for pH_e 8.00 and pH_e 9.00, respectively. Therefore, U87 cells exhibit a higher resistance to basicity than F98 cells. Several studies have reported the existence of a link between the regulation of intracellular acidity and the reduction of cell death (Hackam, Grinstein, and Rotstein, 1996; Rao et al., 2001; Zeng, Yang, and Zhou, 2021; Man et al., 2022). Therefore, in order to minimize the toxic intracellular acidity, tumor cells must regulate the H^+ ions extrusion mechanisms which

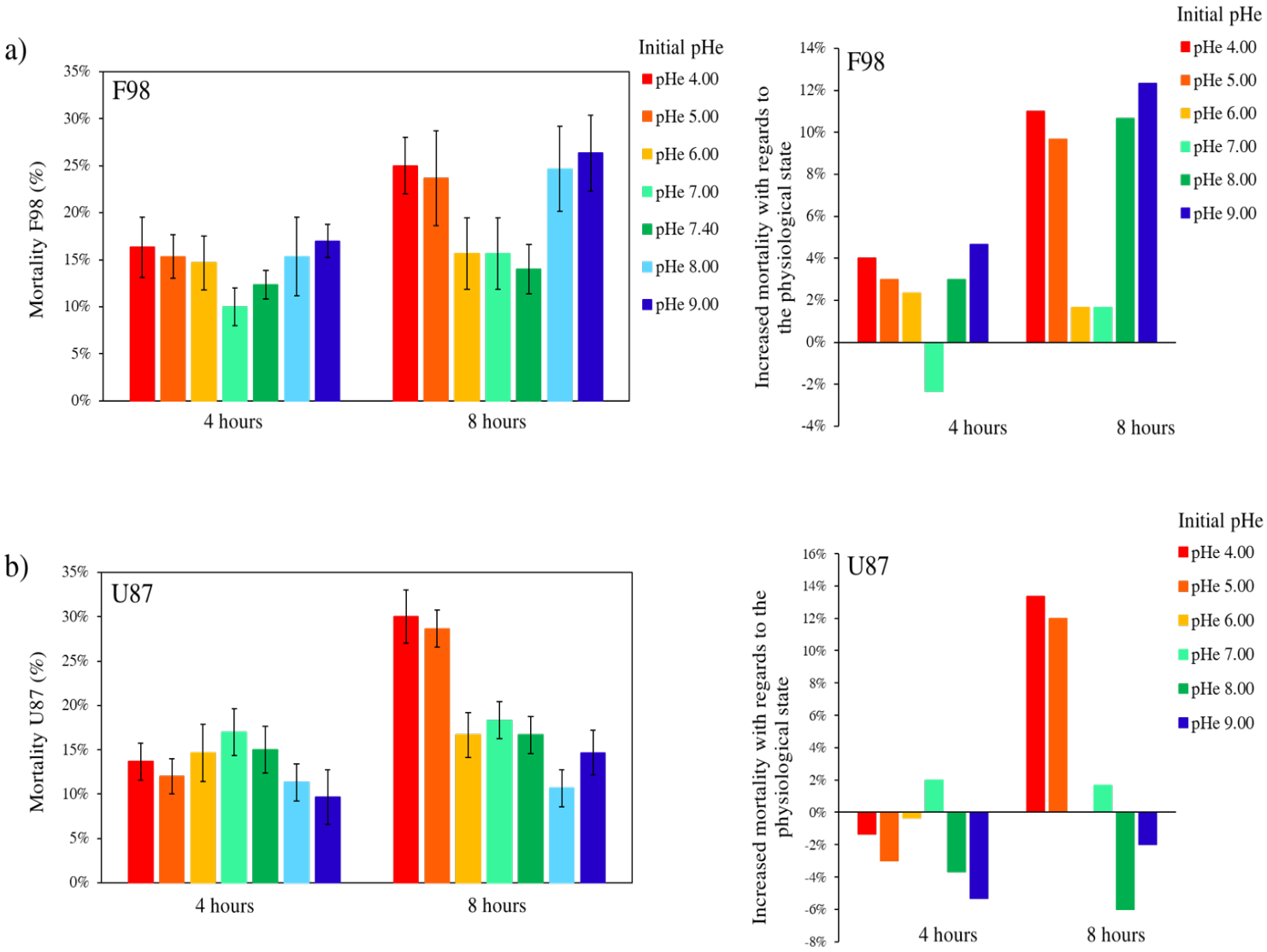

FIGURE 5.8: Cell mortality percentage at 4 and 8 hours of incubation at different pH_e values. a) on F98 cells and b) on U87 cells. The left graphs show the excess mortality compared to the control (which is the standard culture medium with a physiological pH of 7.4). Data are expressed as mean ± SE.

increase the pH_i. Taking these considerations into account, U87 cells that regule intracellular acidity should exhibit lower cell mortality than F98 cells that do no regulate intracellular acidity. However, that is not the case here. U87 cells exhibit higher mortalities under acidic conditions. In this case, the regulation of intracellular acidity does not constitute an adaptive response. These appears to be a key finding of our study. Therefore, how can we explain these results ?

F98 cells that do not regulate intracellular acidity preserve protons inside the cells. In turn, the intracellular protons will produce a toxic effect on many cellular processes such as enzyme activities, metabolism, and gene expression, thus leading to cell death (Tannock and Rotin, 1989; Wahl et al., 2000). However, this is not the case with F98 cells. F98 cells showed a high resistance to intracellular acidity. Are the protons conserved in a way that does not disturb cellular functions?
Accumulating evidence suggests that in addition to the well characterized ion pumps and exchangers in the plasma membrane, cancer cell lysosomes allow to avoid potentially toxic acidification of the intracellular milieu (Piao and Amaravadi, 2015; Tang et al., 2020; Chen, Jäättelä, and Liu, 2020). The lysosome is an intracytoplasmic organelle responsible for the degradation and recycling of intra- or extracellular components. It is very heterogeneous in its size and essentially contains 50 to 60 hydrolases (phosphatases, glycosidases, lipases, nucleases, sulfatases and proteases) active at acidic pH. It has been reported that the pH of lysosomes is maintained at 4.5–5 and the concentration of H^+ ions in lysosomes is almost 1000 times higher than in the cytosol (Chen, Jäättelä, and Liu, 2020; Banerjee and Kane, 2020). Therefore, the lysosome is not only a place of protein degradation but also a storage compartment for H^+ ions. The pH of lysosomes is regulated by V-ATPase, a pump located in the membrane of these organelles, which brings H^+ ions into these vesicles and acidifies the contents. As we suggested that H^+ ions were encapsulated in F98 cells, we therefore assume that F98 cells activate at acidic pH the V-ATpase pump to bring H^+ ions into the lysosomes.

U87 cells that are found to regulate intracellular acidity use the NHE exchanger to export H^+ ions outside the cells. Fluxes through the NHE are driven only by the combined chemical gradients of Na^+ and H^+ and therefore do not directly consume metabolic energy (Kinsella and Aronson, 1980). However, it has been found that the presence of physiological levels of ATP in certain cell lines is necessary for optimal Na^+/H^+ exchange (Cassel, Katz, and Rotman, 1986; Brown et al., 1991; Levine et al., 1993; Kapus et al., 1994). As already seen, U87 cells were able to reduce intracellular acidity by Na^+/H^+ exchange over 8 hours (Figure 5.5, b); The exchanger operated normally during this period. Assuming that the activity of a NHE exchanger in U87 cells depends on the availability of intracellular ATP, the NHE exchanger might have exhausted the intracellular ATP necessary for the various mitochondrial functions, in particular for maintaining the membrane potential gradient which stimulates cell survival and proliferation (Brown et al., 2006; Vasan et al., 2022). The depletion of ATP by the NHE exchanger therefore leads to cell death.

Very few studies have been conducted to investigate the effect of alkaline pH_e on cell survival (Langer, 1985; Wanandi et al., 2017; Khajah et al., 2013; Avnet et al., 2016; Güvenalp and Güvenç, 2020). These studies did not focus on the study of cellular metabolism but rather on the effect of extracellular alkalinization on the permeability of the plasma membrane (Langer, 1985; Avnet et al., 2016; Güvenalp and Güvenç, 2020). It was found that the morphology of cells was altered in alkalinized culture. The spindle-shaped cells, like F98 cells, formed small patches of round cells at basic pH_e (Güvenalp and Güvenç, 2020). Moreover, the cells had lost their ability to adhesion. Consequently, the membrane potential of mitochondria was altered leading to permeability transition, pore opening, and thus cell death (Ichas and Mazat, 1998; Mazzio et al., 2012). Cells that grow as cell aggregates such as U87 cells, are therefore more resistant to cell death under basic pH_e.

5.4 Intracellular pH heterogeneity

By combining confocal microscopy and the BCECF probe, we were able not only to measure dynamic changes in pH_i, but also to spatially assess the distribution of pH_i at the population level or even at the single-cell level. Within a large cell population, cells are not identical and differences in pH_i levels may be important indicators of heterogeneity that could be relevant in clinical practice, especially in personalized medicine (Özel et al., 2015; Korenchan and Flavell, 2019; Koltai, 2020). Therefore, in this part, we will discuss the methodology available to quantify pH_i heterogeneity accross a population of glioma cells. Accordingly, confocal fluorescence images of glioma cells labeled with the BCECF pH probe were analyzed with ImageJ/Fiji software to map the pH_i.

5.4.1 Methodology

The first part of the analysis deals with the segmentation of these images to isolate only the pixels contributing to the intracellular signal. This operation was performed by an automatic thresholding technique based on image entropy using Li's iterative algorithm for minimum cross entropy thresholding, which best fits images of glioma cells. Consequently, binary images only containing the relevant information (object), with pixels set to 1 and background pixels set to 0, were obtained. The binary images are therefore used as masks for further operations.

As we now know, glioma cells were successively excited by two lasers, 405 nm and 488 nm. At each laser excitation, the saved confocal image presents 32 channels extend over the 420-720 nm emission range. Therefore, for images of F98 cells, the 517 nm channel of the 405 nm confocal image, and the 546 nm channel of the 488 nm image were multiplied by the masks, and then the 517 nm channel was divided by the 546 nm channel in ImageJ (pixel by pixel) to obtain a 32-bit ratiometric image. For images of U87 cells, the 517 nm channel of the 488 nm confocal image and the 556 nm channel of the 405 nm image were multiplied by the masks, and a pixel by pixel division between the 517 nm channel and the 556 nm channel was performed to obtain ratiometric image. These final images represent the relative pH_i values for the experiment. The "mpl-viridis" LUT was applied to represent the pH_i values by

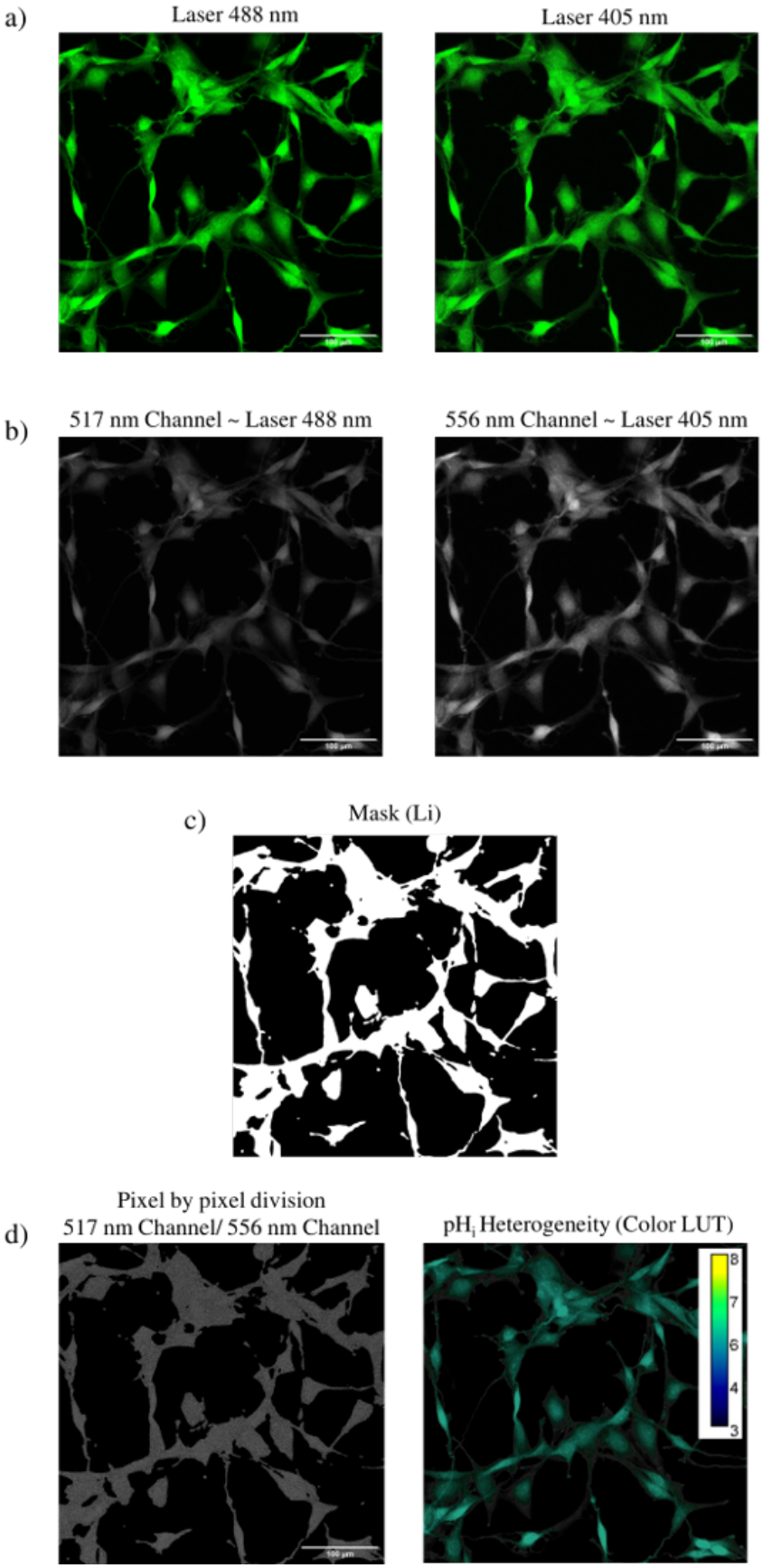

FIGURE 5.9: Image analysis to assess intracellular pH heterogeneity. a) Confocal fluorescence images of U87 cells excited by the 488 and the 405 nm lasers (32 channels per image). Image processing: b) Each channel stack was multiplied by the masks (c), and then a pixel by pixel division between images was performed to get the pH image. The "mpl-viridis" LUT was applied to represent the pH_i values by colors.

colors (Figure 5.9).
Figure 5.10 and Figure 5.11 show the pH_i distributions in glioma cells at different pH_e values. Nine pH_e were presented, and the analyzed images were taken by our set-up 8 hours after exposure of the cells to a given pH_e. Our 20x objective has a numerical aperture (NA) of 0.75. This resulted in a resolution that was not high enough to precisely measure pH_i compartment at the single cell level. The distribution of pH_i was therefore assessed at the level of the cell population.

5.4.2 pH_i heterogeneity at the cell population level

In order to quantitatively analyze the pH_i distributions at the cell population level, pH_i was first calculated pixel-by-pixel using the Li's threshold method (previously described) with ImageJ software. Then, we introduced the parameters pH_i(min) and pH_i(max) as the minimum and the maximum pH_i value, respectively, obtained among all the pixels in the confocal image. These two values show the pH_i range measured on the entire population. Figure 5.12 shows the mean pH_i values of both glioma cells thus illustrating, in gray, the range of pH_i obtained over the cell population. Note that the mean pH_i value (m) of the whole population is given by:

$$m = \frac{\sum_{i=1}^{n} x_i}{n} \tag{5.2}$$

where x_i is the pH_i value of the single pixel i and n is the number of pixels within the cell population. From our data, we measure a wide range of pH_i values within distributions, a criterion used to assess pH_i is heterogeneous at the population level. Moreover, For a pH_e of 5.00, F98 cells exhibit a pH_i range between 4.1 and 7.2. This range becomes wider by increasing the pH_e. Above a pH_e of 6.8, F98 cells exhibit a pH_i distribution between 4.3 and 9.1. The analysis of U87 cells shows a narrower distribution of pH_i compared to the F98 cells. For a pH_e of 5.00, U87 cells exhibit a pH_i range between 5.0 and 7.2. Above a pH_e of 6.8, U87 cells exhibit a pH_i distribution between 5.8 and 9.1.
In order to properly quantify the heterogeneity of glioma cells, we introduced the standard deviation of the pH_i, *std*(pH_i), defined as:

$$std(pH_i) = \sqrt{\frac{\sum_{i=1}^{n}(x_i - m)^2}{n-1}} \tag{5.3}$$

This was used as a metric to describe the pH_i distributions within the cell population.
Statistical analysis showed that the *std*(pH_i) of all experiments was greater than 0.35 pH units, which is considered to be significant. In the case of U87 cells, the *std*(pH_i) is not sensitive to pH_e changes. Regardless of the pH_e tested, statistical analysis showed a *std*(pH_i) of approximately 0.34. However, in the case of F98 cells, the *std*(pH_i) changes as a response to pH_e. For pH_e above 6.8, F98 cells showed a higher *std*(pH_i), of approximately 0.52. For acidic pH_e, *std*(pH_i) dropped to around 0.37.

Firt of all, we assume that the heterogeneity, define as *std*(pH_i), of both cell lines is due

to changes in organelles pH specifically in cytosolic and lysosome pH, as they are the largest contributors to the pH_i heterogeneity (Johnson et al., 2016; Li et al., 2019; Chen, Jäättelä, and Liu, 2020). However, because of the constraints on our set-up, we were not able to precisely measure cytosolic and lysosome pH values for cells. Consequently, we found it interesting to switch our approach from determining pH_i values of individual organelles to determining a general pH_i heterogeneity between cells. Which means to evaluate the *intercellular* heterogeneity. The analysis of intercellular heterogeneity is therefore detailed in the next section. Moreover, we hypothesize that the changes in $std(pH_i)$ between F98 and U87 cells is probably caused by differences in pH_i regulation mechanisms, due to differences in membrane composition between the various organelles.
When in F98 cells, the $std(pH_i)$ decreases in acidic conditions. We assume that this decrease is caused by a combination of permeability changes and acidic deactivation of transporters and pumps in the membranes. A differential change in permeability could result in the plasma membrane becoming very permeable to protons as the pH changes while the lysosome membrane is less sensitive to pH changes. This would lead to a drop in the cytosolic pH towards the lysosome pH, thus reducing the variability of the pH_i.

5.4.3 pH_i heterogeneity at the intercellular level

In order to quantitatively analyze the content of the cell population, the confocal images were segmented with the Cellpose algorithm, recently developed by Stringer et al., 2020. Cellpose is a deep learning-based segmentation algorithm which can very precisely segment a wide range of cell images, both fluorescence and bright-field images, without requiring parameter adjustments. The tool can be used either online (`https://www.cellpose.org/`) or local or via notebooks. Image segmentation by cellpose is achieved by post-processing the input image into a combined gradient vector field, after which gradient tracking calculations ultimately result in cell outlines and a label map. The output image is a mask in which every segmented cell has a different gray value (Figure 5.13). This image is saved for further processing.
In order to measure the pH_i in each segmented cell, the grayscale mask obtained by Cellpose was projected on the map image showing the pH_i distribution at the population level. Accordingly, a pH_i value was associated to each segmented cell (Figure 5.14). The mean pH_i (M) obtained over all the segmented cells is given by:

$$M = \frac{\sum_{i=1}^{N} X_i}{N} \tag{5.4}$$

Where X_i is the mean pH_i of a single cell and N is the number of segmented cells within a cell population.
This time, We introduced the term standard deviation of the pH_i ($std(pH_i)$) to describe the pH_i distributions between cells which is the *intercellular* distribution. In this case, the $std(pH_i)$ is given by:

$$std(pH_i) = \sqrt{\frac{\sum_{i=1}^{N} (X_i - M)^2}{N-1}} \tag{5.5}$$

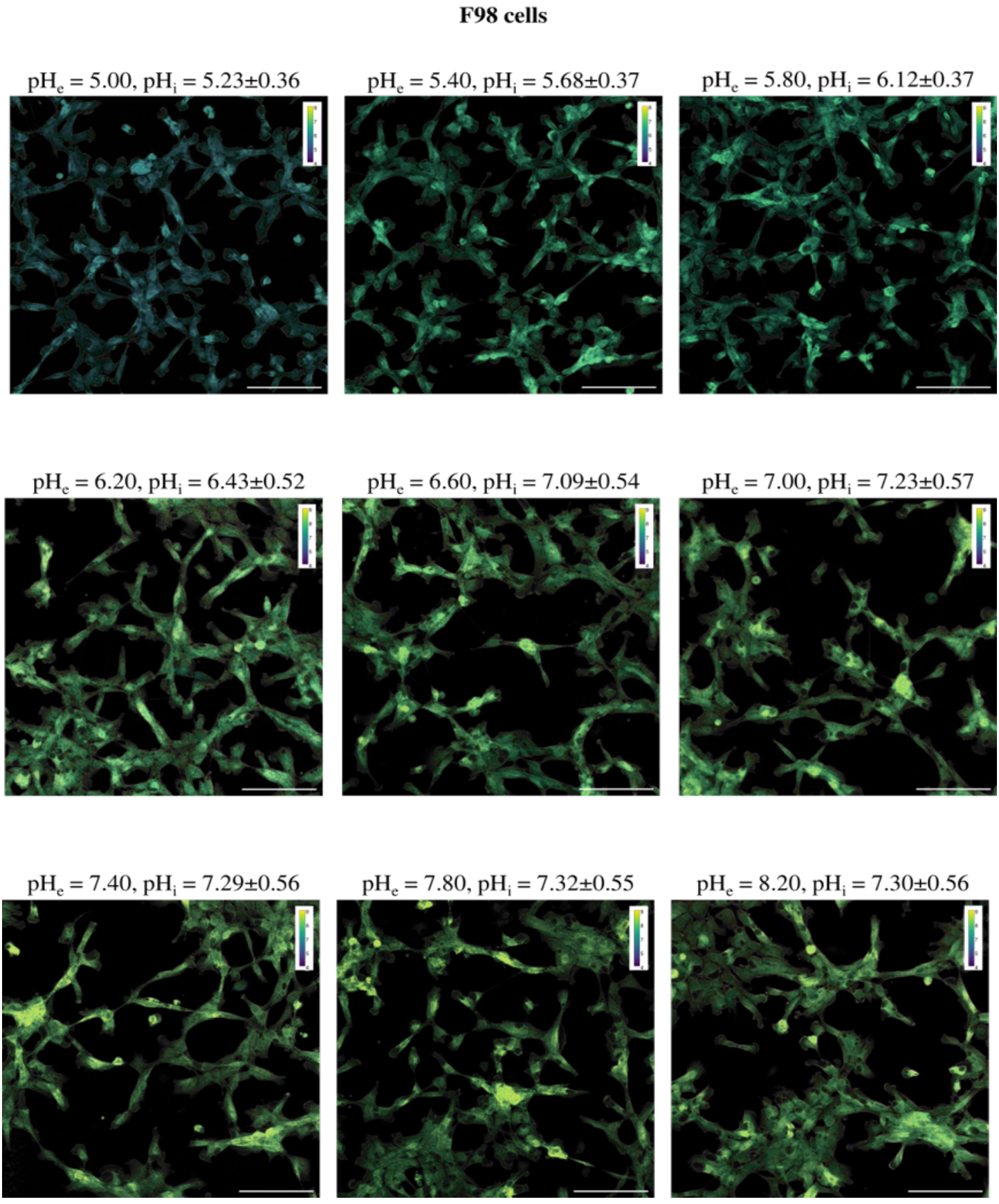

FIGURE 5.10: pH$_i$ distributions in F98 cells at different pH$_e$ values. The analyzed images were taken by our set-up 8 hours after exposure of the cells to a given pH$_e$. The mean pH$_i$ value obtained over the cell population is shown. Scale bar= 100 μm

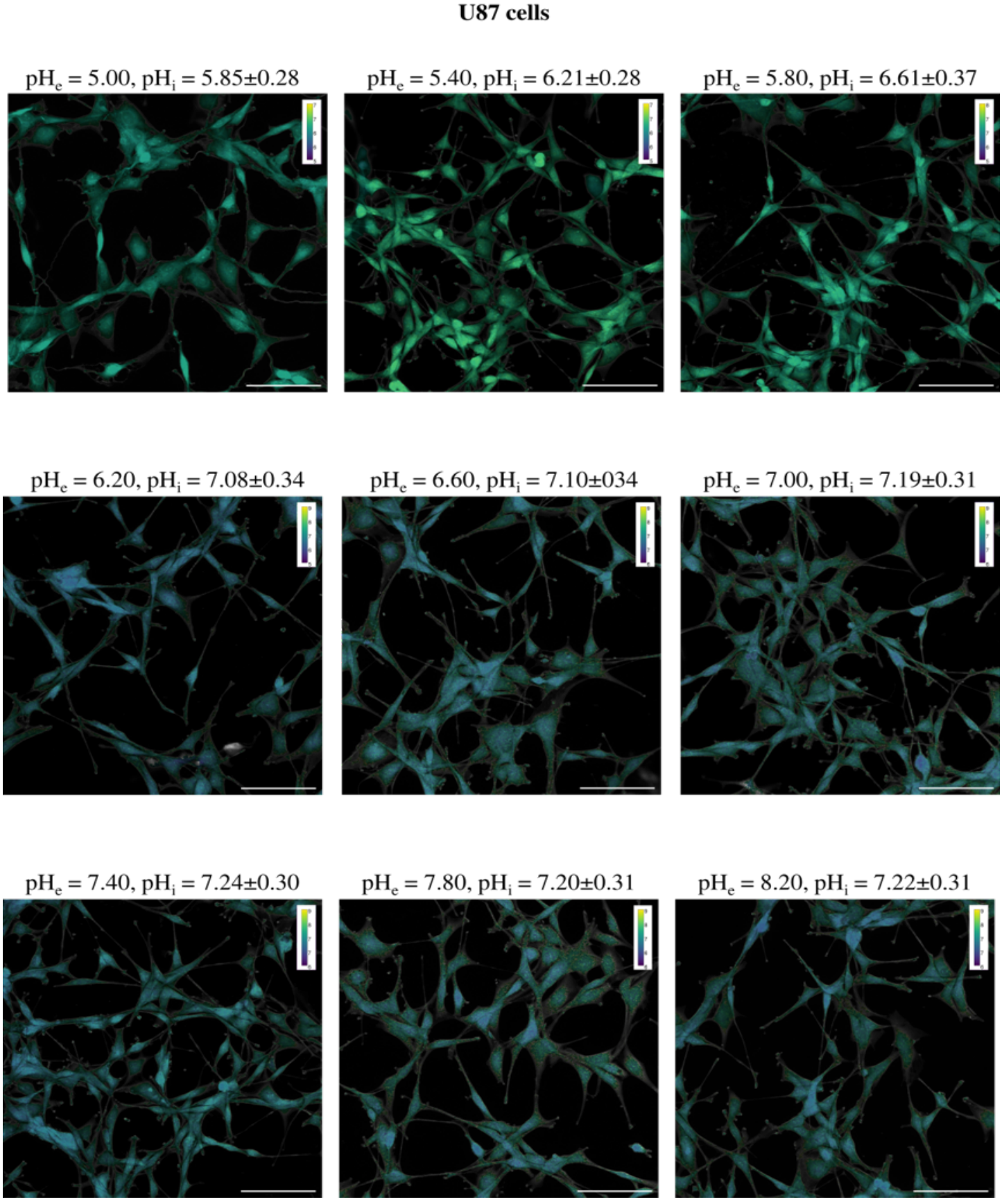

FIGURE 5.11: pH$_i$ distributions in U87 cells at different pH$_e$ values. The analyzed images were taken by our set-up 8 hours after exposure of the cells to a given pH$_e$. The mean pH$_i$ value obtained over the cell population is shown. Scale bar= 100 μm

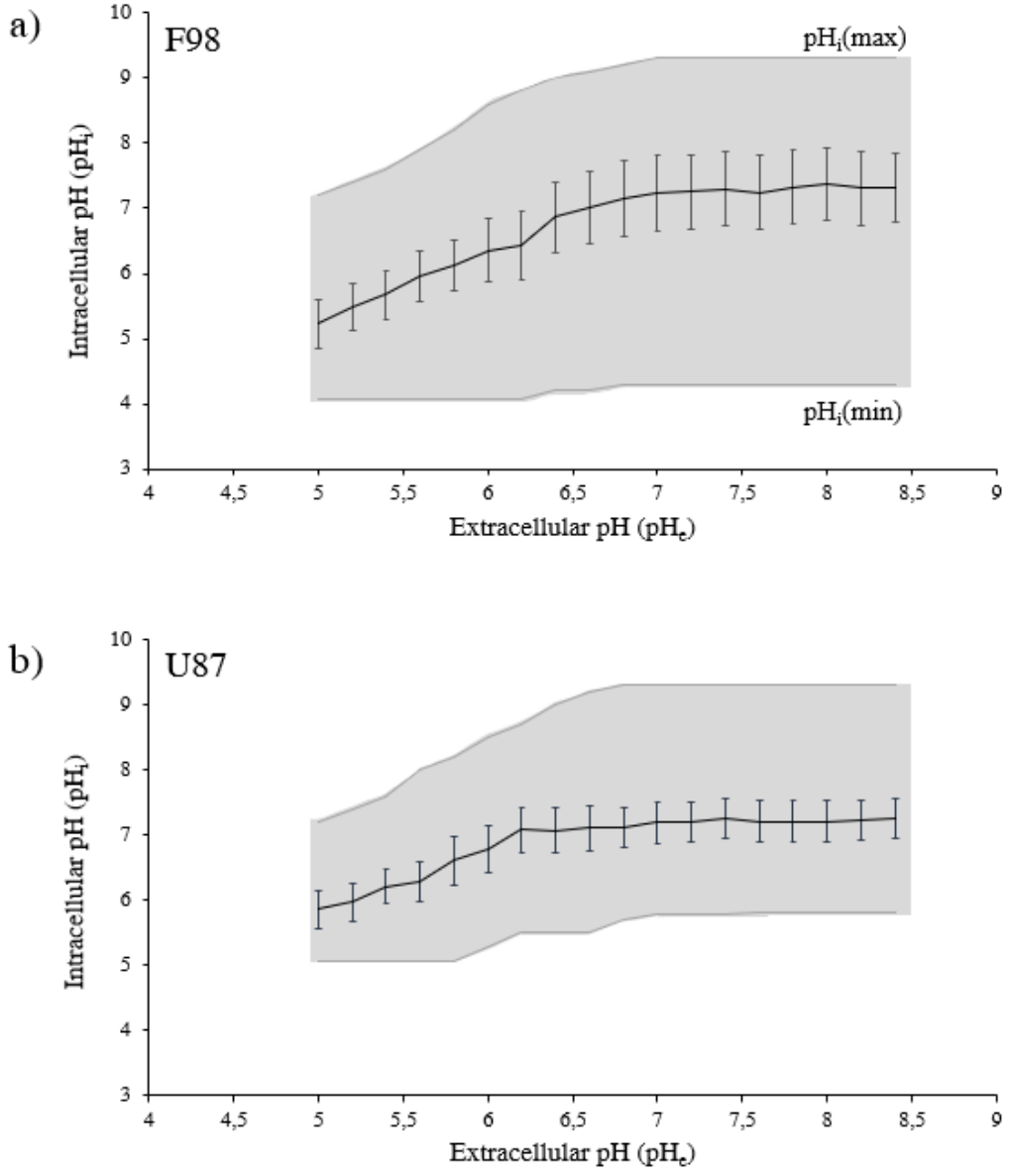

FIGURE 5.12: Investigation of the pH_i distribution at cell population, after incubation in DMEM medium of different pH_e values. Both glioma cells were analyzed: a) F98 and b) U87.

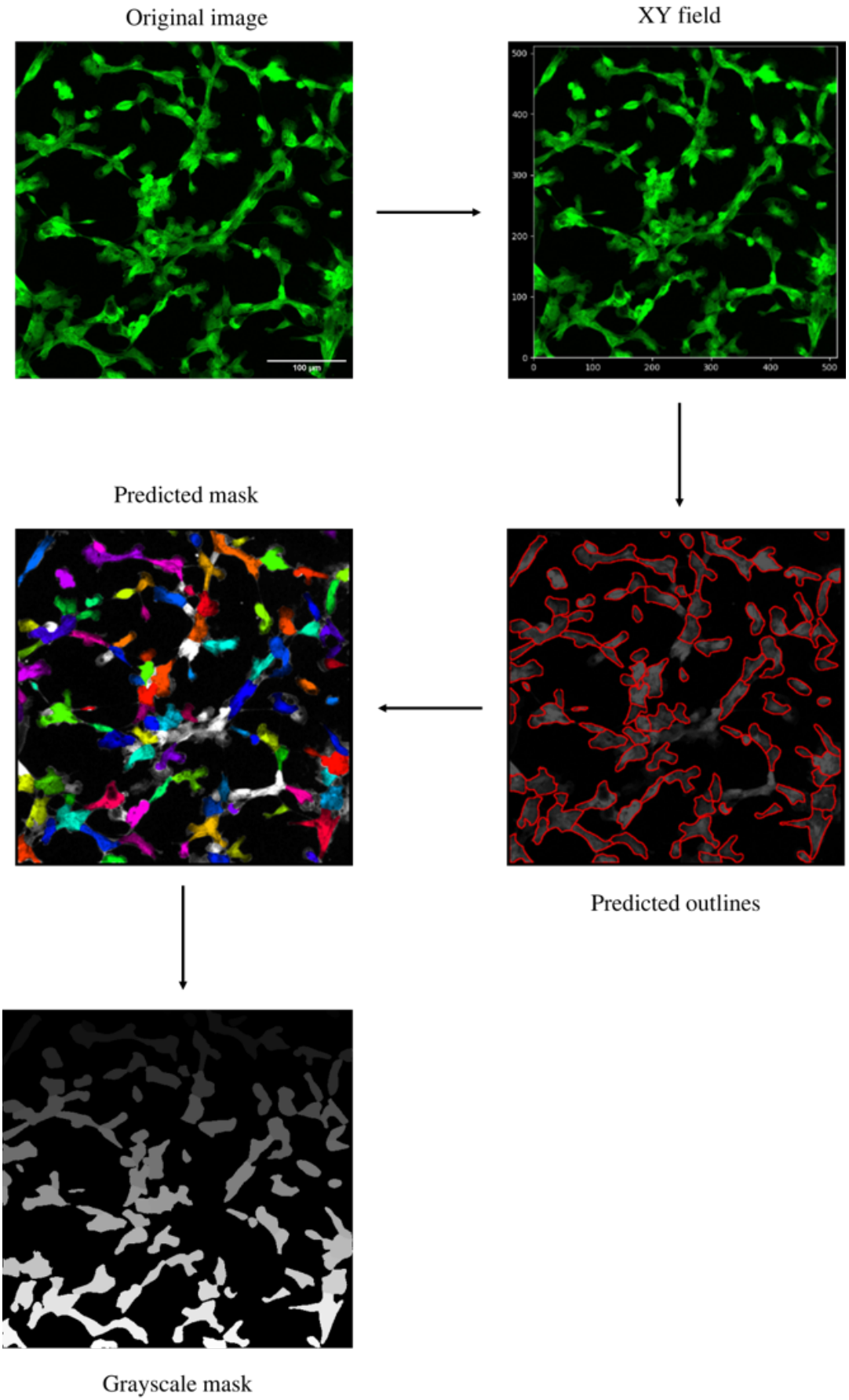

FIGURE 5.13: Cellpose processing steps. Cellpose runs the gradient prediction algorithm in the XY direction, in order to calculate a gradient image. Predicted labels are shown as pseudo-random colored overlay or displayed as a red outline. The final image is a mask in which every segmented cell has a different gray value.

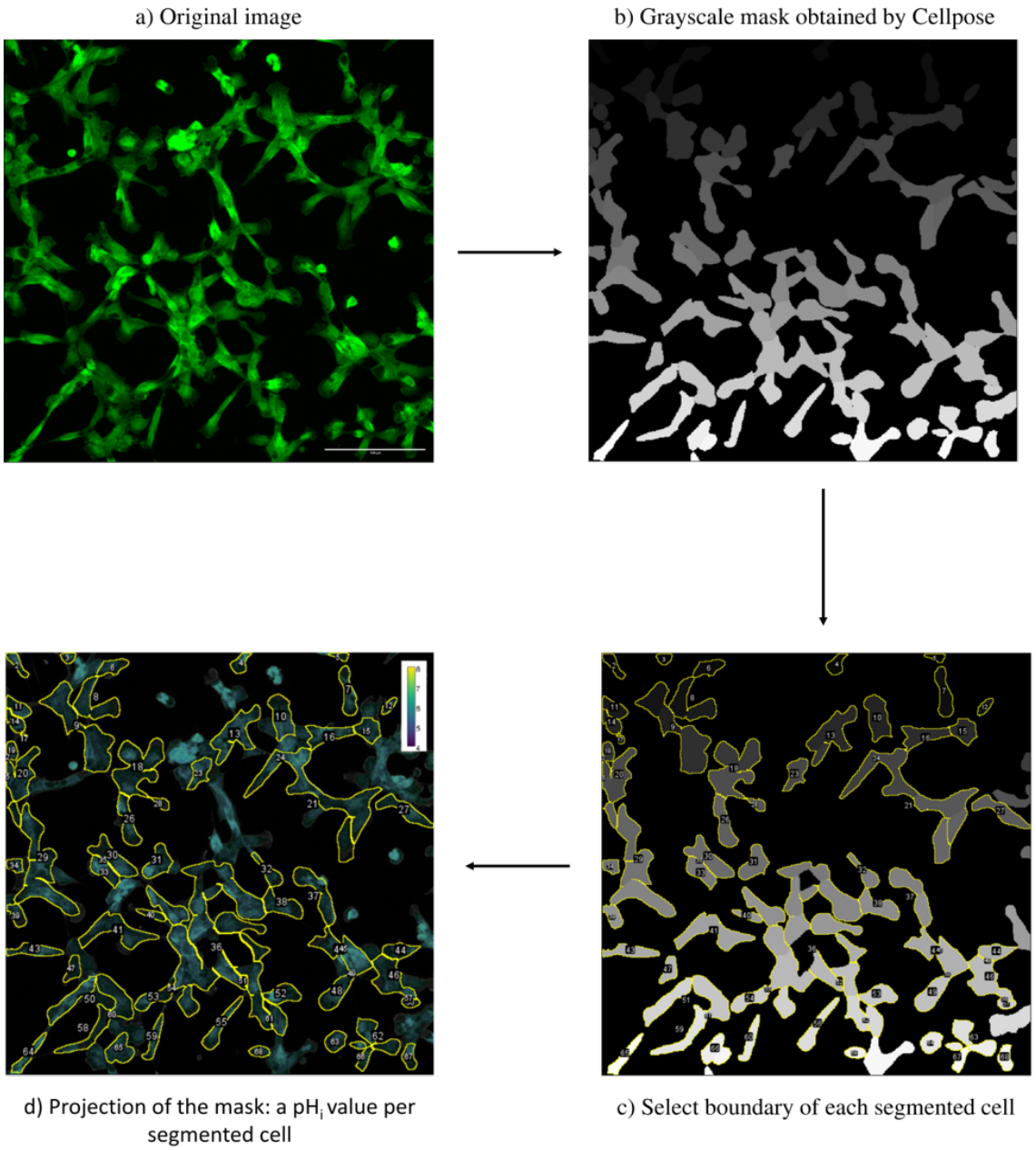

FIGURE 5.14: Intracellular pH quantification. The grayscale mask obtained by Cellpose was projected on the pH$_i$ distrubtion. A pH$_i$ value was associated with each segmented cell.

Therefore, given a pH_e, Figure 5.15 shows the mean pH_i values (M) obtained over all the segmented cells thus illustrating, in gray, the range of pH_i obtained at the *intercellular* level. From our data, we measure a very narrow range of pH_i values between cells, which means that the pH_i is very homogeneous at the *intercellular* level. As an additional criteria, both cell lines exhibit a low *intercellular std*(pH_i), independent of pH_e, of approximately 0.11 and 0.09 for F98 and U87 cells, respectively.
In fact pH_i heterogeneity may exist on the *intercellular* level of tissues. In the tumor, hypoxic cells are generally confronted by intracellular acidosis due to the accumulation of metabolic acids such as lactate and CO_2, which can accentuate pH_i heterogeneity. A strong example is tumor spheroids which, unlike conventional monolayer 2D cultures, allow the study of tumor heterogeneity and have a tissue organization with a much greater density evolution which generates hypoxia which makes them closer to *in vivo* conditions. Accessible from the edges of the spheroid, oxygen is consumed first by the cells of the periphery leading to depletion at the core of the tissue. Hence the pH_i gradient from the periphery to the core of the spheroid. However, cells in 2D monolayer cultures generally have the same oxygen supply, which explains the intercellular pH_i homogeneity.

5.5 Conclusion

Measuring pH in tumors provides useful information for describing the complex dynamics of the tumor microenvironment. Spatial heterogeneity surrounding, between and within cells plays a major role in driving the aggressive tumor phenotype. Rather than acting as a by-product of altered metabolism, intracellular pH variation generates the conditions necessary to alter protein functions, maintain cell differentiation capacity, reduce therapeutic uptake, arrest antitumor immune activity and promote cell migration and metastasis. Additionally, kinetic processes affecting pH can hold a wealth of information regarding tumor initiation, metabolism, and progression. Many imaging and measurement techniques have been developed to study both pH_i and pH_e and further development of these and other *in vivo* pH measurement techniques will help reveal the complex role that plays the transport of protons in the development and treatment of tumors.

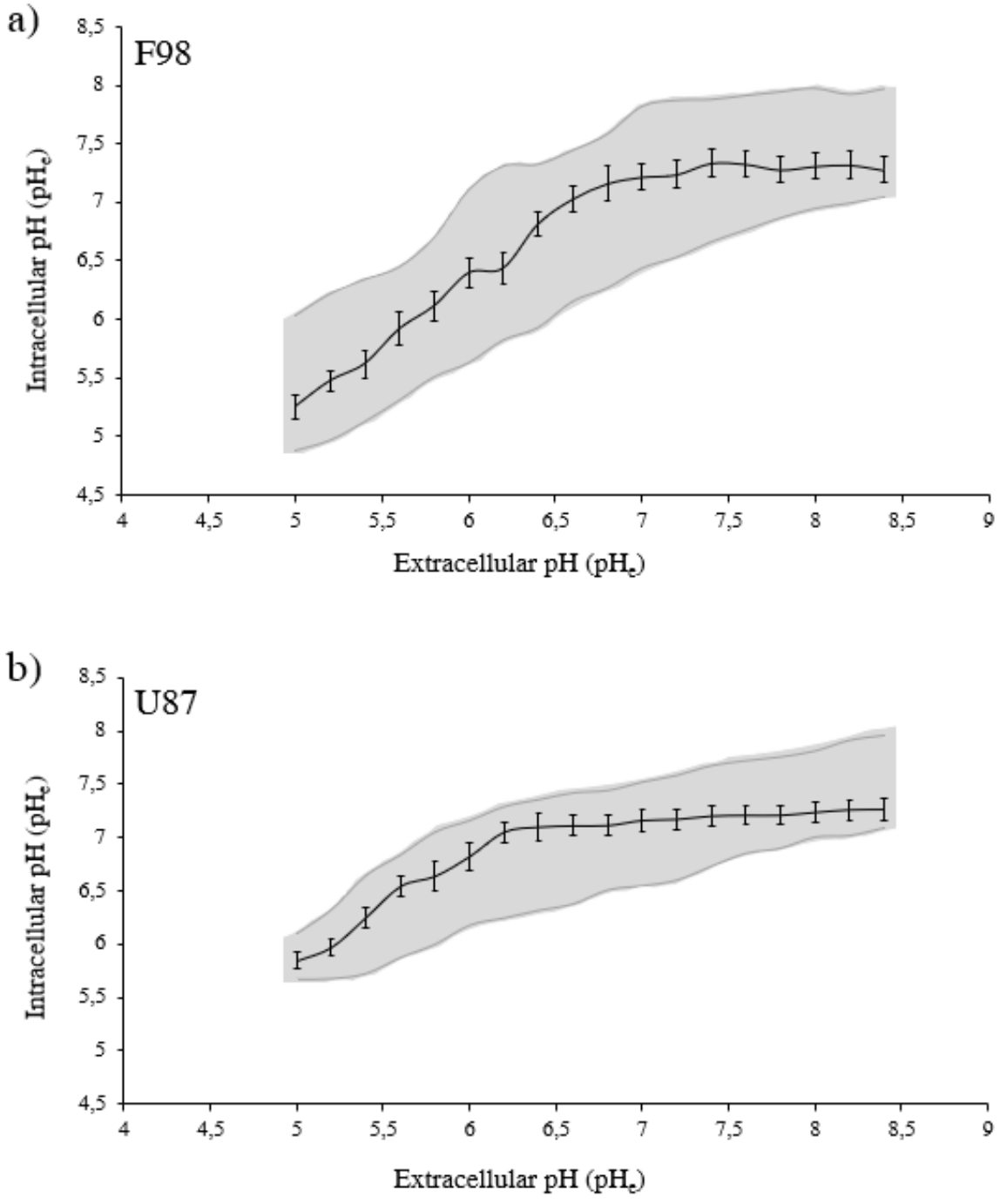

FIGURE 5.15: Investigation of the "*intercellular*" pH_i distribution. Both glioma cells were analyzed: a) F98 and b) U87.

Chapter 6

Intracellular pH evaluation in 3D spheroids

6.1 Introduction

Progress in basic cancer biology research has long suffered from the lack of experimental *in vitro* culture models capable of reproducing the main mechanical, physicochemical and biochemical characteristics of solid tumors. *In vitro* models of tumor cells cultured on 2D substrates proved poor in reproducing or "mimicking" the characteristics of a solid tumor and, were unable to reproduce the successive microenvironments corresponding to the main stages of tumor development, from the generation of an initial tumor at its primary site with the formation of a stroma infiltrated by various cells, and then the migration via the vascular endothelium to tissues of secondary sites of implantation in different organs (metastases) (Bhadriraju and Chen, 2002; Yamada and Cukierman, 2007; Kenny et al., 2007; Weigelt and Bissell, 2008). In view of these complex events still partially elucidated, traditional 2D culture models have, however, facilitated the acquisition of fundamental mechanistic data such as the concepts of oncogenes and tumor suppressor genes or even signaling, since all in all, they simplified mechanistic studies by capturing only limited aspects, of such an aspect of tumor cell biology, for example cell proliferation (Kapałczyńska et al., 2016). On the other hand, these 2D models could not claim to reproduce the biology of a tumor and the integration of relevant biochemical and metabolic parameters, such as the values of the gradients of oxygen and nutrients delivered to the cells according to their localization within the tumor (Barbosa et al., 2021). Moreover, even if 2D tumor cultures could be used with some success for preliminary tests of potentially anti-oncogenic molecules, significant differences between the effects obtained with these cultures and on animal models were observed, which limited particularly the recourse to appreciate their relevance as study models of new antitumor agents. This set of observations has justified the search for *in vitro* cellular models really suitable for the production of three-dimensional or 3D structures approaching if not reproducing the characteristics of different solid tumors, including their respective specificities. A large number of studies have been and continue to be devoted to the *in vitro* reproduction of the structural characteristics of tumor architecture. One of the most studied models is that of the spheroid since it is the most suitable for recreating the conditions of the microenvironment observed *in vivo*, including the recreation of functional properties of real tissues.

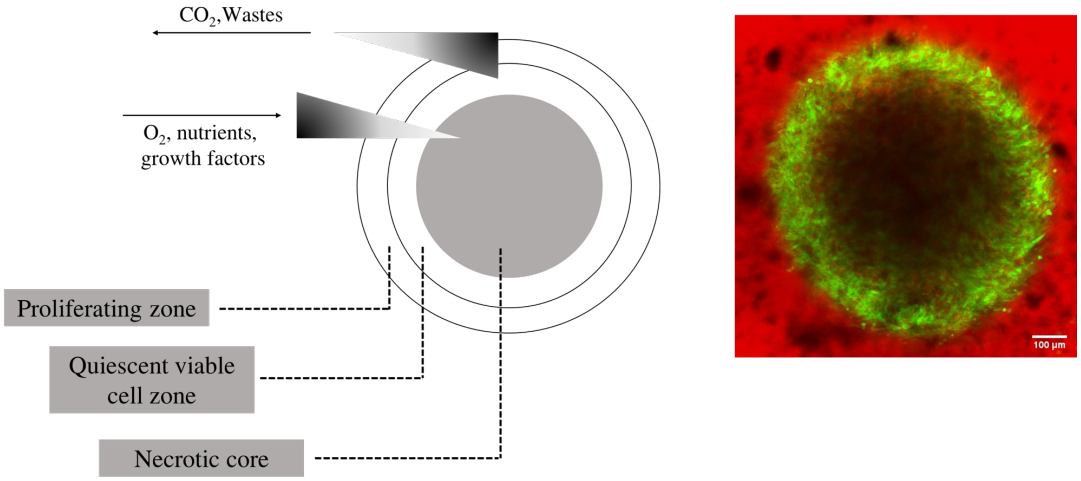

FIGURE 6.1: Schematic representation (on the left) of the spherical geometry of a tumor. Due to their 3D conformation, oxygen gradient is generated between the surface and the core of the spheroid, leading to three distinct layers: a necrotic core, a layer of resting cells and an outer layer of proliferating cells. Right: Picture of a spheroid grown for 30 days. Cells were marked using the fluorescent proteins Green FLuorescent Protein (GFP) and Sulforhodamine B (SRB) is used to mark the dying cells. Living cells are colored in green, dying cells appear in red. The centre of the tumour is composed of hypoxic and dead cells, both do not emit fluorescence.

6.2 The spheroids

According to a general definition (Katt et al., 2016), spheroids are aggregates of cells growing three-dimensionally in suspension and developing complex interactions between cells or with a three-dimensional matrix (e.g. matrigel).

It has been shown that membrane receptors involved in the regulation of cell adhesion and metabolism are expressed in spheroids. This is important for cell aggregation and cell to cell interaction (Fujisawa et al., 2020). Due to the 3D tissue conformation, an oxygen gradient is generated between the surface and the core of the tumor spheroid, which leads to three distinct layers: a necrotic core in the center of the spheroid (hypoxic zone), a layer of resting cells (reversible state in which the cell does not divide due to the reduce oxygen availability) and an outer layer of proliferating cells (which have a direct access to oxygen) (Hirschhaeuser et al., 2010; Breslin and O'Driscoll, 2013; Lazzari, Couvreur, and Mura, 2017) (Figure 6.1). The spheroid has a critical size (of the order of a few hundred µm), beyond which necrosis phenomena can appear (Franko et al., 1998). The heterogeneous microenvironment within a spheroid, in terms of oxygen, nutrients, results in metabolic heterogeneities. Moreover, the production of lactate by hypoxic cells leads to the generation of an acidic environment at the core of tumors. Therefore, the generation of a pH_i gradient associated to an accumulation of lactate is observed in spheroids.

Given the above considerations, tumor spheroids and fluorescent pH-probes are helpful to increase our knowledge on pH fluctuations during tumor formation. So we describe here a method for intracellular pH sensing in glioma tumor spheroids, using the ratiometric BCECF probe in association with confocal fluorescence microscopy.

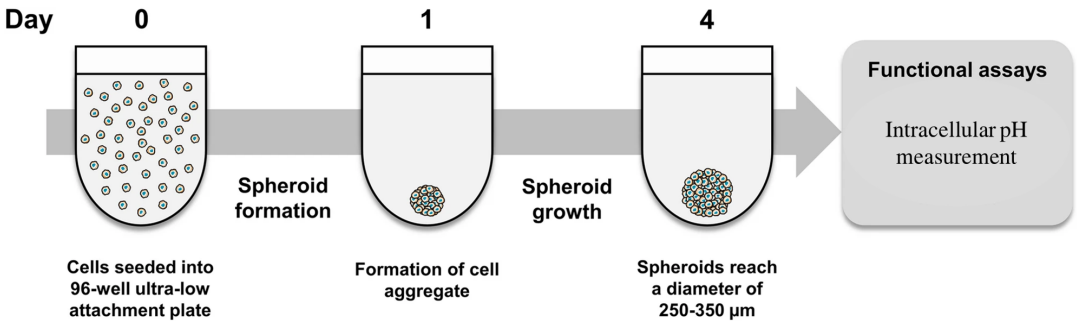

FIGURE 6.2: Spheroid formation using 96-well ultra-low attachment, round-bottom plate. On day 0, cells are harvested and seeded at 1000 cells per well to achieve 3D spheroids with a diameter of 250–350 µm by day 4. The 3D spheroids were then used to measure intracellular pH. Apdated from Roper et al., 2021

6.3 Formation of spheroids

Different cell lines have very different adhesion properties and the most appropriate spheroid formation protocol must be established in each case. We found that U87 and F98 cells are suitable for spontaneous spheroid formation and do not require the addition of reconstituted basement membrane to successfully form spheroids. Therefore, a simple way to achieve the formation of a three-dimensional spheroid is to limit the adhesion of cells to the support by modifying the properties of the surface. This is made possible thanks to the round bottom ultra-low attachment plates which allow the establishment of cell-cell interactions to the detriment of cell-support interactions and promotes the formation of spheroids.

Thus, during our experiments, glioma spheroids were cultured in CELLSTAR® 96 well, round bottom ultra-low attachment plates. F98 and U87 cells were seeded on day 1 at a density of $1{\times}10^3$ cells per well in a volume of 200 μL of medium.The cells are always maintained at standard culture conditions in an incubator at 37°C in a humid atmosphere, composed of 95% air and 5% CO_2. 24 hours after plating, we see the formation of spheroids (1 spheroid per well) (Figure 6.2). The experiment is ended on culture day 4, on which pH_i is assessed. As in 2D cultures, measurements of pH_i in glioma spheroids were implemented using the protocol described in Chapter 2.

pH_i measurements were initiated on day 4 by adding 5μM of BCECF to the culture medium. Afer 60 min of incubation with BCECF, spheroid were washed 3 times with fresh medium (pH ~ 7.4) to remove the probes not taken by the cells. The spheroids were then exposed to different DMEM media with three different pH_e values (5.00, 6.00 and 7.40).

6.4 Fluorescence microscopy

8 hours after incubation with a given pH_e, confocal fluorescence images were recorded by successively exciting each spheroid at 405 nm and 488 nm. Starting from one pole of each

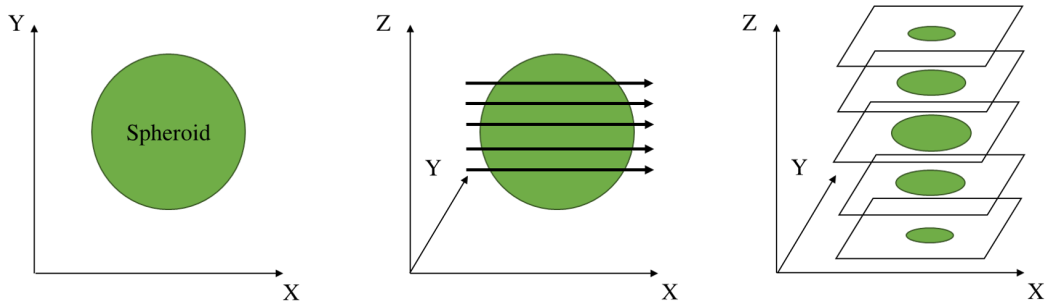

FIGURE 6.3: Confocal z-stacks. Starting from one pole of each spheroid, confocal z-stacks were obtained through them with a step size of 5 μm between adjacent optical planes.

spheroid, the excitations are carried out by optical sections along the Z axis (confocal z-stack) through the spheroid with a Z-slice spacing of 5 μm between adjacent optical planes (Figure 6.3). Figure 6.4 shows a confocal Z-stack, of 50 slices, through a U87 spheroid (diameter 330 μm) incubated at pH_e 7.40. As can be seen, the penetration depth of imaging was very restricted, demonstrated by the early onset of signal attenuation. This is due to the constituents of the 3D biological sample and the lack of transparency of light scattering, which reduce the performance of confocal microscopy. In addition, refractive index (RI) mismatches between media and sample limit the ability to image the entire depth of spheroids, resulting in low contrast and reduced spatial resolution with depth. With our setup, at a depth of 150 µm, there was very little apparent signal (Figure 6.5).
On the other hand, as the depth in the spheroid increases, a central dark area devoid of BCECF signal, and surrounded by a thin viable rim of cells is observed (Figure 6.4). It could be due to necrosis. However, without necrosis staining, it is difficult to discern whether the central dark area was due to necrosis or limited light penetration into the spheroid. Indeed, previous studies reported that beyond a diameter of 500 μm, most spheroids develop hypoxia leading to a necrotic core surrounded by a viable rim of cells (Kunz-Shughart, Kreutz, and Knuechel, 1998; Hirschhaeuser et al., 2010). However, in our culture conditions, we collected spheroids with a diameter < 500 μm (Figure 6.6). Therefore, we assume that the central dark area is rather due to limited light penetration into the spheroid.

Under identical culture conditions, F98 spheroids (diameter 430-490 μm) are larger than U87 spheroids (diameter 290-330 μm) (Figure 6.6). It has been reported that the size of spheroids, ranging from tens to hundreds of microns in diameter, is critical for cellular functions and model applications, thus spheroids of different sizes do not exhibit the same properties (Friedrich et al., 2009). For example, spheroids with a diameter < 150 μm will not develop chemical gradients (pH_i, oxygen nutrients etc.). These gradients are usually generated in spheroids with diameters > 200 μm and increase with increasing spheroid size (Friedrich et al., 2009; Murphy et al., 2017). Therefore, due to a size-induced oxygen difference, we expect to find a larger pH_i gradient in F98 spheroids than in U87 spheroids.
Moreover, it is clear that F98 spheroids are much more spherical than U87 spheroids with a denser and more compact shape. Therefore, the nature of cell-cell interactions is probably

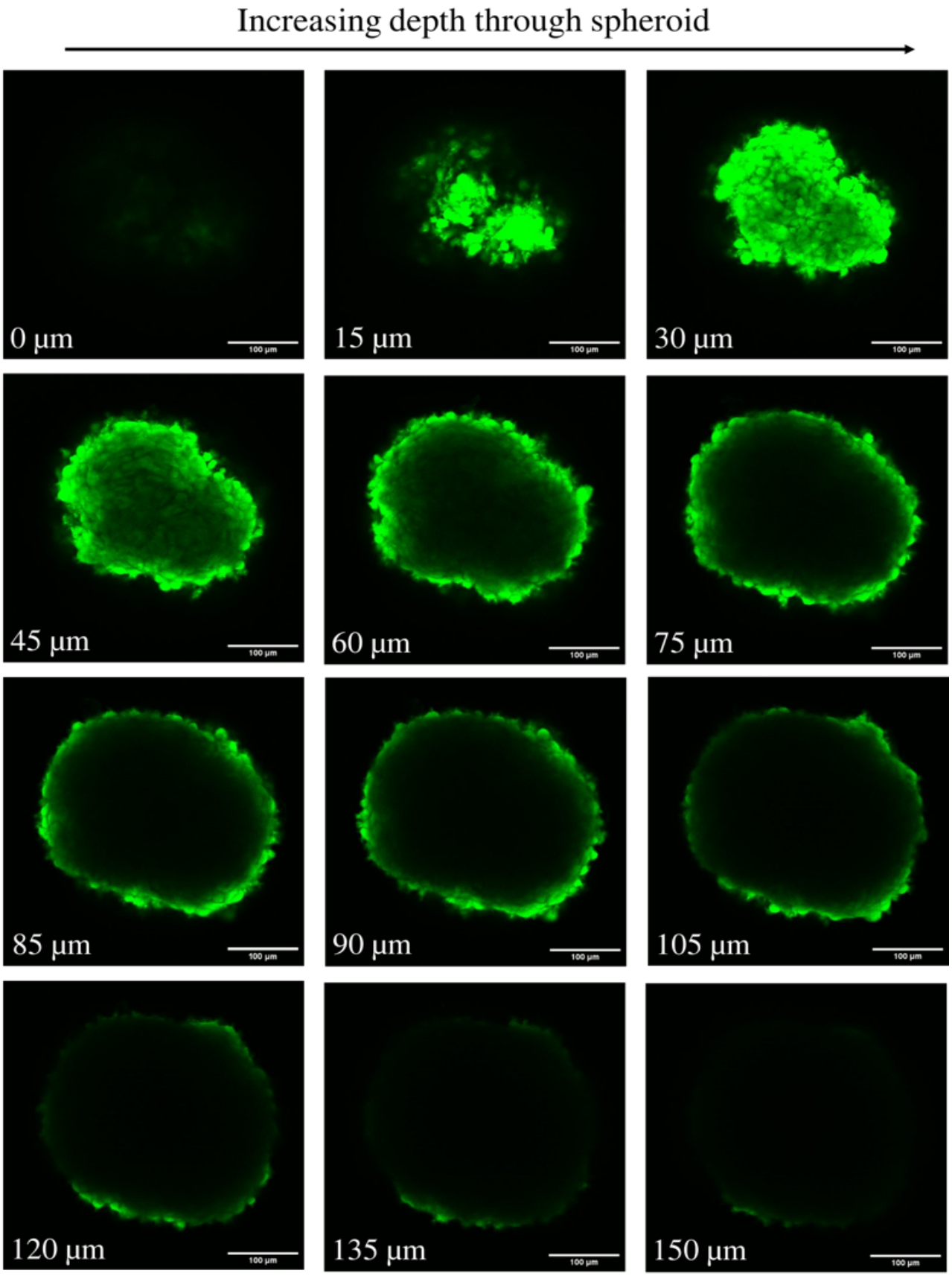

FIGURE 6.4: An example for a confocal z-stack through a U87 spheroid incubated at pH_e 7.4. Starting from one pole of the spheroid, confocal z-stacks were obtained through them with a step size of 5 μm between adjacent optical planes. Depth of scanning is indicated on the images. Scale bar = 100 μm. Excitation = 488 nm.

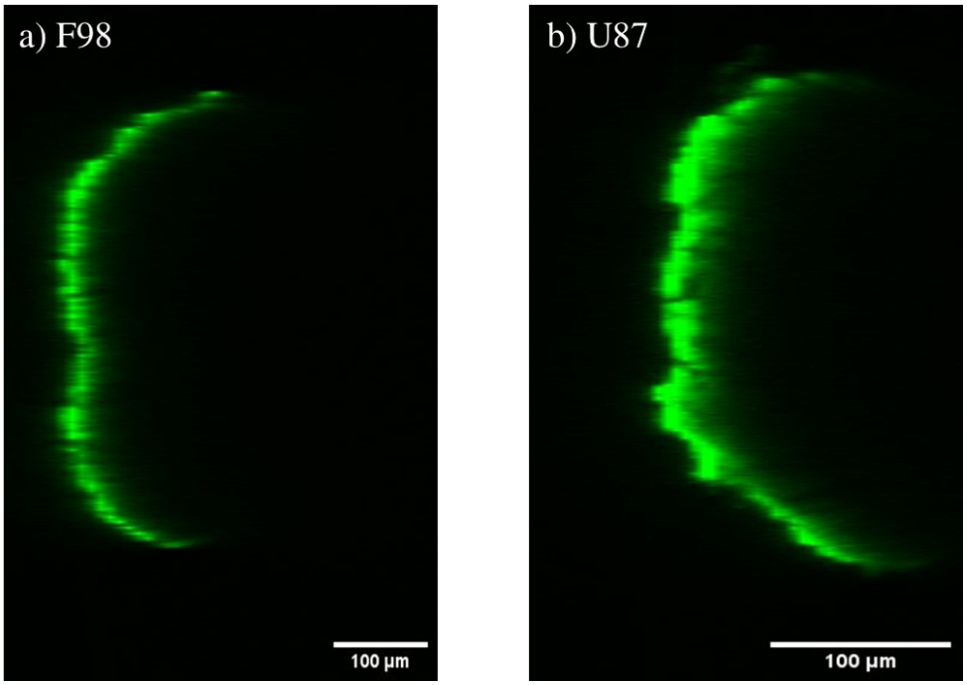

FIGURE 6.5: Orthogonal views of (a) a F98 cell spheroid and (b) a U87 cell spheroid suspended in DMEM medium at pH_e 7.4. The views are reconstructed, with ImageJ, from a Z-stack of confocal images with excitation of BCECF at 488 nm. With our setup, an imaging penetration depth of 150 μm was achieved

different between the two cell lines and the compacted shape of the F98 spheroid may be associated with an increased number of cell-cell contacts inside the spheroid.

6.5 Image processing

To monitor pH_i in tumor spheroids, the fluorescence images were processed with Julia software (https://julialang.org/). The background signal, taken from an empty region, was subtracted from the measurements, and the ratio of emission intensity resulting from excitation at the two wavelengths (488 nm and 405 nm) was calculated pixel-to-pixel. To convert the ratio signals to pH_i values in the spheroids we used the appropriate calibration curves obtained for monolayered cells (Chapter 2). As shown in the Figure 6.7, a pH_i distortion at the depths greater than 85 μm was observed, owing to the poor permeability to light. To avoid any distortion, the pH_i measurement was limited to a depth of 85 μm.

In total, 18 spheroids were treated (see Appendix A) but the best of replicates are presented: three spheroids for each cell line (U87 and F98) incubated at different pH_e values (5.00, 6.00 and 7.40). For each spheroid, pH_i map in the slice located at a depth of 85 µm is presented in Figure 6.8. The following paragraphs are dedicated to the analysis of these images

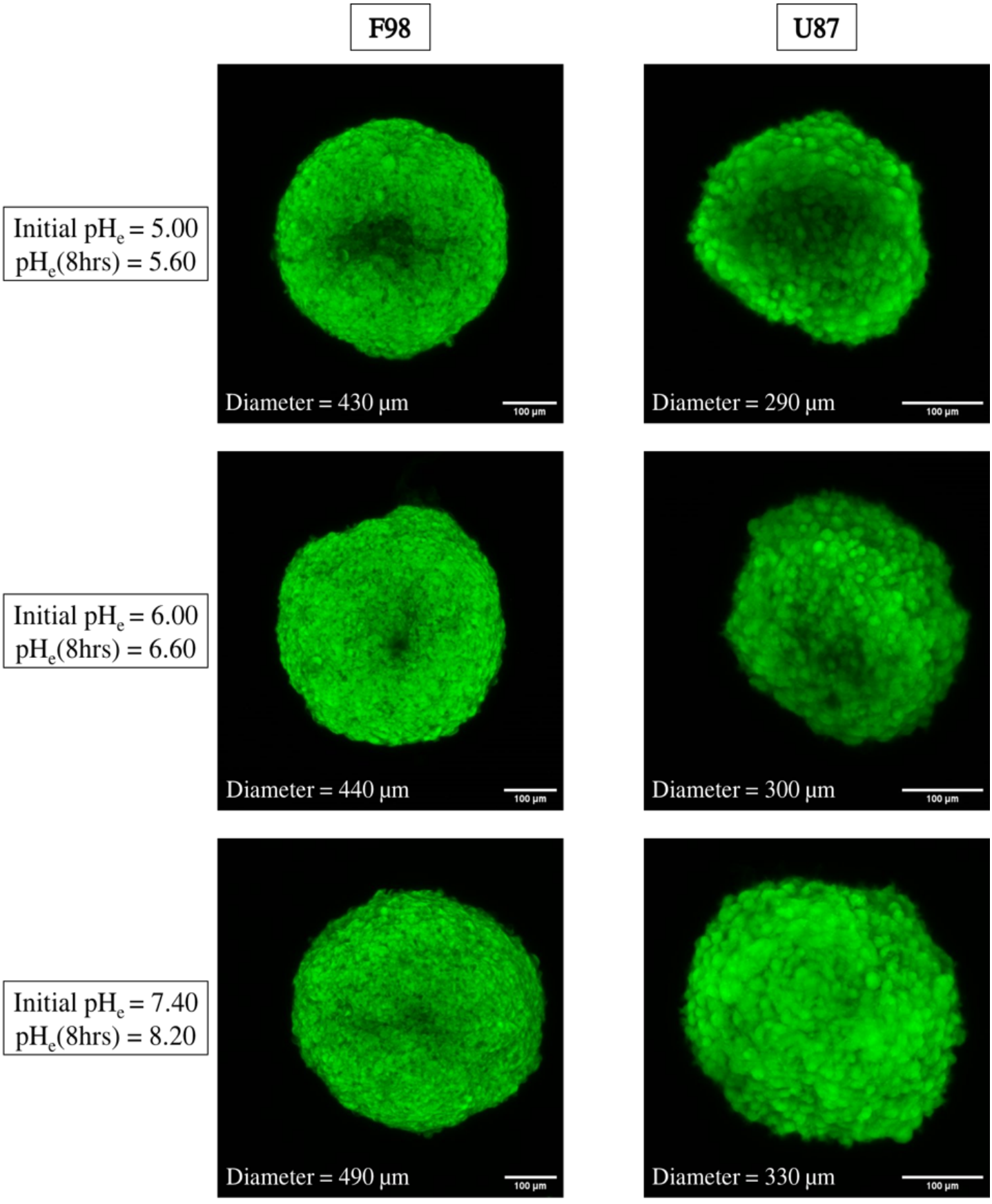

FIGURE 6.6: Z-projection images generated by first collecting a stack of fluorescent images with a step size of 5 μm along the Z-direction and projected them down to a high quality 2D-image using sum slices projection (ImageJ). The spheroids were incubated at different pH$_e$ values and confocal Z-stak images were recorded 8 hours after incubation. Scale bar = 100 μm

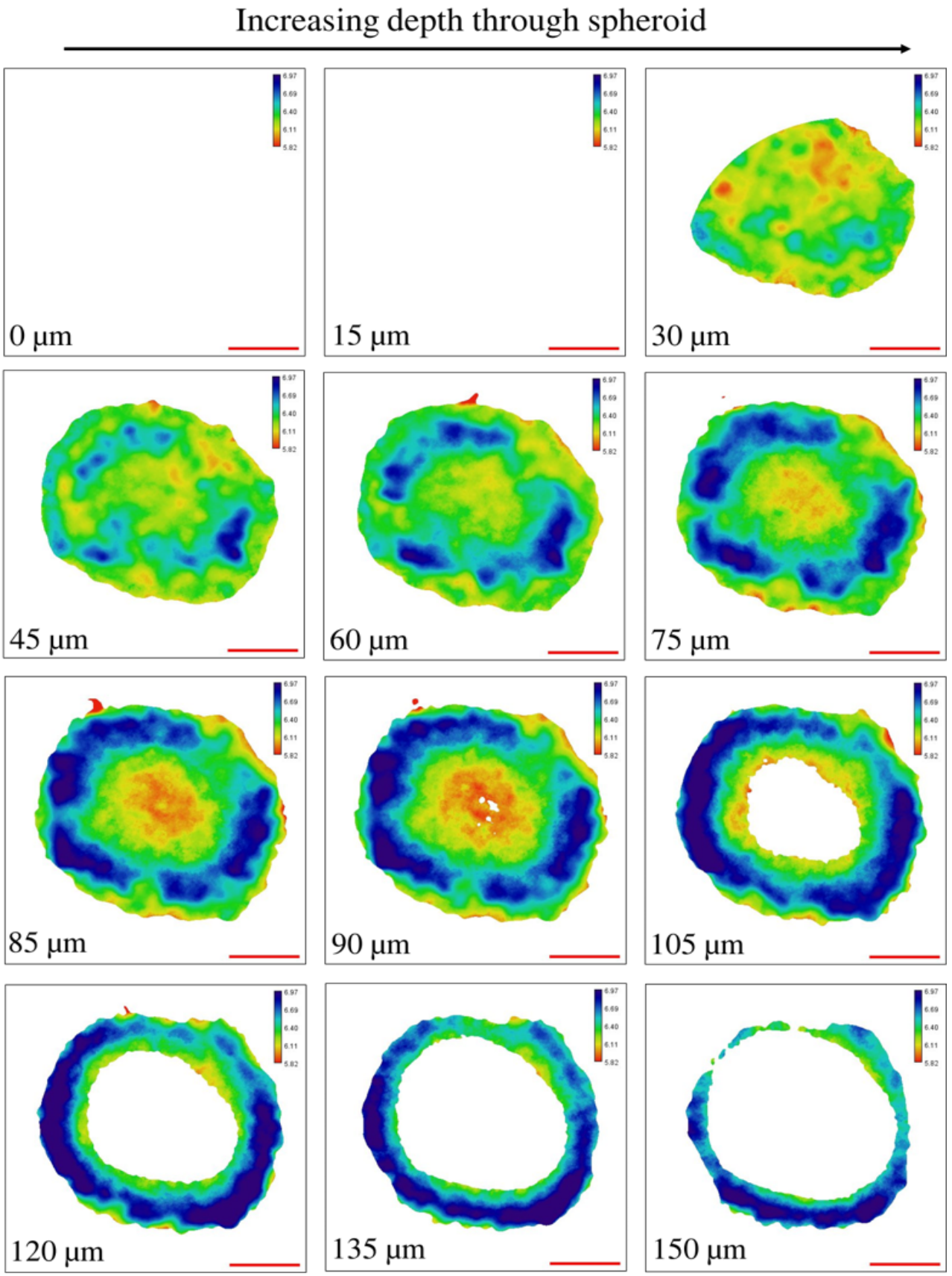

FIGURE 6.7: pH_i maps in the U87 spheroid (Figure 6.4) incubated at pH_e 7.40. A pH_i map for each slice is obtained. Due to the poor permeability to light, a pH_i distortion at the depths greater than 85 μm was noticed. scale bar= 100 μm

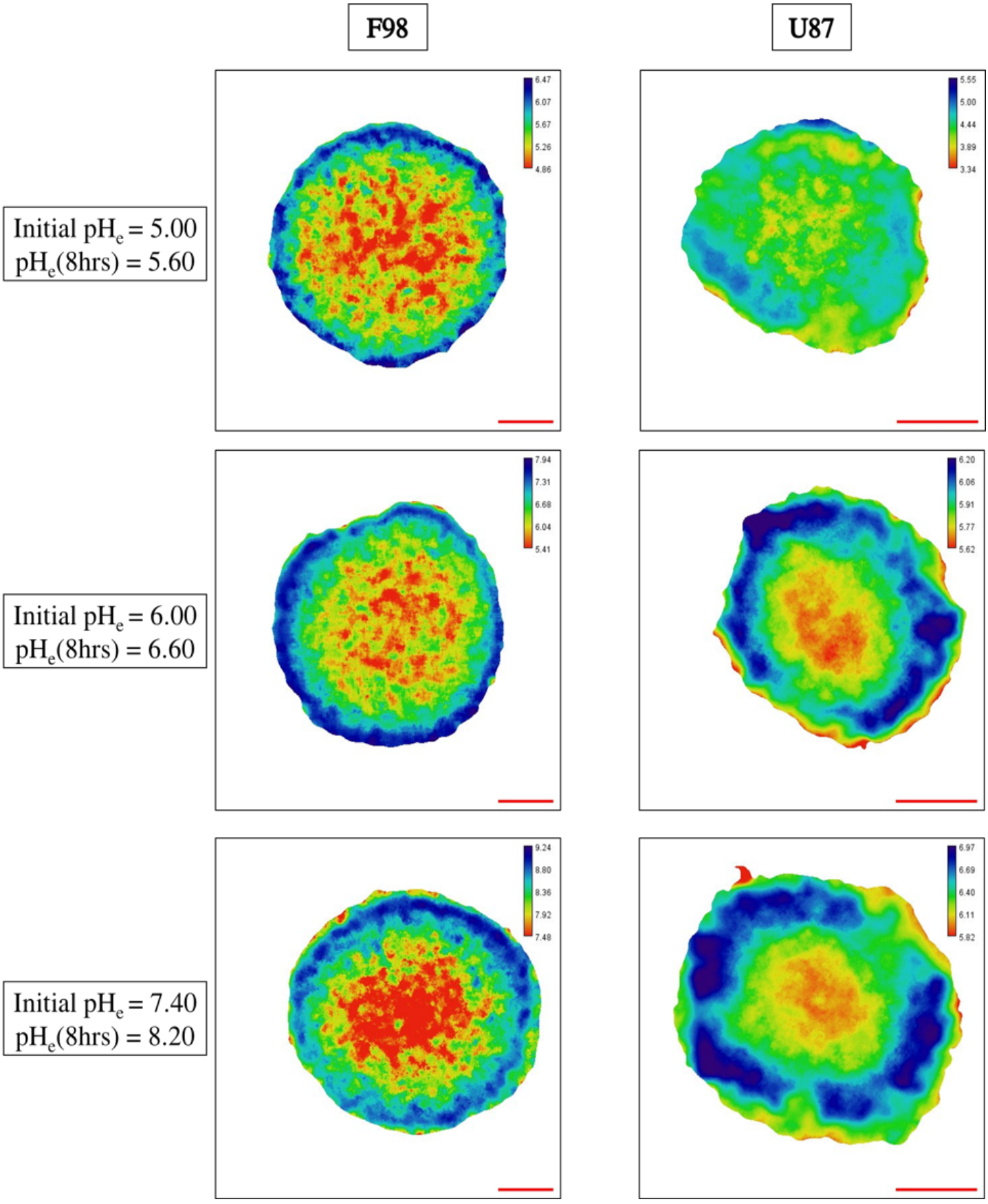

FIGURE 6.8: pH$_i$ map in the slice located at a depth of 85 μm. Scale bar = 100 μm

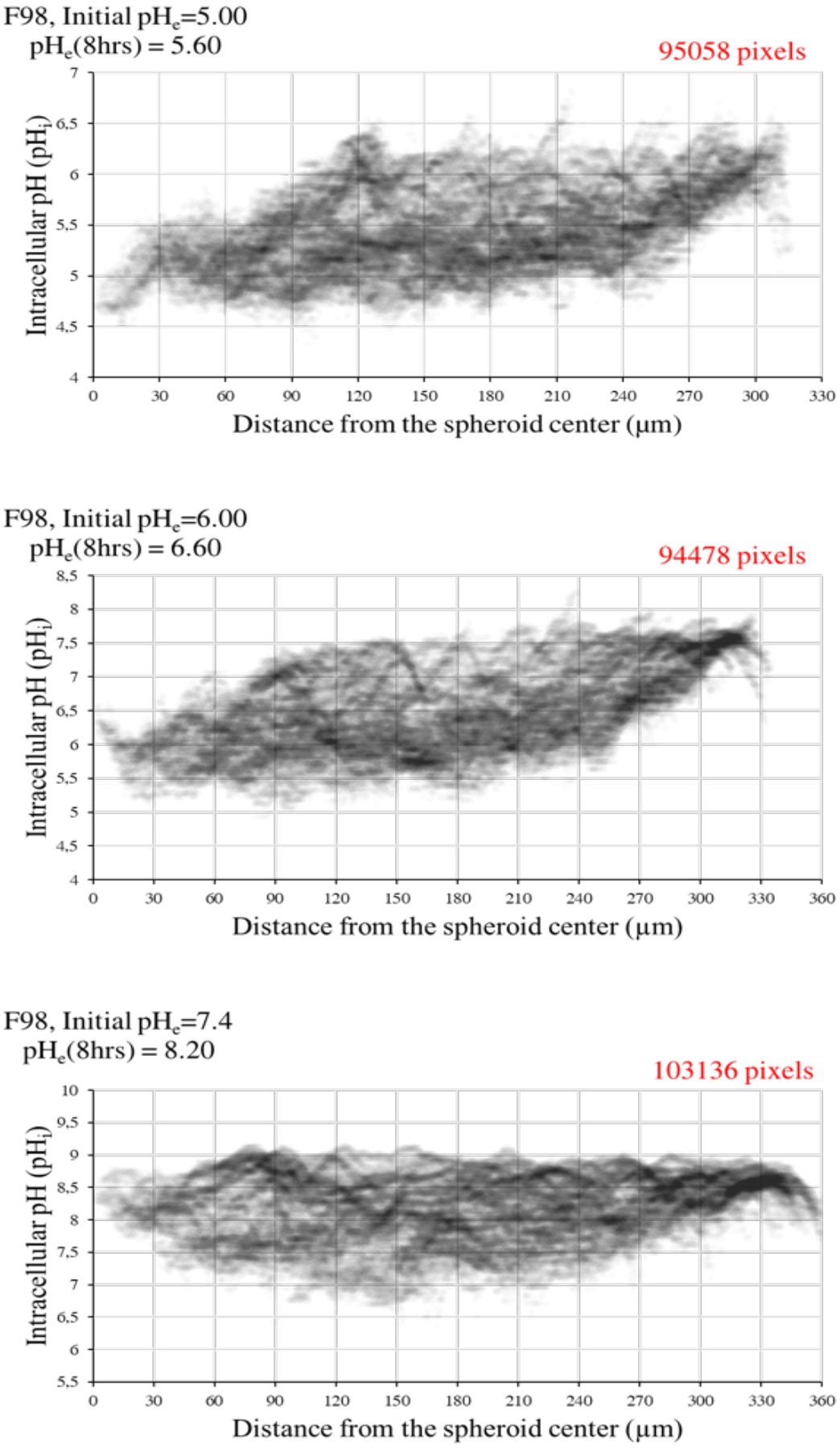

FIGURE 6.9: Radial profiles of F98 spheroids incubated at different pH$_e$ values. Each point corresponds to a pixel in the pH$_i$ map and, each pixel has a pH$_i$ value and is located at a certain distance from the center of the spheroid. The number of pixels in each pH$_i$ map are displayed.

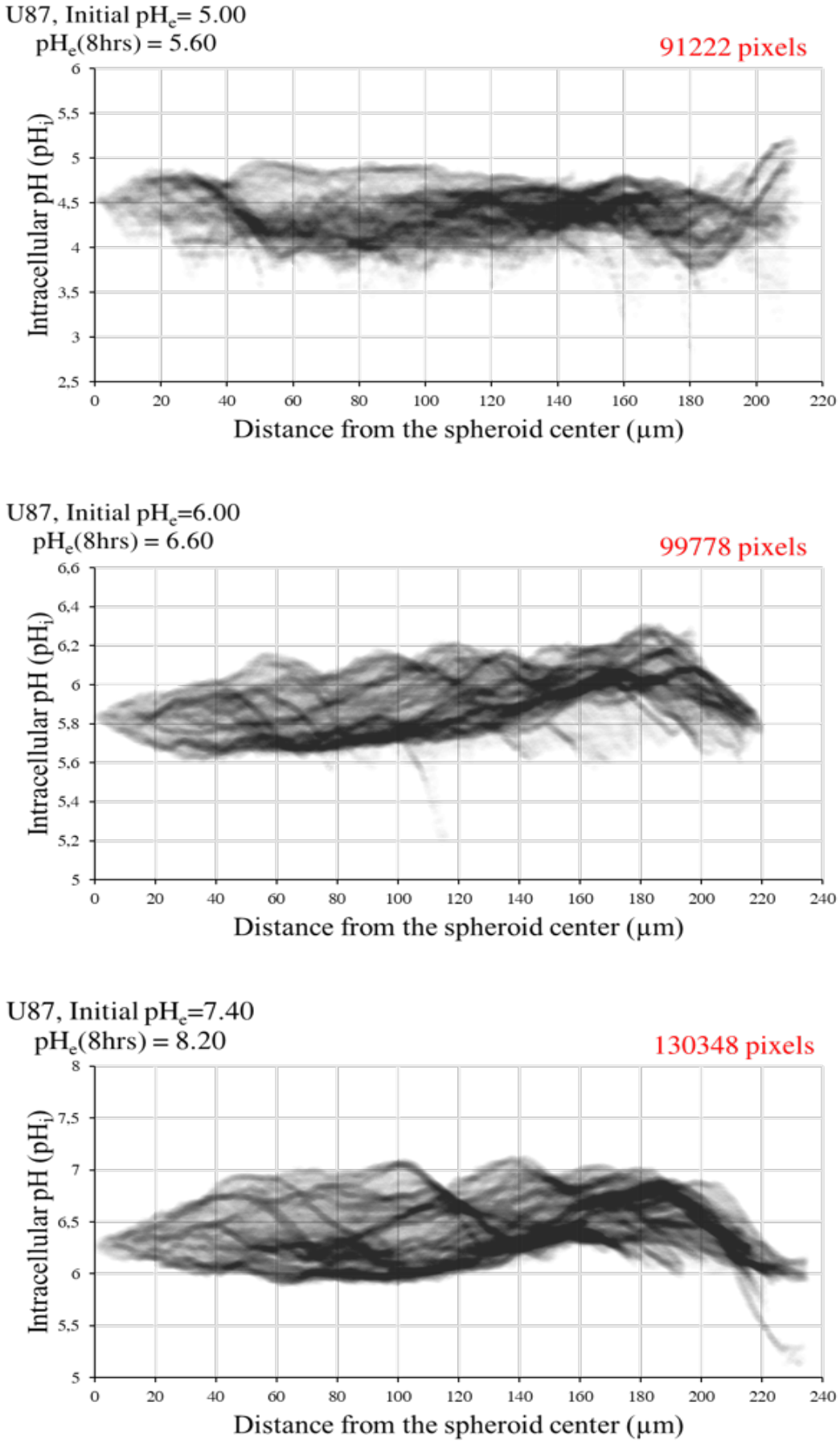

FIGURE 6.10: Radial profiles of U87 spheroids incubated at different pH$_e$ values. Each point corresponds to a pixel in the pH$_i$ map and, each pixel has a pH$_i$ value and is located at a certain distance from the center of the spheroid. The number of pixels in each pH$_i$ map are displayed.

6.6 Intracellular pH in tumor spheroids

Figure 6.8 shows the pH_i distribution in the slice located at a depth of 85 μm in F98 and U87 spheroids. First, we clearly see the emergence of different pH_i zones that show a pH_i gradient with the lower pH_i at the core. These gradients are directly correlated to the depletion of nutrients, from the periphery to the core of the spheroid, including glucose, ATP and oxygen. Moreover, F98 spheroids, larger than U87 spheroids, exhibit a more "grainy" pH_i gradient than U87 spheroids which however show a "smoother" pH_i gradient. These gradients will be quantified later.
In order to quantitatively analyze the pH_i in U87 and F87 spheroids, we processed the map images (Figure 6.8) in two ways: First of all, we plotted the distribution of the pH_i measured for each pixel as a function of the pixel distance from the center of the spheroid. The added value of this presentation in to retain the spatial information contained in the pH_i map image. Second, the spheroids have been treated by generating 3 zones in the spheroids: central zone, intermediate zone and peripheral zone. A mean pH_i value is associated with each zone. The following two paragraphs are devoted to these two types of analysis.

Just before the analysis, it is important to take into account the pH drift of the DMEM culture medium discussed in Chapter 4. Table 7.1 summarizes the drift for each initial pH_e tested (5.00, 6.00 or 7.40), 8 hours after incubation at 37°C and 5% CO_2.

Initial pH_e	pH_e (t=48hrs)
5.00	5.60
6.00	6.60
7.40	8.20

TABLE 6.1: pH drift of DMEM medium after 8 hours of incubation at 37°C and 5% CO_2

6.6.1 Intracellular pH and spatial heterogeneity

First of all, the pH_i maps (Figure 6.8) were processed as follows: each pixel in the map image has a pH_i value and is located at a certain distance from the center of the spheroid. The distribution of the pH_i measured for each pixel as a function of the pixel distance from the center of the spheroid was therefore plotted. All pixel data are summarized in figure 6.9 (F98) and Figure 6.10 (U87). Note that each gray point on the pH_i distribution represents a pixel of the map image. Thus, the pixel size is 1.24 μm and 0.83 μm for F98 and U87 images, respectively, both are much smaller than the size of a cell. In this case, we also assess cellular heterogeneity as a cell has pH_i values spread over several pixels.
In addition, on the pH_i distribution, the darker the gray level, the more superimposed pixels there are (density indicator).

Firstly, all the pH_i distributions of F98 spheroids show a wide dispersion of points in the intermediate zone of the spheroids (Figure 6.9). However, this dispersion becomes less

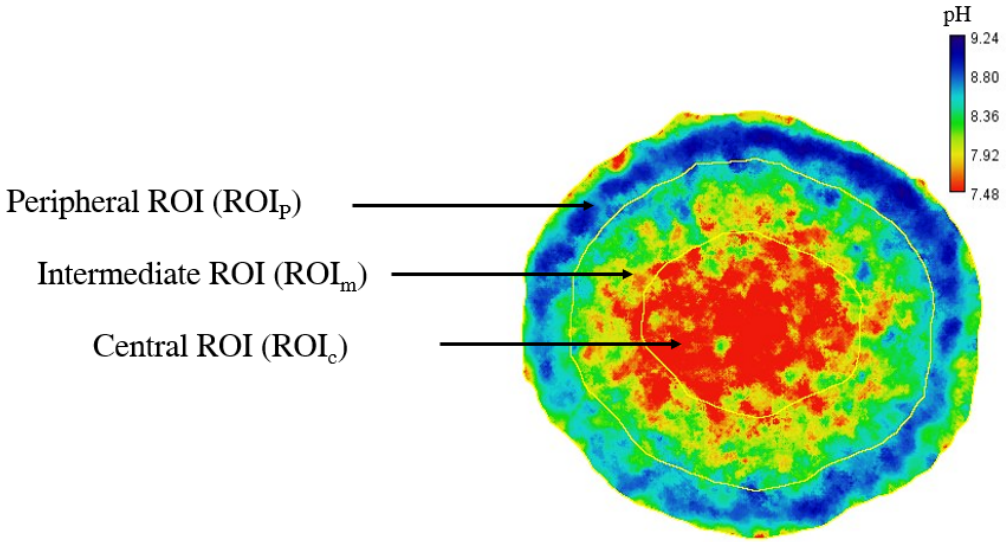

FIGURE 6.11: The equatorial plane of the spheroid was used to generate 3 regions of interest (ROIs) of width equal to a third of the spheroid radius. ROI_c was defined as ROI at the core, ROI_m was defined as the intermediate ROI, and ROI_p was defined as the peripheral ROI.

important approaching the core and the periphery (Figure 6.9). The distribution of pH_i is therefore quite heterogeneous in the intermediate zone of the F98 spheroids.
In addition, by examining the density of the points, we notice that the majority of cells in the intermediate zone have a pH_i between [5.00-5.50], [5.50-6.50] and [8.00-9.00] when incubated at a pH_e of 5.60, 6.60 and 8.20, respectively. However, by following the evolution of the pH_i as we move away from the center of the spheroid, we can see that a large group of central cells tend to increase their pH_i above 5.50 and 6.50 when incubated at a pH_e of 5.60 and 6.60, respectively. On the other hand, and under basic conditions, although the majority of central F98 cells have a pH_i between [9.00-8.00], a small group of cells tend to decrease their pH_i below 8.00. It therefore seems that the F98 intermediate cells attempt to regulate their pH_i towards a physiological state.

Secondly, the pH_i distributions of U87 spheroids (Figure 6.10) show a dispersion of points much less important than F98 cells and which follows the shape of a plateau as we move away from the center of the spheroid. The distribution of pH_i is almost homogeneous in the U87 spheroids. In addition, depending on the point density, we see that the majority of points have a pH_i between [4.00-4.50], [5.00-6.00] and [6.00-6.00] when incubated at a pH_e of 5.60, 6.60 and 8.20, respectively. Therefore, U87 spheroids do not regulate pH_i and are more acidic than F98 spheroid.

It has been reported that pH_i depends on the adhesive interactions of cells with neighboring cells and cell-cell contact interactions regulate cell activities via modulation of pH_i (Galkina, Sud'ina, and Margolis, 1996; Galkina et al., 1995). The fact that central F98 cells tend to

regulate their pH_i may be associated with an increase in the number of cell-cell contacts inside the spheroid.

6.6.2 pH_i gradients in the spheroid

Since tumor spheroids represent heterogeneous 3D structures in terms of pH_i, in which the cells of the outer proliferative layer are known to have a more alkaline pH_i than the quiescent cells inside (Zagaynova et al., 2017), pH_i measurements were performed separately for the inner and outer layers of the spheroids. For this, the map images (Figure 6.8) were used to identify the equatorial plane of the spheroid and to produce a spheroid outline. This contour was used to generate 3 concentric, nonoverlapping layered regions of interest (ROIs) of width equal to a third of the spheroid radius (Figure 6.11). ROI_c was defined as ROI at the core, ROI_m was defined as the intermediate ROI, and ROI_p was defined as the peripheral ROI. A mean pH_i value is therefore associated with each zone. Radial pH_i data are summarized in Figure 6.12.

pH_i in F98 Spheroids

Analysis of pH_i separately in the core and on the periphery of the F98 spheroids showed a statistically significant difference between the central and peripheral parts (Figure 6.12, top). Quantitative analysis of the pH_i values revealed that the pH_i in the central areas was 5.08 ± 0.21, 5.87 ± 0.28 and 7.51 ± 0.31 for spheroids incubated at a pH_e of 5.60, 6.60, 8.20, respectively. Whereas, the pH_i in peripheral parts of these spheroids was 5,97 ± 0,21, 7,18 ± 0,33 and 8,57 ± 0,27, respectively. F98 spheroids showed therefore 0.89, 1,31 and 1,06 units of difference in pH_i between the center and the periphery, when incubated at a pH_e of 5.60, 6.60 and 8.20 respectively.
Regardless of pH_e, F98 spheroids develop therefore significant radial gradients of pH_i, with the lowest levels reached at the core.

pH_i in U87 Spheroids

Quantitative analysis of the pH_i values revealed that the pH_i in the central areas was 4,17 ± 0,16, 5,72 ± 0,04 and 6,06 ± 0.08 for U87 spheroids incubated at a pH_e of 5.60, 6.60, 8.20, respectively (Figure 6.12, bottom). Whereas, the pH_i in peripheral parts of these spheroids was 4,41 ± 0,25, 6,03 ± 0,09 and 6,65 ± 0,20, respectively. U87 spheroids showed therefore 0.24, 0,31 and 0,59 units of difference in pH_i between the center and the periphery, when incubated at a of pH_e 5.60, 6.60 and 8.20 respectively.
According to another observation, the gradient of pH_i decreases with decreasing pH_e and the distribution becomes quasi-homogeneous under very acidic conditions.

In order to compare the pH_i gradients between the two spheroids F98 and U87, we calculated the slope of each gradient (Figure 6.12, see next to each gradient). F98 spheroids show a pH_i gradient with a slope of 0.0063, 0.0112 and 0.008 when incubated at a pH_e of 5.60, 6.60 and 8.20 respectively. While the U87 spheroids show a pH_i gradient with a slope

of 0,003, 0,0034 and 0,0062 when incubated at a pH_e of 5.60, 6.60 and 8.20 respectively. For a given pH_e, the U87 spheroids present pH_i gradients with always a smaller slope than those obtained for the gradients of F98 spheroids. U87 spheroids develop therefore lower radial pH_i gradients compared to F98 spheroids, with always the lowest pH_i levels reached at the core.

6.7 Interpretation

In our study, a core-periphery difference in the pH_i was recorded in glioma spheroids, indicating a spatial pH_i gradient, with the lower pH_i in the core. In general, the methods for measuring pH_i in spheroids are limited. Similar results had previously been demonstrated using synthetic fluorescent pH-sensitive dyes and fluorescence microscopy. Using the membrane-permeant form of carboxy-SNARF-1, Swietach et al. found that spheroids of RT112 bladder carcinoma cells have an acidic core with a pH_i 0.25 units lower than at the surface (Swietach et al., 2008). Hulikova et al. also studied pH_i in spheroids loaded with carboxy-SNARF-1 and showed 0.1-0.2 units of difference in pH_i between the center and the periphery for both human colorectal carcinoma lines HT29 and HCT116 spheroids, with the more acidic pH_i in their cores (Hulikova, Vaughan-Jones, and Swietach, 2011). pH_i imaging in 3D models of metastatic ovarian cancer OvCa, using SNARF-4 F, demonstrated a pH gradient along their radii, with more acidic cores being observed consistently for both small and large spheroids (Evans et al., 2011). The possibility to measure pH_i with the use of the pH-sensitive fluorescent dye BCECF has also been demonstrated on human duodenum-derived spheroids (Weinlich et al., 2002).

It is generally accepted that the development of pH_i gradients in spheroids correlates with the gradients in nutrient concentration, including glucose, ATP and oxygen, resulting in the reorganization of metabolic pathways and changes in the growth probability of cells. Insufficient penetration of oxygen, nutrients in combination with a lack of a transport system to remove waste from the center of the spheroid leads to a hypoxia-induced accumulation of metabolic by-products, mostly lactate, in the cell cytoplasm. However, the exact mechanisms responsible for the regulation of pH_i in such a heterogeneous microenvironment are yet to be established.

It has been reported that the expression of the enzyme carbonic anhydrase IX (CA9/CA IX) is correlated with hypoxia (McDonald and Dedhar, 2014; Marie-Egyptienne et al., 2016; Tan et al., 2009; Swinson et al., 2003) and is regulated by hypoxia-inducible factor 1α (HIF-1α) (Wykoff et al., 2000). Thus, CA9 allows intracellular alkalinization by facilitating the extracellular export of CO_2. This action participates in the acidification of the extracellular microenvironment (Švastová et al., 2004). Therefore, because CO_2 is readily membrane-permeant, it will pass through the extracellular space of the spheroid to its core. Cells growing near the central regions of spheroids are more subject to hypoxia, and the expression of CA9 allows CO_2 to be exported into the extracellular space of the spheroid, resulting in an increase in pH_i. At the same time, the extracellular space of the spheroid is acidified: changes in pH_e will be mirrored by opposite changes in pH_i. This has been proven

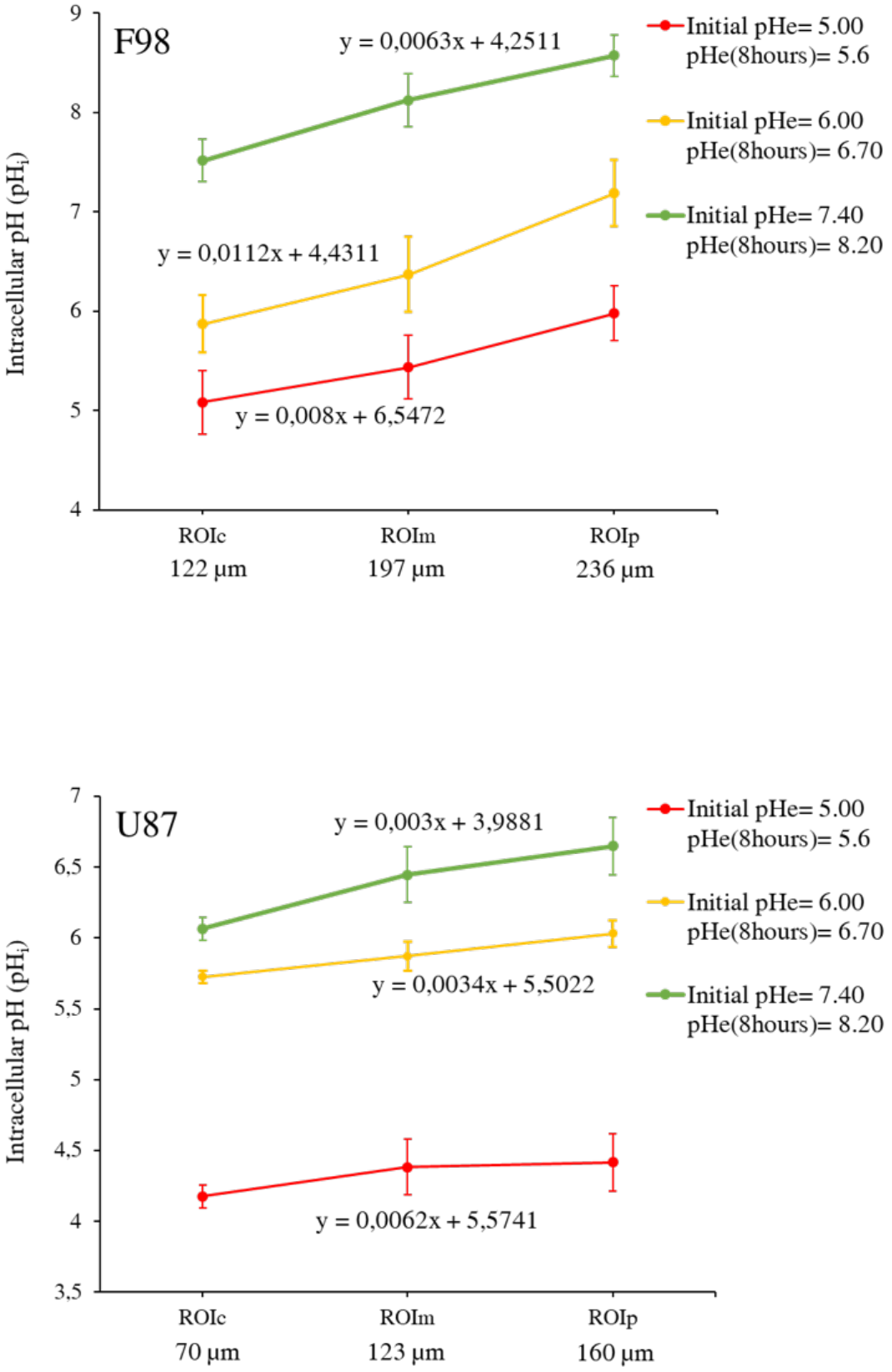

FIGURE 6.12: Intracellular pH gradient in F98 spheroids (top) and U87 spheroids (bottom) incubated at different pH_e values.

on CA9-expressing spheroids of HCT116 human colon carcinoma cells and RT112 bladder carcinoma cells that developed intracellular and extracellular acidosis that was greatest at the core (Swietach et al., 2008; Swietach et al., 2009). In addition, CA9 inhibition with AP105 (1-([4-sulfamoylphenyl)ethyl]-2,4,6-trimethyl pyridinium perchlorate) reduced the radial pH_e gradient but increased the radial pH_i gradient (Swietach et al., 2009). In other words, in the absence of CA9 activity, large spatial pH_i gradients were evident.
Based on our data, quantitative analyzes of pH_i gradients are not sufficient to comment on the ability of CA expression by glioma cells. It is important to investigate whether inhibition of intracellular CA isoforms has an additional effect on pH_i and even pH_e gradients. The expression of CA9 in many tumors has raised questions about its importance for cancer growth. Its potential for spatial control of pH_i offers a clear tumor survival advantage, especially since CA9 has one of the highest catalytic rates of all isoforms (Wingo et al., 2001). CA9 can benefit the tumor not only by increasing pH_i, but also by decreasing pH_e. Selective inhibition of CA9 activity by drugs or antibodies may provide a way to control tumor progression, by disrupting pH_i coordination and pH_e acidification. Although membrane-permeable CA inhibitors have been shown to attenuate tumor growth, the use of membrane-permeable CA inhibitors, such as AP105, to selectively target extracellular CA9 may provide a new therapeutic approach.
Early studies in tissue culture have suggested that under the microenvironmental conditions that exist in the acidic regions of tumor, the Na^+/H^+ exchanger is likely to be responsible for the majority of pH_i regulation (Boyer and Tannock, 1992; Boyer et al., 1993). Agents that inhibit the functioning of the Na^+/H^+ exchanger have a high potential to cause pHe-dependent cytotoxicity and thus selective killing of the cells in acidic regions of solid tumors. The development of these agents requires understanding how the pH regulation of tumor cells is modulated by the acidic environment of tumors. For this reason, they investigated whether the set of microenvironmental conditions encountered in tumor spheroids influence the functioning of the Na^+/H^+ exchanger. The results indicated that cells close to the central regions of the spheroids tend to have slightly higher activity of their Na^+/H^+ exchangers than those at the periphery. In MGH Ul human bladder-carcinoma spheroids, this effect was observed in the medium at pH_e 7.4, while in murine EMT-6 spheroids, it was necessary to lower the pH_e level of the medium to observe this effect. Surprisingly, in EMT-6 spheroids, Na^+/H^+ exchanger activity in peripheral cells was not higher when spheroids were grown in pH_e 6.6 medium than when grown at pH_e 7.4. They hypothesized that when this cell line is grown in spheroid form, lower pH_e levels are required to stimulate overexpression of the Na^+/H^+ exchanger. The last paragraph is dedicated to this comparison

In order to complete the interpretation of our results, it is important to make a comparison between the results obtained in 2D monolayer cultures and in 3D spheroids.

6.8 2D *vs.* 3D cultures

In order to make a comparison between 2D monolayer cultures and 3D spheroids, we plotted, on the same graph, the relationship between pH_e and pH_i obtained in these two types of

culture (8 hours after incubation at a given pH_e). It should be noted that the pH_e of the medium used for the culture of the 3D spheroids was measured by the non-permeable probe BCECF (Figure 6.13). Moreover, our objective was to measure the pH_e inside the spheroids but unfortunately we could not detect any extracellular BCECF signal in the spheroids. This may be related to the low diffusion of the extracellular BCECF probe in the spheroids which in turn may be related to the high cell density and compact shape of the spheroids.
Figure 6.14 shows the differences between 2D cell cultures and 3D spheroids. The 3 solid lines show the pH_i values obtained for the 3 regions of interest in the spheroid (ROI_c, ROI_m and ROI_p). The dotted line shows the pH_i values obtained in monolayer cultures. Under acidic and neutral conditions, The peripheral F98 cells show a response quite similar to that of the cells in 2D cultures. Under basic conditions, peripheral cells tend to raise their pH_i compared to the 2D model. Having already assumed that the F98 cells in the 2D cultures used, under basic conditions, the Cl^-/HCO_3^- exchanger to export the HCO_3^- ions outside the cells, we can therefore hypothesize that the activity of the Cl^-/HCO_3^- exchanger is inhibited in 3D cultures. However, whatever the pH_e, the peripheral U87 cells show a completely different activity compared to the 2D cultures. Peripheral U87 cells tend to lower their pH_i compared to the 2D model. We have already assumed that the U87 cells in the 2D cultures used, under acid conditions, the Na^+/H^+ exchanger to export the H^+ ions outside the cells. The fact that the U87 peripheral cells lowered, under acidic conditions, their intracellular pH can be explained by the inhibition of the Na^+/H^+ exchanger; the H^+ ions are therefore conserved in the peripheral cells. However, unlike peripheral F98 cells, the decrease in pH_i under basic conditions allows us to hypothesize that peripheral U87 cells "overexpress" Na^+/H^+.

6.9 Conclusion

We have shown, for the first time, the possibility of using the BCECF probe for ratiometric pH_i imaging in glioma spheroids. Our results demonstrate that pH_i imaging can be a valuable tool for assessing metabolic status and tumor progression in glioma models.
In addition, there are differences between 2D and 3D experiences that cannot be controlled. In the monolayer experiments, the only modified factor was the pH_e level. In contrast, cells growing in a spheroid are exposed not only to reduced pH_e levels, but also to hypoxia and starvation of other nutrients. These conditions can combine to inhibit energy metabolism or protein synthesis and prevent the regulation of exchanges such as Na^+/H^+ (Tidwell et al., 2022). Thus, the presence of growth factors could modulate the response of cells to microenvironmental conditions (Zhang, 2010).
In addition, an important factor regulating the activity of many cells is adhesion to other cells. It has been reported that pH_i depends on the adhesive interactions of cells with neighboring cells and cell-cell contacts regulate cell activities via modulation of pH_i (Galkina, Sud'Ina, and Margolis, 1992; Galkina et al., 1995).

Finally, tumor spheroids, in combination with fluorescent pH-indicators, offer a promising

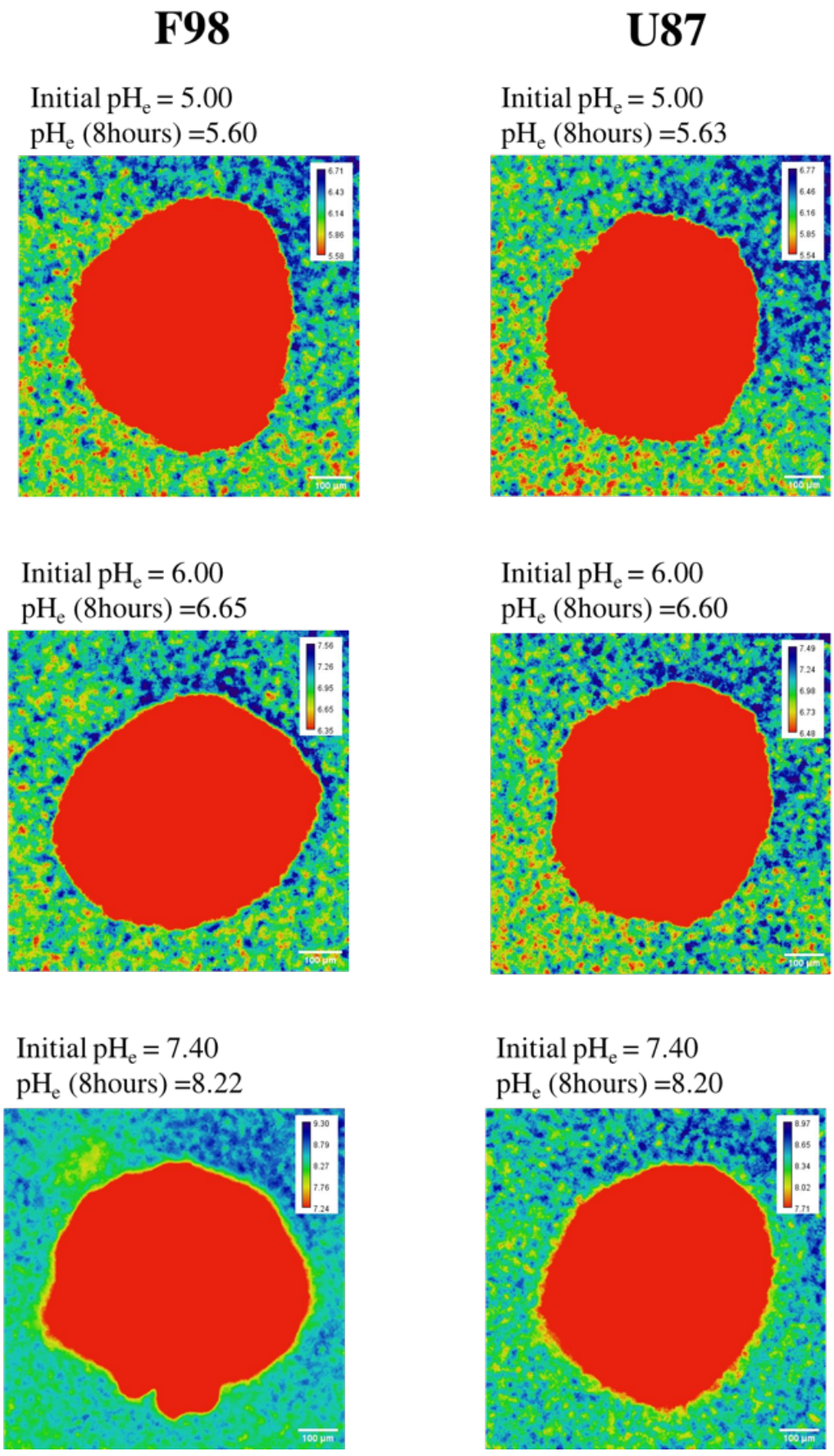

FIGURE 6.13: pH drift of the DMEM culture medium in 3D culture spheroids. Note that the blue spots present at the top corner of the images were due to an experimental artifact (Dust on the laser). pH$_e$ was measured in the corners not showing these spots.

approach for imaging of the cytoplasmic pH in cancer cells in providing both high accuracy and spatial resolution.

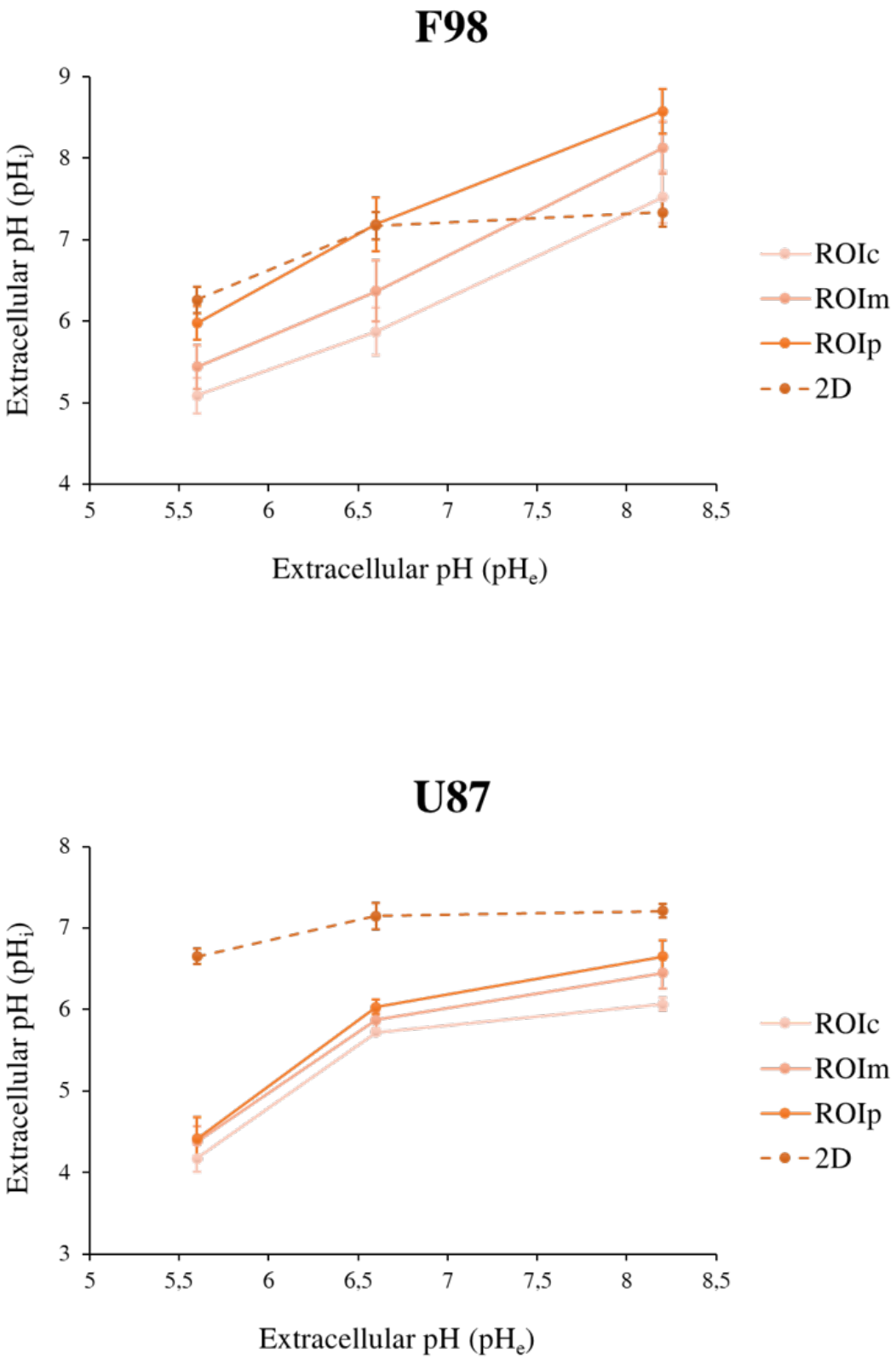

FIGURE 6.14: Relationship between pH_e and pH_i of F98 and U87 cells incubated in monolayer cultures (2D) and in 3D spheroids. The cells are incubated at different pH_e values and the pH_i was measured 8 hours after incubation.

Chapter 7

Extracellular pH as a therapeutic target to optimize the efficacy of temozolomide

7.1 Introduction

Currently, temozolomide (TMZ) is the standard treatment for glioblastoma (GBM) since it is one of the rare molecules able to cross the blood brain barrier. However, there are serious drawbacks, mainly related to the invasive nature of this tumor, and to the inherent and acquired resistance, which can ultimately lead to treatment failure. Therefore, there is an urgent need for novel therapeutic strategies that enhance the benefits of TMZ in terms of patient survival and quality of life.

The effect of TMZ is highly pH dependent. TMZ is stable under acidic conditions, while this reaction occurs at physiological and basic pH conditions. However, since tumor cells can acidify their microenvironment, this may influence the efficacy of TMZ. Therefore, there is only a small pH range favoring TMZ-induced damage in tumor cells. In this context, we are interested in this chapter to study the influence of the extracellular pH (pH_e) on the efficiency of the TMZ complex, and to then find the optimal pH_e of this molecule on the two cell lines of interest, U87 and F98.

7.2 Drug dose-response

Drug dose-response study is an experiment that is performed to test the efficacy of a drug in cell lines. It is widely used in cancer research to prioritize drugs to be tested in patients. This type of studies is only possible *in vitro*. In a dose-response study of an anti-cancer drug, cell cultures of a specific cancer are treated with a specific drug in increasing concentrations, and the percentage of cell viability is measured. The lower the % of cell viability, the more effective the tested drug is against the specific cancer cell line.

In fact, drug dose-response study is necessary to determine the half-maximal inhibitory concentration (IC_{50}) which is the most widely used and informative measure of drug efficacy. IC_{50} indicates the amount of drug required to inhibit cell viability by half, thus providing a measure of the potency of an antagonist drug in pharmacological research. IC_{50} is calculated

to decide the optimum dosage of the drugs for further studies.
Given the above, in order to test the effect of TMZ on glioma cells by manipulating extracellular pH, it is important first to determine the IC_{50} concentrations of U87 and F98 cells. The following paragraph will therefore be dedicated to presenting the method used to determine these concentrations.

7.2.1 Cell viability and IC_{50} values

In order to test the effect of TMZ on cell viability, we used the 3-(4,5-dimethylthiazol-2-yl)-2,5-diphenyltetrazolium bromide (MTT) assay, according to the standard protocol. Briefly, glioma cells are seeded on Day0 (D0) in a 96-well plate at the rate of 1×10^4 cells per well in 200 μL of culture medium. On D3, cells were washed twice with PBS and incubated 48 hours with TMZ at different concentrations (0, 50, 100, 200, 300, 400, 500 and 1000 μM) in a final volume of 100 μL per well (pH_e 7.4). Control cells were treated with DMSO only. At the end of the incubation period, 10 μL of an MTT solution is added to achieve a final concentration of 0.5 mg/mL. The cells were then incubated for 3 hours at 37°C, 5% CO_2 and protected from light. The Formazan crystals formed after incubation were dissolved by adding 100 μL of dimethylsulfoxide to each well. Finally, the number of live cells was quantified by an absorbance reading at 570 nm and results were expressed as the mean of three replicates as a percentage of control (taken as 100%). The extent of cytotoxicity was defined as the relative reduction of the optical density (OD), which correlated to the amount of viable cells in relation to cell control (100%). The cell viability was plotted in a graph and the IC_{50} was calculated accordingly to decide the optimum dosage of the drug for further studies. From Figure 7.1, it was observed that the level of cell survival generally decreased with increasing TMZ concentration indicating a dose-dependent behavior. The IC50 value (i.e., the drug concentration that results in 50% cell viability) was almost 200μM and 250 μM for F98 and U87, respectively. Further experiments were performed with the above-mentioned drug concentrations.

7.3 Toxicities of TMZ in F98 and U87 monolayer cultures (2D)

The majority of previously published drug toxicity research is conducted using commercially available cell media with a pH above 7, which is typical of healthy tissues. These experiments do not reflect the actual conditions of pathological cell division and growth; therefore, to perform biological experiments under conditions similar to cancer cells, it is important to adjust the pH of cell media to the appropriate value. The experiments in this work were carried out in neutral and acidified cell media and the influence of pH on the toxicity results on the U87 and F98 cell lines was evaluated.

7.3.1 Methodology

1×10^4 cells of F98 and U87 cells were seeded on day0 (D0) onto 96-well plates in 200 μL of standard cell culture medium 48 h before experiments. On D3, TMZ was first diluted

a)

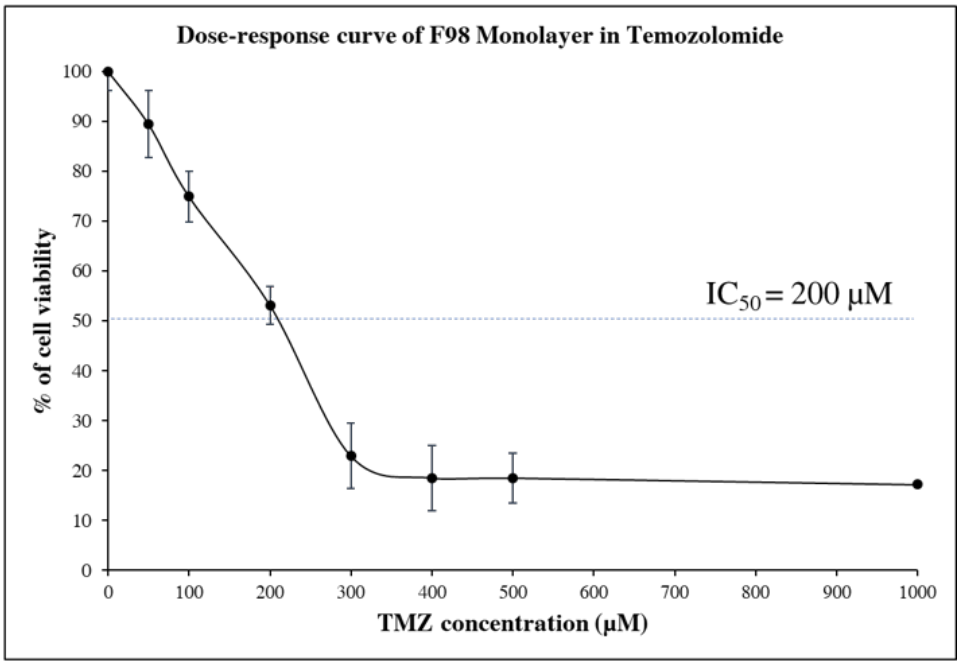

b)

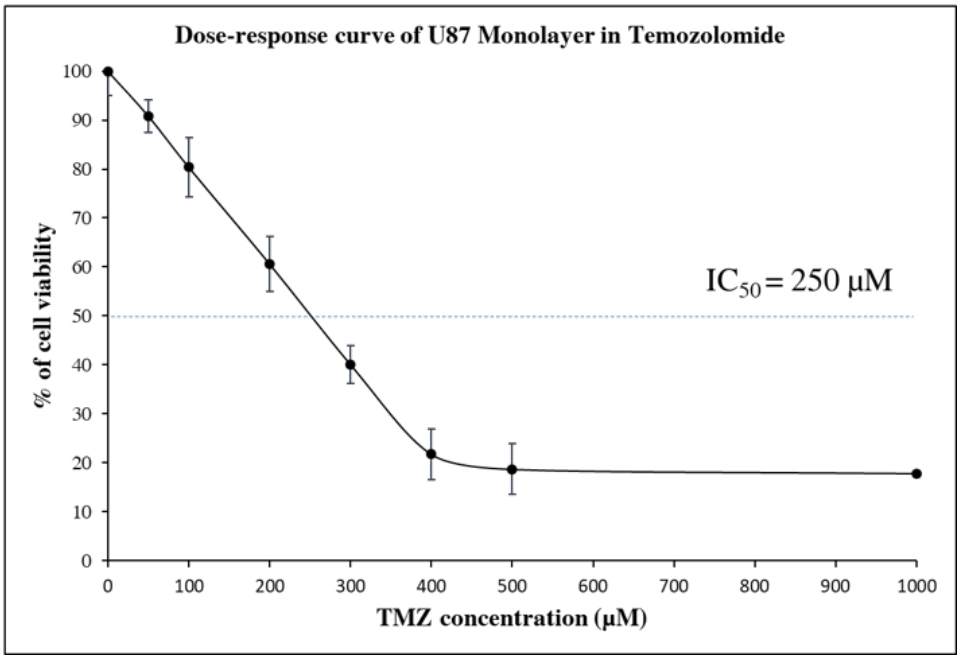

FIGURE 7.1: Dose-response curve of F97 and U87 monolayers of the drug Temozolomide

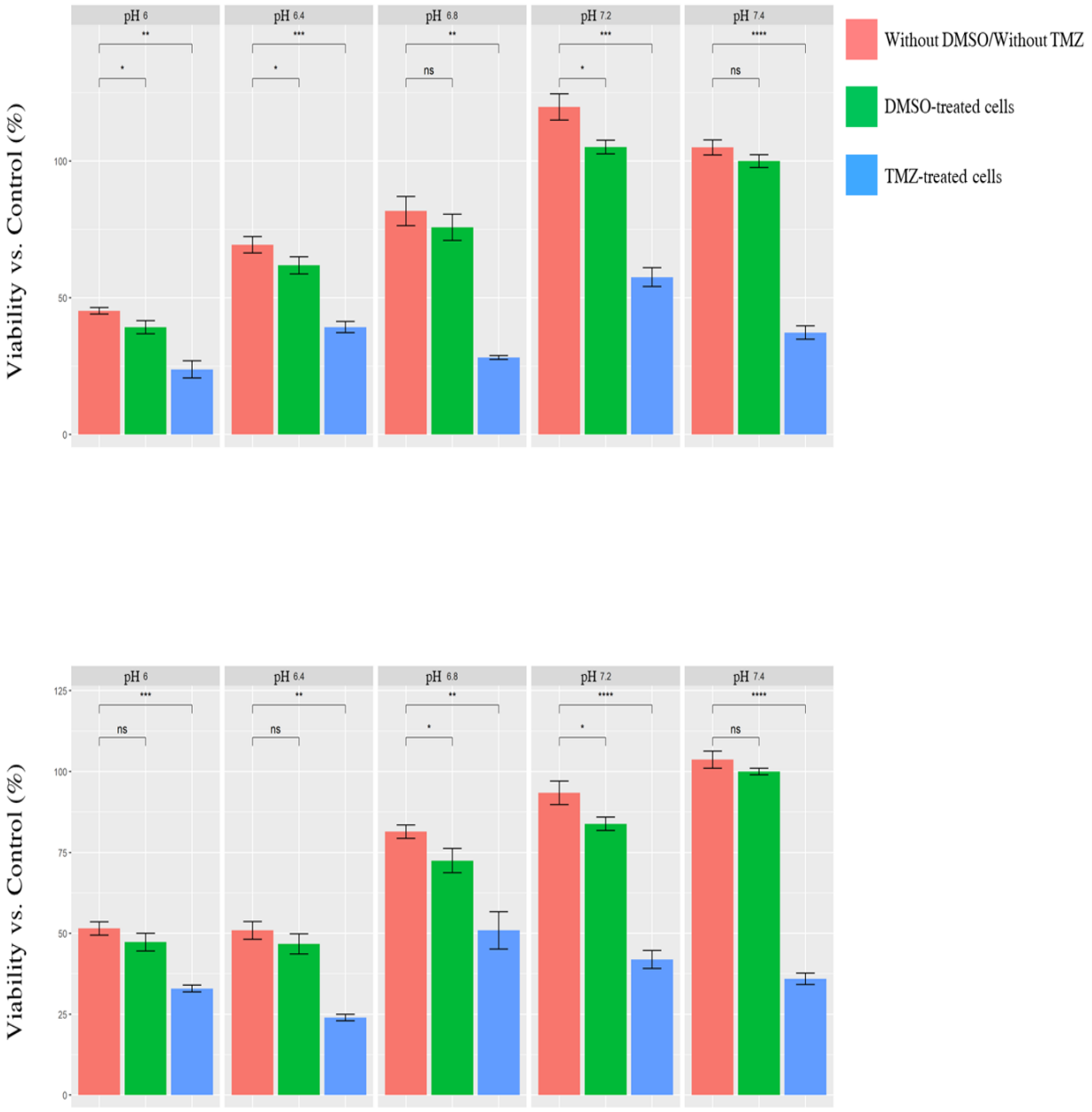

FIGURE 7.2: The dependence of TMZ toxicity on the pH_e of the medium itself (2D monolayer cultures)

with the cell culture medium with pH, i.e. pH_e, 6.00, 6.40, 6.80, 7.20 or 7.40 to a final TMZ concentration of 200 μM (F98 cells) or 250 μM (U89 cells). The standard cell culture medium was then replaced with 100 μL of medium containing tested compounds and cells were treated after 48 hours (two DNA replication cycles). Note that the cell culture medium at pH_e 6.00, 6.40, 6.80, 7.20 or 7.40 was used as untreated controls and medium with DMSO was used as control. Results of the MTT test were normalized to the control (pH_e= 7.4, DMSO-treated cells).

Before presenting the results, it is important to always take into account the pH drift of the DMEM culture medium discussed in Chapter 4. Table 7.1 summarizes the drift for each initial pH_e tested (6.00, 6.40, 6.80, 7.20 or 7.40), 48 hours after incubation at 37°C and 5% CO_2.

Initial pH_e	pH_e (t=48hrs)
5.00	6.07
6.00	6.91
6.40	7.33
6.80	7.67
7.20	8.15
7.40	8.52

TABLE 7.1: pH drift of DMEM medium after 48 hours of incubation at 37°C and 5% CO_2

7.3.2 Results

Figure 7.2 shows the dependence of TMZ toxicity on the pH_e of the medium itself, 48 hours after exposure. First, no significant difference was noted between control cultures with DMSO alone and cultures without DMSO.
Witout treatment of F98 cells, the viability values was 39.28 ± 2.38, 61.90 ± 3,14 , 75.79 ± 4.81, 105.15 ± 2.47 and 100 ± 2.99% (control) at pH_e 6.91, 7.33, 7.67, 8.15 and 8.52, respectively. After treatment, the viability values was 23.80 ± 3.31, 39.28 ± 2,09, 28.17 ± 0.68, 57.53 ± 3.43 and 37 ± 2.47% at pH_e 6.91, 7.33, 7.67, 8.15 and 8.52, respectively (Figure 7.2, top). Therefore, statistical analysis showed a percentage of cell viability vs. control (see Note[1]) of approximately 61, 63, 37, 55, 37% when exposure to pH_e 6.91, 7.33, 7.67, 8.15 and 8.52, respectively (Table 7.2).

In the other side, without treatment of U87 cells, the viability values was 47.30 ± 2.74, 48.30 ± 3,11 , 72.45 ± 3.73, 83.83 ± 2.07 and 100 ± 1.03% (control) at pH_e 6.91, 7.33, 7.67, 8.15 and 8.52, respectively. After treatment, the viability values was 32.93 ± 2.74, 23.95 ± 3,11, 50.89 ± 3.73, 41.91 ± 2.07 and 35.92 ± 1.03% at pH_e 6.91, 7.33, 7.67, 8.15 and 8.52, respectively (Figure 7.2, bottom). Therefore, statistical analysis showed a percentage of cell viability vs. control of approximately 70, 51, 70, 50, 36% when exposure to pH_e 6.91, 7.33,

[1]Viability vs. control (%)= $\frac{\%of cell viability after TMZ treatment}{\%of cell viability before treatment (Control)} \times 100$

Extracellular pH (pH_e)	% cell viability without treatment (Control)	% cell viability after TMZ treatment	Viability vs. control (%)
6.91	39.28 ± 2.38	23.80 ± 3.31	61
7.33	61.90 ± 3,14	39.28 ± 2,09	63
7.67	75.79 ± 4.81	28.17 ± 0.68	37
8.15	105.15 ± 2.47	57.53 ± 3.43	55
8.52	100 ± 2.99	37 ± 2.47	37

TABLE 7.2: % inhibition of cell viability after treatment of F98 (2D) with TMZ.

7.67, 8.15 and 8.52, respectively (Table 7.3).

Extracellular pH (pH_e)	% cell viability before treatment (Control)	% cell viability after TMZ treatment	Viability vs. control (%)
6.91	47.30 ± 2.74	32.93 ± 2.74	70
7.33	48.30 ± 3,11	23.95 ± 3,11	51
7.67	72.45 ± 3.73	50.89 ± 3.73	70
8.15	83.83 ± 2.07	41.91 ± 2.07	50
8.52	100 ± 1.03	35.92 ± 1.03	36

TABLE 7.3: Viability vs. control (%) after treatment of U87 (2D) with TMZ.

Results showed that, for both cell lines, a pH_e of 8.52 provides a good efficiency of the drug. In addition, F98 cancerous cells exhibited higher sensitivity toward TMZ treatment at pH_e 7.67. The vability vs. control was 37% for F98 cells while it was 70% for U87 cells. In addition, at pH_e 6.91, both cell lines showed low sensitivity to TMZ; they were resistant to TMZ treatment with viability vs. control of approximately 61% and 70% for U87 and F98 cells, respectively.

In principle, the lower viability vs. control (%), the optimal efficiency of TMZ. Therefore, for both cell lines, we conclude that the optimal pH_e for TMZ efficiency is 8.52 (Figure 7.3). We have defined the optimal pH_e range as the pH_e values inducing lower viability vs. control,

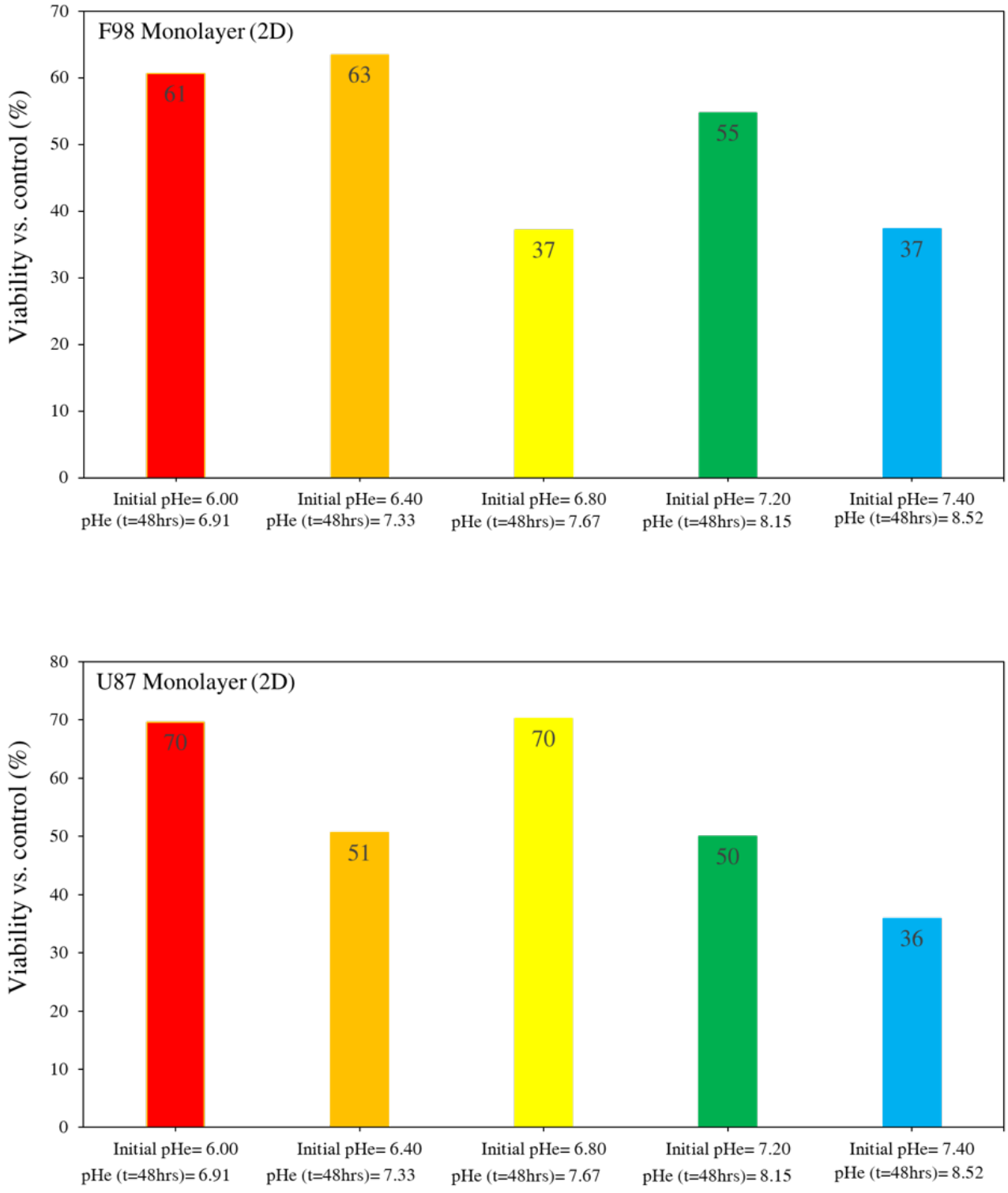

FIGURE 7.3: Cell viability vs. control (%) after treatment of F98 and U87 with TMZ (2D monolayer cultures).

2D monolayer cultures	Optimal pH_e	Optimal pH_e range
F98	8.52	7.67-8.52
U87	8.52	8.15-8.52

TABLE 7.4: Optimal pH_e and optimal pH_e range for TMZ efficiency for F98 and U87 cells (2D cultures).

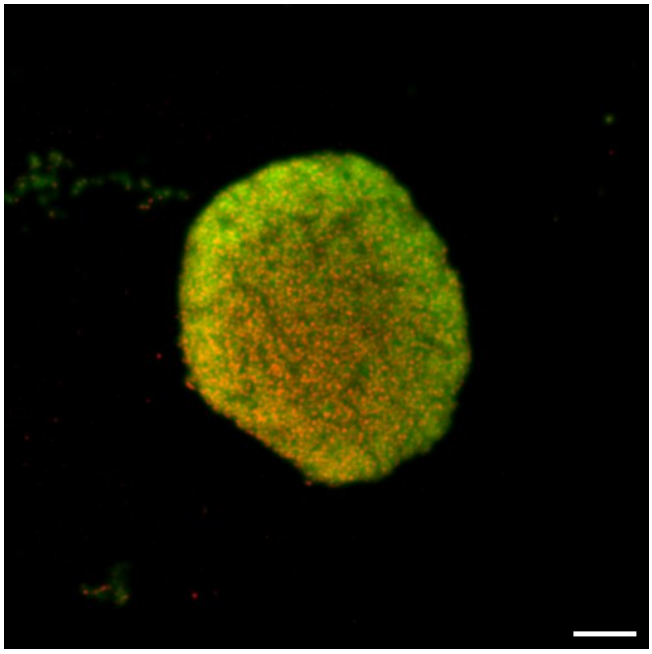

FIGURE 7.4: Spheroid F98 incubated at pH_e 7.4 in the presence of 200 μM of TMZ. The BCECF probe (green) marks all the cells, living and dead, while the sulforodhamine B probe (SRB, red) marks the dead cells. scale bar= 100 μm

below 51%. Therefore the optimal pH_e range for TMZ efficiency is 7.67-8.52 for F98 cells, while is 8.15-8.52 for U87 cells (Table 7.4).

7.4 Toxicities of TMZ in F98 and U87 spheroids (3D)

7.4.1 Methodology

The measurement of drug sensitivity was repeated in spheroid (3D) cell culture models. F98 and U87 cells were seeded on D0 in CELLSTAR® 96 well, round bottom ultra-low attachment plates, at a density of 1×10^3 cells per well in a volume of 200 μL. In day 3 The standard cell culture medium was replaced with 100 μL of medium containing TMZ at final concentration of 200 μM (F98 cells) or 250 μM (U89 cells). The cell culture medium at initial pH_e 5.00, 6.00 and 7.40 was used as untreated controls and medium with DMSO was used as control. The experiment was ended on culture D5, on which cell viability was assessed taking into account the pH drift of the culture medium (Table 7.1).

In 3D spheroid cultures, the cell viability was evaluated by confocal microscopy using two

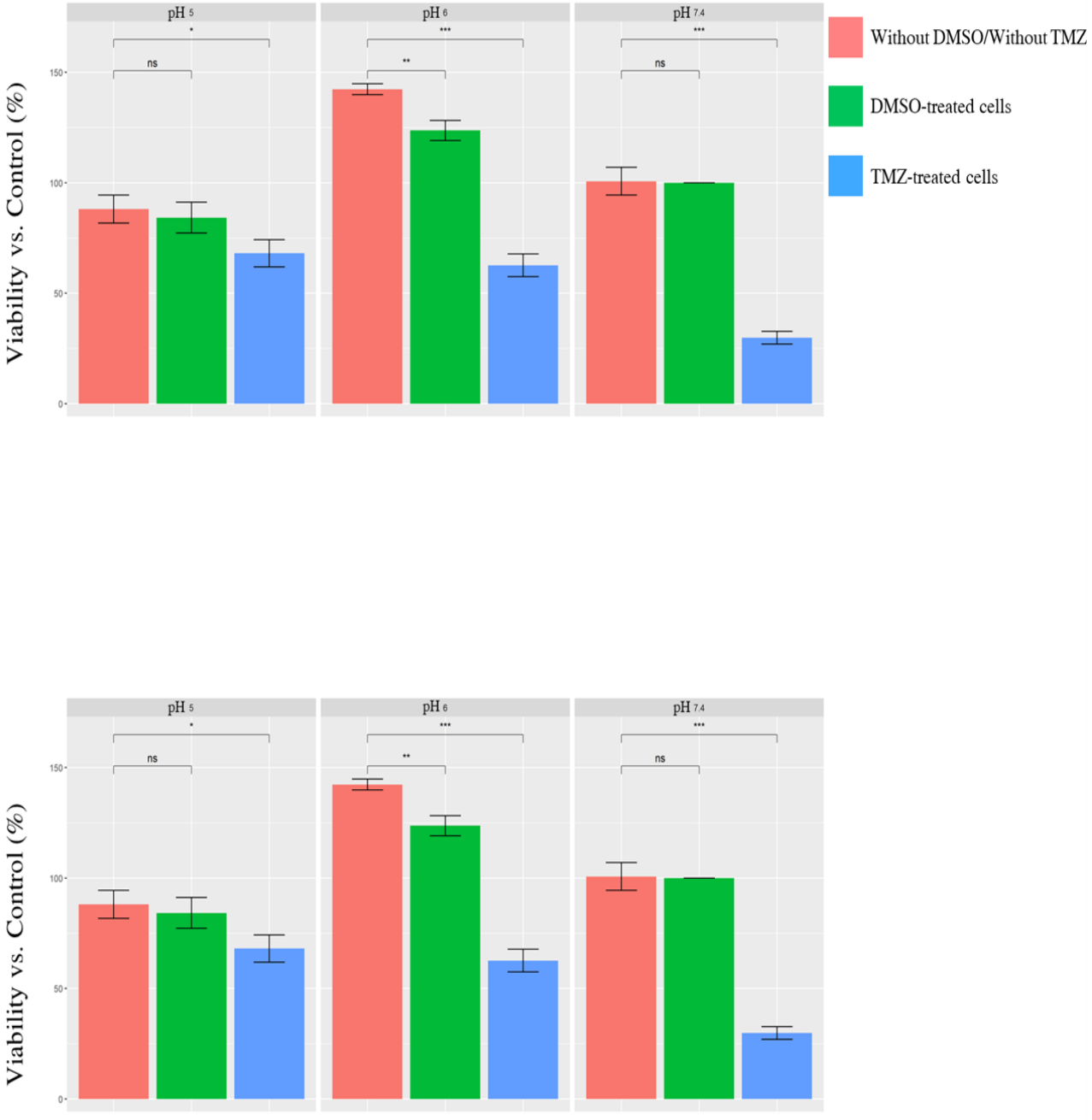

FIGURE 7.5: The dependence of TMZ toxicity on the pH_e of the medium (3D spheroid cultures).

probes: the BCECF probe used as a powerful probe that allows labeling entire cells and the sulforodamine B probe that marks the dead cells. The difference between these two fluorescent signals gives us the number of living cells in the spheroid (Figure 7.4).

7.4.2 Results

The toxicity of TMZ differed between the pH_e values tested (Figure 7.5). Without treatment of F98 spheroids, the viability value was 84.44 ± 7,21, 123.13 ± 7.89 and 100 ± 8.64% (control) at pH_e 6.07, 6.91 and 8.52 respectively. After treatment of F98 spheroids, the viability value was 68.27 ± 3,58, 62.27 ± 4.72 and 29.83 ± 6.81% at pH_e 6.07, 6.91 and 8.52, respectively (Figure 7.5, top). Therefore, statistical analysis showed a viability vs. control (%) of approximately 81, 51 and 30% when exposure to pH_e 6.07, 6.91 and 8.52, respectively (Table 7.5).

Furthermore, the effect of TMZ is clearly visible on the size of F98 spheroids. TMZ inhibited the growth of F98 spheroids and the inhibition was significant for pH_e 6.91 and pH_e 8.52 (Figure 7.6).

Extracellular pH (pH_e)	% cell viability before treatment (Control)	% cell viability after TMZ treatment	Viability vs. control (%)
6.07	84.44 ± 7,21	68.27 ± 3,58	81
6.91	123.13 ± 7.89	62.27 ± 4.72	51
8.52	100 ± 8.64	29.83 ± 6.81	30

TABLE 7.5: Viability vs. control (%) after treatment of F98 spheroids (3D) with TMZ.

Extracellular pH (pH_e)	% cell viability before treatment (Control)	% cell viability after TMZ treatment	Viability vs. control (%)
6.07	80.49 ± 6.89	67.99 ± 5.36	84
6.91	121.73 ± 6,21	78.11 ± 5,29	64
8.52	100 ± 3.31	35.62 ± 4.84	36

TABLE 7.6: Viability vs. control (%) after treatment of U87 spheroids (3D) with TMZ.

In the other side, without treatment of U87 spheroids, the viability value was 80.49 ± 6.89, 121.73 ± 6,21 and 100 ± 3.31% (control) at pH_e 6.07, 6.91 and 8.52 respectively. After treatment of U87 spheroids, the viability value was 67.99 ± 5.36, 78.11 ± 5,29 and 35.62 ± 4.84% at pH_e 6.07, 6.91 and 8.52, respectively (Figure 7.5, bottom). Therefore, analysis

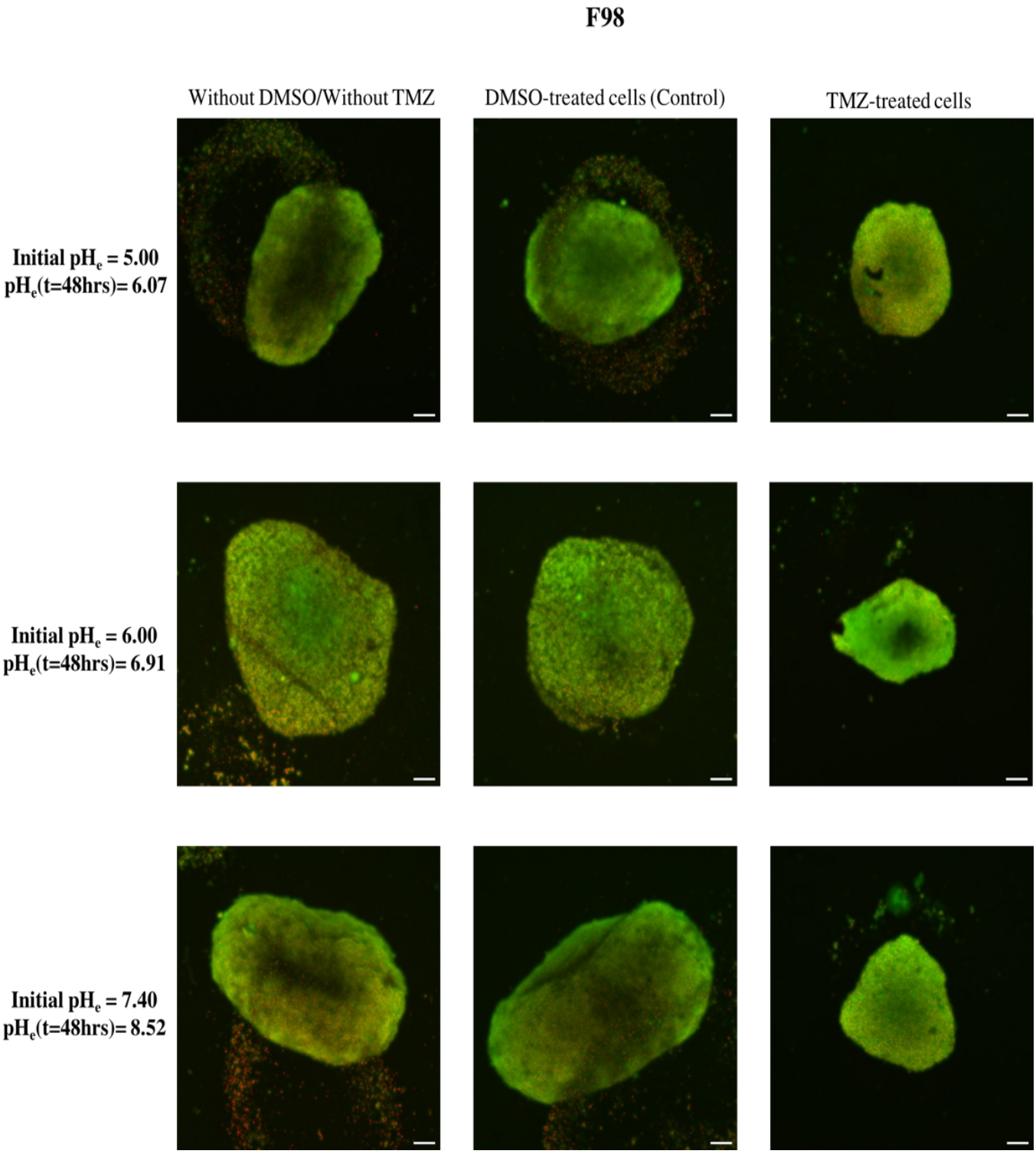

FIGURE 7.6: Effect of TMZ on F98 spheroides under different conditions.
Scae bar= 100 μm

showed a viability vs. control (%) of approximately 84, 64 and 36% when exposure to pH_e 6.07, 6.91 and 8.52, respectively (Table 7.6). In addition, TMZ also inhibited the growth of U87 spheroids and the inhibition was significant for pH_e 8.52 (Figure 7.7).

Results show that the toxicity of TMZ decreased with the decrease of the pH_e value and a pH_e of 8.52 provides a good efficiency of the drug in 3D spheroid cultures. Moreover, for a very acidic pH_e (pH_e 6.07), both cell lines behaved similarly. U87 and F98 spheroids showed low sensitivity to TMZ: they were resistant to TMZ treatment with a viability vs. control of approximately 81 and 84% for F98 and U87 cells, respectively.
In addition, we note that the efficiency of TMZ is much greater on F98 spheroids than on U87 spheroids: statistical analysis showed a a viability vs. control of approximately 51 and 30 % when F98 spheroids are incubated at pH_e 6.91 and 8.52, respectively, while analysis showed a viability vs. control of approximately 64 and 36 % when U87 spheroids are incubated at pH_e 6.91 and 8.52, respectively. These results show that the efficacy of TMZ depends on the cell type, which gives an argument to consider pH_e as a personalized therapeutic target.
Finally, as 2D cultures, the lower viability vs. control was obtained for a pH_e of 8.52 (Figure 7.8). Therefore, for both cell lines, the optimal pH_e for TMZ efficiency is therefore 8.52. In addition, we have defined the optimal pH_e range as the pH_e values inducing viability vs. control below 51%. For U87 spheroids, testing pH_e between 6.07 and 6.91 will be an interesting test to properly quantify the optimal pH range. But at first sight, we can say that the optimal pH_e range for the two lines, in 3D cultures, is 6.91-8.52 (Table 7.7).

3D spheroid cultures	Optimal pH_e	Optimal pH_e range
F98	8.52	6.91-8.52
U87	8.52	6.91-8.52

TABLE 7.7: Optimal pH_e and optimal pH_e range for TMZ efficiency for F98 and U87 cells (3D cultures).

7.5 Conclusion

We hypothesized that a change in the pH_e will result in predictable changes in drug toxicity. The data presented here are consistent with this hypothesis in the case of Temozolomide; TMZ toxicity is strongly pH-dependent. In addition, these results consistently show that selective tumor alkalinization is likely to result in an enhancement in the anti-tumor activity of TMZ. However, selective acidification reduced the cytotoxic efficacy of the chemotherapeutic drug. The differences in toxicity at normal and acidic pH can be attributed to the protonation level of temozolomide. The neutral, uncharged form of TMZ is readily permeable through the cell membrane, while the protonated, ionized form does not penetrate it efficiently, due to the diffusive character of drug transport (Born and Eichholtz-Wirth, 1981; Patil et al., 2010; Mahoney et al., 2003).

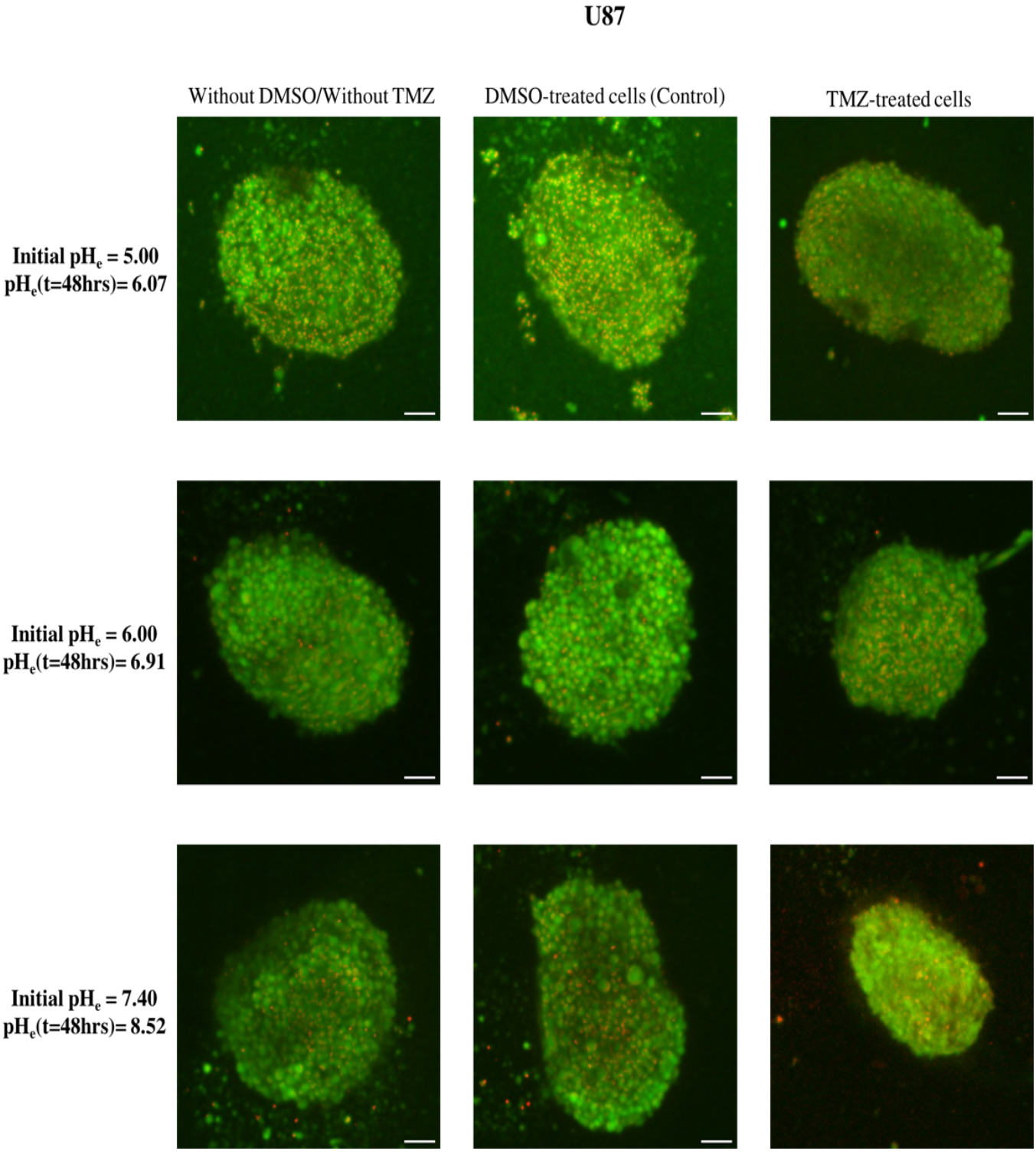

FIGURE 7.7: Effect of TMZ on U87 spheroides under different conditions.

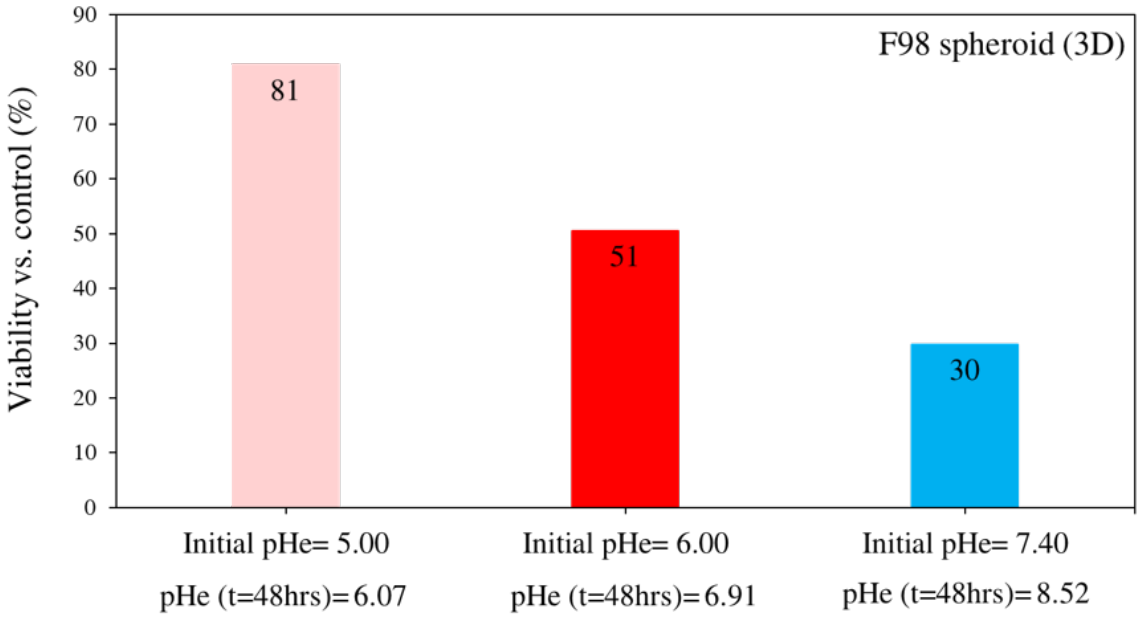

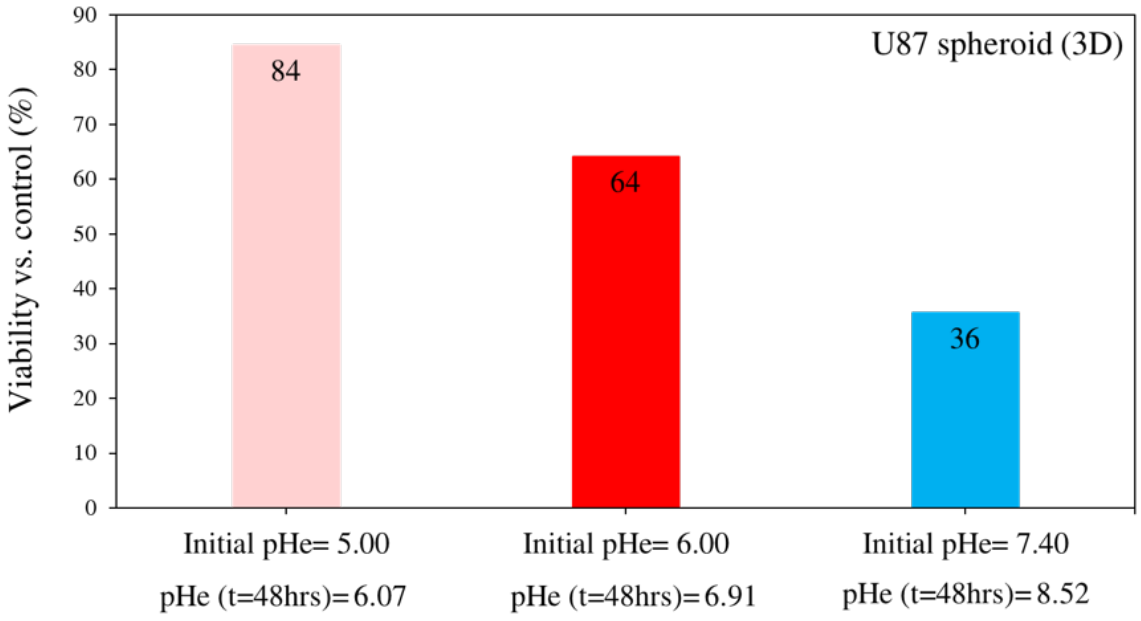

FIGURE 7.8: % inhibition of cell viability after treatment of F98 and U87 with TMZ (3D spheroid cultures).

Our results are particularly important because the pH_e of the glioma cells is lower than the pH_e of the healthy tissue and, the biological tests must be carried out in acidified media simulating the chemical properties of the natural environment of the malignant tissue instead of that of the healthy one. In other words, in order to reproduce the environmental conditions resulting from the presence of metabolic products of cancer cell glycolysis, the concentrations of hydrogen ions in the cell medium should be carefully considered when designing biomedical experiments.

Although we found the same optimal pH_e for both cell lines, either in 2D monolayer cultures or in 3D spheroids, we found that the TMZ molecule is more effective on F98 cells than on U87 cells. In other words, the efficacy of TMZ depends on the cell type. The set of all results gives therefore an argument for considering pH_e as a personalized therapeutic target for future research based on the combination of TMZ with pH-regulating agents.

Conclusion and Perspective

Many cellular processes and therapeutic agents are known to be highly pH-dependent, making the study of intracellular pH (pH_i) regulation of paramount importance. Therefore, this thesis made it possible to focus on the regulation of the pH_i of two brain tumor cells using fluorescence microscopy. We observed that the tumor regulation of acidity is not the same for the two cell lines and as a consequence, our results do not support the common idea that tumor cells behave in a similarly way. On the other hand, pH_i regulation appears highly cell-dependent.

In order to interpret our results, we have put forward hypotheses to explain the mechanisms involved in the regulation of pH_i. In 2D monolayer cultures, we assumed that F98 rat glioma cells do not regulate intracellular acidity, preserve protons inside the cells by activating the V-ATpase pump at acidic pH to bring H^+ ions into lysosomes. The study of the effect of the inhibition of the V-ATpase pump, by bafilomycin A1 (Wang et al., 2021), on the pH_i would be an excellent tool to validate our interpretation. On the other hand, we hypothesized that human glioblastoma U87 cells, that are found to regulate intracellular acidity, use the Na^+/H^+ exchanger to export H^+ ions outside the cells. Therefore, testing amiloride as a Na^+/H^+ exchanger inhibitor (Masereel, 2003) can be an effective tool to validate our hypothesis.

In addition, in order to properly characterize the tumor regulation of pH_i, it is crucial to study it at the scale of a spheroid. This 3D model constitute an intermediate biological model between 2D cell cultures and animal models and develop a relationship between the cells and their heterogeneous environment characterized by substrates fluxes and gradients. More precisely, cells growing in a spheroid are exposed not only to reduced pH_e levels, as 2D monolayer cultures, but also to a limitation of the supply of nutrients and oxygen, due to their diffusion inside the spheroid. Differences in results between 2D and 3D experiments were therefore expected. Tidwell et al., 2022 have recently shown that the combination of hypoxia, starvation of other nutrients and extracellular acidity inhibit energy metabolism or protein synthesis and prevent the regulation of exchanges such as Na^+/H^+ in 3D spheroids. This is in a great agreement with the results obtained on the U87 spheroids: contrary to the results obtained in 2D monolayer cultures, the fact that the U87 spheroids lowered under acidic conditions their pH_i can be explained by the inhibition of the Na^+/H^+ exchanger.

The effect of Tomozolomide (TMZ), the cornerstone drug used against brain tumors, is highly pH-dependent. Since tumor cells can acidify their microenvironment, regulating their intracellular pH, this may influence the efficacy of TMZ. Therefore, the effect of TMZ was

studied on our two cell lines by manipulating the extracellular pH (pH_e). The results has allowed us to show that drug efficiency depend on the cell type and on the pH_e, which gives an argument for considering pH as a personalized therapeutic target for future research based on the combination of TMZ with pH-regulating agents.

Despite the original results of this thesis, there are nevertheless several limitations. First of all, during the first two years of the thesis, several breakdowns and incidents, such as a gas leak and the failure of the incubator, delayed the realization of the experiments. In addition, the containment of covid in 2020 has aggravated this delay. For this we could not finish all the planned tasks and unfortunately we did not have time to manipulate on patient-derived glioblastoma cell lines (PDCL).

The second limitation we encountered is the pH drift of the culture medium used for cell incubation during the *in vitro* studies. A relatively rapid and notable rise in the pH of the DMEM culture medium has been observed, and values greater than 8.5 could be reached after 8 hours of incubation. This pH drift was found to be independent of the presence of cells. After quantifying the pH drift of the DMEM culture medium, we concluded that increasing the CO_2 level of the incubator beyond 5% can be a worthwhile exercise to avoid significant pH fluctuations. However, it has become convention to use 5% CO_2 with DMEM and most cell line suppliers will advise this. In order to overcome the pH drift, we therefore monitored in parallel the pH_e and the pH_i. In other words, a pH_e value was associated to a corresponding pH_i value measured at the same instant.

Another strong limitation is the characterization of pH_i regulation over short times. The evolution of the pH_i was followed as function of pH_e only over 8 hours. Despite the impact observed over short periods of time, it would have been interesting to characterize the regulation of intracellular acidity over the long term during, for example, cell-cycle progression and growth state transition. But we lacked time to do this.

Despite the limitations encountered, this thesis has yielded original results. We have shown, for the first time, the possibility of using the BCECF probe for ratiometric pH_i imaging in glioma. Our results demonstrate therefore that pH_i imaging can be a valuable tool for assessing metabolic status in glioma models. The characterization data collected for each glioma cell will be used to parameterize the regulation networks implemented in the mathematical model developed by Stéphanou and Ballesta, 2019 which provide a computational framework towards enhanced efficacy of TMZ-based personalized therapy.

Appendix A

Intracellular pH evaluation in 3D spheroids

A.1 pH_i in tumor spheroids

Here we present the 18 spheroids treated to assess pH_i in tumor spheroids.

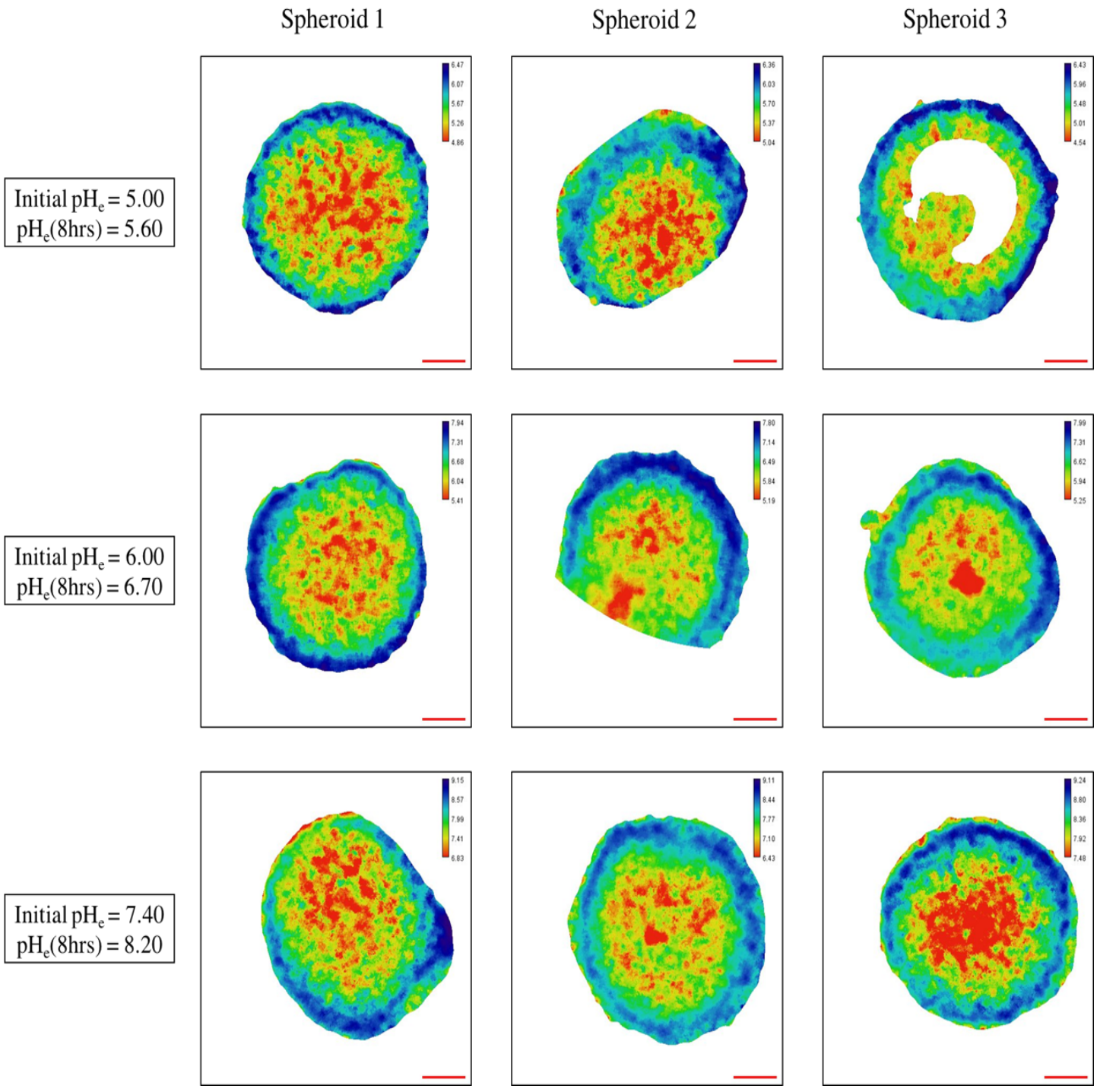

FIGURE A.1: F98 shephroids incubated at different pH$_e$ values. Spheroid triplicates were included for each condition tested. Each pH$_i$ map represents the slice located at a depth of 85 μm. Scale bar = 100 μm

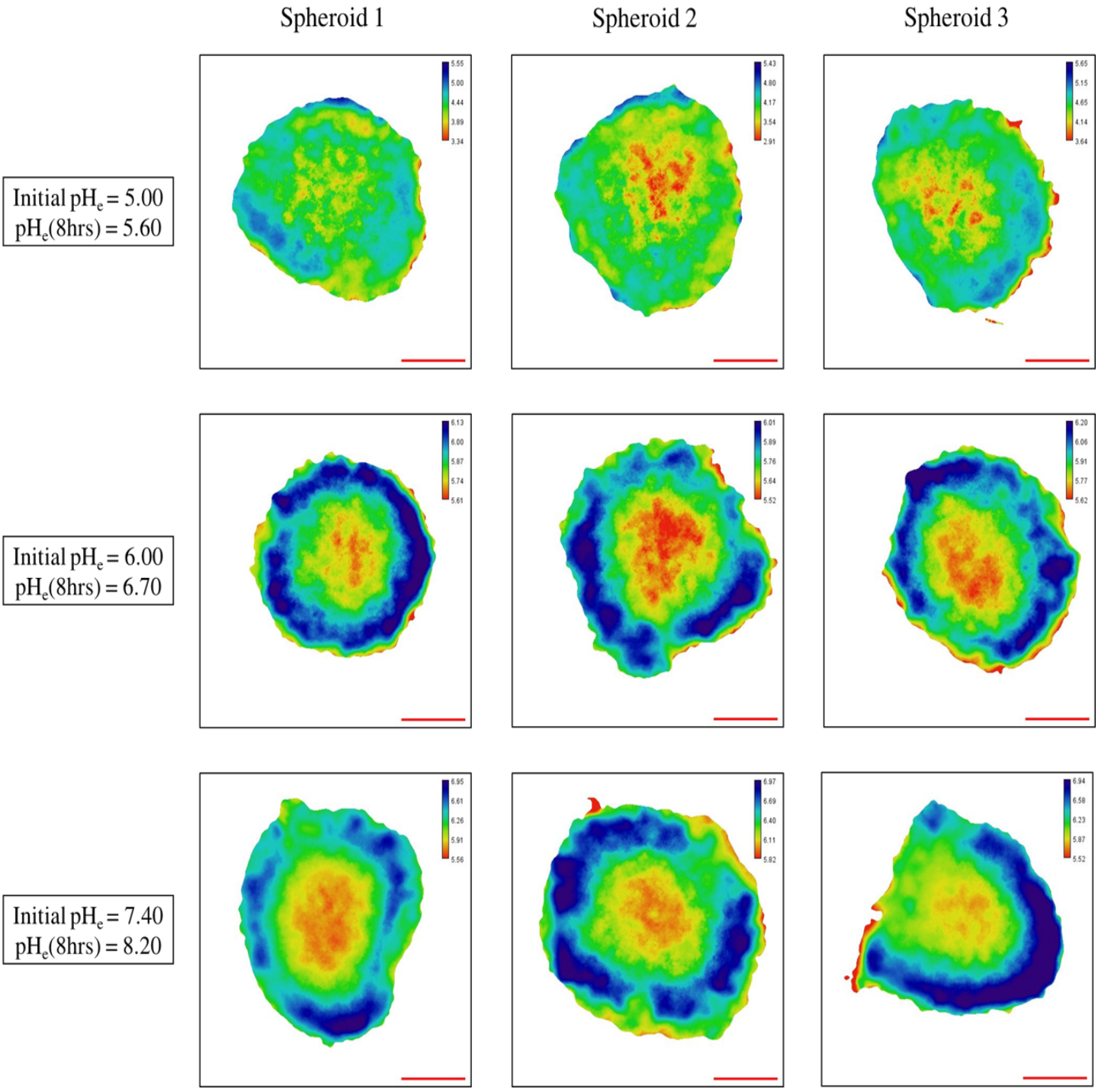

FIGURE A.2: U87 shephroids incubated at different pH_e values. Spheroid triplicates were included for each condition tested. Each pH_i map represents the slice located at a depth of 85 μm. Scale bar = 100 μm

Bibliography

Ackerman, J J et al. (1981). "The role of intrarenal pH in regulation of ammoniagenesis: [31P]NMR studies of the isolated perfused rat kidney." In: *The Journal of Physiology* 319.1, pp. 65–79. DOI: 10.1113/jphysiol.1981.sp013892.

Adam, W. R., A. P. Koretsky, and M. W. Weiner (1985). "Measurement of Renal Intracellular pH by 31P NMR". In: *Contributions to Nephrology*. S. Karger AG, pp. 15–21. DOI: 10.1159/000411204.

— (1986). "31P-NMR in vivo measurement of renal intracellular pH: effects of acidosis and K depletion in rats". In: *American Journal of Physiology-Renal Physiology* 251.5, F904–F910. DOI: 10.1152/ajprenal.1986.251.5.f904.

Albani, Jihad Rene (2008). *Principles and Applications of Fluorescence Spectroscopy*. Wiley Sons, Incorporated, John, p. 264. ISBN: 9780470691335.

Alterio, Vincenzo et al. (2009). "Crystal structure of the catalytic domain of the tumor-associated human carbonic anhydrase IX". In: *Proceedings of the National Academy of Sciences* 106.38, pp. 16233–16238. DOI: 10.1073/pnas.0908301106.

Andersen, Anne Poder, José M. A. Moreira, and Stine Falsig Pedersen (2014). "Interactions of ion transporters and channels with cancer cell metabolism and the tumour microenvironment". In: 369, p. 20130098. ISSN: 0962-8436. DOI: 10.1098/rstb.2013.0098.

Andreucci, Elena et al. (2020). "The acidic tumor microenvironment drives a stem-like phenotype in melanoma cells". In: *Journal of Molecular Medicine* 98.10, pp. 1431–1446. DOI: 10.1007/s00109-020-01959-y.

Audero, Madelaine Magalì, Natalia Prevarskaya, and Alessandra Fiorio Pla (2022). "Ca2 Signalling and Hypoxia/Acidic Tumour Microenvironment Interplay in Tumour Progression". In: *International Journal of Molecular Sciences* 23.13, p. 7377. DOI: 10.3390/ijms23137377.

Auerbach, R (1988). "Patterns of tumor metastasis: organ selectivity in the spread of cancer cells". In: *Laboratory investigation; a journal of technical methods and pathology* 58.4, 361—364. ISSN: 0023-6837. URL: http://europepmc.org/abstract/MED/3282122.

Avnet, Sofia et al. (2016). "Altered pH gradient at the plasma membrane of osteosarcoma cells is a key mechanism of drug resistance". In: *Oncotarget* 7.39, pp. 63408–63423. DOI: 10.18632/oncotarget.11503.

Babcock, D F (1983). "Examination of the intracellular ionic environment and of ionophore action by null point measurements employing the fluorescein chromophore." In: *Journal of Biological Chemistry* 258.10, pp. 6380–6389. DOI: 10.1016/s0021-9258(18)32420-7.

Bailey, Robert E., Andrew M. Smith, and Shuming Nie (2005). "Quantum Dots in Biology and Medicine". In: *ChemInform* 36.22. DOI: 10.1002/chin.200522288.

Bakhoda, Shokoufeh et al. (2018). "Application of Quantum Dot nanocrystal in Luminescent solar concentrators". In: *IOP Conference Series: Materials Science and Engineering* 328, p. 012022. DOI: 10.1088/1757-899x/328/1/012022.

Balkay, Laszlo et al. (June 1997). "Flow cytometric determination of intracellular free K+ concentration". In: *Cytometry* 28, pp. 42–9. DOI: 10.1002/(SICI)1097-0320(19970501)28:1<42::AID-CYTO5>3.0.CO;2-J.

Ballesta, A et al. (2014). "Multiscale Design of Cell-Type-Specific Pharmacokinetic/Pharmacodynamic Models for Personalized Medicine: Application to Temozolomide in Brain Tumors". In: *CPT: Pharmacometrics &amp Systems Pharmacology* 3.4, p. 112. DOI: 10.1038/psp.2014.9.

Balleza, Enrique, J Mark Kim, and Philippe Cluzel (2017). "Systematic characterization of maturation time of fluorescent proteins in living cells". In: *Nature Methods* 15.1, pp. 47–51. DOI: 10.1038/nmeth.4509.

Baltz, J.M., J.D. Biggers, and C. Lechene (1993). "A novel H permeability dominating intracellular pH in the early mouse embryo". In: *Development* 118.4, pp. 1353–1361. DOI: 10.1242/dev.118.4.1353.

Banerjee, Subhrajit and Patricia M. Kane (2020). "Regulation of V-ATPase Activity and Organelle pH by Phosphatidylinositol Phosphate Lipids". In: *Frontiers in Cell and Developmental Biology* 8. DOI: 10.3389/fcell.2020.00510.

Barathova, M et al. (2007). "Alternative splicing variant of the hypoxia marker carbonic anhydrase IX expressed independently of hypoxia and tumour phenotype". In: *British Journal of Cancer* 98.1, pp. 129–136. DOI: 10.1038/sj.bjc.6604111.

Barbosa, Mélanie A. G. et al. (2021). "3D Cell Culture Models as Recapitulators of the Tumor Microenvironment for the Screening of Anti-Cancer Drugs". In: *Cancers* 14.1, p. 190. DOI: 10.3390/cancers14010190.

Barth, Rolf F. (1998). In: *Journal of Neuro-Oncology* 36.1, pp. 91–102. DOI: 10.1023/a:1005805203044.

Barth, Rolf F., Weilian Yang, and Jeffrey A. Coderre (2003). "Rat brain tumor models to assess the efficacy of boron neutron capture therapy: a critical evaluation". In: *Journal of Neuro-oncology* 62.1-2, pp. 61–74. DOI: 10.1007/bf02699934.

Barth, Rolf F et al. (2000). "Boron neutron capture therapy of brain tumors: enhanced survival and cure following blood–brain barrier disruption and intracarotid injection of sodium borocaptate and boronophenylalanine". In: *International Journal of Radiation Oncology∗Biology∗Physics* 47.1, pp. 209–218. DOI: 10.1016/s0360-3016(00)00421-1.

Bartošová, Mária et al. (2002). "Expression of carbonic anhydrase IX in breast is associated with malignant tissues and is related to overexpression of c-erbB2". In: *The Journal of Pathology* 197.3, pp. 314–321. DOI: 10.1002/path.1120.

Bastús, Neus G. et al. (2014). "Synthesis of Highly Monodisperse Citrate-Stabilized Silver Nanoparticles of up to 200 nm: Kinetic Control and Catalytic Properties". In: *Chemistry of Materials* 26.9, pp. 2836–2846. DOI: 10.1021/cm500316k.

Bhadriraju, Kiran and Christopher S Chen (2002). "Engineering cellular microenvironments to improve cell-based drug testing". In: *Drug Discovery Today* 7.11, pp. 612–620. DOI: 10.1016/s1359-6446(02)02273-0.

Bond, Jennifer and Julie Varley (2005). "Use of flow cytometry and SNARF to calibrate and measure intracellular pH in NS0 cells". In: *Cytometry Part A* 64A.1, pp. 43–50. DOI: 10.1002/cyto.a.20066.

Born, R and H Eichholtz-Wirth (1981). "Effect of different physiological conditions on the action of adriamycin on Chinese hamster cells in vitro". In: *British Journal of Cancer* 44.2, pp. 241–246. DOI: 10.1038/bjc.1981.175.

Bourguignon, Lilly Y.W. et al. (2004). "CD44 Interaction with Na-H Exchanger (NHE1) Creates Acidic Microenvironments Leading to Hyaluronidase-2 and Cathepsin B Activation and Breast Tumor Cell Invasion". In: *Journal of Biological Chemistry* 279.26, pp. 26991–27007. DOI: 10.1074/jbc.m311838200.

Boussouf, Abdelhamid and Stéphane Gaillard (2000). "Intracellular pH changes during oligodendrocyte differentiation in primary culture". In: *Journal of Neuroscience Research* 59.6, pp. 731–739. DOI: 10.1002/(sici)1097-4547(20000315)59:6<731::aid-jnr5>3.0.co;2-g.

Boyer, Michael J. and Ian F. Tannock (Aug. 1992). "Regulation of Intracellular pH in Tumor Cell Lines: Influence of Microenvironmental Conditions1". In: *Cancer Research* 52.16, pp. 4441–4447. ISSN: 0008-5472. eprint: https://aacrjournals.org/cancerres/article-pdf/52/16/4441/2447730/cr0520164441.pdf.

Boyer, MJ et al. (1993). "Regulation of intracellular pH in subpopulations of cells derived from spheroids and solid tumours". In: *British Journal of Cancer* 68.5, pp. 890–897. DOI: 10.1038/bjc.1993.451.

Breslin, Susan and Lorraine O'Driscoll (2013). "Three-dimensional cell culture: the missing link in drug discovery". In: *Drug Discovery Today* 18.5-6, pp. 240–249. DOI: 10.1016/j.drudis.2012.10.003.

Brindle, Kevin M. et al. (1988). "31P NMR measurements of myocardial pH invivo". In: *Biochemical and Biophysical Research Communications* 151.1, pp. 70–77. DOI: 10.1016/0006-291x(88)90560-8.

Brisson, Lucie et al. (2012). "pH regulators in invadosomal functioning: Proton delivery for matrix tasting". In: 91, pp. 847–860. ISSN: 0171-9335. DOI: 10.1016/j.ejcb.2012.04.004.

Brophy, Gregory T. and N.E. Sladek (1983). "Influence of pH on the cytotoxic activity of chlorambucil". In: *Biochemical Pharmacology* 32.1, pp. 79–84. DOI: 10.1016/0006-2952(83)90656-1.

Brown, D, S Gluck, and J Hartwig (1987). "Structure of the novel membrane-coating material in proton-secreting epithelial cells and identification as an HATPase." In: *Journal of Cell Biology* 105.4, pp. 1637–1648. DOI: 10.1083/jcb.105.4.1637.

Brown, D A and J Garthwaite (1979). "Intracellular pH and the distribution of weak acids and bases in isolated rat superior cervical ganglia." In: *The Journal of Physiology* 297.1, pp. 597–620. DOI: 10.1113/jphysiol.1979.sp013059.

Brown, S. E. et al. (1991). "ATP-sensitive Na()-H antiport in type II alveolar epithelial cells". In: *American Journal of Physiology-Cell Physiology* 261.6, pp. C954–C963. DOI: 10.1152/ajpcell.1991.261.6.c954.

Brown, Silvia V. et al. (2006). "ATP Synthase Is Responsible for Maintaining Mitochondrial Membrane Potential in Bloodstream Form iTrypanosoma brucei/i". In: *Eukaryotic Cell* 5.1, pp. 45–53. DOI: 10.1128/ec.5.1.45-53.2006.

Bueno, Valquiria et al. (2007). "The Specific Monocarboxylate Transporter (MCT1) Inhibitor, AR-C117977, a Novel Immunosuppressant, Prolongs Allograft Survival in the Mouse". In: *Transplantation* 84.9, pp. 1204–1207. DOI: 10.1097/01.tp.0000287543.91765.41.

Calcinotto, Arianna et al. (2012). "Modulation of Microenvironment Acidity Reverses Anergy in Human and Murine Tumor-Infiltrating T Lymphocytes". In: *Cancer Research* 72.11, pp. 2746–2756. DOI: 10.1158/0008-5472.can-11-1272.

Caldwell, Peter C. (1956). "Intracellular pH". In: *International Review of Cytology*. Elsevier, pp. 229–277. DOI: 10.1016/s0074-7696(08)62572-3.

Campbell, Tessa N. (2001). "The Effect of pH on Green Fluorescent Protein: a Brief Review". In.

Cardone, Rosa A., Valeria Casavola, and Stephan J. Reshkin (2005). "The role of disturbed pH dynamics and the Na/H exchanger in metastasis". In: *Nature Reviews Cancer* 5.10, pp. 786–795. DOI: 10.1038/nrc1713.

Carmeliet, Peter and Rakesh K. Jain (2000). "Angiogenesis in cancer and other diseases". In: *Nature* 407.6801, pp. 249–257. DOI: 10.1038/35025220.

Carmelo, Vanda, Helena Santos, and Isabel Sá-Correia (1997). "Effect of extracellular acidification on the activity of plasma membrane ATPase and on the cytosolic and vacuolar pH of Saccharomyces cerevisiae". In: *Biochimica et Biophysica Acta (BBA) - Biomembranes* 1325.1, pp. 63–70. DOI: 10.1016/s0005-2736(96)00245-3.

Cassel, D, M Katz, and M Rotman (1986). "Depletion of cellular ATP inhibits Na/H antiport in cultured human cells. Modulation of the regulatory effect of intracellular protons on the antiporter activity." In: *Journal of Biological Chemistry* 261.12, pp. 5460–5466. DOI: 10.1016/s0021-9258(19)57238-6.

Chalfie, Martin et al. (1994). "Green Fluorescent Protein as a Marker for Gene Expression". In: *Science* 263.5148, pp. 802–805. DOI: 10.1126/science.8303295.

Chen, Jian et al. (2012). "A restricted cell population propagates glioblastoma growth after chemotherapy". In: *Nature* 488.7412, pp. 522–526. DOI: 10.1038/nature11287.

Chen, Ran, Marja Jäättelä, and Bin Liu (2020). "Lysosome as a Central Hub for Rewiring PH Homeostasis in Tumors". In: *Cancers* 12.9, p. 2437. DOI: 10.3390/cancers12092437.

Chen, Thomas et al. (2018). "Rare Stochastic Expression of O6-Methylguanine- DNA Methyltransferase (MGMT) in MGMT-Negative Melanoma Cells Determines Immediate Emergence of Drug-Resistant Populations upon Treatment with Temozolomide In Vitro and In Vivo". In: *Cancers* 10.10, p. 362. DOI: 10.3390/cancers10100362.

Chen, Yingche, Kelvin Tsao, and Jeffrey W. Keillor (2015). "Fluorogenic protein labelling: a review of photophysical quench mechanisms and principles of fluorogen design". In: *Canadian Journal of Chemistry* 93.4, pp. 389–398. DOI: 10.1139/cjc-2014-0405.

Cheng, Grace M. Y. and Kenneth K. W. To (2012). "Adverse Cell Culture Conditions Mimicking the Tumor Microenvironment Upregulate ABCG2 to Mediate Multidrug Resistance and a More Malignant Phenotype". In: *ISRN Oncology* 2012, pp. 1–10. DOI: 10.5402/2012/746025.

Chiche, Johanna, M. Christiane Brahimi-Horn, and Jacques Pouysségur (2010). "Tumour hypoxia induces a metabolic shift causing acidosis: a common feature in cancer". In: 14, pp. 771–794. ISSN: 1582-1838. DOI: 10.1111/j.1582-4934.2009.00994.x.

Chiche, Johanna et al. (2008). "Hypoxia-Inducible Carbonic Anhydrase IX and XII Promote Tumor Cell Growth by Counteracting Acidosis through the Regulation of the Intracellular pH". In: *Cancer Research* 69.1, pp. 358–368. DOI: 10.1158/0008-5472.can-08-2470.

Claire, C. and R. C. Thomas (1977). "Micro-electrode measurement of the intracellular pH and buffering power of mouse soleus muscle fibres." In: *The Journal of Physiology* 267.3, pp. 791–810. DOI: 10.1113/jphysiol.1977.sp011838.

Clarke, Jennifer, Nicholas Butowski, and Susan Chang (2010). "Recent Advances in Therapy for Glioblastoma". In: *Archives of Neurology* 67.3. DOI: 10.1001/archneurol.2010.5.

Clarke, Kieran et al. (1993). "Extracellular volume and transsarcolemmal proton movement during ischemia and reperfusion: A31P NMR spectroscopic study of the isovolumic rat heart". In: *NMR in Biomedicine* 6.4, pp. 278–286. DOI: 10.1002/nbm.1940060407.

Clavreul, Anne et al. (2019). "The French glioblastoma biobank (FGB): a national clinicobiological database". In: 17. ISSN: 1479-5876. DOI: 10.1186/s12967-019-1859-6.

Conchello, José-Angel and Jeff W Lichtman (2005). "Optical sectioning microscopy". In: *Nature Methods* 2.12, pp. 920–931. DOI: 10.1038/nmeth815.

Corbet, Cyril and Olivier Feron (2017). "Tumour acidosis: from the passenger to the driver's seat". In: *Nature Reviews Cancer* 17.10, pp. 577–593. DOI: 10.1038/nrc.2017.77.

Damaghi, Mehdi, Jonathan W. Wojtkowiak, and Robert J. Gillies (2013). "pH sensing and regulation in cancer". In: *Frontiers in Physiology* 4. DOI: 10.3389/fphys.2013.00370.

Dean, Kevin M and Amy E Palmer (2014). "Advances in fluorescence labeling strategies for dynamic cellular imaging". In: *Nature Chemical Biology* 10.7, pp. 512–523. DOI: 10.1038/nchembio.1556.

deMello, Andrew J. (2006). "Control and detection of chemical reactions in microfluidic systems". In: *Nature* 442.7101, pp. 394–402. DOI: 10.1038/nature05062.

Denker, Sheryl P et al. (2000). "Direct Binding of the Na–H Exchanger NHE1 to ERM Proteins Regulates the Cortical Cytoskeleton and Cell Shape Independently of H Translocation". In: *Molecular Cell* 6.6, pp. 1425–1436. DOI: 10.1016/s1097-2765(00)00139-8.

Denny, Brian J. et al. (1994). "NMR and Molecular Modeling Investigation of the Mechanism of Activation of the Antitumor Drug Temozolomide and Its Interaction with DNA". In: *Biochemistry* 33.31, pp. 9045–9051. DOI: 10.1021/bi00197a003.

Doyen, Denis et al. (2022). "Intracellular pH Control by Membrane Transport in Mammalian Cells. Insights Into the Selective Advantages of Functional Redundancy". In: *Frontiers in Molecular Biosciences* 9. DOI: 10.3389/fmolb.2022.825028.

Druzhkova, Irina et al. (2015). *Registration of intracellular pH in cancer cells with genetically encoded ratiometric sensor*. DOI: 10.1364/ecbo.2015.953710.

Ekberg, Henrik et al. (2007). "The Specific Monocarboxylate Transporter-1 (MCT-1) Inhibitor, AR-C117977, Induces Donor-Specific Suppression, Reducing Acute and Chronic Allograft Rejection in the Rat". In: *Transplantation* 84.9, pp. 1191–1199. DOI: 10.1097/01.tp.0000287541.53389.be.

Ellis, D. and R. C. Thomas (1976). "Microelectrode measurement of the intracellular pH of mammalian heart cells". In: *Nature* 262.5565, pp. 224–225. DOI: 10.1038/262224a0.

Enerson, Bradley E. and Lester R. Drewes (2003). "Molecular Features, Regulation, and Function of Monocarboxylate Transporters: Implications for Drug Delivery". In: *Journal of Pharmaceutical Sciences* 92.8, pp. 1531–1544. DOI: 10.1002/jps.10389.

Estrella, Veronica et al. (2013). "Acidity Generated by the Tumor Microenvironment Drives Local Invasion". In: *Cancer Research* 73.5, pp. 1524–1535. DOI: 10.1158/0008-5472.can-12-2796.

Evans, Conor L. et al. (2011). "Killing Hypoxic Cell Populations in a 3D Tumor Model with EtNBS-PDT". In: *PLoS ONE* 6.8. Ed. by Eric J. Bernhard, e23434. DOI: 10.1371/journal.pone.0023434.

Fan, S et al. (2012). "LASS2 enhances chemosensitivity of breast cancer by counteracting acidic tumor microenvironment through inhibiting activity of V-ATPase proton pump". In: *Oncogene* 32.13, pp. 1682–1690. DOI: 10.1038/onc.2012.183.

Fang, Jennifer S., Robert D. Gillies, and Robert A. Gatenby (2008). "Adaptation to hypoxia and acidosis in carcinogenesis and tumor progression". In: *Seminars in Cancer Biology* 18.5, pp. 330–337. DOI: 10.1016/j.semcancer.2008.03.011.

Federici, Cristina et al. (2014). "Exosome Release and Low pH Belong to a Framework of Resistance of Human Melanoma Cells to Cisplatin". In: *PLoS ONE* 9.2. Ed. by Irina V. Lebedeva, e88193. DOI: 10.1371/journal.pone.0088193.

Fernández, Victor M. (1983). "An electrochemical cell for reduction of biochemicals: Its application to the study of the effect of pH and redox potential on the activity of hydrogenases". In: *Analytical Biochemistry* 130.1, pp. 54–59. DOI: 10.1016/0003-2697(83)90648-6.

Fidler, Isaiah J. (2003). "The pathogenesis of cancer metastasis: the 'seed and soil' hypothesis revisited". In: *Nature Reviews Cancer* 3.6, pp. 453–458. DOI: 10.1038/nrc1098.

Fischer, Karin et al. (2007). "Inhibitory effect of tumor cell–derived lactic acid on human T cells". In: *Blood* 109.9, pp. 3812–3819. DOI: 10.1182/blood-2006-07-035972.

Folkman, Judah and Mark Hochberg (1973). "SELF-REGULATION OF GROWTH IN THREE DIMENSIONS". In: *Journal of Experimental Medicine* 138.4, pp. 745–753. DOI: 10.1084/jem.138.4.745.

Forgac, M. (1989). "Structure and function of vacuolar class of ATP-driven proton pumps". In: *Physiological Reviews* 69.3, pp. 765–796. DOI: 10.1152/physrev.1989.69.3.765.

Frank, Natasha Y. et al. (2005). "ABCB5-Mediated Doxorubicin Transport and Chemoresistance in Human Malignant Melanoma". In: *Cancer Research* 65.10, pp. 4320–4333. DOI: 10.1158/0008-5472.can-04-3327.

Franko, AJ et al. (1998). "Variable presence of hypoxia in M006 human glioma spheroids and in spheroids and xenografts of clonally derived sublines". In: *British Journal of Cancer* 78.10, pp. 1261–1268. DOI: 10.1038/bjc.1998.669.

Freyer, J. P. and R. M. Sutherland (1985). "A reduction in the in situ rates of oxygen and glucose consumption of cells in EMT6/Ro spheroids during growth". In: *Journal of Cellular Physiology* 124.3, pp. 516–524. DOI: 10.1002/jcp.1041240323.

Friedrich, Juergen et al. (2009). "Spheroid-based drug screen: considerations and practical approach". In: *Nature Protocols* 4.3, pp. 309–324. DOI: 10.1038/nprot.2008.226.

Froberg, M. Kent et al. (2001). "Expression of monocarboxylate transporter MCT1 in normal and neoplastic human CNS tissues". In: *Neuroreport* 12.4, pp. 761–765. DOI: 10.1097/00001756-200103260-00030.

Fujisawa, Koichi et al. (2020). "Metabolic Alterations in Spheroid-Cultured Hepatic Stellate Cells". In: *International Journal of Molecular Sciences* 21.10, p. 3451. DOI: 10.3390/ijms21103451.

Fuster, Daniel, Orson W. Moe, and Donald W. Hilgemann (2004). "Lipid- and mechanosensitivities of sodium/hydrogen exchangers analyzed by electrical methods". In: *Proceedings of the National Academy of Sciences* 101.28, pp. 10482–10487. DOI: 10.1073/pnas.0403930101.

Galkina, S.I., G.F. Sud'Ina, and L.B. Margolis (1992). "Cell-cell contacts alter intracellular pH". In: *Experimental Cell Research* 200.1, pp. 211–214. DOI: 10.1016/s0014-4827(05)80090-4.

Galkina, S.I., G.F. Sud'ina, and L.B. Margolis (1996). "Regulation of intracellular pH by phospholipase A2 and protein kinase C upon neutrophil adhesion to solid substrata". In: *FEBS Letters* 393.1, pp. 117–120. DOI: 10.1016/0014-5793(96)00864-2.

Galkina, S.I. et al. (1995). "Regulation of intracellular pH by cell-cell adhesive interactions". In: *FEBS Letters* 374.1, pp. 17–20. DOI: 10.1016/0014-5793(95)00969-g.

Gallagher, Shannon M. et al. (2007). "Monocarboxylate Transporter 4 Regulates Maturation and Trafficking of CD147 to the Plasma Membrane in the Metastatic Breast Cancer Cell Line MDA-MB-231". In: *Cancer Research* 67.9, pp. 4182–4189. DOI: 10.1158/0008-5472.can-06-3184.

Garry, Robert F. et al. (1988). "Cell surface effects of human immunodeficiency virus". In: *Bioscience Reports* 8.1, pp. 35–48. DOI: 10.1007/bf01128970.

Genovese, Ilaria et al. (2017). "Not only P-glycoprotein: Amplification of the ABCB1- containing chromosome region 7q21 confers multidrug resistance upon cancer cells by coordinated overexpression of an assortment of resistance-related proteins". In: *Drug Resistance Updates* 32, pp. 23–46. DOI: 10.1016/j.drup.2017.10.003.

Gentric, Géraldine, Virginie Mieulet, and Fatima Mechta-Grigoriou (2017). "Heterogeneity in Cancer Metabolism: New Concepts in an Old Field". In: 26, pp. 462–485. ISSN: 1523-0864. DOI: 10.1089/ars.2016.6750.

Georgakoudi, Irene et al. (2008). "Optical Spectroscopy and Imaging for the Noninvasive Evaluation of Engineered Tissues". In: *Tissue Engineering Part B: Reviews* 14.4, pp. 321–340. DOI: 10.1089/ten.teb.2008.0248.

Gillet, J and J Remacle (n.d.). In: ().

Gillies, Robert J. et al. (2002). "MRI of the tumor microenvironment". In: *Journal of Magnetic Resonance Imaging* 16.4, pp. 430–450. DOI: 10.1002/jmri.10181.

Gilmour, K.M. (2010). "Perspectives on carbonic anhydrase". In: *Comparative Biochemistry and Physiology Part A: Molecular &amp Integrative Physiology* 157.3, pp. 193–197. DOI: 10.1016/j.cbpa.2010.06.161.

Glunde, Kristine et al. (2002). "Na/H exchange subtype 1 inhibition during extracellular acidification and hypoxia in glioma cells". In: *Journal of Neurochemistry* 80.1, pp. 36–44. DOI: 10.1046/j.0022-3042.2001.00661.x.

Gonçalves, M. Sameiro T. (2008). "Fluorescent Labeling of Biomolecules with Organic Probes". In: *Chemical Reviews* 109.1, pp. 190–212. DOI: 10.1021/cr0783840.

Gores, G J et al. (1989). "Intracellular pH during "chemical hypoxia" in cultured rat hepatocytes. Protection by intracellular acidosis against the onset of cell death." In: *Journal of Clinical Investigation* 83.2, pp. 386–396. DOI: 10.1172/jci113896.

Graber, Mark L. et al. (1986). "Characteristics of fluoroprobes for measuring intracellular pH". In: *Analytical Biochemistry* 156.1, pp. 202–212. DOI: 10.1016/0003-2697(86)90174-0.

Grabmaier, Karin et al. (2004). "Strict regulation of CAIXG250/MN by HIF-1α in clear cell renal cell carcinoma". In: *Oncogene* 23.33, pp. 5624–5631. DOI: 10.1038/sj.onc.1207764.

Griesbeck, Oliver et al. (2001). "Reducing the Environmental Sensitivity of Yellow Fluorescent Protein". In: *Journal of Biological Chemistry* 276.31, pp. 29188–29194. DOI: 10.1074/jbc.m102815200.

Grillon, Emmanuelle et al. (2011). "The Spatial Organization of Proton and Lactate Transport in a Rat Brain Tumor". In: *PLoS ONE* 6.2. Ed. by Joseph Najbauer, e17416. DOI: 10.1371/journal.pone.0017416.

Güvenalp, Neşe and Dilek Güvenç (2020). "HepG2 hücre hattının canlılığı üzerine medium pH'sının etkisinin incelenmesi". In: *Etlik Veteriner Mikrobiyoloji Dergisi*. DOI: 10.35864/evmd.742482.

Hackam, David J., Sergio Grinstein, and Ori D. Rotstein (1996). "INTRACELLULAR pH REGULATION IN LEUKOCYTES". In: *Shock* 5.1, pp. 17–21. DOI: 10.1097/00024382-199601000-00005.

Hagberg, H., S. Larsson, and H. Haljamae (1983). "A new design of double-barrelled microelectrodes for intracellular pH-measurement in vivo". In: *Acta Physiologica Scandinavica* 118.2, pp. 149–153. DOI: 10.1111/j.1748-1716.1983.tb07255.x.

Hamm, L. Lee, Nazih Nakhoul, and Kathleen S. Hering-Smith (2015). "Acid-Base Homeostasis". In: *Clinical Journal of the American Society of Nephrology* 10.12, pp. 2232–2242. DOI: 10.2215/cjn.07400715.

Hanahan, Douglas and Robert A. Weinberg (2000). "The Hallmarks of Cancer". In: 100, pp. 57–70. ISSN: 0092-8674. DOI: 10.1016/s0092-8674(00)81683-9.

— (2011). "Hallmarks of Cancer: The Next Generation". In: *Cell* 144.5, pp. 646–674. DOI: 10.1016/j.cell.2011.02.013.

Harguindey, Salvador et al. (2005). "The role of pH dynamics and the Na/H antiporter in the etiopathogenesis and treatment of cancer. Two faces of the same coin—one single nature". In: *Biochimica et Biophysica Acta (BBA) - Reviews on Cancer* 1756.1, pp. 1–24. DOI: 10.1016/j.bbcan.2005.06.004.

Harguindey, Salvador et al. (2009). "Proton Transport Inhibitors as Potentially Selective Anticancer Drugs". In: *Anticancer Research* 29.6, pp. 2127–2136. ISSN: 0250-7005. eprint: https://ar.iiarjournals.org/content/29/6/2127.full.pdf. URL: https://ar.iiarjournals.org/content/29/6/2127.

Haugland, Richard P. (2005). *A Guide to Fluorescent Probes and Labeling Technologies*. Molecular Probes, p. 1126. ISBN: 9780971063648.

Hawe, Andrea, Marc Sutter, and Wim Jiskoot (2008). "Extrinsic Fluorescent Dyes as Tools for Protein Characterization". In: *Pharmaceutical Research* 25.7, pp. 1487–1499. DOI: 10.1007/s11095-007-9516-9.

Hedeskov, C. J. (1968). "Early effects of phytohaemagglutinin on glucose metabolism of normal human lymphocytes". In: *Biochemical Journal* 110.2, pp. 373–380. DOI: 10.1042/bj1100373.

Heiden, Matthew G. Vander, Lewis C. Cantley, and Craig B. Thompson (2009). "Understanding the Warburg Effect: The Metabolic Requirements of Cell Proliferation". In: *Science* 324.5930, pp. 1029–1033. DOI: 10.1126/science.1160809.

Heim, Roger and Roger Y Tsien (1996). "Engineering green fluorescent protein for improved brightness, longer wavelengths and fluorescence resonance energy transfer". In: *Current Biology* 6.2, pp. 178–182. DOI: 10.1016/s0960-9822(02)00450-5.

Heiple, J M and D L Taylor (1980). "Intracellular pH in single motile cells." In: *Journal of Cell Biology* 86.3, pp. 885–890. DOI: 10.1083/jcb.86.3.885.

Held, Paul (2018). "Using Phenol Red to Assess pH in Tissue Culture Media". In.

Hemptinne, A. de (1980). "Intracellular pH and surface pH in skeletal and cardiac muscle measured with a double-barrelled pH microelectrode". In: *Pflügers Archiv* 386.2, pp. 121–126. DOI: 10.1007/bf00584198.

Heston, W.E. (1948). "Genetics of Cancer". In: *Advances in Genetics*. Elsevier, pp. 99–125. DOI: 10.1016/s0065-2660(08)60467-8.

Hight, Matthew R. et al. (2011). "Multispectral fluorescence imaging to assess pH in biological specimens". In: *Journal of Biomedical Optics* 16.1, p. 016007. DOI: 10.1117/1.3533264.

Hindenburg, A. A. et al. (Aug. 1989). "Intracellular distribution and pharmacokinetics of daunorubicin in anthracycline-sensitive and -resistant HL-60 cells." In: *Cancer research* 49 (16), pp. 4607–4614. ISSN: 0008-5472. ppublish.

Hinton, Ayana et al. (2009). "Function of a Subunit Isoforms of the V-ATPase in pH Homeostasis and in Vitro Invasion of MDA-MB231 Human Breast Cancer Cells". In: *Journal of Biological Chemistry* 284.24, pp. 16400–16408. DOI: 10.1074/jbc.m901201200.

Hirschhaeuser, Franziska et al. (2010). "Multicellular tumor spheroids: An underestimated tool is catching up again". In: *Journal of Biotechnology* 148.1, pp. 3–15. DOI: 10.1016/j.jbiotec.2010.01.012.

Hjelmeland, A B et al. (2010). "Acidic stress promotes a glioma stem cell phenotype". In: *Cell Death &amp Differentiation* 18.5, pp. 829–840. DOI: 10.1038/cdd.2010.150.

Holohan, Caitriona et al. (2013). "Cancer drug resistance: an evolving paradigm". In: *Nature Reviews Cancer* 13.10, pp. 714–726. DOI: 10.1038/nrc3599.

Hulikova, Alzbeta, Richard D. Vaughan-Jones, and Pawel Swietach (2011). "Dual Role of CO2/HCO3- Buffer in the Regulation of Intracellular pH of Three-dimensional Tumor Growths". In: *Journal of Biological Chemistry* 286.16, pp. 13815–13826. DOI: 10.1074/jbc.m111.219899.

Ibrahim-Hashim, Arig and Veronica Estrella (2019). "Acidosis and cancer: from mechanism to neutralization". In: 38, pp. 149–155. ISSN: 0167-7659. DOI: 10.1007/s10555-019-09787-4.

Ichas, François and Jean-Pierre Mazat (1998). "From calcium signaling to cell death: two conformations for the mitochondrial permeability transition pore. Switching from low- to high-conductance state". In: *Biochimica et Biophysica Acta (BBA) - Bioenergetics* 1366.1-2, pp. 33–50. DOI: 10.1016/s0005-2728(98)00119-4.

Imai, Takeo and Toshihiko Ohno (1995). "Measurement of yeast intracellular pH by image processing and the change it undergoes during growth phase". In: *Journal of Biotechnology* 38.2, pp. 165–172. DOI: 10.1016/0168-1656(94)00130-5.

Ivanov, Sergey et al. (2001). "Expression of Hypoxia-Inducible Cell-Surface Transmembrane Carbonic Anhydrases in Human Cancer". In: *The American Journal of Pathology* 158.3, pp. 905–919. DOI: 10.1016/s0002-9440(10)64038-2.

Ivanov, Sergey V. et al. (1998). "Down-regulation of transmembrane carbonic anhydrases in renal cell carcinoma cell lines by wild-type von Hippel-Lindau transgenes". In: *Proceedings of the National Academy of Sciences* 95.21, pp. 12596–12601. DOI: 10.1073/pnas.95.21.12596.

Izumi, Hiroto et al. (2011). "Monocarboxylate transporters 1 and 4 are involved in the invasion activity of human lung cancer cells". In: *Cancer Science* 102.5, pp. 1007–1013. DOI: 10.1111/j.1349-7006.2011.01908.x.

Izutsu, K. T. (1972). "Intracellular pH, H ion flux and H ion permeability coefficient in bullfrog toe muscle". In: *The Journal of Physiology* 221.1, pp. 15–27. DOI: 10.1113/jphysiol.1972.sp009735.

Jablonski, A. (1933). "Efficiency of Anti-Stokes Fluorescence in Dyes". In: *Nature* 131.3319, pp. 839–840. DOI: 10.1038/131839b0.

Jacquet, Pierre and Angélique Stéphanou (2021). "Metabolic Reprogramming, Questioning, and Implications for Cancer". In: *Biology* 10.2, p. 129. DOI: 10.3390/biology10020129. URL: https://hal.archives-ouvertes.fr/hal-03151101.

Jares-Erijman, Elizabeth A and Thomas M Jovin (2003). "FRET imaging". In: *Nature Biotechnology* 21.11, pp. 1387–1395. DOI: 10.1038/nbt896.

Jähde, Eckhard, Karl-Heinz Glüsenkamp, and Manfred F. Rajewsky (1990). "Protection of cultured malignant cells from mitoxantrone cytotoxicity by low extracellular pH: A possible mechanism for chemoresistance in vivo". In: *European Journal of Cancer and Clinical Oncology* 26.2, pp. 101–106. DOI: 10.1016/0277-5379(90)90290-a.

Ji, Xiwei et al. (2019). "Chemoresistance mechanisms of breast cancer and their countermeasures". In: *Biomedicine &amp Pharmacotherapy* 114, p. 108800. DOI: 10.1016/j.biopha.2019.108800.

Johannessen, Tor-Christian Aase, Rolf Bjerkvig, and Berit Bølge Tysnes (2008). "DNA repair and cancer stem-like cells – Potential partners in glioma drug resistance?" In: *Cancer Treatment Reviews* 34.6, pp. 558–567. DOI: 10.1016/j.ctrv.2008.03.125.

Johnson, Danielle E. et al. (2016). "The position of lysosomes within the cell determines their luminal pH". In: *Journal of Cell Biology* 212.6, pp. 677–692. DOI: 10.1083/jcb.201507112.

Justus, Calvin R., Lixue Dong, and Li V. Yang (2013). "Acidic tumor microenvironment and pH-sensing G protein-coupled receptors". In: *Frontiers in Physiology* 4. DOI: 10.3389/fphys.2013.00354.

Kallinowski, F. and P. Vaupel (1988). "pH distributions in spontaneous and isotransplanted rat tumours". In: 58, pp. 314–321. ISSN: 0007-0920. DOI: 10.1038/bjc.1988.210.

Kapałczyńska, Marta et al. (2016). "2D and 3D cell cultures – a comparison of different types of cancer cell cultures". In: *Archives of Medical Science*. DOI: 10.5114/aoms.2016.63743.

Kapus, A. et al. (1994). "Functional characterization of three isoforms of the Na/H exchanger stably expressed in Chinese hamster ovary cells. ATP dependence, osmotic sensitivity, and role in cell proliferation." In: *Journal of Biological Chemistry* 269.38, pp. 23544–23552. DOI: 10.1016/s0021-9258(17)31550-8.

Karayan-Tapon, Lucie et al. (2009). "Prognostic value of O6-methylguanine-DNA methyltransferase status in glioblastoma patients, assessed by five different methods". In: *Journal of Neuro-Oncology* 97.3, pp. 311–322. DOI: 10.1007/s11060-009-0031-1.

Kato, Yasumasa et al. (2005). "Acidic Extracellular pH Induces Matrix Metalloproteinase-9 Expression in Mouse Metastatic Melanoma Cells through the Phospholipase D-Mitogen-activated Protein Kinase Signaling". In: *Journal of Biological Chemistry* 280.12, pp. 10938–10944. DOI: 10.1074/jbc.m411313200.

Katt, Moriah E. et al. (2016). "In Vitro Tumor Models: Advantages, Disadvantages, Variables, and Selecting the Right Platform". In: *Frontiers in Bioengineering and Biotechnology* 4. DOI: 10.3389/fbioe.2016.00012.

Kenny, Paraic A. et al. (2007). "The morphologies of breast cancer cell lines in three-dimensional assays correlate with their profiles of gene expression". In: *Molecular Oncology* 1.1, pp. 84–96. DOI: 10.1016/j.molonc.2007.02.004.

Kerbel, Robert and Judah Folkman (2002). "Clinical translation of angiogenesis inhibitors". In: 2, pp. 727–739. ISSN: 1474-175X. DOI: 10.1038/nrc905.

Khajah, Maitham A. et al. (2013). "Extracellular Alkaline pH Leads to Increased Metastatic Potential of Estrogen Receptor Silenced Endocrine Resistant Breast Cancer Cells". In: *PLoS ONE* 8.10. Ed. by Chih-Hsin Tang, e76327. DOI: 10.1371/journal.pone.0076327.

Kinsella, J. L. and P. S. Aronson (1980). "Properties of the Na-H exchanger in renal microvillus membrane vesicles". In: *American Journal of Physiology-Renal Physiology* 238.6, F461–F469. DOI: 10.1152/ajprenal.1980.238.6.f461.

Ko, L., A. Koestner, and W. Wechsler (1980). "Morphological characterization of nitrosourea-induced glioma cell lines and clones". In: *Acta Neuropathologica* 51.1, pp. 23–31. DOI: 10.1007/bf00688846.

Koltai, Tomas (2020). "Targeting the pH Paradigm at the Bedside: A Practical Approach". In: *International Journal of Molecular Sciences* 21.23, p. 9221. DOI: 10.3390/ijms21239221.

Koppenol, Willem H., Patricia L. Bounds, and Chi V. Dang (2011). "Otto Warburg's contributions to current concepts of cancer metabolism". In: 11, pp. 325–337. ISSN: 1474-175X. DOI: 10.1038/nrc3038.

Korenchan, David E. and Robert R. Flavell (2019). "Spatiotemporal pH Heterogeneity as a Promoter of Cancer Progression and Therapeutic Resistance". In: *Cancers* 11.7, p. 1026. DOI: 10.3390/cancers11071026.

Kreso, Antonija and John E. Dick (2014). "Evolution of the Cancer Stem Cell Model". In: *Cell Stem Cell* 14.3, pp. 275–291. DOI: 10.1016/j.stem.2014.02.006.

Kunz-Shughart, Leoni A., Marina Kreutz, and Ruth Knuechel (1998). "Multicellular spheroids: a three-dimensionaliin vitro/iculture system to study tumour biology". In: *International Journal of Experimental Pathology* 79.1, pp. 1–23. DOI: 10.1046/j.1365-2613.1998.00051.x.

Lacoste, I., B.J. Harvey, and J. Ehrenfeld (1991). "Cl- permeability of the basolateral membrane of the Rana esculenta epithelium: activation of Cl-/HCO3- exchange by alkaline intracellular pH". In: *Biochimica et Biophysica Acta (BBA) - Biomembranes* 1063.1, pp. 103–110. DOI: 10.1016/0005-2736(91)90359-g.

Lagadic-Gossmann, D., J. M. Chesnais, and D. Feuvray (1988). "Intracellular pH regulation in papillary muscle cells from streptozotocin diabetic rats: an ion-sensitive microelectrode study". In: *Pflügers Archiv - European Journal of Physiology* 412.6, pp. 613–617. DOI: 10.1007/bf00583762.

Lakowicz, Joseph R. (1999). *Principles of Fluorescence Spectroscopy*. Springer US. DOI: 10.1007/978-1-4757-3061-6.

Lam, Fred C. et al. (2001). "β-Amyloid efflux mediated by p-glycoprotein". In: *Journal of Neurochemistry* 76.4, pp. 1121–1128. DOI: 10.1046/j.1471-4159.2001.00113.x.

Lang, Wenjie et al. (2020). "Recent advances in construction of small molecule-based fluorophore-drug conjugates". In: *Journal of Pharmaceutical Analysis* 10.5, pp. 434–443. DOI: 10.1016/j.jpha.2020.08.006.

Langer, G A (1985). "The effect of pH on cellular and membrane calcium binding and contraction of myocardium. A possible role for sarcolemmal phospholipid in EC coupling." In: *Circulation Research* 57.3, pp. 374–382. DOI: 10.1161/01.res.57.3.374.

Larsen, Annette K., Alexandre E. Escargueil, and Andrzej Skladanowski (2000). "Resistance mechanisms associated with altered intracellular distribution of anticancer agents". In: *Pharmacology &amp Therapeutics* 85.3, pp. 217–229. DOI: 10.1016/s0163-7258(99)00073-x.

Lavis, Luke D. and Ronald T. Raines (2008). "Bright Ideas for Chemical Biology". In: *ACS Chemical Biology* 3.3, pp. 142–155. DOI: 10.1021/cb700248m.

Lazzari, Gianpiero, Patrick Couvreur, and Simona Mura (2017). "Multicellular tumor spheroids: a relevant 3D model for the in vitro preclinical investigation of polymer nanomedicines". In: *Polymer Chemistry* 8.34, pp. 4947–4969. DOI: 10.1039/c7py00559h.

Lee, Eun Seong, Zhonggao Gao, and You Han Bae (Dec. 2008). "Recent progress in tumor pH targeting nanotechnology." In: *Journal of controlled release : official journal of the Controlled Release Society* 132 (3), pp. 164–170. ISSN: 1873-4995. DOI: 10.1016/j.jconrel.2008.05.003. ppublish.

Lee, Sang Y. (2016). "Temozolomide resistance in glioblastoma multiforme". In: *Genes &amp Diseases* 3.3, pp. 198–210. DOI: 10.1016/j.gendis.2016.04.007.

Lei, Hao, Kamil Ugurbil, and Wei Chen (2003). "Measurement of unidirectional P subi/sub to ATP flux in human visual cortex at 7 T by using iin vivo/i sup31/sup P magnetic resonance spectroscopy". In: *Proceedings of the National Academy of Sciences* 100.24, pp. 14409–14414. DOI: 10.1073/pnas.2332656100.

Lei, Hao et al. (2003). "In vivo31P magnetic resonance spectroscopy of human brain at 7 T: An initial experience". In: *Magnetic Resonance in Medicine* 49.2, pp. 199–205. DOI: 10.1002/mrm.10379.

Lenting, Krissie et al. (2017). "Glioma: experimental models and reality". In: *Acta Neuropathologica* 133.2, pp. 263–282. DOI: 10.1007/s00401-017-1671-4.

Levine, S. A. et al. (1993). "Kinetics and regulation of three cloned mammalian Na+/H+ exchangers stably expressed in a fibroblast cell line." In: 268, pp. 25527–25535. ISSN: 0021-9258. DOI: 10.1016/s0021-9258(19)74423-8.

Leyval, Damien et al. (1997). "Flow cytometry for the intracellular pH measurement of glutamate producing Corynebacterium glutamicum". In: *Journal of Microbiological Methods* 29.2, pp. 121–127. DOI: 10.1016/s0167-7012(97)00031-6.

Li, Houshen et al. (2013). "Simple Synthesis of Monodisperse, Quasi-spherical, Citrate-Stabilized Silver Nanocrystals in Water". In: *Langmuir* 29.16, pp. 5074–5079. DOI: 10.1021/la400214x.

Li, Shan-Shan et al. (2019). "Monitoring the Changes of pH in Lysosomes during Autophagy and Apoptosis by Plasmon Enhanced Raman Imaging". In: *Analytical Chemistry* 91.13, pp. 8398–8405. DOI: 10.1021/acs.analchem.9b01250.

Li, Ying et al. (2009). "Expression and Activity of Carbonic Anhydrase IX Is Associated With Metabolic Dysfunction in MDA-MB-231 Breast Cancer Cells". In: *Cancer Investigation* 27.6, pp. 613–623. DOI: 10.1080/07357900802653464.

Lichtman, Jeff W and José-Angel Conchello (2005). "Fluorescence microscopy". In: *Nature Methods* 2.12, pp. 910–919. DOI: 10.1038/nmeth817.

Liu, Jing et al. (2020). "Intracellular Labeling with Extrinsic Probes: Delivery Strategies and Applications". In: *Small* 16.22, p. 2000146. DOI: 10.1002/smll.202000146.

Liu, Jixiang, Zhenjun Diwu, and Wai-Yee Leung (2001). "Synthesis and photophysical properties of new fluorinated benzo[c]xanthene dyes as intracellular pH indicators". In: *Bioorganic &amp Medicinal Chemistry Letters* 11.22, pp. 2903–2905. DOI: 10.1016/s0960-894x(01)00595-9.

Llaguno, Sheila Alcantara et al. (2009). "Malignant Astrocytomas Originate from Neural Stem/Progenitor Cells in a Somatic Tumor Suppressor Mouse Model". In: *Cancer Cell* 15.1, pp. 45–56. DOI: 10.1016/j.ccr.2008.12.006.

Loiselle, Frederick B. and Joseph R. Casey (2010). "Measurement of Intracellular pH". In: *Methods in Molecular Biology*. Humana Press, pp. 311–331. DOI: 10.1007/978-1-60761-700-6_17.

Loizzi, Vera et al. (2017). "Biological Pathways Involved in Tumor Angiogenesis and Bevacizumab Based Anti-Angiogenic Therapy with Special References to Ovarian Cancer". In: *International Journal of Molecular Sciences* 18.9, p. 1967. DOI: 10.3390/ijms18091967.

Louis, David N. et al. (2007). "The 2007 WHO Classification of Tumours of the Central Nervous System". In: 114, pp. 97–109. ISSN: 0001-6322. DOI: 10.1007/s00401-007-0243-4.

Lunt, Sophia Y. and Matthew G. Vander Heiden (2011). "Aerobic Glycolysis: Meeting the Metabolic Requirements of Cell Proliferation". In: *Annual Review of Cell and Developmental Biology* 27.1, pp. 441–464. DOI: 10.1146/annurev-cellbio-092910-154237.

Ly, A. (2014). "Ondes électromagnétiques, risques et cancers". In: *Journal Africain du Cancer / African Journal of Cancer* 6.4, pp. 189–193. DOI: 10.1007/s12558-014-0350-9.

Madshus, I H (1988). "Regulation of intracellular pH in eukaryotic cells". In: *Biochemical Journal* 250.1, pp. 1–8. DOI: 10.1042/bj2500001.

Magg, T and Michael Albert (Nov. 2007). "Tracking cell proliferation using the far red fluorescent dye SNARF-1". In: *Cytometry. Part B, Clinical cytometry* 72, pp. 458–64. DOI: 10.1002/cyto.b.20180.

Mahoney, Brent P. et al. (2003). "Tumor acidity, ion trapping and chemotherapeutics". In: *Biochemical Pharmacology* 66.7, pp. 1207–1218. DOI: 10.1016/s0006-2952(03)00467-2.

Makutonina, A et al. (1996). "Human immunodeficiency virus infection of T-lymphoblastoid cells reduces intracellular pH". In: *Journal of Virology* 70.10, pp. 7049–7055. DOI: 10.1128/jvi.70.10.7049-7055.1996.

Man, Cheuk Him et al. (2022). "Proton export alkalinizes intracellular pH and reprograms carbon metabolism to drive normal and malignant cell growth". In: *Blood* 139.4, pp. 502–522. DOI: 10.1182/blood.2021011563.

Marie-Egyptienne, Delphine Tamara et al. (2016). "Cancer initiating-cells are enriched in the CA9 positive fraction of primary cervix cancer xenografts". In: *Oncotarget* 8.1, pp. 1392–1404. DOI: 10.18632/oncotarget.13625.

Martinez-Zaguilan, R. et al. (1993). "Vacuolar-type H(+)-ATPases are functionally expressed in plasma membranes of human tumor cells". In: 265, pp. C1015–C1029. ISSN: 0363-6143. DOI: 10.1152/ajpcell.1993.265.4.c1015.

Martinez-Zaguilan Raul ; Gillies, Robert J. (1992). "A Plasma Membrane V-type H+-ATPase May Contribute to Elevated Intracellular pH (pHin)in Some Human Tumor Cells". In: 671, pp. 478–480. ISSN: 0077-8923. DOI: 10.1111/j.1749-6632.1992.tb43834.x.

Martínez-Zaguilán, R. et al. (Mar. 1996). "Acidic pH enhances the invasive behavior of human melanoma cells." In: *Clinical experimental metastasis* 14 (2), pp. 176–186. ISSN: 0262-0898. DOI: 10.1007/BF00121214. ppublish.

Martínez-Zaguilán, Raul et al. (1998). "Distinct regulation of pHin and [Ca2+]in in human melanoma cells with different metastatic potential". In: 176, pp. 196–205. ISSN: 0021-9541. DOI: 10.1002/(sici)1097-4652(199807)176:1<196::aid-jcp21>3.0.co;2-4.

Masereel, B (2003). "An overview of inhibitors of Na/H exchanger". In: *European Journal of Medicinal Chemistry* 38.6, pp. 547–554. DOI: 10.1016/s0223-5234(03)00100-4.

Mathews, Marlon S. et al. (2012). "Photochemical internalization of bleomycin for glioma treatment". In: *Journal of Biomedical Optics* 17.5, p. 058001. DOI: 10.1117/1.jbo.17.5.058001.

Mazzio, Elizabeth A. et al. (2012). "Pericellular pH homeostasis is a primary function of the Warburg effect: Inversion of metabolic systems to control lactate steady state in tumor cells". In: *Cancer Science* 103.3, pp. 422–432. DOI: 10.1111/j.1349-7006.2012.02206.x.

Mccarty, Mark F. and Julian Whitaker (2010). "Manipulating tumor acidification as a cancer treatment strategy." In: *Alternative medicine review : a journal of clinical therapeutic* 15 3, pp. 264–72.

McDonald, Paul C. and Shoukat Dedhar (2014). *Carbonic Anhydrase IX (CAIX) as a Mediator of Hypoxia-Induced Stress Response in Cancer Cells*. DOI: 10.1007/978-94-007-7359-2_13.

Meldrum, N. U. and F. J. W. Roughton (1933). "Carbonic anhydrase. Its preparation and properties". In: *The Journal of Physiology* 80.2, pp. 113–142. DOI: 10.1113/jphysiol.1933.sp003077.

Mellor, Howard R. and Richard Callaghan (2011). "Accumulation and distribution of doxorubicin in tumour spheroids: the influence of acidity and expression of P-glycoprotein". In: *Cancer Chemotherapy and Pharmacology* 68.5, pp. 1179–1190. DOI: 10.1007/s00280-011-1598-8.

Merchant, Fatima A. et al. (2005). "Confocal Microscopy". In: *Handbook of Image and Video Processing*. Elsevier, pp. 1291–XLI. DOI: 10.1016/b978-012119792-6/50135-2.

Mesrati, Malak Hassn et al. (2020). "Understanding Glioblastoma Biomarkers: Knocking a Mountain with a Hammer". In: *Cells* 9.5, p. 1236. DOI: 10.3390/cells9051236.

Messaoudi, Khaled, Anne Clavreul, and Frédéric Lagarce (2015). "Toward an effective strategy in glioblastoma treatment. Part I: resistance mechanisms and strategies to overcome resistance of glioblastoma to temozolomide". In: *Drug Discovery Today* 20.7, pp. 899–905. DOI: 10.1016/j.drudis.2015.02.011.

Milito, Angelo De et al. (2009). "pH-dependent antitumor activity of proton pump inhibitors against human melanoma is mediated by inhibition of tumor acidity". In: *International Journal of Cancer* 127.1, pp. 207–219. DOI: 10.1002/ijc.25009.

Minta, A, J P Y Kao, and R Y Tsien (1989). "Fluorescent indicators for cytosolic calcium based on rhodamine and fluorescein chromophores". In: *Journal of Biological Chemistry* 264.14, pp. 8171–8178. DOI: 10.1016/s0021-9258(18)83165-9.

Miraglia, Erica et al. (2005). "Na/H exchanger activity is increased in doxorubicin-resistant human colon cancer cells and its modulation modifies the sensitivity of the cells to doxorubicin". In: *International Journal of Cancer* 115.6, pp. 924–929. DOI: 10.1002/ijc.20959.

Mirrett, Stanley (1982). "Acridine Orange Stain". In: *Infection Control* 3.3, pp. 250–253. DOI: 10.1017/s0195941700056198.

Moellering, Raymond E. et al. (2008). "Acid treatment of melanoma cells selects for invasive phenotypes". In: *Clinical &amp Experimental Metastasis* 25.4, pp. 411–425. DOI: 10.1007/s10585-008-9145-7.

Mojas, Nina, Massimo Lopes, and Josef Jiricny (2007). "Mismatch repair-dependent processing of methylation damage gives rise to persistent single-stranded gaps in newly replicated DNA". In: *Genes &amp Development* 21.24, pp. 3342–3355. DOI: 10.1101/gad.455407.

Molenaar, Douwe, Tjakko Abee, and Wil N. Konings (1991). "Continuous measurement of the cytoplasmic pH in Lactococcus lactis with a fluorescent pH indicator". In: *Biochimica et Biophysica Acta (BBA) - General Subjects* 1115.1, pp. 75–83. DOI: 10.1016/0304-4165(91)90014-8.

Montcourrier, Philippe et al. (1997). In: *Clinical and Experimental Metastasis* 15.4, pp. 382–392. DOI: 10.1023/a:1018446104071.

Moon, Richard B. and John H. Richards (1973). "Determination of Intracellular pH by 31P Magnetic Resonance". In: 248, pp. 7276–7278. ISSN: 0021-9258. DOI: 10.1016/s0021-9258(19)43389-9.

Moore, Richard D. (1983). "Effects of insulin upon ion transport". In: *Biochimica et Biophysica Acta (BBA) - Reviews on Biomembranes* 737.1, pp. 1–49. DOI: 10.1016/0304-4157(83)90013-8.

Morita, T. et al. (1992). "Clastogenicity of low pH to various cultured mammalian cells". In: 268, pp. 297–305. ISSN: 0027-5107. DOI: 10.1016/0027-5107(92)90235-t.

Murakami, Tadashi et al. (2001). "Elevated expression of vacuolar proton pump genes and cellular ph in cisplatin resistance". In: *International Journal of Cancer* 93.6, pp. 869–874. DOI: 10.1002/ijc.1418.

Murphy, Kaitlin C. et al. (2017). "Measurement of oxygen tension within mesenchymal stem cell spheroids". In: *Journal of The Royal Society Interface* 14.127, p. 20160851. DOI: 10.1098/rsif.2016.0851.

Nagai, Takeharu et al. (2002). "A variant of yellow fluorescent protein with fast and efficient maturation for cell-biological applications". In: *Nature Biotechnology* 20.1, pp. 87–90. DOI: 10.1038/nbt0102-87.

Neri, Dario and Claudiu T. Supuran (2011). "Interfering with pH regulation in tumours as a therapeutic strategy". In: 10, pp. 767–777. ISSN: 1474-1776. DOI: 10.1038/nrd3554.

Nett, W. and J.W. Deitmer (1996). "Simultaneous measurements of intracellular pH in the leech giant glial cell using 2',7'-bis-(2-carboxyethyl)-5,6-carboxyfluorescein and ion-sensitive microelectrodes". In: *Biophysical Journal* 71.1, pp. 394–402. DOI: 10.1016/s0006-3495(96)79240-8.

Nguyen, Annalee W and Patrick S Daugherty (2005). "Evolutionary optimization of fluorescent proteins for intracellular FRET". In: *Nature Biotechnology* 23.3, pp. 355–360. DOI: 10.1038/nbt1066.

Nordfors, Kristiina et al. (2010). "The tumour-associated carbonic anhydrases CA II, CA IX and CA XII in a group of medulloblastomas and supratentorial primitive neuroectodermal tumours: an association of CA IX with poor prognosis". In: *BMC Cancer* 10.1. DOI: 10.1186/1471-2407-10-148.

Ohkuma, S and B Poole (1978). "Fluorescence probe measurement of the intralysosomal pH in living cells and the perturbation of pH by various agents." In: *Proceedings of the National Academy of Sciences* 75.7, pp. 3327–3331. DOI: 10.1073/pnas.75.7.3327.

Ohtsubo, T. et al. (Sept. 1997). "p53-dependent induction of WAF1 by a low-pH culture condition in human glioblastoma cells." In: *Cancer research* 57 (18), pp. 3910–3913. ISSN: 0008-5472. ppublish.

Onuigbo, WI (1975). "Human model for studying seed-soil factors in blood-borne metastasis". In: *Archives of pathology* 99.6, 342—343. ISSN: 0363-0153. URL: http://europepmc.org/abstract/MED/167699.

Oraiopoulou, M.-E. et al. (2017). "iIn Vitro/In Silico/i Study on the Role of Doubling Time Heterogeneity among Primary Glioblastoma Cell Lines". In: *BioMed Research International* 2017, pp. 1–12. DOI: 10.1155/2017/8569328.

Ormö, Mats et al. (1996). "Crystal Structure of the b iAequorea victoria/i /b Green Fluorescent Protein". In: *Science* 273.5280, pp. 1392–1395. DOI: 10.1126/science.273.5280.1392.

Ostrom, Q. T. et al. (2014). "CBTRUS Statistical Report: Primary Brain and Central Nervous System Tumors Diagnosed in the United States in 2007-2011". In: 16, pp. iv1–iv63. ISSN: 1522-8517. DOI: 10.1093/neuonc/nou223.

Owen, Charles S. (1992). "Comparison of spectrum-shifting intracellular pH probes 5′(and 6′)-carboxy-10-dimethylamino-3-hydroxyspiro[7H-benzo[c]xanthene-7, 1′(3′H)-isobenzofuran]-3′-one and 2′,7′-biscarboxyethyl-5(and 6)-carboxyfluorescein". In: *Analytical Biochemistry* 204.1, pp. 65–71. DOI: 10.1016/0003-2697(92)90140-3.

Oxtoby, David W., H. Pat Gillis, and Laurie J. Butler (2015). *Principles of modern chemistry*. [Andover] : Brooks/Cole Cengage Learning, 2015. ISBN: 9781305079113.

Padan, Etana, Dan Zilberstein, and Shimon Schuldiner (1981). "pH homesstasis in bacteria". In: *Biochimica et Biophysica Acta (BBA) - Reviews on Biomembranes* 650.2-3, pp. 151–166. DOI: 10.1016/0304-4157(81)90004-6.

Paget, Stephen (1889). "THE DISTRIBUTION OF SECONDARY GROWTHS IN CANCER OF THE BREAST." In: *The Lancet* 133.3421, pp. 571–573. DOI: 10.1016/s0140-6736(00)49915-0.

Pampaloni, Francesco, Emmanuel G. Reynaud, and Ernst H. K. Stelzer (2007). "The third dimension bridges the gap between cell culture and live tissue". In: *Nature Reviews Molecular Cell Biology* 8.10, pp. 839–845. DOI: 10.1038/nrm2236.

Pan, Peiwen et al. (2006). "Carbonic anhydrase gene expression in CA II-deficient (iCar2sup-/-/sup/i) and CA IX-deficient (iCar9sup-/-/sup/i) mice". In: *The Journal of Physiology* 571.2, pp. 319–327. DOI: 10.1113/jphysiol.2005.102590.

Parkkila, Anna-Kaisa et al. (1995). "Immunohistochemical demonstration of human carbonic anhydrase isoenzyme II in brain tumours". In: 27, pp. 974–982. ISSN: 0018-2214. DOI: 10.1007/bf02389687.

Parkkila, Seppo et al. (2010). "Carbonic anhydrase II. A novel biomarker for gastrointestinal stromal tumors". In: *Modern Pathology* 23.5, pp. 743–750. DOI: 10.1038/modpathol.2009.189.

Parks, Scott K., Johanna Chiche, and Jacques Pouyssegur (2010). "pH control mechanisms of tumor survival and growth". In: *Journal of Cellular Physiology* 226.2, pp. 299–308. DOI: 10.1002/jcp.22400.

Parks, Scott K., Johanna Chiche, and Jacques Pouysségur (2013). "Disrupting proton dynamics and energy metabolism for cancer therapy". In: 13, pp. 611–623. ISSN: 1474-175X. DOI: 10.1038/nrc3579.

Parks, Scott K., Yann Cormerais, and Jacques Pouysségur (2017). "Hypoxia and cellular metabolism in tumour pathophysiology". In: *The Journal of Physiology* 595.8, pp. 2439–2450. DOI: 10.1113/jp273309.

Parks, Scott K. et al. (2013). "Hypoxia promotes tumor cell survival in acidic conditions by preserving ATP levels". In: *Journal of Cellular Physiology* 228.9, pp. 1854–1862. DOI: 10.1002/jcp.24346.

Pastorekova, Silvia et al. (2004). "Review Article". In: *Journal of Enzyme Inhibition and Medicinal Chemistry* 19.3, pp. 199–229. DOI: 10.1080/14756360410001689540.

Patil, Rameshwar et al. (2010). "Temozolomide Delivery to Tumor Cells by a Multifunctional Nano Vehicle Based on Poly(β-L-malic acid)". In: *Pharmaceutical Research* 27.11, pp. 2317–2329. DOI: 10.1007/s11095-010-0091-0.

Pérez-Herrero, Edgar and Alberto Fernández-Medarde (2021). "The reversed intra- and extracellular pH in tumors as a unified strategy to chemotherapeutic delivery using targeted nanocarriers". In: *Acta Pharmaceutica Sinica B* 11.8, pp. 2243–2264. DOI: 10.1016/j.apsb.2021.01.012.

Piao, Shengfu and Ravi K. Amaravadi (2015). "Targeting the lysosome in cancer". In: *Annals of the New York Academy of Sciences* 1371.1, pp. 45–54. DOI: 10.1111/nyas.12953.

Piasentin, Nicola, Edoardo Milotti, and Roberto Chignola (2020). "The control of acidity in tumor cells: a biophysical model". In: *Scientific Reports* 10.1. DOI: 10.1038/s41598-020-70396-1.

Pillai, Smitha R. et al. (2019). "Causes, consequences, and therapy of tumors acidosis". In: *Cancer and Metastasis Reviews* 38.1-2, pp. 205–222. DOI: 10.1007/s10555-019-09792-7.

Ponte-Sucre, Alicia (2007). "Availability and applications of ATP-binding cassette (ABC) transporter blockers". In: *Applied Microbiology and Biotechnology* 76.2, pp. 279–286. DOI: 10.1007/s00253-007-1017-6.

Pontén, Jan and Elizabeth H. Macintyre (1968). "Long term culture of normal and neoplastic human glia". In: *Acta Pathologica Microbiologica Scandinavica* 74.4, pp. 465–486. DOI: 10.1111/j.1699-0463.1968.tb03502.x.

Pouysségur, J et al. (1982). "Growth factor activation of an amiloride-sensitive Na/H exchange system in quiescent fibroblasts: coupling to ribosomal protein S6 phosphorylation." In: *Proceedings of the National Academy of Sciences* 79.13, pp. 3935–3939. DOI: 10.1073/pnas.79.13.3935.

Pouysségur, Jacques, Frédéric Dayan, and Nathalie M. Mazure (2006). "Hypoxia signalling in cancer and approaches to enforce tumour regression". In: *Nature* 441.7092, pp. 437–443. DOI: 10.1038/nature04871.

Pressman, Berton and Norberto deGuzman (Feb. 1977). "Biological Applications and Evolutionary Origins of Ionophores". In: *Advances in experimental medicine and biology* 84, pp. 285–300. DOI: 10.1007/978-1-4684-3279-4_14.

Putney, Luanna K. and Diane L. Barber (2003). "Na-H Exchange-dependent Increase in Intracellular pH Times G2/M Entry and Transition". In: 278, pp. 44645–44649. ISSN: 0021-9258. DOI: 10.1074/jbc.m308099200.

Ranganathan, Rama, Mark A. Wall, and Michael Socolich (2000). In: *Nature Structural Biology* 7.12, pp. 1133–1138. DOI: 10.1038/81992.

Rao, Min et al. (2001). "Intracellular pH regulation by Mycobacterium smegmatis and Mycobacterium bovis BCG". In: *Microbiology* 147.4, pp. 1017–1024. DOI: 10.1099/00221287-147-4-1017.

Rattigan, Yanique I. et al. (2012). "Lactate is a mediator of metabolic cooperation between stromal carcinoma associated fibroblasts and glycolytic tumor cells in the tumor microenvironment". In: *Experimental Cell Research* 318.4, pp. 326–335. DOI: 10.1016/j.yexcr.2011.11.014.

Razungles, Julie et al. (2013). "L'effet Warburg. De la théorie du cancer aux applications thérapeutiques en cancérologie". In: 29, pp. 1026–1033. ISSN: 0767-0974. DOI: 10.1051/medsci/20132911020.

Rebillard, Ame

lie et al. (2007). "Cisplatin-Induced Apoptosis Involves Membrane Fluidification via Inhibition of NHE1 in Human Colon Cancer Cells". In: *Cancer Research* 67.16, pp. 7865–7874. DOI: 10.1158/0008-5472.can-07-0353.

Reshkin, Stephan et al. (July 2003). "Paclitaxel induces apoptosis via protein kinase A- and p38 mitogen-activated protein-dependent inhibition of the Na+/H+ exchanger (NHE) NHE isoform 1 in human breast cancer cells". In: *Clinical cancer research : an official journal of the American Association for Cancer Research* 9, pp. 2366–73.

Rhoades, Rodney (2013). *Medical physiology principles for clinical medicine. principles for clinical medicine*. Wolters Kluwer Health/Lippincott Williams Wilkins. ISBN: 9781609134273.

Rink, T J, R Y Tsien, and T Pozzan (1982). "Cytoplasmic pH and free Mg2 in lymphocytes." In: *Journal of Cell Biology* 95.1, pp. 189–196. DOI: 10.1083/jcb.95.1.189.

Rino, Jose et al. (2009). "Frontiers in fluorescence microscopy". In: *The International Journal of Developmental Biology* 53.8-9-10, pp. 1569–1579. DOI: 10.1387/ijdb.072351jr.

Rivarola, Valeria et al. (2005). "Functional and Molecular Adaptation of Cl&ltsup&gt-&lt/sup&gt/HCO&ltsub&gt3&lt/sub&gt&ltsup&gt-&lt/sup&gt Exchanger to Chronic Alkaline Media in RenalCells". In: *Cellular Physiology and Biochemistry* 16.4-6, pp. 271–280. DOI: 10.1159/000089853.

Robey, Ian F. and Lance A. Nesbit (2013). "Investigating Mechanisms of Alkalinization for Reducing Primary Breast Tumor Invasion". In: *BioMed Research International* 2013, pp. 1–10. DOI: 10.1155/2013/485196.

Roos, A and W F Boron (1981). "Intracellular pH." In: *Physiological Reviews* 61.2, pp. 296–434. DOI: 10.1152/physrev.1981.61.2.296.

Roos, D. and J.A. Loos (1973). "Changes in the carbohydrate metabolism of mitogenically stimulated human peripheral lymphocytes". In: *Experimental Cell Research* 77.1-2, pp. 127–135. DOI: 10.1016/0014-4827(73)90561-2.

Roper, Sophie J. et al. (2021). "3D spheroid models of paediatric SHH medulloblastoma mimic tumour biology, drug response and metastatic dissemination". In: *Scientific Reports* 11.1. DOI: 10.1038/s41598-021-83809-6.

Rotin, Daniela et al. (1987). "Cytotoxicity of compounds that interfere with the regulation of intracellular pH: a potential new class of anticancer drugs." In: *Cancer research* 47 6, pp. 1497–504.

Rozhin, Jurij et al. (1994). "Pericellular pH affects distribution and secretion of cathepsin B in malignant cells." In: *Cancer research* 54 24, pp. 6517–25.

Sadava, David E. et al. (2014). *Life The Science of Biology. The Science of Biology*. W. H. Freeman, p. 1267. ISBN: 9781429298643.

Salhany, J (1979). "31P nuclear magnetic resonance measurement of cardiac pH in perfused guinea-pig hearts". In: *Journal of Molecular and Cellular Cardiology* 11.6, pp. 601–610. DOI: 10.1016/0022-2828(79)90434-6.

Salvati, Maurizio et al. (2020). "Glioblastoma: Molecular profile and immunophenotypic analysis as prognostic tools for tailored therapy and decision making in a recent surgical series". In: *Interdisciplinary Neurosurgery* 20, p. 100697. DOI: 10.1016/j.inat.2020.100697.

Salvi, Aline, J. Mark Quillan, and Wolfgang Sadée (2002). "Monitoring intracellular pH changes in response to osmotic stress and membrane transport activity using 5-chloromethylfluorescein". In: *AAPS PharmSci* 4.4, pp. 21–28. DOI: 10.1208/ps040421.

Schroeder, Marie A. et al. (2009). "Measuring intracellular pH in the heart using hyperpolarized carbon dioxide and bicarbonate: a 13C and 31P magnetic resonance spectroscopy study". In: *Cardiovascular Research* 86.1, pp. 82–91. DOI: 10.1093/cvr/cvp396.

Seksek, O. and J. Bolard (1996). "Nuclear pH gradient in mammalian cells revealed by laser microspectrofluorimetry". In: *Journal of Cell Science* 109.1, pp. 257–262. DOI: 10.1242/jcs.109.1.257.

Seksek, Olivier et al. (1991). "SNARF-1 as an intracellular pH indicator in laser microspectrofluorometry: A critical assessment". In: *Analytical Biochemistry* 193.1, pp. 49–54. DOI: 10.1016/0003-2697(91)90042-r.

Sennoune, Souad R. et al. (2004). "Vacuolar Hsup/sup-ATPase in human breast cancer cells with distinct metastatic potential: distribution and functional activity". In: *American Journal of Physiology-Cell Physiology* 286.6, pp. C1443–C1452. DOI: 10.1152/ajpcell.00407.2003.

Serres, Sébastien, Emma R. O'Brien, and Nicola R. Sibson (2014). *Imaging Angiogenesis, Inflammation, and Metastasis in the Tumor Microenvironment with Magnetic Resonance Imaging*. DOI: 10.1007/978-1-4614-5915-6_12.

Shackleton, Mark et al. (2009). "Heterogeneity in Cancer: Cancer Stem Cells versus Clonal Evolution". In: *Cell* 138.5, pp. 822–829. DOI: 10.1016/j.cell.2009.08.017.

Shaner, Nathan C et al. (2004). "Improved monomeric red, orange and yellow fluorescent proteins derived from Discosoma sp. red fluorescent protein". In: *Nature Biotechnology* 22.12, pp. 1567–1572. DOI: 10.1038/nbt1037.

Sharma, Mohit et al. (2015). "pH Gradient Reversal: An Emerging Hallmark of Cancers". In: *Recent Patents on Anti-Cancer Drug Discovery* 10.3, pp. 244–258. DOI: 10.2174/1574892810666150708110608.

Shieh, Peyton and Carolyn R. Bertozzi (2014). "Design strategies for bioorthogonal smart probes". In: *Org. Biomol. Chem.* 12.46, pp. 9307–9320. DOI: 10.1039/c4ob01632g.

Shimomura, Osamu, Frank H. Johnson, and Yo Saiga (1962). "Extraction, Purification and Properties of Aequorin, a Bioluminescent Protein from the Luminous Hydromedusan,Aequorea". In: *Journal of Cellular and Comparative Physiology* 59.3, pp. 223–239. DOI: 10.1002/jcp.1030590302.

Shirmanova, Marina V. et al. (2015). "Intracellular pH imaging in cancer cells in vitro and tumors in vivo using the new genetically encoded sensor SypHer2". In: *Biochimica et Biophysica Acta (BBA) - General Subjects* 1850.9, pp. 1905–1911. DOI: 10.1016/j.bbagen.2015.05.001.

Singh, Neha et al. (2020). "Mechanisms of temozolomide resistance in glioblastoma - a comprehensive review". In: *Cancer Drug Resistance*. DOI: 10.20517/cdr.2020.79.

Skarsgard, L. D. et al. (1995). "The cytotoxicity of melphalan and its relationship to pH, hypoxia and drug uptake." In: *Anticancer research* 15 (1), pp. 219–223. ISSN: 0250-7005. ppublish.

Slyusareva, E. A. et al. (2011). "Spectral and fluorescent indication of the acid-base properties of biopolymer solutions". In: *Russian Physics Journal* 54.4, pp. 485–492. DOI: 10.1007/s11182-011-9643-y.

Smallbone, Kieran, Philip K. Maini, and Robert A. Gatenby (2010). "Episodic, transient systemic acidosis delays evolution of the malignant phenotype: Possible mechanism for cancer prevention by increased physical activity". In: 5, p. 22. ISSN: 1745-6150. DOI: 10.1186/1745-6150-5-22.

Smallbone, Kieran et al. (2005). "The role of acidity in solid tumour growth and invasion". In: *Journal of Theoretical Biology* 235.4, pp. 476–484. DOI: 10.1016/j.jtbi.2005.02.001.

Sodek, Katharine L., Maurice J. Ringuette, and Theodore J. Brown (2009). "Compact spheroid formation by ovarian cancer cells is associated with contractile behavior and an invasive phenotype". In: *International Journal of Cancer* 124.9, pp. 2060–2070. DOI: 10.1002/ijc.24188.

Song, Shuangshuang et al. (2014). "Multifunctional Tumor-Targeting Nanocarriers Based on Hyaluronic Acid-Mediated and pH-Sensitive Properties for Efficient Delivery of Docetaxel". In: 31, pp. 1032–1045. ISSN: 0724-8741. DOI: 10.1007/s11095-013-1225-y.

Sonveaux, Pierre et al. (2008). "Targeting lactate-fueled respiration selectively kills hypoxic tumor cells in mice". In: *Journal of Clinical Investigation*. DOI: 10.1172/jci36843.

Spugnini, Enrico P, Gennaro Citro, and Stefano Fais (2010). "Proton pump inhibitors as anti vacuolar-ATPases drugs: a novel anticancer strategy". In: *Journal of Experimental &amp Clinical Cancer Research* 29.1. DOI: 10.1186/1756-9966-29-44.

Steyern, F Vult von, J O Josefsson, and S Tågerud (1996). "Rhodamine B, a fluorescent probe for acidic organelles in denervated skeletal muscle." In: *Journal of Histochemistry &amp Cytochemistry* 44.3, pp. 267–274. DOI: 10.1177/44.3.8648087.

Stock, Christian and Albrecht Schwab (2009). "Protons make tumor cells move like clockwork". In: *Pflügers Archiv - European Journal of Physiology* 458.5, pp. 981–992. DOI: 10.1007/s00424-009-0677-8.

Stokes, George (1853). "XVI. On the change of refrangibility of light.—No. II". In: *Philosophical Transactions of the Royal Society of London* 143, pp. 385–396. DOI: 10.1098/rstl.1853.0016.

Stéphanou, Angélique and Annabelle Ballesta (2019). "pH as a potential therapeutic target to improve temozolomide antitumor efficacy : A mechanistic modeling study". In: 7, e00454. ISSN: 2052-1707. DOI: 10.1002/prp2.454.

Stringer, Carsen et al. (2020). "Cellpose: a generalist algorithm for cellular segmentation". In: *Nature Methods* 18.1, pp. 100–106. DOI: 10.1038/s41592-020-01018-x.

Strobel, Hannah et al. (2019). "Temozolomide and Other Alkylating Agents in Glioblastoma Therapy". In: *Biomedicines* 7.3, p. 69. DOI: 10.3390/biomedicines7030069.

Strong, Leonell C. (1950). "GENETICS AND CANCER". In: *Scientific American* 183.1, pp. 44–47. ISSN: 00368733, 19467087. URL: http://www.jstor.org/stable/24967496 (visited on 09/05/2022).

Stupp, Roger et al. (2005). "Radiotherapy plus Concomitant and Adjuvant Temozolomide for Glioblastoma". In: *New England Journal of Medicine* 352.10, pp. 987–996. DOI: 10.1056/nejmoa043330.

Stupp, Roger et al. (2009). "Effects of radiotherapy with concomitant and adjuvant temozolomide versus radiotherapy alone on survival in glioblastoma in a randomised phase III study: 5-year analysis of the EORTC-NCIC trial". In: *The Lancet Oncology* 10.5, pp. 459–466. DOI: 10.1016/s1470-2045(09)70025-7.

Supuran, Claudiu T. et al. (2010). "Recent Advances in Structural Studies of the Carbonic Anhydrase Family: The Crystal Structure of Human CA IX and CA XIII". In: *Current Pharmaceutical Design* 16.29, pp. 3246–3254. DOI: 10.2174/138161210793429841.

Sutherland, Robert M. (1988). "Cell and Environment Interactions in Tumor Microregions: The Multicell Spheroid Model". In: *Science* 240.4849, pp. 177–184. DOI: 10.1126/science.2451290.

Švastová, Eliška et al. (2004). "Hypoxia activates the capacity of tumor-associated carbonic anhydrase IX to acidify extracellular pH". In: *FEBS Letters* 577.3, pp. 439–445. DOI: 10.1016/j.febslet.2004.10.043.

Swietach, Pawel, Richard D. Vaughan-Jones, and Adrian L. Harris (2007). "Regulation of tumor pH and the role of carbonic anhydrase 9". In: *Cancer and Metastasis Reviews* 26.2, pp. 299–310. DOI: 10.1007/s10555-007-9064-0.

Swietach, Pawel et al. (2008). "Tumor-associated Carbonic Anhydrase 9 Spatially Coordinates Intracellular pH in Three-dimensional Multicellular Growths". In: *Journal of Biological Chemistry* 283.29, pp. 20473–20483. DOI: 10.1074/jbc.m801330200.

Swietach, Pawel et al. (2009). "The Role of Carbonic Anhydrase 9 in Regulating Extracellular and Intracellular pH in Three-dimensional Tumor Cell Growths". In: *Journal of Biological Chemistry* 284.30, pp. 20299–20310. DOI: 10.1074/jbc.m109.006478.

Swietach, Pawel et al. (2014). "The chemistry, physiology and pathology of pH in cancer". In: *Philosophical Transactions of the Royal Society B: Biological Sciences* 369.1638, p. 20130099. DOI: 10.1098/rstb.2013.0099.

Swinson, Daniel E. B. et al. (2003). "Carbonic Anhydrase IX Expression, a Novel Surrogate Marker of Tumor Hypoxia, Is Associated With a Poor Prognosis in Non–Small-Cell Lung Cancer". In: 21, pp. 473–482. ISSN: 0732-183X. DOI: 10.1200/jco.2003.11.132.

Tan, E Y et al. (2009). "The key hypoxia regulated gene CAIX is upregulated in basal-like breast tumours and is associated with resistance to chemotherapy". In: *British Journal of Cancer* 100.2, pp. 405–411. DOI: 10.1038/sj.bjc.6604844.

Tang, Tao et al. (2020). "The role of lysosomes in cancer development and progression". In: *Cell &amp Bioscience* 10.1. DOI: 10.1186/s13578-020-00489-x.

Tannen, R. L. (1978). "Ammonia metabolism". In: *American Journal of Physiology-Renal Physiology* 235.4, F265–F277. DOI: 10.1152/ajprenal.1978.235.4.f265.

Tannock, Ian F. and Daniela Rotin (1989). "Acid pH in tumors and its potential for therapeutic exploitation." In: *Cancer research* 49 16, pp. 4373–84.

Tarling, Elizabeth J., Thomas Q. de Aguiar Vallim, and Peter A. Edwards (2013). "Role of ABC transporters in lipid transport and human disease". In: *Trends in Endocrinology &amp Metabolism* 24.7, pp. 342–350. DOI: 10.1016/j.tem.2013.01.006.

Tentori, Lucio and Grazia Graziani (2002). "Pharmacological Strategies to Increase the Anti-tumor Activity of Methylating Agents". In: *Current Medicinal Chemistry* 9.13, pp. 1285–1301. DOI: 10.2174/0929867023369916.

Thews, Oliver et al. (2006). "Impact of Extracellular Acidity on the Activity of P-glycoprotein and the Cytotoxicity of Chemotherapeutic Drugs". In: *Neoplasia* 8.2, pp. 143–152. DOI: 10.1593/neo.05697.

Thews, Oliver et al. (2014). "Impact of Hypoxia-Related Tumor Acidosis on Cytotoxicity of Different Chemotherapeutic Drugs In Vitro and In Vivo". In: *Advances in Experimental Medicine and Biology*. Springer New York, pp. 51–58. DOI: 10.1007/978-1-4939-0620-8_7.

Thomas, Anish et al. (2017). "Temozolomide in the Era of Precision Medicine". In: *Cancer Research* 77.4, pp. 823–826. DOI: 10.1158/0008-5472.can-16-2983.

Thomas, John A. et al. (1979). "Intracellular pH measurements in Ehrlich ascites tumor cells utilizing spectroscopic probes generated in situ". In: *Biochemistry* 18.11, pp. 2210–2218. DOI: 10.1021/bi00578a012.

Thomas, R. C. (1974). "Intracellular pH of snail neurones measured with a new pH-sensitive glass micro-electrode". In: *The Journal of Physiology* 238.1, pp. 159–180. DOI: 10.1113/jphysiol.1974.sp010516.

Tidwell, Tia R. et al. (2022). "Metabolic flux analysis of 3D spheroids reveals significant differences in glucose metabolism from matched 2D cultures of colorectal cancer and pancreatic ductal adenocarcinoma cell lines". In: *Cancer &amp Metabolism* 10.1. DOI: 10.1186/s40170-022-00285-w.

Todaro, Matilde et al. (2007). "Colon Cancer Stem Cells Dictate Tumor Growth and Resist Cell Death by Production of Interleukin-4". In: *Cell Stem Cell* 1.4, pp. 389–402. DOI: 10.1016/j.stem.2007.08.001.

Tomita, Yutaka et al. (2005). "Long-Term iin Vivo/i Investigation of Mouse Cerebral Microcirculation by Fluorescence Confocal Microscopy in the Area of Focal Ischemia". In: *Journal of Cerebral Blood Flow &amp Metabolism* 25.7, pp. 858–867. DOI: 10.1038/sj.jcbfm.9600077.

Torigoe, Takayuki et al. (2002). "Enhanced Expression of the Human Vacuolar H-ATPase c subunit Gene (ATP6L) in Response to Anticancer Agents". In: *Journal of Biological Chemistry* 277.39, pp. 36534–36543. DOI: 10.1074/jbc.m202605200.

Toseland, Christopher P. (2013). "Fluorescent labeling and modification of proteins". In: *Journal of Chemical Biology* 6.3, pp. 85–95. DOI: 10.1007/s12154-013-0094-5.

Tourkya, Belal (July 2009). "Mise au point de la spectroscopie de fluorescence pour la taxonomie des Pseudomonads. Application à la caractérisation d'isolats d'ateliers carnés". Theses. Université Blaise Pascal - Clermont-Ferrand II ; Université d'Auvergne - Clermont-Ferrand I. URL: https://tel.archives-ouvertes.fr/tel-00725447.

Tsien, R. Y. (1981). "A non-disruptive technique for loading calcium buffers and indicators into cells". In: *Nature* 290.5806, pp. 527–528. DOI: 10.1038/290527a0.

Turchi, Laurent et al. (2000). "Evidence for a Direct Correlation between c-Jun NH2 Terminal Kinase 1 Activation, Cyclin D2 Expression, and G1/S Phase Transition in the Murine Hybridoma 7TD1 Cells". In: *Experimental Cell Research* 261.1, pp. 220–228. DOI: 10.1006/excr.2000.5060.

Turner, Dennis A. and David Cory Adamson (2011). "Neuronal-Astrocyte Metabolic Interactions: Understanding the Transition Into Abnormal Astrocytoma Metabolism". In: *Journal of Neuropathology &amp Experimental Neurology* 70.3, pp. 167–176. DOI: 10.1097/nen.0b013e31820e1152.

Uzman, J.Akif et al. (1998). "The Role of Intracellular Alkalinization in the Establishment of Anterior Neural Fate inXenopus". In: *Developmental Biology* 193.1, pp. 10–20. DOI: 10.1006/dbio.1997.8782.

Vasan, Karthik et al. (2022). "Genes Involved in Maintaining Mitochondrial Membrane Potential Upon Electron Transport Chain Disruption". In: *Frontiers in Cell and Developmental Biology* 10. DOI: 10.3389/fcell.2022.781558.

Vaupel, P., F. Kallinowski, and P. Okunieff (Dec. 1989). "Blood flow, oxygen and nutrient supply, and metabolic microenvironment of human tumors: a review." In: *Cancer research* 49 (23), pp. 6449–6465. ISSN: 0008-5472. ppublish.

Végran, Frédérique et al. (2011). "Lactate Influx through the Endothelial Cell Monocarboxylate Transporter MCT1 Supports an NF-κB/IL-8 Pathway that Drives Tumor Angiogenesis". In: *Cancer Research* 71.7, pp. 2550–2560. DOI: 10.1158/0008-5472.can-10-2828.

Verbeek, B. et al. (2008). "O6-Methylguanine-DNA methyltransferase inactivation and chemotherapy". In: *British Medical Bulletin* 85.1, pp. 17–33. DOI: 10.1093/bmb/ldm036.

Vilariño, Natalia et al. (1998). "Role of HCO-3Ions in Cytosolic pH Regulation in Rat Mast Cells: Evidence for a New Na-Independent, HCO-3-Dependent Alkalinizing Mechanism". In: *Biochemical and Biophysical Research Communications* 253.2, pp. 320–324. DOI: 10.1006/bbrc.1998.9615.

Visioli, Fernanda et al. (2014). "Glucose-Regulated Protein 78 (Grp78) Confers Chemoresistance to Tumor Endothelial Cells under Acidic Stress". In: *PLoS ONE* 9.6. Ed. by Yuanpu Peter Di, e101053. DOI: 10.1371/journal.pone.0101053.

Visvader, Jane E. and Geoffrey J. Lindeman (2012). "Cancer Stem Cells: Current Status and Evolving Complexities". In: *Cell Stem Cell* 10.6, pp. 717–728. DOI: 10.1016/j.stem.2012.05.007.

Voss, T G et al. (1996). "Alteration of intracellular potassium and sodium concentrations correlates with induction of cytopathic effects by human immunodeficiency virus". In: *Journal of Virology* 70.8, pp. 5447–5454. DOI: 10.1128/jvi.70.8.5447-5454.1996.

Vukovic, V and IF Tannock (1997). "Influence of low pH on cytotoxicity of paclitaxel, mitoxantrone and topotecan". In: *British Journal of Cancer* 75.8, pp. 1167–1172. DOI: 10.1038/bjc.1997.201.

Waddell, William J. and Thomas C. Butler (1959). "CALCULATION OF INTRACELLULAR pH FROM THE DISTRIBUTION OF 5,5-DIMETHYL-2,4-OXAZOLIDINEDIONE (DMO). APPLICATION TO SKELETAL MUSCLE OF THE DOG*". In: *Journal of Clinical Investigation* 38.5, pp. 720–729. DOI: 10.1172/jci103852.

Wahl, Miriam L. et al. (2000). "Intracellular pH regulation in a nonmalignant and a derived malignant human breast cell line". In: *Journal of Cellular Physiology* 183.3, pp. 373–380. DOI: 10.1002/(sici)1097-4652(200006)183:3<373::aid-jcp10>3.0.co;2-s.

Wanandi, S.I. et al. (2017). "Impact of extracellular alkalinization on the survival of human CD24-/CD44 breast cancer stem cells associated with cellular metabolic shifts". In: *Brazilian Journal of Medical and Biological Research* 50.8. DOI: 10.1590/1414-431x20176538.

Wang, Rong et al. (2021). "Molecular basis of V-ATPase inhibition by bafilomycin A1". In: *Nature Communications* 12.1. DOI: 10.1038/s41467-021-22111-5.

Wang, Tingchung, Cathleen Marquardt, and John Foker (1976). "Aerobic glycolysis during lymphocyte proliferation". In: *Nature* 261.5562, pp. 702–705. DOI: 10.1038/261702a0.

Wang, Xuan, Haiyun Zhang, and Xiaozhuo Chen (2019). "Drug resistance and combating drug resistance in cancer". In: *Cancer Drug Resistance*. DOI: 10.20517/cdr.2019.10.

Warburg, Otto (1926). "Ueber den Stoffwechsel der Tumoren: Arbeiten aus dem Kaiser Wilhelm-Institut für Biologie, Berlin-Dahlem." In: 87, p. 1671. ISSN: 0098-7484. DOI: 10.1001/jama.1926.02680200071042.

— (1956). "On the Origin of Cancer Cells". In: 123, pp. 309–314. ISSN: 0036-8075. DOI: 10.1126/science.123.3191.309.

Ward, Carol et al. (2020). "The impact of tumour pH on cancer progression: strategies for clinical intervention". In: *Exploration of Targeted Anti-tumor Therapy* 1.2, pp. 71–100. DOI: 10.37349/etat.2020.00005.

Ward, Patrick S. and Craig B. Thompson (2012). "Metabolic Reprogramming: A Cancer Hallmark Even Warburg Did Not Anticipate". In: 21, pp. 297–308. ISSN: 1535-6108. DOI: 10.1016/j.ccr.2012.02.014.

Weigelt, Britta and Mina J. Bissell (2008). "Unraveling the microenvironmental influences on the normal mammary gland and breast cancer". In: *Seminars in Cancer Biology* 18.5, pp. 311–321. DOI: 10.1016/j.semcancer.2008.03.013.

Weinlich, Michael et al. (2002). "Human Duodenal Spheroids for Noninvasive intracellular pH measurement and quantification of regulation mechanisms under physiological conditions". In: *In Vitro Cellular &amp Developmental Biology - Animal* 38.1, p. 7. DOI: 10.1290/1071-2690(2002)038<0007:hdsfni>2.0.co;2.

Widmaier, Eric P., Hershel Raff, and Kevin T. Strang (2014). *Vander's human physiology : the mechanisms of body function - 13. ed.* McGraw-Hill Educación. ISBN: 9780073378305.

Williams, A. C., T. J. Collard, and C. Paraskeva (1999). "An acidic environment leads to p53 dependent induction of apoptosis in human adenoma and carcinoma cell lines:

implications for clonal selection during colorectal carcinogenesis". In: 18, pp. 3199–3204. ISSN: 0950-9232. DOI: 10.1038/sj.onc.1202660.

Williamson, John R. et al. (1976). "Contribution of tissue acidosis to ischemic injury in the perfused rat heart." In: *Circulation* 53 3 Suppl, pp. I3–14.

Wingo, Thomas et al. (2001). "The Catalytic Properties of Human Carbonic Anhydrase IX". In: *Biochemical and Biophysical Research Communications* 288.3, pp. 666–669. DOI: 10.1006/bbrc.2001.5824.

Wu, Hao, Minfeng Ying, and Xun Hu (2016). "Lactic acidosis switches cancer cells from aerobic glycolysis back to dominant oxidative phosphorylation". In: 7, pp. 40621–40629. ISSN: 1949-2553. DOI: 10.18632/oncotarget.9746.

Wykoff, C. C. et al. (Dec. 2000). "Hypoxia-inducible expression of tumor-associated carbonic anhydrases." In: *Cancer research* 60, pp. 7075–7083. ISSN: 0008-5472.

Xiao, Hai et al. (2003). "Acidic pH induces topoisomerase II-mediated DNA damage". In: 100, pp. 5205–5210. ISSN: 0027-8424. DOI: 10.1073/pnas.0935978100.

Xu, Wang et al. (2016). "Discerning the Chemistry in Individual Organelles with Small-Molecule Fluorescent Probes". In: *Angewandte Chemie International Edition* 55.44, pp. 13658–13699. DOI: 10.1002/anie.201510721.

Yamada, Kenneth M. and Edna Cukierman (2007). "Modeling Tissue Morphogenesis and Cancer in 3D". In: *Cell* 130.4, pp. 601–610. DOI: 10.1016/j.cell.2007.08.006.

Yamagata, M and IF Tannock (1996). "The chronic administration of drugs that inhibit the regulation of intracellular pH: in vitro and anti-tumour effects". In: *British Journal of Cancer* 73.11, pp. 1328–1334. DOI: 10.1038/bjc.1996.254.

Yang, Xuekang et al. (2010). "Inhibition of Na/H exchanger 1 by 5-(N-ethyl-N-isopropyl) amiloride reduces hypoxia-induced hepatocellular carcinoma invasion and motility". In: *Cancer Letters* 295.2, pp. 198–204. DOI: 10.1016/j.canlet.2010.03.001.

Yip, Stephen et al. (2009). "iMSH6/i Mutations Arise in Glioblastomas during Temozolomide Therapy and Mediate Temozolomide Resistance". In: *Clinical Cancer Research* 15.14, pp. 4622–4629. DOI: 10.1158/1078-0432.ccr-08-3012.

Yoshimoto, Koji et al. (2012). "Complex DNA repair pathways as possible therapeutic targets to overcome temozolomide resistance in glioblastoma". In: *Frontiers in Oncology* 2. DOI: 10.3389/fonc.2012.00186.

Zagaynova, Elena V. et al. (2017). "Imaging of Intracellular pH in Tumor Spheroids Using Genetically Encoded Sensor SypHer2". In: *Advances in Experimental Medicine and Biology*. Springer International Publishing, pp. 105–119. DOI: 10.1007/978-3-319-67358-5_7.

Özel, Rıfat Emrah et al. (2015). "Single-cell intracellular nano-pH probes". In: *RSC Advances* 5.65, pp. 52436–52443. DOI: 10.1039/c5ra06721a.

Zeng, Wei ping, Shuangshuang Yang, and Baohua Zhou (2021). "Intracellular pH-regulated Cell Intrinsic Control of Death and Proliferation of Lymphocytes in Immune Response and Tumor Cells". In: DOI: 10.1101/2021.10.29.466539.

Zeuthen, Thomas (1980). "Chapter 3 How to Make and Use Double-Barreled Ion-Selective Microelectrodes". In: *Current Topics in Membranes and Transport*. Elsevier, pp. 31–47. DOI: 10.1016/s0070-2161(08)60271-3.

Zhang, Guohong, Vanessa Gurtu, and Steven R. Kain (1996). "An Enhanced Green Fluorescent Protein Allows Sensitive Detection of Gene Transfer in Mammalian Cells". In: *Biochemical and Biophysical Research Communications* 227.3, pp. 707–711. DOI: 10.1006/bbrc.1996.1573.

Zhang, Jihong, Malcolm F.G. Stevens, and Tracey D. Bradshaw (2012). "Temozolomide: Mechanisms of Action, Repair and Resistance". In: *Current Molecular Pharmacology* 5.1, pp. 102–114. DOI: 10.2174/1874467211205010102.

Zhang, Xuejing (2010). "Growth factors in tumor microenvironment". In: *Frontiers in Bioscience* 15.1, p. 151. DOI: 10.2741/3612.

Zhou, Weidong, Lance A. Liotta, and Emanuel F. Petricoin (2015). "Cancer metabolism and mass spectrometry-based proteomics". In: *Cancer Letters* 356.2, pp. 176–183. DOI: 10.1016/j.canlet.2013.11.003.

Zhu, Aizhi, Daniel Lee, and Hyunsuk Shim (2011). "Metabolic Positron Emission Tomography Imaging in Cancer Detection and Therapy Response". In: *Seminars in Oncology* 38.1, pp. 55–69. DOI: 10.1053/j.seminoncol.2010.11.012.

Zhu, Hao et al. (2016). "Fluorescent Probes for Sensing and Imaging within Specific Cellular Organelles". In: *Accounts of Chemical Research* 49.10, pp. 2115–2126. DOI: 10.1021/acs.accounts.6b00292.

Zhuang, Ying Xin et al. (1984). "Characterization of potent sodium/proton exchange inhibitors from the amiloride series in A431 cells". In: *Biochemistry* 23.19, pp. 4481–4488. DOI: 10.1021/bi00314a038.